

REPORT DOCUMENTATION PAGE			Form Approved OMB No. 0704-0188	
Public reporting burden for this collection of information is estimated to average 1 hour per response, including the time for reviewing instructions, searching existing data sources, gathering and maintaining the data needed, and completing and reviewing the collection of information. Send comments regarding this burden estimate or any other aspect of this collection of information, including suggestions for reducing this burden, to Washington Headquarters Services, Directorate for Information Operations and Reports, 1215 Jefferson Davis Highway, Suite 1204, Arlington, VA 22202-4302, and to the Office of Management and Budget, Paperwork Reduction Project (0704-0188), Washington, DC 20503.				
1. AGENCY USE ONLY (Leave blank)		2. REPORT DATE 14.Aug.02		3. REPORT TYPE AND DATES COVERED DISSERTATION
4. TITLE AND SUBTITLE YOUR REQUESTS FOR PUBLIC RELAEASE APPROVAL, "COUPLING RETINAL SCANNING DISPLAYS TO THE HIMAN VISUAL SYSTEM"			5. FUNDING NUMBERS	
6. AUTHOR(S) MAJ TURNER STUART L				
7. PERFORMING ORGANIZATION NAME(S) AND ADDRESS(ES) UNIVERSITY OF WASHINGTON			8. PERFORMING ORGANIZATION REPORT NUMBER CI02-131	
9. SPONSORING/MONITORING AGENCY NAME(S) AND ADDRESS(ES) THE DEPARTMENT OF THE AIR FORCE AFIT/CIA, BLDG 125 2950 P STREET WPAFB OH 45433			10. SPONSORING/MONITORING AGENCY REPORT NUMBER	
11. SUPPLEMENTARY NOTES				
12a. DISTRIBUTION AVAILABILITY STATEMENT Unlimited distribution In Accordance With AFI 35-205/AFIT Sup 1			12b. DISTRIBUTION CODE	
13. ABSTRACT (Maximum 200 words)				
<div style="display: flex; justify-content: space-between; align-items: center;"> <div style="text-align: center;"> DISTRIBUTION STATEMENT A Approved for Public Release Distribution Unlimited </div> <div style="font-size: 2em; font-weight: bold;">20020829 039</div> </div>				
14. SUBJECT TERMS			15. NUMBER OF PAGES 272	
			16. PRICE CODE	
17. SECURITY CLASSIFICATION OF REPORT	18. SECURITY CLASSIFICATION OF THIS PAGE	19. SECURITY CLASSIFICATION OF ABSTRACT	20. LIMITATION OF ABSTRACT	

University of Washington

Abstract

**Coupling Retinal Scanning Displays to the Human Visual System:
Visual System Response and Engineering Considerations**

Stuart L. Turner

Chair of the Supervisory Committee:

Professor Thomas A. Furness, III

Department of Industrial Engineering

A retinal scanning display (RSD) is a visual display that presents an image to an observer via a modulated beam of light that is directed through the eye's pupil and rapidly scanned in a raster-like pattern across the retina. As compared to conventional displays that create a real image for viewing, the RSD induces a virtual image only in the mind of the observer. The spatio-temporal characteristics of the RSD retinal stimulation are unique, as are the optical geometries of the small Maxwellian view exit pupil and the entry of image forming rays into the eye. This body of research examined the retinal and opto-physiological responses of the human visual system to RSD stimuli and derived human interface and engineering concepts founded upon unique visual system responses. The retinal response to RSD stimuli was found to be consistent with accepted theories of human visual response. The physiological response of the eye pupil to the Maxwellian view RSD was found to be different from natural view pupillary response models in literature. A broad set of RSD pupillary response models was empirically derived from experimental data. An examination of the RSD interface concept of arrayed small Maxwellian view exit pupils was conducted. The arrayed exit pupil concept was found to be a viable solution to some RSD interfacing challenges. Fundamental perceptual characteristics of arrayed exit pupil RSD's were qualified and basic human observer preferences for arrayed pupil parameters was modeled. Human factors engineering guidelines for implementation of arrayed exit pupil displays were derived.

**Coupling Retinal Scanning Displays to the Human Visual
System: Visual System Response and Engineering
Considerations**

Stuart L. Turner

A dissertation submitted in partial fulfillment of the requirements for
the degree of

Doctor of Philosophy

University of Washington

2002

Program Authorized to Offer Degree: Industrial Engineering

University of Washington
Graduate School

This is to certify that I have examined this copy of a doctoral dissertation by

Stuart L. Turner

and have found that it is complete and satisfactory in all respects,
and that any and all revisions required by the final
examining committee have been made.

Chair of Supervisory Committee:



Thomas A. Furness, III

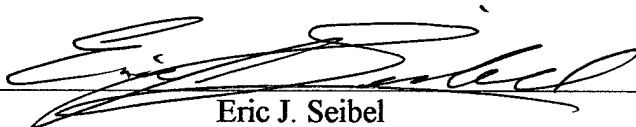
Reading Committee:



Thomas A. Furness, III



Tony C. Woo



Eric J. Seibel

Date:

6 JUNE 2002

The views expressed in this article are those of the author and do not reflect the official policy or position of the United States Air Force, Department of Defense, or the U. S. Government.

In presenting this dissertation in partial fulfillment of the requirements for the Doctoral degree at the University of Washington, I agree that the Library shall make its copies freely available for inspection. I further agree that extensive copying of the dissertation is allowable only for scholarly purposes, consistent with "fair use" as prescribed in the U.S. Copyright Law. Requests for copying or reproduction of this dissertation may be referred to Bell and Howell Information and Learning, 300 North Zeeb Road, Ann Arbor, MI 48106-1346, to whom the author has granted "the right to reproduced and sell (a) copies of the manuscript in microform and/or (b) printed copies of the manuscript made from microform."

Signature Stuart L. Levine

Date 6 JUNE 2002

University of Washington

Abstract

**Coupling Retinal Scanning Displays to the Human Visual System:
Visual System Response and Engineering Considerations**

Stuart L. Turner

Chair of the Supervisory Committee:

Professor Thomas A. Furness, III

Department of Industrial Engineering

A retinal scanning display (RSD) is a visual display that presents an image to an observer via a modulated beam of light that is directed through the eye's pupil and rapidly scanned in a raster-like pattern across the retina. As compared to conventional displays that create a real image for viewing, the RSD induces a virtual image only in the mind of the observer. The spatio-temporal characteristics of the RSD retinal stimulation are unique, as are the optical geometries of the small Maxwellian view exit pupil and the entry of image forming rays into the eye. This body of research examined the retinal and opto-physiological responses of the human visual system to RSD stimuli and derived human interface and engineering concepts founded upon unique visual system responses. The retinal response to RSD stimuli was found to be consistent with accepted theories of human visual response. The physiological response of the eye pupil to the Maxwellian view RSD was found to be different from natural view pupillary response models in literature. A broad set of RSD pupillary response models was empirically derived from experimental data. An examination of the RSD interface concept of arrayed small Maxwellian view exit pupils was conducted. The arrayed exit pupil concept was found to be a viable solution to some RSD interfacing challenges. Fundamental perceptual characteristics of arrayed exit pupil RSD's were qualified and basic human observer preferences for arrayed pupil parameters was modeled. Human factors engineering guidelines for implementation of arrayed exit pupil displays were derived.

Table of Contents

Table of Contents	i
List of Figures	vi
List of Tables	ix
Chapter 1: Introduction	1
1.1 Overview	1
1.2 Research Overview	4
1.3 Research Benefits	8
1.4 Dissertation Structure	9
Chapter 2. Background and Literature Review	10
2.1 Apparatus	10
2.1.1 Virtual Retinal Display	10
2.1.2 The VRD Emulator	14
2.1.2.1 VRD Emulator Opto-mechanical Design	14
2.1.2.2 VRD Emulator Driving Electronics	17
2.1.2.3 VRD Emulator Stimuli and Display Limitations	18
2.1.3 Arrayed Exit Pupil Emulator	20
2.1.4 Pupillometer	21
2.2 Literature Review	24
2.2.1 Human Visual System Function	24
2.2.1.1 Cornea to Cortex	24
2.2.1.2 Brightness (Luminosity) Perception and Measurement	26
2.2.1.3 Flicker Perception	34
2.2.1.4 Spatial Perception and Spatiotemporal Considerations	38
2.2.1.5 Chromatic Considerations	42
2.2.1.6 Pupil Response	43
2.2.1.7 Accommodation Response	45
2.2.2 Retinal Scanning Display Considerations	47
2.2.3 Arrayed Small Exit Pupil Display Considerations	50
2.2.3.1 Rationale for Arrayed Small Exit Pupil Displays	50
2.2.3.2 Considerations in the Optical Geometry of Pupil Coupling and Pupil Array Generation	55
2.2.3.3 General Engineering Concepts and Assumptions for Arrayed Pupil RSD's	60
2.2.4 Light Metrology Considerations with Retinal Scanning Displays	63
2.3 Conclusions from Background and Literature Review Considerations	66

Table of Contents, continued...

Chapter 3: General Hypotheses	85
3.1 Hypothesis 1: Retinal response to, and visual perception of, retinal scanning display stimuli is not anomalous.	85
3.1.1 Sub-hypothesis 1a: Brightness Perception	85
3.1.2 Sub-hypothesis 1b: Flicker Perception	87
3.2 Hypothesis 2: Pupillary responses of the visual system to small exit pupil retinal scanning displays differ from the responses to equivalently perceived conventional displays.	89
3.2.1 Sub-hypothesis 2a: Binocular Opaque View Pupillary Response	90
3.2.2 Sub-hypothesis 2b: Binocular Augmented View Pupillary Response	92
3.2.3 Sub-hypothesis 2c: Monocular View Pupillary Response	93
3.3 Hypothesis 3: Arrays of small exit pupils are an effective method of preserving the optical advantages of small exit pupil RSD's while offering expanded exit pupil area to the observer.	95
3.3.1 Sub-hypothesis 3a: Image Perception with Arrayed Exit Pupils	96
3.3.2 Sub-hypothesis 3b: Model of Preferred Optimum Exit Pupil Separation	97
Chapter 4: Retinal Response in the Temporal Domain: Flicker Experiments	102
4.1 Flicker Contrast Threshold Comparison: VRD vs. CRT	102
4.1.1 Objectives and Hypotheses	102
4.1.2 Apparatus and Experimental Setup	103
4.1.3 Calibrations and Corrections	105
4.1.3.1 Luminance Calibration	105
4.1.3.2 Display Homogeneity Tests	107
4.1.4 Subjects	108
4.1.5 Procedure	109
4.1.5.1 Perceptual Luminance Match	109
4.1.5.2 Flicker Detection Trials	111
4.1.6 Analysis	112
4.1.7 Results	113
4.1.8 Discussion and Conclusions	114
4.2 Critical Flicker Frequency Comparison	117
4.2.1 Objectives and Hypothesis	117
4.2.2 Apparatus and Experimental Set-up	118
4.2.3 Subjects	119
4.2.4 Procedure	120
4.2.5 Analysis	120

Table of Contents, continued...

4.2.6 Results	121
4.2.7 Discussion and Conclusions	121
Chapter 5: Retinal Response in the Intensity Domain: Brightness Experiments	130
5.1 Brightness Comparisons of Scanning and Non-scanning Maxwellian Sources	131
5.1.1 Objectives and Hypothesis	132
5.1.2 Apparatus and Experimental Set-up	133
5.1.3 Subjects	136
5.1.4 Procedure	136
5.1.5 Analysis	137
5.1.6 Results	137
5.1.7 Discussion and Conclusions	138
Chapter 6: Opto-physiological Response: Pupillary Response Model Development	141
6.1 Objectives and Hypotheses	141
6.2 Apparatus, Experimental Setup, and Calibrations	144
6.2.1 Calibration of Pupillary Response Experiment Stimuli	146
6.3 Subjects	148
6.4 Method and Procedure	148
6.4.1 Binocular Display Alignment	149
6.4.2 Stimuli and Data Collection in Opaque View	151
6.4.3 Data Collection in Augmented View	154
6.4.4 Pupillary Response Pilot Study and Experimental Design Revisions	155
6.5 Analysis	156
6.6 Results	157
6.6.1 All Background Luminance Conditions Results	157
6.6.2 Opaque View Background Condition Results	156
6.6.3 Background Condition 10 cd/m ² Results	162
6.6.4 Background Condition 100 cd/m ² Results	165
6.6.5 Background Condition 1000 cd/m ² Results	167
6.7 Discussion and Conclusions	168
6.7.1 Binocular Opaque View RSD Model of Pupil Response	169
6.7.2 Binocular Augmented View RSD Models of Pupil Response	175
6.7.3 Monocular versus Binocular RSD View Pupil Response	177
6.7.4 Monocular View RSD Models of Pupil Response	179
6.7.5 Consolidated General Discussion and Conclusions	181

Table of Contents, continued...

Chapter 7: Small Exit Pupil Arrays: Concept Explorations and Exit Pupil Separation Preference Experiment	197
7.1 Basic Explorations of Arrayed Small Exit Pupil Concepts	197
7.1.1 Objectives and Hypotheses	198
7.1.2 Apparatus	199
7.1.3 Observers	199
7.1.4 Procedures	199
7.1.5 Results and Discussion	200
7.1.5.1 General Perceptual Characteristics and the Region of Coupling Confusion	200
7.1.5.2 Display Content Density and Saccadic Suppression	203
7.1.5.3 Miscellaneous Additional Observation Results	205
7.1.5.4 Visual Perceptual Effects of z-Axis Pupil Coupling Error	207
7.1.6 Conclusions	209
7.2 Optimum Exit Pupil Separation Distance Preference Experiment	210
7.2.1 Objectives and Hypotheses	210
7.2.2 Apparatus and Experimental Setup	211
7.2.3 Subjects	213
7.2.4 Methods and Procedure	213
7.2.5 Analysis	215
7.2.6 Results	216
7.2.7 Discussion and Conclusions	218
7.3 Additional Arrayed Small Exit Pupil Observations and Explorations	224
7.4 Conclusions	227
Chapter 8: General Discussion and Conclusions	231
8.1 Visual Response in the Intensity Domain	231
8.2 Visual Response in the Temporal Domain	233
8.3 Human Pupillary Response with Small Exit Pupil RSD's	235
8.4 Arrayed Small Exit Pupil Displays	237
8.5 Human Factors Engineering Guidelines for Arrayed Small Exit Pupil RSD's	240
8.6 Recommended Research and Future RSD Concepts	244
8.7 Closing Comments	249
End Notes	252

Bibliography	260
Appendix A: List of Pupillary Response Experiment RSD Conditions	268
Appendix B: List of Pupillary Response Experiment RSD Conditions	269
Appendix C: Example Stimuli Used in Pupillary Response Pilot Study and Exit Pupil Separation Study	270

List of Figures

Chapter 2

2.1 Virtual Retinal Display Component Diagram	69
2.2 Virtual Retinal Display Optical Bench	70
2.3 VRD Scan Mechanism and Viewing Optics	71
2.4 VRD Scanning Mechanisms	72
2.5 Viewing Optics of Virtual Retinal Display	73
2.6 VRD Emulator Optical Component Diagram	74
2.7 Basic VRD Emulator Control Logic Diagram	75
2.8 Arrayed Exit Pupil Emulator (APE)	76
2.9 Pupillometer and Output Data	77
2.10 Cross Section of Human Eye	78
2.11 Pathways of Neural Signals from the Retina	78
2.12 Scotopic and Photopic Luminous Efficiency Functions	79
2.13 Cone Photoreceptor Relative Sensitivities	79
2.14 Rod and Cone Photoreceptor Cells	80
2.15 Human Sensitivity to Flicker	80
2.16 Contrast Sensitivity Function	81
2.17 Eye Pupil Size as a Function of Scene Luminance	81
2.18 Maxwellian Viewing Arrangement	82
2.19 Geometry of Eye Rotations with Small Exit Pupils	83
2.20 Simplified Geometry of Parallel and Non-parallel Beam Scans as Applied to Pupil Coupling	84
2.21 Simplified Geometry of Parallel and Non-parallel Beam Scan Generation	84

Chapter 3

3.1 Pupil Diameter as a Function of Corneal Flux Density	101
--	-----

Chapter 4

4.1 VRD Augmented for Flicker Contrast Threshold Experiment	124
4.2 Temporal Signature of VRD Pixels	125
4.3 Relative Error of Actual Contrasts and Target Contrasts	125

List of Figures, continued...

4.4 Counter Phased HFP Stimuli for Perceptual Luminance Match	125
4.5 Simulated Frames of 30 Hz Gaussian Flickering Stimulus	126
4.6 Range of Flicker Contrast Threshold Psychometric Functions by 2AFC Method	126
4.7 Flicker Contrast Thresholds and Threshold Ratios	127
4.8 Flicker Contrast Thresholds by the Method of Adjustment	128
4.9 Relationship of VRD/CRT Contrast Threshold Ratios to VRD/CRT Retinal Illumination Estimates Ratios	128
4.10 VRD Emulator Modified for CFF Experiment	129

Chapter 5

5.1 VRD Emulator Modified for Brightness Matching Experiment	140
5.2 Illustration of Oscilloscope Measurement Display for Brightness Matching Experiment Measurements	141
5.3 Summary of Retinal Illumination Ratios for Brightness Matching Experiment	141

Chapter 6

6.1 VRD Emulator Binocular Display Arrangement	187
6.2 Augmented Photograph of VRD Emulator Binocular Display Arrangement	188
6.3 Summary of All Subjects' Mean Pupil Responses	189
6.4 Comparison of Results with Pupil Response Models	189
6.5 Linear Comparison of Results with Hypothetical Model	190
6.6 Comparison of Binocular RSD Mean Pupil Response by Background Luminance and by Subject	191
6.7 Comparison of Monocular RSD Mean Pupil Response by Background Luminance and by Subject	192
6.8 Binocular RSD Family of Pupil Response Functions	193
6.9 Binocular RSD Standard Deviation with Background Luminance	193
6.10 Pupil Diameter Difference, Monocular RSD – Binocular RSD	194
6.11 Mean Range and Standard Deviations of Pupil Diameter Means, Monocular versus Binocular	195

List of Figures, continued...

6.12 Monocular RSD Family of Pupil Response Functions	196
6.13 Monocular RSD Standard Deviation with Background Luminance	196

Chapter 7

7.1 Geometry of z-axis Pupil Coupling Error	228
7.2 Infrared Image of Subject Eye During Arrayed Exit Pupil Separation Experiment	229
7.3 Pupil Separation Preference Study Summary of Results	229
7.4 Eye Pupil Diameter Measurements Compared with Model Predictions	230
7.5 Illustration of 10 Exit Pupil Array Presented About Eye Pupil	230

Chapter 8

8.1 Relationship Among Eye Pupil Diameter, Exit Pupil Optimum Separation, and RSD Field of View Accessibility	251
--	-----

List of Tables

Chapter 2

Table 2.1 Spatial Cut-off Frequency	39
Table 2.2 Estimations of Eye Rotation Limits for Pupil Coupling	57

Chapter 4

Table 4.1 Mean Critical Flicker Frequency Values	121
--	-----

Chapter 6

Table 6.1 ANOVA Summary of Significant Pupil Response Effects (all background conditions considered)	158
Table 6.2 Homogeneous Subsets of Background Luminance by Pupil Diameter	158
Table 6.3 Homogeneous Subsets of RSD Field of View by Pupil Diameter	159
Table 6.4 Homogeneous Subsets of RSD Corneal Flux Density by Pupil Diameter	160
Table 6.5 ANOVA Summary of Significant Pupil Response Effects (opaque view conditions only)	160
Table 6.6 Homogeneous Subsets of RSD Corneal Flux Density by Pupil Diameter (opaque view conditions only)	161
Table 6.7 ANOVA Summary of Significant Pupil Response Effects (10 cd/m ² background conditions only)	163
Table 6.8 Homogeneous Subsets of RSD Field of View by Pupil Diameter (10 cd/m ² background conditions only)	163
Table 6.9 Homogeneous Subsets of RSD Corneal Flux Density by Pupil Diameter (10 cd/m ² background conditions only)	164
Table 6.10 ANOVA Summary of Significant Pupil Response Effects (100 cd/m ² background conditions only)	165
Table 6.11 Homogeneous Subsets of RSD Corneal Flux Density by Pupil Diameter (10 cd/m ² background conditions only)	166
Table 6.12 Models of Binocular Augmented View Pupil Response	176
Table 6.13 Monocular Versus Binocular RSD View Pupil Response Difference	178
Table 6.14 Models of Monocular Augmented View Pupil Response	180
Table 6.15 Summary of All Asserted Pupil Response Models	182

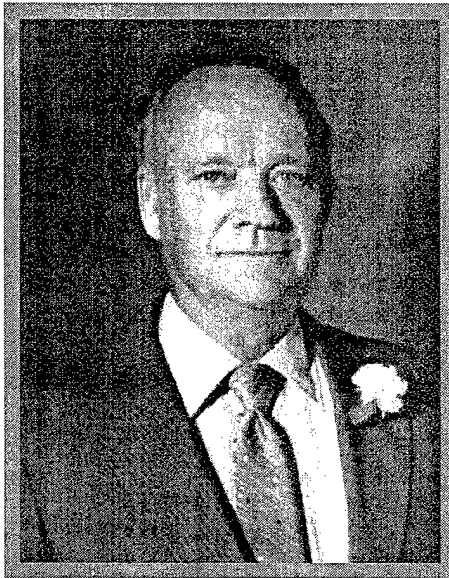
List of Tables, continued...

Chapter 7

Table 7.1 Best Fit Linear Functions to Exit Pupil Separation Data	216
Table 7.2: Linear Functions Fitting Slopes and Ordinate Intercepts of Pupil Separation Functions	217
Table 7.3: Comparison of SC-1 Efficiency Ratios to Coupled Pupil Area Ratios for the 1.0 mm Exit Pupil Condition	219
Table 7.4: Comparison of SC-1 Efficiency Ratios to Coupled Pupil Area Ratios for the 0.5 mm Exit Pupil Condition	220

Dedication

This dissertation is dedicated in loving memory to my late father, Obie L. Turner, who instilled in me at a very young age his own love of science, technology, and engineering. Daddy, you would have loved this stuff!



Chapter 1: Introduction

1.1 Overview

The human is a visual animal. By far, the processing of visual information in the human brain employs more cortical resources than any other sensory function [1]. Our well developed visual ability facilitates the effortless creation of distal, physical world models within our minds by which we think, predict, and speculate about our interactions with the world. This ability promotes success in overcoming the challenges in the environment, thereby preserving and enhancing life. We are dependent upon our visual sense for our livelihood, and indeed, for our very existence. We have become, through design and natural forces, dominated by our sense of vision.

As such visually dominated beings, we have devoted enormous resources and effort to the development of technologies that stimulate our visual senses. More than ever before, human activity is modulated by technologies designed specifically to deliver visual information to the brain. Photography, cinema, television, and computers are typical examples of visual display technology by which we work, relax, entertain, learn, and enhance our thinking. *Mobile computing* has recently emerged as a major industry segment, requiring small and lightweight displays that are still able to deliver ample quantities of visual information. Visual display technology has become ubiquitous in modern civilization, critical to our every day operations, and we continue to develop, innovate, and improve our visual display technology at breathtaking pace.

Why? Why, this heavy investment in visual displays? Why, the impetuous race to further advance visual display technology? Clearly, the modern world is increasingly driven by information. Information is now readily available in quantities much too vast to be wholly assimilated by the individual human, but we still are driven by necessity, by basic desires, and by curiosity to absorb as much information as possible. In agreement with the dominant role vision assumes in our psyches, perceptual psychology has shown that the most efficient means of acquiring information is through the visual channel. In engineering terms, vision provides greater bandwidth to the brain than any other perceptual modality. Thus, improved visual display technology, including visual displays that provide information in environments and conditions that previously precluded their use, holds the potential of expanding our ability to assimilate more

information with greater efficiency than ever before. Greater bandwidth to the brain is the fundamental goal of advancing visual display technology.

The primary role of the human factors engineer (HFE) is to evaluate and improve interfaces between humans and machines, thereby improving efficiency and safety of operations. Put another way, the HFE is tasked to gauge the bandwidth to the brain provided by an interface, as well as its effects on task performance, and to seek methods of increasing both bandwidth and performance. With respect to visual display technology interfacing, the HFE is concerned with the coupling of displays to the human visual system, ensuring a good match of image presentation and information formatting with human visual capacity and task demands. This role is frequently a multidisciplinary one, blending study of perceptual psychology, cognitive psychology, and psychophysics with that of display engineering and the physical sciences.

A multidisciplinary approach to human factors research is imperative with the advent of entirely new visual display technology, especially if the technology employs novel or unconventional methods of stimulating the human visual system. The HFE must endeavor to explore the nature of the new stimulus and examine its effects on imagery perception. Based on the perceptual characteristics, the HFE must seek implementations of the new technology that produce efficient and effective coupling with the human visual system and promote enhancement of task performance. The physical nature of light stimuli, the physiology of the human visual system, the psychology of perception and cognition, and the engineering of visual displays form a complex multidisciplinary nexus that must be addressed for the HFE to meet his responsibilities in the advancement of new visual display technology.

Indeed, a unique new genre of visual display technology is currently under development, holding tremendous potential for new and exciting applications. Known collectively as *retinal scanning displays*, or *RSD's*, these displays provide no real image for visualization. Rather, RSD's stimulate the eye's retina with a rapidly scanning beam of light to induce a virtual image in the mind of the observer [2, 3]. This virtual image is perceived superimposed with any real world scene being viewed (augmented view), or as an independent image if real world imagery is blocked (opaque view). This display technology offers distinct advantages over more conventional extended source displays, such as cathode ray tubes (CRT) or liquid crystal displays (LCD), and it introduces some intriguing new questions across disciplinary boundaries. The research effort described here addresses the multidisciplinary nexus surrounding the coupling of RSD technology with the human visual system.

The most obvious difference between RSD's and conventional display technologies is the absence of a real image. With conventional display systems, an extended photon emitting source is provided for the observer's eye to image onto the retina. Typically, the emitting source providing the real image is a variably energized phosphor deposit or other glowing substance, or an illuminated array of configurable liquid crystals. These techniques are typified by CRT and LCD technology. The resulting retinal image stimulates photoreceptors that relay signals to the visual processing centers of the brain, causing the perception of an image coarsely analogous to the variable photon emissions of the extended physical light source.

However, RSD's provide no extended emitting source for real imaging. Instead, only a single, narrow, scanning beam illuminates the retina after passing through the pupil and ocular media of the eye [2, 3]. The beam's energy is modulated in synchrony with its scanning pattern and in accordance with the imagery to be presented. The result is variable stimulation of the retinal photoreceptors by the beam in a spatiotemporal pattern that is integrated by the observer's visual processing system and perceived as a stable, vivid virtual image.

This novel method of stimulating the human visual system offers some interesting advantages over conventional display methods. The RSD has the potential to efficiently deliver a great amount of energy to the retina, providing a very bright display with very low energy consumption. Large depth of field (near to far focus) can be achieved with a small RSD exit pupil without severe reductions in image quality, making the display ideal for many augmented reality applications [4, 5]. Since an RSD is not reliant upon an extended photon emitting "screen", it has the potential to be small and lightweight while providing a large field of view with excellent resolution [5]. Finally, the RSD is completely private, as no real image exists for imaging by other's eyes.

Numerous potential applications for RSD's exist, and many are currently being explored by academic, commercial, and government researchers [6-10]. The high brightness feature may offer enhanced augmented information display in bright ambient light environments, such as military aircraft cockpits. The large depth of field characteristic may provide a simple method of maintaining a well focused augmented display for applications requiring substantial real world accommodation changes, such as manufacturing environments. The potential for small, lightweight, and private displays may prove to be a boon to the burgeoning mobile computing and personal digital device industry. Already, RSD applications are being tested in the medical arena, providing patient data to doctors and nurses, and displaying augmented imagery and information

to surgeons performing delicate procedures [11, 12]. As RSD display engineering and miniaturization matures, it is clear that RSD's will grow to be a significant means of information display across a wide range of military, commercial, and civil applications.

However, new unknowns are introduced by the advent of RSD's. The perceptual effects of the unique spatiotemporal stimulation of the retina by RSD's, providing a very bright but very brief display "pixel time," have not been adequately quantified. When viewing a small exit pupil RSD along with a natural view, the physiological response of the eye's pupil is poorly understood. Pupil changes will modulate natural scene retinal illumination, but not RSD retinal illumination. The longitudinal effects of the eye's accommodation response to the small exit pupil display's large depth of field are poorly understood, particularly under augmented viewing conditions. Effective methods for interfacing small exit pupil displays with the human visual system are largely unexplored. Methods for maintaining precise coupling alignment of a tiny RSD exit pupil with the eye's entrance pupil are undeveloped.

Because this display technology is new, and because commercial RSD's are still quite rare, little basic perceptual or human factors research has been conducted with RSD's. Since this method of stimulating the retina is unique for a visual display, and since the optical properties of RSD's are novel, it is prudent to closely examine perceptual characteristics and human factors issues with RSD's to ensure their proper and effective implementation as information display devices. Thus, the general goals of this research effort are: 1) to conduct an investigation of human visual system response to RSD stimulation, 2) to identify any unique perceptual and/or physiological characteristics associated with RSD visual stimulation, 3) to explore general engineering concepts for practical implementation and interfacing of RSD's with the human visual system, and 4) to compile human factors data related to RSD interfacing that will assist engineers in solving some of the human factors challenges of RSD implementation.

1.2 Research Overview

This body of research covers a broad spectrum of interdisciplinary issues related to the coupling of RSD's to the human visual system. Obviously, basic perceptual and physiological responses of the visual system have a significant impact on the design and implementation of visual display technologies. This research is aimed at uncovering and defining any unique perceptual and physiological responses to RSD stimulation, predicting the impact of these visual system

responses on RSD display interfacing methods, and initiating an exploration of RSD interface concepts that will allow unique advantage of RSD's to be maximized. The general conceptual framework for these research topics follows.

Any dynamic visual display must function within three main perceptual dimensions. A display of some *spatial* extent changes in *intensity* over *time*. Thus, a thorough investigation of RSD perceptual effects should consider the spatial, temporal, and intensity (brightness and contrast) domains. Complicating this simple taxonomy is the fact that these three dimensions are interdependent, as characteristics along one dimension affect perceptions along the others. Additional complications arise with physiological considerations of the human visual system. In each of the domains, distinction must be made between perceptual effects originating at the level of the retina and effects related to other opto-physiological factors. Finally, the impact of retinal and opto-physiological factors on display design and implementation must be considered within the context of human factors engineering to ensure display viability in real world contexts.

In studying human visual perception, spatial factors concern the ability to resolve patterns of various sizes, quantified in units of subtended visual angle. This seemingly simple definition is greatly complicated by the interdependence of spatial and intensity factors, specifically the relationship between spatial extent and contrast. The contrast required for pattern detection varies with the spatial extent of the pattern. The human *contrast sensitivity function* (CSF) describes this relationship, and the relationship varies with stimuli that are temporally modulated to the extent that "flicker" is perceptible.

With visual display technology, consideration of the temporal domain typically focuses on the perception of flicker. Flicker perception is a function of spatial extent, contrast, and brightness, as larger, higher contrasting, and brighter temporally modulated stimuli are more easily perceived as flickering. The *critical flicker frequency* (CFF) is the rate of temporal modulation at which a given stimulus is no longer perceived as flickering, but rather as a steady source. Flicker is an undesirable characteristic for most information displays, and it is alleviated by refreshing displays rapidly, typically at 60 Hz. or greater.

The intensity domain, when not considering contrast and CSF's, is largely concerned with the *percept* brightness, or *luminosity*. Brightness is distinguished from luminance, a physically measurable quantity of light energy in a particular direction. Brightness implies the perception of luminance, and is only coarsely correlated with stimulus physical luminance. The human visual system is subject to retinal gain changes, pupil attenuation changes, and psychological factors that

affect brightness perception. Contrast, temporal modulation, and spatial extent affect brightness perception in complex ways. Brightness is best quantified by comparison with other stimuli or standard luminance sources.

The retina contains a vast and complex array of interconnected photoreceptive cells that absorb light quanta and respond with electrochemical excitation of neural cells. Illumination of these photoreceptive cells by light passing through the optics of the eye is the initiation of all visual experience. If visual perception is altered in any dimension by the RSD's unique stimulus, the source of that altered perception may be due to a unique retinal response to the stimulus. Visual physiological responses are typically dependent upon retinal response, thus retinal perceptual factors will be considered in initial studies. Opto-physiological response studies will follow the completion of retinal response studies.

Opto-physiological factors include the physical optics of the eye's cornea, lens, and humors, and particularly the response of the eye's pupillary and accommodation response mechanisms. The eye's optics must still be traversed by RSD stimuli, and the scanning light beam must be imaged onto the retina with these optics. More significantly, normal physiological responses of the pupil and lens may be circumvented by the small exit pupil RSD. A bright RSD image presented with an exit pupil of less than two millimeters diameter will not be attenuated by the eye's pupil contracting in response to the bright stimulus. The unique small pupil optical geometry may also induce enhanced brightness perception, as light rays are longitudinally aligned with photoreceptive cells, improving phototransduction efficiency and perhaps altering pupil response. The small exit pupil RSD image, with large depth of field, may induce abnormal oscillations in the dynamics of the eye's lens with unknown long term implications for accommodation, acuity, and comfort [13].

Thus, unique perceptual experiences could arise due to the unique conditions caused by RSD stimuli and related to opto-physiological factors. Any anomalous visual system responses due to opto-physiological factors must be distinguished from any novel retinal responses occurring with RSD stimulation, and the impact of these visual system responses on display interfacing should be carefully examined. In particular, unique pupillary response to RSD stimulation may have significant impact on the coupling of small exit pupil RSD's with the visual system. Therefore, following an examination of retinal response, research into pupillary response in the opto-physiological realm will be conducted.

Related to the opto-physiological factors are interface engineering issues with display implementation, particularly in head-mounted display scenarios. The optical characteristics of RSD's, coupled with the characteristics of the human visual system, introduce many questions and novel human factors engineering challenges that must be addressed before most envisioned RSD applications can be viable. Of particular interest is the implementation of RSD displays that preserve the RSD's small exit pupil and related optical and energy efficiency advantages. Maintaining proper coupling of small exit pupils with the eye's entrance pupil offers some significant challenges. Studies characterizing the opto-physiological response of the eye pupil to RSD stimuli provide a natural lead-in to the study of strategies for maintaining proper pupil coupling.

Small exit pupil displays must remain well aligned with the eye's entrance pupil or the display image is lost to the observer. In high luminance environments where the eye's pupil is constricted, the pupil coupling precision required to maintain image capture may be less than two millimeters. Further, because eye rotation is necessary for central vision examination across an RSD image, small eye pupils preclude imaging the entirety of a wide field of view display on the fovea for central vision inspection. The exit pupil will become decoupled from the eye's entrance pupil as the observer attempts to scan around the extremities of an image or as environmental factors induce relative motion between eye and display. The image will disappear from view when pupils are decoupled due to these eye-display relative movements. This is a severe disadvantage associated with small exit pupil displays that must be overcome before practical implementations can be realized.

Displaying multiple small exit pupils in an array about the eye's pupil may improve pupil coupling area, or *effective exit pupil area*. This may allow the observer to fully view wide field imagery with central vision and maintain the RSD image even with substantial eye-display relative motion, while also preserving small exit pupil advantages. However, the perceptual effectiveness of this approach is unknown, and display engineering challenges related to the creation of exit pupil arrays seem likely to necessitate some unique display compromises that may affect visual perception of the display. Further, little knowledge has been catalogued of human pupillary response to the small exit pupil RSD conditions that will impact the implementation of arrayed exit pupil displays. Therefore, following research into the pupillary response to RSD stimulation, an exploration of the concept of arrayed exit pupil displays will be launched. This

exploration will focus on basic perceptual characteristics of this display concept and the resultant impact on RSD coupling with the human visual system.

In accordance with these topics, this research has five major objectives:

1. Explore the intensity domain with RSD's to identify and quantify any anomalous perceptual effects due to retinal response.
2. Explore the temporal domain with RSD's to identify and quantify any anomalous perceptual effects due to retinal response.
3. Explore the pupillary response to small exit pupil RSD's and model the behavior of the pupillary system under RSD stimuli conditions.
4. Explore interface engineering options for preserving the advantages of small exit pupil display with arrays of small exit pupils and model human preference for basic arrayed pupil display characteristics.
5. Derive human factors engineering guidelines for implementing RSD's with arrayed small exit pupils.

1.3 Research Benefits

The potential benefits of this research include:

- Enhanced understanding of the human factors engineering issues and visual perceptual issues associated with the implementation of RSD's.
- Possible visual perceptual discoveries revealing new fundamental characteristics of the human visual system.
- Greater understanding of the opto-physiological responses of the eye to RSD stimuli, and the impact of these responses on RSD perception and implementation.
- Models for predicting eye pupil response to small exit pupil RSD stimuli upon which improved display engineering concepts may be based.
- Development of human factors guidelines governing the implementation of arrayed small exit pupil RSD's for improved effective exit pupil area.
- Expanded RSD engineering concepts for the improvement of display quality and efficiency.

Certainly, with the expanding implementation of RSD's, the engineering communities advancing these displays will benefit from the pupil response models and implementation guidelines for

arrayed small exit pupil RSD's. An understanding of the impact of opto-physiological responses is critical to ensuring that RSD's are designed for safe and efficient utilization, avoiding user discomfort or strain. Further, the psychophysics community may benefit from basic perceptual data if any unusual or unexpected perceptual anomalies are uncovered with this unique stimulation of the visual system. The human factors engineering community may benefit most from the revelation of utilization issues and challenges, pointing the way to research that will be necessary to make the RSD an effective display technology for human use.

1.4 Dissertation Structure

This dissertation is presented in the following format. Chapter 2 provides detailed background information relevant to the new research. First, because of the unique nature of the display technology applied in this research, engineering descriptions of the RSD technology and other apparatus are detailed. Second, a literature review is presented summarizing pertinent aspects of human visual perception, visual system physiology and anatomy that the reader may need for subsequent interpretation of experiments and findings. Third, engineering considerations with RSD and arrayed exit pupil displays are reviewed that are pertinent to display interfacing concepts explored in this body of research. Chapter 3 presents a synthesis of the RSD engineering and human visual system considerations of Chapter 2, from which general hypotheses are established. Chapter 4 describes RSD retinal response research in the temporal domain. Chapter 5 describes RSD retinal response research in the intensity domain. Chapter 6 describes RSD opto-physiological pupillary response research. Chapter 7 describes explorations and research with arrayed exit pupil display concepts. Chapter 8 summarizes and integrates new research findings with literature and introduces additional RSD concepts and recommended additional research.

Within each subsequent chapter, figures referenced by number in the text are compiled in numerical order at the end of each chapter. Tables are inserted within the body of the text near the text numerical reference. All figures and tables are identified numerically by chapter number and numerical sequence number.

Chapter 2. Background and Literature Review

Before the new research efforts can be fully expounded, a detailed description of VRD technology is necessary, as well as a description of derived devices custom engineered exclusively for this new research. Additionally, a review of relevant human visual system characteristics and related research literature is prudent.

2.1 Apparatus

The Human Interface Technology Laboratory (HITL) at the University of Washington was the seminal organization for RSD development [2, 6]. The Virtual Retinal Display™, or VRD, is an RSD invented by the laboratory's director, Dr. Thomas A. Furness, III and Joel Kollin, a research engineer at the laboratory [14]. Under Dr. Furness' leadership, investigations of RSD technologies have continued since the VRD's inception in the early 1990's. All new research reported herein was conducted at HITL using VRD and VRD derivative technologies. The two primary display devices utilized in this research were the upgraded original prototype Virtual Retinal Display and a variable display parameter RSD with limited modulation capability dubbed the *VRD Emulator* (VRDE).

2.1.1 Virtual Retinal Display

The original VRD constructed at HITL is an engineering device mounted on an optical bench platform [3, 6]. It has undergone several design upgrade iterations since its original implementation, but the basic functional components have not changed significantly:

1. Photon generation is accomplished by laser emission.
2. Laser intensity modulation is accomplished with acousto-optic modulators (AOM) in accordance with an interpreted VGA computer video signal.
3. Modulated laser light is routed via optical fibers to a dual mirror, 2-D scanning mechanism.
4. The pattern of scanned modulated laser light is converged by optical elements to form a small display exit pupil for viewing.

The VRD is viewed by placing the entrance pupil of the observer's eye coincident with the converged display exit pupil, allowing the scanning beam to pass through the eye's pupil and causing the retina to be illuminated by the expanding scan pattern beyond the exit pupil position. Figure 2.1 depicts a component diagram of the basic functionality of the VRD. Figure 2.2 is an augmented photograph of the VRD optical bench depicting the system architecture, and Figure 2.3 is an augmented photograph of the scanning mechanism and viewing optics arrangement depicting the formation of a converged, small exit pupil.

Two lasers are used to provide three distinct wavelengths of coherent light perceived as red, blue, and green. A helium-neon gas laser radiating at 633 nm (Melles Griot model 05-LHP-121) provides the red beam, while an argon ion laser (Omnichrome model 532R-A-A04) provides both green and blue beams at 514 nm and 458 nm, respectively. The 514 nm and 458 nm wavelength beams are separated from the multiple wavelength emitting beam of the argon ion laser with dichroic mirrors selected to reflect only a narrow range of wavelengths while passing all others. Typical of laser energy, each beam is coherent and monochromatic, and each beam is linearly polarized from the point of emission. Each beam is independently routed into an acousto-optic modulator to affect intensity modulations. Each beam is modulated in accordance with a standard computer video signal that has been converted to drive the AOM's.

The video source is a red-green-blue (RGB) VGA computer signal. Each channel's analog signal is digitally sampled and read into a memory buffer for temporary storage. The VGA raster scan synchronization signals are also captured to facilitate proper coordination of light modulation with display scan position. An entire display "line" of RGB intensity values is sampled and stored as discrete digital values for 640 pixel positions comprising a horizontal display line. In reading out these discrete display line values, the buffering electronics implement a unique pattern of first-in, first-out (FIFO) and first-in, last-out (FILO), alternatively. That is, every other display line's values are read out of the buffer in reverse order to that in which they were read in, or FIFO - FILO - FIFO - FILO, etc. This method of read out is necessary due to the bi-directional operation of the VRD's horizontal scanning mechanism that is described in more detail subsequently. Display line values are read in and read out in accordance with the video synchronization signals, and each pixel's values for RGB intensity are converted into a format suitable for the control electronics of the AOM systems [6].

Three acousto-optic modulation systems by Neos Technologies (modulator model N15260 and driver model N21260-7ASSY) are used to adjust the intensity of the laser beams.

The reformatted video signal modulates the output of the AOM systems' RF driver modules. These modules produce a 260 MHz carrier frequency that is amplitude modulated in accordance with the reformatted video signal input. The RF carrier wave is directed to the AOM's modulator module, where a mechanical standing wave is induced by the RF energy within a transparent crystal. The optical properties of the crystal change rapidly with modulation of the RF-induced mechanical wave such that it acts as a variable refractive index grating, diffracting the laser light as a function of the mechanical wave's frequency and amplitude. The result is separation by diffraction of the laser energy into emission modes (separate beams) that are emitted from the crystal at various angles to the main (zero order) beam. Each of these laser modes is intensity modulated as a function of the amplitude of the crystal's mechanical standing wave. (Diffraction angle changes may be induced by frequency modulations, but that function is not implemented in the VRD.) The moded beams of greatest intensity for each of the RGB channels, the 1st order beams, are directed into fiber optics to be used as scanned display beams. Thus, the VGA video signal, via reformatting electronics and AOM systems, ultimately provides rapid intensity modulation of the 1st order RGB laser beams used for visual stimulation with the VRD. This rather inefficient method of modulation is used because it offers modulation speed sufficient for 60 Hz refreshed video (Robert Burstein, VRD engineer, 1998, personal communication).

Each 1st order laser beam is focused onto the entrance aperture of a 3.1 μm core diameter optical fiber using a microscope objective lens and a micrometer positioning stage. The three fibers, separately guiding red, green, and blue modulated laser light, are blended together to form a single 3.1 μm fiber guiding the combined RGB beams of laser light. The fiber combiner (Canadian Instrumentation and Research, Limited) was custom constructed from a HITL design (Eric Seibel, Human Interface Technology Laboratory, Personal Contact). The single combined fiber terminates within the VRD scanning mechanism.

The laser emissions from the optical fiber pass through a small focusing lens immediately upon exiting the fiber and illuminate a dual mirror scanning mechanism. Two mechanical devices with mirrored surfaces produce the 2-D scan of the laser as depicted in graphic *A* of Figure 2.4 [3]. The horizontal, or "line," scan is created with a HITL invented device called the mechanical resonant scanner (MRS) [15]. This device is a small oscillating mirror mounted on spring plates and driven with induction coils, as depicted in graphic *B* of Figure 2.4. It oscillates with a sinusoidal period and a frequency of 15.75 kHz, offering speed sufficient for horizontal scanning at VGA video rates [3]. As mentioned above, the MRS scans out horizontal display

lines bi-directionally as the mirror oscillates, requiring the FIFO-FILO video data read-out. The vertical scan is accomplished with a mirrored galvanometer (Cambridge Technologies model 6800). As both mirrored surfaces oscillate in raster synchrony and deflect the incident laser beam, a rectangular 2-D scan of laser light is directed toward the VRD viewing optics.

As depicted in Figure 2.1 step 4 and step 5, and in Figure 2.3, the scanning beam exits the scan mechanism and is directed through an optical combiner/beam splitter. This beam splitter passes 70% of the light energy and reflects 30%. The 70% portion of the beam continues to a 100 mm focal length reflecting optic. This spherical reflector converges the scan pattern while reflecting the beam back along its path to the combiner. Again, 70% of the light energy passes through the combiner, and 30% is reflected toward the observer's eye. Only 21% of the light exiting the scan mechanism remains in the viewing path. The scan pattern converges at a position in front of the viewing optic arrangement forming a small exit pupil of approximately beam width diameter (approximately 1 mm diameter). When the eye's entrance pupil is positioned coincident with the display exit pupil, the retina is illuminated by the scanning beam.

The spherical reflector converges the scanning pattern of the beam to form the exit pupil, but it also has an optical effect on the beam itself. Without careful engineering, the beam would be converged by the spherical reflector, making it difficult or impossible for the eye to focus the beam on the retina. Recall from above that a small lens at the termination of the optical fiber has a converging affect on the beam. This lens was selected to bring the beam to a focus at a position in the optical path above the scanning mechanism and below the combiner. The spherical reflecting optic was then positioned 100 mm beyond the beam's focal point. Since the spherical reflector has a 100 mm focal length, the beam is reflected from the spherical surface with a high degree of collimation. A well collimated scanning beam is the result, allowing the eye to comfortably view the beam by accommodating near optical infinity. Figure 2.5 illustrates the collimation and viewing scenario for three scanning positions of the beam.

By the methods described above, a single laser "spot" is moved across the eye's retina in a pattern depicting approximately 500 horizontal lines, each line modulated in intensity and chromaticity up to 640 times across it's length. The pattern is repeated at a rate of 60 Hz to present a dynamic, full color image. However, the image is virtual, existing only in the mind of the display observer.

2.1.2 The VRD Emulator

The VRD Emulator (VRDE) was designed and constructed at HITL by the author and HITL staff engineer Robert Burstein. The current version of the VRDE is a modification of an earlier design that was aborted due to unanticipated engineering problems. A new engineering approach by the author resolved the problems, and the VRDE was constructed using most of the apparatus acquired for the original design along with new acquisitions. It is a unique display device designed to emulate the stimuli provided by the VRD and to facilitate the exploration of visual perception of RSD stimuli.

The VRD Emulator provides retinal illumination in a manner nearly identical to that of the VRD. However, the apparatus comprising the VRDE and generating the illumination is substantially different from the original VRD. The opto-mechanical design and the driving electronics differ significantly from the VRD. These differences allow a broad range of variable display parameters that are impossible with the rigidly designed original VRD. Unfortunately, these same differences limit the VRDE to display of only simple imagery. Nevertheless, the VRDE is a valuable tool for investigating basic visual perception of small exit pupil RSD's.

Although the VRDE apparatus is quite different from the original VRD, the basic functional components are quite similar:

1. Photon generation is accomplished by laser emission.
2. Laser intensity modulation is accomplished with an acousto-optic modulator in accordance with synchronization signals generated by the VRDE.
3. Modulated laser light is directed by standard optical components to a 2-D scanning mechanism.
4. The pattern of scanned modulated laser light is converged by optical elements to form a small exit pupil for viewing.

2.1.2.1 VRD Emulator Opto-mechanical Design

Three main optical engineering differences from the VRD are notable. 1) No optical fibers are used to direct the VRDE laser emissions, thereby avoiding a significant power loss associated with injection of the light into the fiber. 2) The scanning mechanism employs a spinning mirrored polygon for the horizontal scan, rather than the Mechanical Resonant Scanner, providing

a broad range of horizontal scan speeds and unidirectional scanning. 3) Lens optics converge the scan and collimate the beam for viewing, in lieu of the spherical reflecting optic of the VRD.

Figure 2.6 depicts a component diagram of the basic optical configuration of the VRDE. Neutral density filters, selectable over a four logarithmic range, attenuate the laser beam immediately upon emission. The red laser is a linearly polarized, 633 nm, helium-neon gas tube laser (Melles-Griot model 05-LHP-121).

The attenuated beam is directed into an acousto-optic modulator (Neos Technologies modulator model 48062-1.0-.55-W and driver model 64040-75-.1-4CH) for intensity modulation. In the aborted VRDE design, this modulator was intended to provide only blanking of the laser beam during vertical retraces of the scan. While the modulator has the bandwidth to modulate line by line, its speed is insufficient for sub-line modulation at the pixel level. For most desired applications, this is a sufficient level of performance.

The first order modulated beam is optically expanded using a negative focal length lens, and subsequently weakly converged by a positive lens. The intent of this beam expansion and weak convergence is to create a long, narrow “waist” in the beam near the scanning mechanism. The long waist is dictated by the scanning mechanism and viewing optics, and this is explained in more detail subsequently. Over an extended path, the beam narrows and passes through a variable neutral density filter (ND wedge) used to make minute adjustments in beam intensity. The beam then encounters the VRDE scanning mechanism to create a 2-D scan pattern similar to that of the original VRD.

In the scanning mechanism, the beam first encounters a mirrored galvanometer (Cambridge Technologies model 6800HP) that deflects the beam vertically. The vertically scanning beam is reflected onto a spinning polygon (Lincoln Laser Company model M225-030-XLIM) with 75 mirrored facets. As the polygon spins, the beam is scanned horizontally. The mirrored galvanometer is synchronized with the polygon to produce a regular, repeated raster scan of the beam. Unlike the sinusoidal, bi-directional scan of the VRD’s oscillating MRS mirror, the spinning polygon scans the beam in only one direction with constant speed.

The scanning beam is reflected from the polygon onto a mirror that directs the beam toward the viewing optics. This mirror reflects only the central portion of the horizontal scan. The edge regions of the scan are discarded because they are of reduced luminance, caused by polygon facet edge effects where the beam is overlapping two facets as the polygon spins. Only a partial beam profile is reflected into the viewing path near the horizontal edges of the scan when

the active polygon facet enters and exits the beam's profile spot. The clipping mirror allows only the full beam profile reflections to continue down the optical path, providing an equiluminous horizontal scan pattern.

The scanning beam passes through a converging lens that collimates the scan pattern and increases the convergence of the beam. The beam comes to a focus 50 mm prior to the viewing optic, and the collimated scan pattern fits within the entrance aperture of the viewing optic. The viewing optic is a 50 mm focal length compound lens assembly that collimates the beam and converges the scan pattern to form a small exit pupil (exit pupil diameter varied with different VRDE implementations between approximately 0.5 and 1.0 mm).

This arrangement is similar to the VRD's optical design, with larger scanning mechanisms, longer beam paths, and with lens optics substituting for the spherical reflector of the VRD. In each case the beam is weakly converged to provide a small profile to fit within the scanning mirror apertures. It is ultimately brought to focus before the viewing optic at a distance equal to the viewing optic's focal length, thereby collimating the beam while converging the scan pattern.

Several complex relationships conspire to dictate the production of a long waist in the beam, as mentioned above. Because the VRDE polygon facets are narrow (3 mm) in the horizontal dimension, a small beam profile is required to avoid excessive reduced luminance edge effects, as described above, while preserving a sufficient horizontal scan extent. The distance between the scanning mechanism and the viewing optic must be relatively long to avoid blocking the beam's path with components and to allow sufficient space for additional components subsequently added to the basic design described here. Further, the beam must be collimated and the scan converged to form the exit pupil. The scan convergence requires a relatively short focal length optic to maintain a large visual angle for the display. Any optical component positioned beyond the scanning mechanism will affect both beam collimation and scan convergence, with success of one goal dictating failure in the other due to the parameters of the optical path lengths and scanning mechanism reflection angles. Thus, the beam must be focused just prior to the viewing optic, the focus must be a long distance from the scanning mechanism, the beam profile must be small at the scanning mechanism, and this must be accomplished with no high positive power optical elements between the scanning mechanism and the viewing optic. The production of a long and narrow waist, as illustrated in Figure 2.6, was a viable and practical solution to the problem.

2.1.2.2 VRD Emulator Driving Electronics

The VRD Emulator is driven and synchronized through a PC computer, but not using the video signal as does the original VRD. Electronic interfacing with VRDE components is accomplished with National Instrument™ I/O boards, while operator control, monitoring, and signal generation is accomplished with LabView™ software routines. Figure 2.7 is a color-coded illustration of the basic control logic of the VRDE.

The spinning mirrored polygon is used as the timing base for synchronizing all VRDE functions. An infrared emitter-detector assembly is positioned near the polygon so that IR reflections from polygon facets are detected as the facets rotate past. A pseudo-sinusoidal analog waveform is output from the emitter detector with each peak corresponding to a facet passing. This analog signal is conditioned into a TTL square wave of equivalent frequency, providing a clocking signal in which each cycle corresponds to the scanning of one horizontal line by the rotation of a single polygon facet through the laser beam's profile. This TTL clocking signal is routed to the I/O board in the computer that provides all waveform generation for the operation of the VRDE.

Through the LabView control interface on the computer, the VRDE operator defines a stair-stepped ramp voltage waveform to drive the mirrored galvanometer affecting the vertical scan. An array defining these voltage levels is loaded onto the I/O board buffer, and the stair-stepped waveform is clocked out to the galvanometer by the polygon's clocking signal. In this manner, the vertical and horizontal scan is synchronized, regardless of the polygon's rate of rotation. By defining ramp waveforms of variable lengths and variable magnitudes, the number of horizontal lines comprising one display frame may be manipulated, as may the vertical separation of the horizontal lines.

With LabView, the operator also defines an I/O buffered array of voltage values equating to modulation levels of each display line. By again accessing the polygon clock signal, these modulation values are sequenced to the AOM in synchrony with both the horizontal and vertical scanning pattern. In this way, individual lines may be modulated to discrete luminance levels, and the beam may be blanked entirely during the vertical retrace time of the mirrored galvanometer between frame presentations.

Also via the LabView control interface, the operator defines a steady TTL square wave signal that is interpreted by the polygon driver as a rotation speed. By varying the TTL signal

frequency, the operator varies the polygon's rotation rate. Since all other synchronization is based upon the polygon's rotation rate, the display may be easily operated with a broad range of scanning speeds and frame refresh rates.

2.1.2.3 VRD Emulator Stimuli and Display Limitations

The VRD Emulator can provide retinal stimulation via a small exit pupil (near 1 mm diameter) in a manner similar to the original VRD. However, some fundamental differences are evident. The mirrored polygon provides unidirectional horizontal scanning in a raster pattern more akin to that provided by a conventional CRT or LCD display. Further, the horizontal scan is constant temporally, in contrast to the sinusoidal oscillations of the VRD's MRS scanner. Avoiding fiber injection, the VRDE can provide much more energy to the retina than the original VRD. A range of approximately four decades of luminous energy are available with the VRDE.

The VRDE can provide a display comprised of any number of horizontal lines from one to more than 750. However, in practical use the number of lines displayed is limited to multiples of 75. This ensures that each horizontal display line is generated by the same polygon facet in each frame refresh. Because the polygon facets have very slight variation in alignment and the resulting reflection angles, allowing different facets to refresh a given display line will cause the line to be displayed in a slightly different position with each frame refresh. The unstable line may appear poorly resolved, or improperly focused. Thus, line number intervals of 75, 150, 225, 300... 750 are practical.

The vertical separation of display lines may be adjusted by defining the discrete voltage steps of the ramp waveform clocked out to the mirrored galvanometer. In most applications, a vertical separation is desirable that does not allow the perception of individual lines. With a Gaussian beam profile, typical of most laser beams, the energy delivered across a display comprised of multiple lines becomes almost constant near the Rayleigh limit. At the Rayleigh limit, the energy from adjacent overlapping Gaussian beams sums to produce a field of light energy that varies by only 10%. That is, the contrast between overlapping horizontal lines' peaks and troughs of luminance is only 10%, and this low level of contrast at high spatial frequencies is near the limit of human detection. The field appears contiguous to most observers when line spacing is at or near the Rayleigh limit.

In summary, the VRD Emulator can display small exit pupil visual stimuli comprised of multiple, contiguous, horizontal scan lines, with each line independently modulated in intensity, and with base display intensity variable over four decades. The number of display lines, line vertical spacing, and the speed of the scan are variable. At the upper limit of scanning speed, a display of 150 lines may be frame refreshed at frequencies exceeding 200 Hz. The upper limit of refresh rate is a function of the maximum polygon rotation rate and the number of lines displayed, with maximum refresh rate being reduced as more display lines are presented. With custom data arrays driving the mirrored galvanometer, the scan may be affected top to bottom, bottom to top, or interlaced in either direction.

Unfortunately, the VRD Emulator cannot display complex imagery. This ability is limited by two factors. First, the bandwidth of the AOM used in the VRDE is insufficient to modulate at pixel rates. Unlike the VRD's AOM's, the VRDE's modulator is designed to modulate up to four different wavelengths of laser energy simultaneously – a feature desired in the earlier, abandoned incarnation of the device. The cost of this capability is reduced response speed, even when modulating a single wavelength. Well synchronized, sub-line modulation was demonstrated during the development of the VRDE, but a faster modulator is required to make pixel modulation feasible. Second, because the VRDE allows variable line numbers and refresh rates, converting a standard video signal to any of the possible VRDE display formats becomes a daunting and impractical task. While buffered array values representing modulation levels for imagery could be synchronized with the polygon clock signal, the arrays necessary for even simple imagery would be vast, and a viable automated method for creating such arrays has not been developed. Further, each such array would have to be constructed for one specific display format, and the imagery would not be properly displayed if the display format was changed from the one intended.

However, most basic visual perceptual experiments planned for the VRDE do not require the presentation of complex imagery. In fact, almost all of the research requires the presentation of homogenous fields of retinal illumination presented with a small (1 mm) exit pupil scanning device -- exactly what the VRDE can best provide. The few planned studies that do need some type of imagery require only simple, static modulation of the display. This can be easily achieved by positioning an intervening acetate slide in the optical path, thereby modulating the beam just prior to the viewing optic as it scans across the slide. Therefore, the cost in time and effort of

engineering the VRDE to display more complex dynamic imagery far exceeded the expected benefit of doing so.

2.1.3 Arrayed Exit Pupil Emulator

A novel optical apparatus was constructed at HITL for the purpose of displaying multiple small exit pupils in various arrayed configurations. Several exit pupils could be simultaneously presented, and the size, geometrical arrangement, and image presented by the pupils could be varied by the experimenter. Figure 2.8 depicts the optical setup of the Arrayed Exit Pupil Emulator (AEPE) as used in a subsequently described experiment (see Chapter 7).

The purpose of the AEPE was to emulate the production of multiple exit pupils by a theoretical modified retinal scanning display system. A method was needed to converge multiple small exit pupils that would each present a clear image on the retina without the necessity for a modulated beam scanning system like that of the VRD. The following simple solution was designed and constructed by the author.

Planar light stops were augmented with apertures covered by translucent filtering material. The translucent acetate material served to scatter illumination passing through the apertures from lamps behind the apertures in the optical path. Rays from these translucent "windows" were folded with two first surface mirrors to create a long optical path in a relatively compact area. Ultimately, the windows were imaged by a minifying compound lens, effectively producing small converged exit pupils. The optical path distance and minifying lens were selected to produce a 12:1 minification ratio. Thus, changes in window size produced 1/12 size changes in exit pupil size. For example, a 12 mm diameter window produced a 1 mm diameter exit pupil. Further, a 12 mm separation distance between two windows produced a 1 mm separation between exit pupils.

The exit pupils were modulated for imaging with a 35mm photographic acetate slide positioned in the path immediately before the converging optic. With the tremendous depth of field provided by very small exit pupils, a clear image from the slide was effectively transmitted to the retina by the modulated light rays of the converging exit pupils. As exit pupil diameters approached 1 mm, mild image defocus was noticeable. With smaller exit pupils, near 0.5 mm diameter, a crisply focused image was perceived.

In some experimental setups, and as depicted in Figure 2.8, two exit pupils were presented in a manner that allowed observer manipulation of the pupil separation distance. The observer adjustments were facilitated by mobilizing one lamp-window combination on a sliding rail mechanism. The observer would grip a handle on the sliding rail and move the mobile lamp-window combination relative to the second, static lamp-window combination. By this method, the observer could manipulate the separation distance between two exit pupils being used for image observation. With the minifying effect of the converging optic, gross movement of the mobile lamp-window combination affected relatively small movement of the exit pupil. A pointer was affixed to the sliding rail adjacent to a fixed ruled scale to allow measurement of observer adjustments. This particular setup is discussed in more detail in the experiments described in Chapter 7. In other setups, arrays of 5 to 12 exit pupils were generated using fixed arrays of translucent windows and a single rear-illuminating lamp.

It is significant to note that exit pupils created in this manner do not produce images on the retina that are perfectly coincident. The spatial separation of any two retinal images is a function of the incident angle of the rays entering the converging optic. The disparity between retinal images with the AEPE system ranged from approximately 0.3 to 1.3 degrees visual angle. This topic and its relevance to display engineering is explored more fully in section 2.2, while the visual perceptual ramifications are explored in Chapter 7.

2.1.4 Pupillometer

A system was designed and constructed at HITL to record precision measurements of human eye pupil diameters. The pupillometer is comprised of a video camera, a PC computer augmented with a video capture card, and custom software to analyze captured video frames. The system has been demonstrated to provide accurate pupil diameter measurements at up to 18 Hz.

The system's camera is a Sony Hi-8 video format with close focusing macro lens and with an optional infrared photo-detection array plus infrared illuminator. The IR detection array and IR illuminator are particularly effective for pupil measurements since measurements may be made under conditions of very low ambient illumination, and the IR light does not significantly affect pupil response. Additionally, the eye's iris is typically a highly IR reflective surface, while the aperture of the pupil reflects very little. Excellent contrast between pupil and iris results, facilitating easy image analysis.

The system's computer is a PC type with Intel Pentium™ processor operating at 1.3 GHz. The video capture board is a Winnov Videum™ VO (PCI) board with capture resolution up to 640 x 480 pixels. The custom software was written in C language by HITL graduate student Richard May.

In a typical application, the camera is positioned along with mirrors or beam splitters to image the eye as close as possible without disrupting the image being viewed by a human subject. The subject is stabilized so that the eye's position does not vary significantly. The video image is collected at a small angle horizontally to the normal of the pupil's plane, providing an oval pupil profile. The standard NTSC video signal is routed to the computer capture card for digital sampling. After a video frame is digitally captured, the software application analyzes it to determine pupil diameter, and the diameter data is appended to an electronic file. Figure 2.9 depicts a typical IR pupil image being analyzed by the pupillometer and its associated data file output, as described below.

For each captured video frame, the software evaluates pixel luminance levels in order to determine the edges of the pupil in the image. A digitized video segment depicting a close-up image of the eye is presented in which the eye is well fixated to minimize movement of the pupil to be measured. The operator uses keyboard commands to position a yellow cursor within the image of the pupil. This position serves as a starting point for the software's search algorithm. The search routine notes the luminance level of the starting position, and it calculates a new search value based upon the starting luminance and an operator-defined additive factor. This new search value, or threshold luminance, is representative of the typical increased luminance level of the iris that forms the edge of the pupil. The routine then sequentially examines pixels beginning at the starting position in the image, moving horizontally (both left and right) until the selected pixels' luminances are equal to or greater than the threshold luminance. Two positions along opposite edges of the oval pupil image are thereby identified, and the linear pixel count separating these two image positions is calculated. The routine then calculates the midpoint of the line connecting the two edge points. This midpoint position lies on the vertical axis of the oval pupil image, regardless of the vertical position of the starting cursor.

A new pixel luminance threshold search begins from this midpoint position, sampling pixels sequentially in the vertical dimension (both up and down from the midpoint). When the threshold pixel luminance value is found along the vertical axis, opposing positions on the top and bottom of the oval pupil are identified. Given a small horizontal offset angle for the pupil

image, these top and bottom pixel positions represent two points diametrically opposed on the pupil, and the distance between them is the true pupil diameter. The routine calculates the linear pixel count between the two edge points and writes this pixel count value to the data file. Based upon an operator-defined calibration value of pixels per millimeter, the algorithm also calculates the pupil diameter in millimeters and writes this value in an adjacent position in the data file. Each such datum is also correlated with an absolute time in milliseconds (from the start of data collection) written to the data file.

An initialization file contains the operator defined values for threshold luminance additive factor and for the pixels per millimeter calibration value. The threshold luminance additive factor may be adjusted with keyboard actions during the system setup prior to actual data collection. The real-time pupil image is presented on the computer monitor, and crossing white lines over the pupil depict the real-time calculation of horizontal and vertical axes, as described above. The operator may adjust the threshold luminance value while examining the diameter lines to ensure precise detection of the actual pupil's edge. The calibration value of pixels per millimeter is determined by using the system to briefly datalog measurements of apertures of known diameter placed at the pupil's measurement position. The pixel count data in these measures are divided by the known aperture diameter to obtain a precise pixel per millimeter calibration value that is subsequently entered into the initialization file.

The resolution of this system is dependent upon the magnification achieved in the image of the eye and pupil. An extremely close image of the pupil will allow a large pixel per millimeter calibration value, while a more distant image will provide fewer image pixels per millimeter of pupil diameter. Most applications allow a calibration value of approximately 20 pixels per millimeter, equating to a resolution of 0.05 mm. Additionally, because this system relies upon pixel luminance values in determining pupil diameter, minor movements of the eye that cause slight pixel value changes will also have a small effect on the threshold determination. These minor pixel value changes are caused by the camera detector array's Nyquist sampling limits as the image of the eye's iris edge moves across the detector array. Tests and evaluation of the system show that this variability is not more than 3 pixels in the diameter count, equating to approximately 0.15 mm maximum error in measurements.

2.2 Literature Review

The human visual system is an enormously complex system. An expansive body of research has been compiled over centuries in attempts to uncover the multiplicity of visual system characteristics. In evaluating a new method of stimulating the retina to provide information display, an examination of relevant discoveries in visual perceptual research will assist in formulating new experimental designs and provide clues for the formulation of hypotheses. Most importantly to the engineering community, more effective display designs may result from detailed consideration of the functioning of the human visual system. The coupling of RSD systems with the human visual system is of primary importance here, and a review of previous efforts in that area is also prudent.

2.2.1 Human Visual System Function

The human visual system transduces light energy entering the eye into electrochemical patterns within neural circuitry, ultimately resulting in visual perception in the mind of the observer. This transduction process begins at the cornea and ends with the stimulation of neurons in the brain. A general overview of this process, from cornea to cortex, is followed by more detailed reviews of literature topics pertinent to new research. The reader interested in more detailed discussion of the process of human vision is referred to Rodieck (1998), Wandell (1995), and Le Grand (1968) [16-18].

2.2.1.1 Cornea to Cortex

Figure 2.10 is an illustration of a cross section of a typical human eye. The cornea and lens are transparent optical elements that refract light to affect focusing of an image onto the retina. Most of the refractive power of the eye's optics is due to the cornea: the protuberance that covers the colored iris and the pupil, and contains a clear fluid called aqueous humor. The lens is a conformable, complex optical element composed of multiple layers of varying refractive power. The layers are arranged much like the layers of an onion, and the shape of the lens is changed by the actuation of small muscles called the ciliary muscles. This shape-shifting varies the refractive

power of the lens and is the mechanism of accommodation. The iris is positioned between the cornea and lens, and its variable aperture forms the pupil of the eye.

The white outer shell of the eye, the sclera, is a tough, fibrous tissue. Just inside the sclera is a rich network of blood vessels and other tissue termed the choroid. The choroid provides the eye and retina an ample supply of oxygenated blood. Within this covering, and filling the bulk of the eye, is a clear fluid called the vitreous humor that helps maintain positive pressure within the ball of the eye.

The retina is a thin layer of neural cells coating the back of the eye inside the choroid. The retina is composed of many different cell types interconnected in a complex neural network, and its primary function is to accomplish the transduction of light energy into electrochemical neural signals. The initiation of the visual experience occurs when light passes through the cornea, pupil, lens, and humors to create a focused image on the retina.

The phototransductive cells of the retina are the rod and cone cells, named for their anatomical appearance. Wavelength sensitive cone cells are packed densely in the fovea, the central region of vision with the greatest resolving capacity, and they are much less densely distributed throughout the remaining parts of the retina. Wavelength univariant rod cells are absent in the fovea, but substantially more populous than cones in the extrafoveal retina. Cones facilitate color vision in high luminance conditions, while rods are the low-luminance “night vision” detectors, unable to encode wavelength information necessary for color perception.

Each type of photoreceptive cell contains photopigment molecules that may absorb light quanta and, as a result, change their molecular geometry. When quanta are absorbed and photopigment molecules change geometry, a cascade of chemical events is triggered within the cell that leads to changes in the cell’s “firing” rate, or rate of sending electrochemical impulses. These firing rate changes encode information about the number of light quanta absorbed by the photoreceptive cell.

Also within the retinal network are ganglion cells that receive and integrate photoreceptor cell signals, and the ganglion’s firing response may be a function of the signals received from numerous photoreceptors. The ganglion cells’ axons are long neural fibers that bundle to form the optic nerve. The optic nerve departs the posterior eye and is the conduit of visual signals to the brain. The ganglions’ firing responses are channeled down their axons within the optic nerve and delivered directly to a node on the brain’s thalamus called the lateral geniculate nucleus (LGN). The LGN is essentially a relay station for visual neural signals. Little processing of

information takes place here. Rather, the retinal signals are reorganized and forwarded to cortex for processing. Figure 2.11 depicts the pathways of neural signals from the retina, to LGN, to primary visual cortex in the posterior brain.

Primary visual cortex (V1) is well structured as a retinotopic map. That is, neurons in V1 respond to stimulation from retinal cells in a manner that is organized topographically with the retinal view of the world. Adjacent cells in the retina, responsible for receiving quanta from adjacent portions of the visual field, stimulate adjacent areas in V1 cortex. Thus, a kind of map of the visual field as seen by the retina is represented in the organization of V1 cortex. Neural activations spread outward from V1 to higher processing cortical areas in the brain that are arranged concentrically about V1. Ultimately, large regions of the occipital lobe, temporal lobe, parietal lobe, and even the frontal lobe of the brain are activated in the processing, interpretation, and conscious experiencing of visual information transduced by the retina.

2.2.1.2 Brightness (Luminosity) Perception and Measurement

Brightness, or luminosity, of a visual stimulus is defined as the attribute according to which the stimulus appears to be more or less intense, or according to which the stimulus seems to emit more or less light [19]. Brightness is purely a perceptual phenomenon, existing only in the mind of the observer. While brightness perception is related to physical measures of light energy, such as luminance (luminous flux density per solid angle), substantial differences in brightness perception result from equiluminous stimuli under differing environmental conditions, with differing individual observers, and with variable temporal and spatial characteristics of the stimulus. Absolute judgments of brightness are imprecise, typically relying upon verbal descriptions, such as “dazzling,” “brilliant,” “bright,” “dim,” and “dark.” Such descriptions are of little use in the effort to quantify the perception of a visual display. In most examinations of brightness effects, a direct comparison of test stimuli with control stimuli is the most effective manner in which to quantify brightness.

Stanley Stevens developed a brightness model called the Steven's Power Law [20, 21]. This model relates brightness perception to stimuli luminances through an interval scale of measure for brightness. Steven's experimental methods generate power functions with parameters determined by specific experimental conditions. Subsequent studies by Bodmann, Haubner, and Marsden expanded Steven's work and promoted a brightness power law of the form

$$B = aL^p - B_0 \quad (\text{eq. 2.1})$$

in which B denotes the estimate of brightness by an observer of a stimulus of luminance L under specific observation conditions [22]. For visual perception, the exponent p has a value of approximately 0.31, while the values of a and B_0 depend upon conditions such as the size of the stimulus and the luminance of its surrounding field. Brightness is plotted on an interval scale and derived by a bisection method of presentation. In this method, subjects are presented two control stimuli of differing luminance and a third independently variable stimulus. The subject adjusts the luminance of the variable stimulus until it is judged to be half way between the two control stimuli in brightness. The luminance of the variable stimulus is recorded and, after repeated trials across a range of control luminances, a power law relationship between luminance and brightness is revealed [20]. In this manner, subjective comparisons of stimuli are used to establish interval scale relationships between the physical parameter luminance and the perceptual phenomenon brightness.

More common are comparisons using only one test stimulus and one control stimulus in which the observer must match the brightness of the stimuli by adjusting the intensity of the test stimulus. The psychophysical *method of adjustment* is used to identify relatively large effects of a test stimulus with good efficiency, requiring small numbers of trials as compared to other, more elaborate, methods [23]. In addition to the obvious direct (side by side) comparison of stimuli, three photometric methods of brightness matching have been widely employed with the method of adjustment that offer improved consistency of results over the direct comparison method: 1) minimally distinct border judgments, 2) heterochromatic flicker photometry, and 3) motion photometry [23].

Minimally distinct border judgments (MDB) are made with visual fields of the test stimuli and control stimuli immediately adjacent to one another. By careful optical design, two stimuli are presented in a precisely juxtaposed bipartite field. When the two stimuli are nearly identical in brightness, the border between the two hemifields appears to blur, or become less distinct than when brightness differences remained. The observer adjusts the luminance of the test field until the border is minimally distinct, thereby making a brightness match with the control field [24, 25]. This method provides consistent results comparable to flicker photometry methods.

Heterochromatic flicker photometry (HFP), or simply flicker photometry, presents the two stimuli with identical geometry and identically positioned in visual space, but in rapid

alternation. By adjusting the luminance of the test stimuli, a condition is achieved in which the perception of flicker of the alternating fields is reduced to a minimum. At the minimum flicker value of the test stimulus luminance, a brightness match with the control stimulus is achieved. Typically, test and control presentations are alternated at 10 to 40 Hz, depending upon specific stimuli conditions. In practice, this method is easy to apply, and it yields consistent results whether or not the two fields are closely matched in chromaticity [26].

Motion photometry presents the two stimuli as a grating, or set of stripes. The grating is set into motion across a display, and the observer adjusts the luminance of the alternate test stripes. The perception of motion is minimized when the two stimuli are closely matched in brightness. This method provides advantages and results very similar to the HFP method [23]. Obviously, this method is primarily used with dynamic video display devices in which the creation of such complex stimuli is feasible.

Using these methods and others, vision researchers have tapped into human perception to derive functions describing human visual sensitivity. Notable examples are functions describing human sensitivity to luminance across the visible spectrum of wavelengths. The *scotopic* and *photopic* sensitivity curves describe luminous spectral sensitivity of the rod photoreceptor system and cone photoreceptor system, respectively. The curves are called the *luminous efficiency functions*, describing the efficiency with which our visual system detects various wavelengths.

Figure 2.12 depicts estimates of the scotopic and photopic luminous efficiency functions. To illustrate the practical relevance of these functions, consider the example of two dim emitters on a dark night where night vision is operative. Each emitter is equivalent in size, viewing distance, directionality, and radiant power emitted. However, one emitter is monochromatic at 500 nm, and the second is monochromatic at 650 nm. In accordance with the scotopic luminous efficiency function (V'_λ) the 500 nm light will be transduced by the retina much more efficiently than will the 650 nm source. Thus, even though the radiant power reaching the retina from each emitter is equivalent, the 500 nm emitter will be perceived significantly brighter than the 650 nm emitter. A similar example may easily be derived from the photopic luminous efficiency function (V_λ) for higher luminance conditions in which cone photoreceptors are functional. Under photopic luminance conditions, peak sensitivity is centered approximately on the 555 nm wavelength. The spectral range of human luminous sensitivity is approximately 400 to 700 nm.

The luminous efficiency functions were derived through psychophysical techniques, relying upon the perception and reporting of human observers. However, the physiological

source of variable spectral sensitivity to luminance is found within the photoreceptors themselves, at the center of the phototransduction process. Scotopic and photopic luminous efficiency is directly attributable to the probability that a photon will be absorbed by the photopigment within a photoreceptive cell. Different photopigments in each of the four different types of photoreceptors (one rod type and three cone types) have different absorption spectra. Quanta of varied wavelengths have varied probabilities of absorption. The absorption probability distributions associated with each photopigment are well matched to the luminous efficiency functions. Further, the response of the photoreceptor has been shown to be univariant to wavelength [27]. That is, once a photon of light has been absorbed by a cell's photopigment, the effect on and by the cell is the same, regardless of the wavelength of the photon or the probability of the absorption occurring.

Wald and Brown (1956) conducted an *in vitro* quantification of the absorption of quanta by *rhodopsin*, the photopigment present in rod photoreceptors [28]. A normalized curve of absorption rate as a function of wavelength was compared with the normalized scotopic luminous efficiency function. After corrections to the rhodopsin absorption function for the absorptive effects of the cornea, lens, and humors, the two functions were identical. Although further confirmation is required, this result suggests that the mechanism of spectral luminous sensitivity is the photochemical properties of the photopigments themselves, and that no additional physiological factors are involved.

Baylor, Nunn, and Schnapf (1987) used an ingenious micropipette apparatus to collect an expansive set of measurements of photocurrents generated by individual *in vitro* cone photoreceptors in response to spectral stimuli [29]. Their measurements spanned the entire visible spectrum of wavelengths and six logarithmic units of intensity, representing a remarkable measurement achievement. As expected, they found three different response functions for each of the three cone types. In spite of a static non-linearity in the photocurrent response of individual photoreceptors to the linear absorption of quanta by the photopigments, a comparison of peak photocurrent response levels between stimuli of different wavelengths satisfies the homogeneity requirements of linear systems analysis with the establishment of a constant ratio among the responses to variable wavelength stimuli. This allows the derivation of the complete spectral responsivity function of a photoreceptor. Assuming that the wavelengths sensitivity is due entirely to the cone photopigment, as in rods, then these functions represent the absorption functions of the cone photopigments [17].

In order for Baylor's derived functions to match human perception of wavelength information in the photopic realm, as Wald and Brown's data had matched scotopic perception, the functions must map linearly onto functions describing human color perception as well as brightness perception. Color perception has been characterized with a set of *color matching functions* that are somewhat arbitrary, but convenient for many engineering endeavors. The Commission Internationale d'Eclairage (CIE; an international standards organization) met in 1931 to establish a standard method of specifying color perception in order to facilitate communications among the scientific community. They developed the *XYZ tristimulus coordinate system*, using three functions extrapolated from the averaged results of perceptual color matching experiments as axes for a numerical system of color and brightness definition [30]. In 1987, Baylor and his colleagues made a comparison of their derived cone photopigment absorption functions with the CIE color matching functions and found a linear transformation relating the two sets of functions [29]. This discovery strongly bolsters the argument that photopigments inherently contain the mechanisms that produce variable wavelength sensitivity in the human visual system. Subsequently, a variety of physiological and psychophysical techniques have yielded results in strong agreement with Baylor's original estimates of cone photopigment absorption spectra [23].

In the brightness realm, Boynton (1979) derived a linear model of the photopic luminous efficiency function (V_λ) from early estimates of the response functions of two of the three cones types [31]. The cones are classified in coarse accordance to the region of the visible spectrum to which they respond. The *long wavelength receptors* (L-cones) and the *middle wavelength receptors* (M-cones) overlap substantially along the spectrum, only slightly deviating in their response to various wavelengths. The *short wavelength receptors* (S-cones) are significantly more differentiated from either the L-cones or M-cones. Figure 2.13 depicts the approximate sensitivities of the three cone types by wavelength. Boynton's model of V_λ has been refined with better estimates of cone response, but it remains a simple weighted sum of the L and M cone responses:

$$V_\lambda = 0.699 L(\lambda) + 0.366 M(\lambda) \quad (\text{eq. 2.2}) [16]$$

Thus, brightness perception under both photopic and scotopic luminance conditions is directly and completely attributable to the response of the photoreceptors, and specifically to the probabilities that photoreceptor pigments will absorb quanta of light. While additional encoding by subsequent stages of visual processing certainly occurs, it seems clear that the perception of

brightness is wholly dependent upon the response of the retinal photoreceptors. For any given set of conditions, equivalent retinal response to stimuli will result in equivalent brightness perception and, under identical conditions, equivalent brightness perception necessitates equivalent retinal response.

However, additional considerations remain concerning the excitation of the photoreceptors themselves. Of particular interest are additional physical properties of light stimuli that may affect the probability of absorption. Photopigment molecules are sensitive to the polarization of light. Specifically, for absorption to take place the axis of the electric vector of the incident radiation must closely parallel the long axis of the pigment molecule. However, the arrangement of photopigment molecular axes is random in the undisturbed photoreceptor, and in vivo absorption rates are identical for polarized or unpolarized light [26].

Light energy may also be coherent to varying degrees, whereby wave packets are emitted from a source (typically a laser) with the oscillations of all electric vectors in phase temporally, spatially, or both [32]. While scattered coherent light results in positive and negative wave summations perceived as *speckle*, no effect of coherence on the probability of absorption by photopigments has been reported in literature. Thus, except for macroscopic effects of speckle, no unique brightness perceptual effects are expected from coherent stimuli as compared to non-coherent stimuli.

Anatomical considerations of the photoreceptors are also pertinent to the perception of brightness. The geometry of photoreceptor cells has an effect on the efficiency with which light is absorbed. The discussion here is limited to cone photoreceptors and the photopic luminance condition.

Photoreceptor cells are long, narrow structures, as depicted in Figure 2.14. The cell's inner segment is oriented toward the entrance pupil of the eye, while the outer segment is positioned to the posterior of the retina. The inner segment receives incident light from the pupil and guides it to the outer segment where photopigment molecules are contained. Because of their linear geometry and cross sectional diameter on the order of the wavelength of incident visible radiation, the photoreceptors act as dielectric wave guides to optical radiation [32, 33]. The two segments of the cell act as two optical waveguide segments, and only the light that is successfully guided down the inner segment and the outer segment is available for absorption by the photopigment molecules [34, 35]. The light available to the outer segment is a function of both

geometric optical considerations of waveguides and electromagnetic propagation mode considerations.

The acceptance angle for light entering a waveguide is a function of the indices of refraction of the waveguide material and the surrounding material. These indices determine the critical angle for total internal reflection of light within the waveguide. For incidence angles greater than the critical angle, all light will be internally reflected down the waveguide. For incidence angles less than the critical angle, only partial internal reflection will occur at each reflective encounter with the interface region forming the "walls" of the waveguide, and greater incidence angles generally dictate greater numbers of internal reflections. Thus, light is transmitted down the waveguide with greater efficiency as incidence angles exceed the critical angle [32].

Further, the variety of radiation modes excited by a waveguide increases with greater acceptance angles, even when the incidence angles are less than the critical angle. The total power available in a wavefront encountering the waveguide is divided among the various propagation modes after encountering the aperture of the waveguide, and only a subset of possible modes remain bound to a waveguide, depending upon the waveguide's optical and electromagnetic properties. The unbound modes radiate into the surrounding media and are not transmitted down the waveguide. Thus, the power coupled into the bound modes tends to decrease with increasing acceptance angles [36]. Combined with the geometric considerations of critical angle above, these electromagnetic mode considerations define a directional sensitivity of photoreceptive cells.

Photoreceptor cells are well aligned within the retina so that the longitudinal axis of the cell points toward the center of the exit pupil of the cornea-lens optical system [37]. That is, the cells are well aligned with the optical path traversed by light rays entering the center of the eye's entrance pupil. As a result, for any given photoreceptor, light rays passing through the center of the eye's pupil have incident angles approximately normal to the entrance aperture of the photoreceptor cell's inner segment. Light rays entering the pupil peripherally are refracted such that the incident angle to the inner segment aperture may exceed 10 degrees from normal. The efficiency with which rays are guided to the photopigment molecules is dictated by waveguide theory. Thus, light rays passing through the central portion of the eye's pupil have a greater chance of absorption by photopigments than peripheral rays because the incidence angle to the photoreceptor waveguide is small and propagation down the waveguide is most efficient. It

follows that phototransduction is most efficient for these centrally passing rays, and less efficient for rays passing through the pupil's periphery.

The macroscopic effect of this phenomenon is termed the Stiles-Crawford effect of the first kind (SC-1), after the discoverers [38]. Given the considerations of the Stiles-Crawford effect, it is obvious that, with the exception of narrow beamed stimuli, the efficiency with which stimuli are transduced is a function of pupil size. As the pupil expands in area, rays of greater peripheral distance pass through the optics of the eye, have greater incidence angles to the photoreceptors, and are less efficiently transduced. Rays passing through the extreme periphery of the natural pupil have as little as 20% the luminous efficiency of those passing through the central pupil [38]. Stacey and Pask in 1994, and Pask and Stacey in 1998, modeled the photoreceptors as two segmented waveguides using a basic photoreceptor model first proposed by Snyder and Pask (1973) [33-35]. Their waveguide models accurately predicted the SC-1 effect, the SC-2 effect describing how the SC-1 effect changes with wavelength, and other visual system effects related to acuity.

Jacobs (1944) first summarized the integrated SC-1 effect as a function of pupil radius based upon data collected by Moon and Spencer (1944) [39, 40]. Jacobs calculated the *effective flux* through a pupil, F_e :

$$F_e = \pi D r^2 - 0.0425 \pi D r^4 + 0.00067 \pi D r^6 \quad (\text{eq. 2.3}) [39]$$

where D is the luminous flux density at the pupil and r is the radius of the pupil. This equation is frequently transformed into an *effectivity ratio* formula as:

$$E = 1 - 0.0106 d^2 + 0.0000419 d^4 \quad (\text{eq. 2.3a}) [19]$$

where E is the effectivity ratio and d is the diameter of the pupil. In this way, the effectivity ratio may be simply applied to luminance measurements as a multiplicative factor [19].

For narrow beam stimuli entering the pupil, the perception of brightness is a function of the entry position within the pupil, consistent with SC-1 functions. Beam stimuli entering through the central portion of the pupil will be most efficiently transduced and will appear brighter than similar stimuli passing through the pupil's periphery. This geometry is particularly pertinent to retinal scanning displays.

In summary, brightness perception is best quantified by direct comparative methods due to the adaptive psychophysical characteristics of the human visual system and due to the extreme sensitivity of the visual system to variable brightness stimuli conditions. The initial physiological mechanism of brightness perception is based in the retina: for any given set of conditions,

equivalent retinal response will result in equivalent brightness perception, and equivalent brightness perception indicates equivalent retinal response. With the exception of wavelength and power, the physical characteristics of light energy have no significant effect on phototransduction and brightness perception. The efficiency of phototransduction is a function of entrance pupil position and the resulting ray projection geometry according to the waveguide properties of the photoreceptors described by the Stiles-Crawford effect of the first kind.

2.2.1.3 Flicker Perception

The physiological mechanisms of human visual system temporal response are less well understood than those relating to brightness and chromaticity. Detailed models of the physiological mechanisms leading to temporal perception have lacked consistency and completeness. However, the effect of visual stimuli characteristics on temporal perception, especially flicker perception, is well catalogued by an expansive body of literature. Discussions here will be limited to those factors directly relevant to the evaluation of flicker perception in retinal scanning displays and to establishing the role of retinal response in flicker perception.

Human sensitivity to flicker is a function of luminance level and temporal modulation rate [41]. Data collected by Kelly (1961) in terms of contrast sensitivity revealed increased sensitivity to flicker with increased luminance. Sensitivity peaks between approximately 5 Hz and 20 Hz depending upon luminance level, with the peak frequency increasing with increased luminance [41]. Figure 2.15 depicts Kelly's findings.

The visual systems seems to operate as a low-pass system, as sensitivity to flicker falls dramatically with higher temporal frequencies. An examination of Kelly's flicker sensitivity plots as a function of temporal frequency across six logarithmic units of luminance clearly indicates a common asymptote of all curves at high frequencies. This asymptote is the high-frequency limit of sensitivity to temporal modulation across the entire photopic response range. As temporal frequencies pass the asymptotic value for a given luminance level, *flicker fusion* is achieved. Flicker fusion is the perception of a temporally modulated stimulus as a constant source, and the temporal frequency at which this occurs is the *critical flicker frequency* (CFF) [26]. For most visual displays, frame refresh rates are desired to be greater than the CFF to avoid the perception of flicker.

Flicker perception is also a function of spatial frequency, or the size of the stimuli. At the higher temporal frequencies near the CFF, sensitivity is greatest at low spatial frequencies, or with large stimuli [42]. The relationship between CFF and stimulus size was first explored by Granit and Harper in 1930 [43]. The Granit-Harper Law relates CFF to stimulus size for circular targets as a logarithmic-linear function, with CFF increasing with increased target size. This characteristic is typified by the mild perception of flicker that some people observe in large, bright CRT computer monitors, particularly when the CRT is refreshed at 60 Hz. A small target displayed on the monitor may not appear to flicker, but flicker may be perceived when the full CRT display is luminous.

Interestingly, the temporal waveform function of the flickering stimulus has very little effect on sensitivity at temporal frequencies above 10 Hz [44]. In his 1958 publication, de Lange detailed the sensitivity to flickering stimuli of multiple temporal waveforms, including sine wave, square wave, sawtooth, and other more complex waveforms. Each waveform produced identical sensitivity functions across three logarithmic units of luminance in the photopic range [45]. Subsequent studies have revealed that the critical temporal factor for flicker perception is the fundamental frequency of the Fourier transformation [46]. This characteristic is based in the fact that the visual system acts as a low-pass filter to temporally modulated stimuli. Thus, the higher frequency components in a Fourier analyzed stimulus have reduced effects on the perception of flicker.

Other factors influence flicker perception. Boff and Lincoln (1988) provide a summary of these [44]. Generally, flickering stimuli are less detectable as background luminance levels increase. Flicker sensitivity is greater in the foveal region of central vision than in the peripheral visual region. The shape or type of visual target can have a small effect on flicker sensitivity, and sensitivity at low temporal frequencies can be increased with visual targets having a surrounding field of luminance near the mean flicker luminance level.

The limiting physiological factors in flicker perception seem to reside primarily at the level of the retina. The temporal retinal response, as recorded by electroretinogram, is modeled as a low pass system roughly consistent with perceptual results. Electroretinograms record the complex combined electrophysiological response of retinal cells from a detector positioned on the surface of the cornea or sclera. Because the recorded response is a macroscopic one, and because more than one cell type may contribute to the recording, electroretinograms are difficult to analyze and interpret precisely (Dr. John Kelly, 2000, personal communication). However, Dodt

(1952) used very intense stimuli (and the resulting strong retinal response) to show by electroretinogram that retinal response followed flickering stimuli up to the CFF for the photopic case [47]. More recently, Wu, Burns, and Elsner (1995) and Burns and Elsner (1996) made electroretinogram recordings with more complex temporally modulated stimuli comprised of summed sine wave forms [48, 49]. They concluded that, at high temporal frequencies, most (but not all) of the attenuation in flicker response is occurring within the initial stages of the retinal processing [49]. They also noted a roughly linear relation between stimulus modulation and retinal response. However, perceptual data indicate a more rapid attenuation of flicker sensitivity with increasing temporal frequency than these electroretinogram data depict. Thus, although the retina may preserve and encode some of the high temporal frequency components of flickering stimuli, subsequent visual processing beyond the retina apparently imposes more restrictive low-pass filtering on the signals.

Given these assumptions, it is reasonable to conclude that equivalent retinal response to flicker will induce equivalent flicker perception. However, if subsequent visual processing plays a role in filtering the retinal response, equivalent flicker perception is not sufficient to assume equivalent retinal response.

Additional temporal perceptual research relates the perception of brief flashes of light to recurring flashes, like that of a refreshed display, and to the perception of brightness. Bloch's law describes the appearance of very brief light sources (much less than 1 second) as a function of luminance (L) and duration (t). The relative brightness of a brief source is dependent upon the product, Lt , and this law holds exactly at all luminance levels [18]. However, in comparison to steady stimuli, brief stimuli are perceived as brighter. Broca and Sulzer (1902) compared brightness perception of brief sources to continuous sources in matching experiments. Their results indicate that for brief source duration of less than one second, the luminosity of the brief source is substantially greater than that of the continuous source [50]. This effect diminishes to equality with flash durations greater than one second, and this effect applies to singular brief events, but not to recurring flashes.

Baumgardt and Segal (1946) examined the effect of two successive brief flashes on the same region of the retina. They found that the luminosity effects of the flashes were additive for intervals between flashes of 0.02 seconds or less, but at longer intervals an inhibitory action lowered the luminosity of the combination [51]. Interestingly, the normal refresh rate of visual

displays (60 Hz), necessary to avoid flicker perception in most observers, produces successive brief stimuli on any given portion of the retina with intervals of approximately 0.016 seconds.

It has long been observed that a very brief flash of light is perceived for a relatively long period, and that the period of persistence is approximately constant for brief pulses regardless of the physical duration of the pulse. This *psychological persistence* was first quantified in 1740 by Seguer who measured the length of the visible arc from a circularly whirled glowing ember and derived the perceived persistence time [52]. More modern investigations of this phenomenon find persistence times of 0.15 to 0.18 seconds, varying slightly with luminance [18].

Investigating the implications of this persistence, Talbot and Plateau (1834) independently evaluated the luminosity of regular successions of brief light sources, or flickering sources. Each made luminosity comparisons of flickering sources with constant sources. From their data they derived a law relating the luminance (L) of a fused flickering source (flicker frequency above CFF) to that of a continuous luminous source (L_m) at brightness match:

$$L_m = \frac{1}{t} \int_0^t L dt \quad (\text{eq. 2.4}) [53]$$

Thus, for equivalent brightness perception, the time averaged luminances of the flickering and continuous sources are equivalent. Exceptions to this law occur only for observation periods less than about two seconds, where the previously described Broca-Sulzer effect causes apparent enhancements in observations [54]. Gilmer (1937) tested this law extensively and found it to hold precisely across a broad spectrum of temporal frequencies and with flash durations down to 8×10^{-9} seconds [55].

In summary, flicker perception is a complex phenomenon dependent upon multiple stimulus variables. Its perception is interrelated with the perception of brightness and spatial frequency. A common asymptote across luminance levels defines the critical flicker frequency, the temporal frequency above which flickering sources are fused, or perceived as constant. Only the fundamental frequency in a temporal waveform has significant effect on the perception of flicker and the determination of CFF. The luminosity, or brightness of a fused flickering source is matched to a constant source when the time averaged luminances of the two sources are equivalent. This Talbot-Plateau law strictly holds for recurrent flash durations at least down to the order of nanoseconds. The physiology of flicker perception is not well known, although much of the low-pass temporal filtering effect of the visual system seems to reside within retinal response mechanisms.

2.2.1.4 Spatial Perception and Spatiotemporal Considerations

The spatial response characteristics of the human visual system are well defined and modeled. The human contrast sensitivity function (CSF) describes the visual system's ability to detect spatial frequencies as a function of contrast. Campbell and Robson (1968) measured the CSF as depicted in Figure 2.16 [56]. Human sensitivity to spatial frequencies, as measured with sine wave gratings, peaks near 5 cycles per degree visual angle and is limited to approximately 60 cycles per degree visual angle (one cycle per arcminute) for an emmetropic (normal, idealized) eye.

The high frequency cut-off characteristic of human visual perception is dictated by two factors that have apparently co-evolved within the biology of the human visual system. First, the array of photoreceptor is most densely packed within the central, foveal region of the retina. Densities of approximately 150,000 cells per square millimeter are typical [16]. This dense spacing equates to approximately one receptor cell diameter per 0.5 arcminute of visual angle in the emmetropic eye, or two photoreceptors per arcminute [23]. Modeling the cells as discrete sampling elements and with due consideration for the Nyquist sampling limit, the photoreceptor array density facilitates a maximum spatial resolving capacity of one cycle per degree. This agrees well with the perceptual limit stated above.

Interestingly, the diffraction limited imaging capacity of the eye's optics allows a minimum retinal "point" image size equating to approximately 0.5 arcminute, matching the diameter of a single photoreceptor cell within the fovea [23]. This optical limitation prohibits the imaging on the retina of spatial frequencies greater than 60 cycles per degree. Higher frequencies would exceed the Nyquist limit, inducing aliasing and the perception of aliasing patterns in the visual field. (This perceptual phenomenon has been demonstrated through the use of dual coherent beam interference techniques to generate sub-Nyquist limit gratings on the retina [23].) The cut-off spatial frequency dictated by the eye's optical transfer function is a function of pupil size due to diffraction effects of the limiting aperture and due to optical aberrations in the cornea, lens, and humors of the eye. For (artificial) pupil sizes up to two millimeters in diameter, the cut-off frequencies are identical to those calculated for a diffraction limited optical system. For pupil sizes greater than approximately 2 mm, optical aberrations limit the cut-off frequency to values lower than the diffraction limited case [57]. Table 2.1 below summarizes incremental estimates of the cut-off frequency for pupil diameters with 555 nm wavelength light and a focal length of

21.6 mm for the human eye. Approximations of visual acuity associated with each cut-off frequency have been added to indicate the image resolving limitation of an RSD system utilizing each pupil size.

Table 2.1: Spatial Cut-off Frequency for 555 nm light [57]

Pupil Diameter (mm)	Cut-off spatial frequency cycles / degree	Equivalent Visual Acuity
0.5	15.6	20/77
1.0	31.3	20/38
1.5	48.0	20/25
2.0	62.6	20/20 (or better)

For pupil sizes greater than 2 mm, optical performance remains relatively constant with the 2 mm case, but it is less than the optimum diffraction limited case for those pupil diameters.

The cut-off frequency values of Table 2.1 are based upon sinusoidal spatial grating frequencies and the Rayleigh limit criteria for distinguishing two sources. An individual grating "line" imaged on the retina will be blurred or "spread" by the optical imperfection of the imaging system, thereby reducing image contrast. Thus, even though the grating lines are distinguishable by slight contrast differences, substantial overlap of the optically spread lines occurs at the quoted table frequencies.

The spread of a theoretical line imaged on the retina for various pupil sizes was estimated by Campbell and Gubisch (1966). According to their estimates, an artificial pupil size of 1 mm will result in a 555 nm line spread (to the relative intensity value $1/e^2$) of approximately 4.6 arcminutes visual angle [58]. In the central fovea, this line width would spread across approximately nine cone photoreceptor diameters. This estimate is in agreement with Rodieck's estimates of photoreceptor coverage due to the imaging of a single star, the closest natural phenomenon to a mathematical point source of illumination [16]. The 1 mm pupil diameter is typical of RSD exit pupil diameters. Thus, the scanned illumination line from the collimated beam of an RSD is similarly limited in the minimum width that may be imaged on the retina. The impact on RSD image resolution is described as the limiting acuities of Table 2.1.

Research by deWit (1997) examined the perceived acuity of small exit pupil systems [5]. Using a non-scanning small exit pupil optical apparatus, text and image resolution charts were

imaged in Maxwellian view with various exit pupil diameters. Perceived acuity was slightly less than the diffraction limited cut-off values listed in Table 2.1. For the 1.0 mm exit pupil diameter a mean acuity of 23 cycles per degree (20/52) was reported, while the 0.5 mm exit pupil case resulted in a mean acuity of 12 cycles per degree (20/100). It is notable that reported acuity plateaued well below diffraction limitations (and well below normal maximum acuity) at approximately 28 cycles per degree (20/42) for exit pupil diameters of 1.5 mm to 2.5 mm, indicating that other factors in this experiment may have limited or affected the image resolution.

Still, deWit's results help to describe the impact that small exit pupil RSD's have on image quality. A 1.0 mm exit pupil system may be expected to have a resolving limit in the range of 25 to 30 cycles per degree (20/48 to 20/40). Comparing this acuity in a modern contextual example, a 17 inch diagonally measured SVGA computer monitor (800 x 600 pixels) at approximately arm's length viewing distance (60 cm) can provide a maximum resolution of approximately 14 cycles per degree, or approximately 20/86 acuity. A 1.0 mm exit pupil RSD providing 25 cycles per degree is equivalent to the same computer monitor generating a pixel array of approximately 1400 x 1050 pixels. The 0.5 mm exit pupil RSD providing just 12 cycles per degree resolution is approximately equivalent to the same 17 inch monitor displaying 640 x 480 pixel VGA quality imagery. While the theoretical maximum image quality of the small exit pupil RSD is degraded by the reduced exit pupil size, the image quality is clearly sufficient for computer-aided visual tasks common today.

Some RSD's may utilize coherent laser light. The transfer function of an optical system with coherent light differs from that of the same system with incoherent light. Specifically, as the level of coherence increases, the contrast achieved at low spatial frequency is improved while the high frequency resolution decreases by as much as one-half [59]. Felipe, Artigas, and Pons (1997) psychophysically evaluated these effects as applied to the human eye and plotted coherent and incoherent CSF curves, as well as similar CSF's considering laser speckle and diffraction pattern noise. Their perceptual data generally depict Thompson's theoretical effects, although their low spatial frequency comparison of coherent and incoherent illumination is confounded with diffraction pattern noise due to particulate matter within the ocular media. This causes a reduced sensitivity in the lower frequencies differing from model expectations [60]. It is significant to note that these studies examine coherent and incoherent illumination of the retina as an extended plane wave source, and not as a scanning beam. The implications of this are discussed in section 2.2.2.

Spatial perception is affected by temporal factors for some temporal and spatial frequency combinations. However, at high temporal frequencies near and above typical photopic CFF, spatial and temporal factors are separable [42]. Thus, the temporal CSF (TCSF) is identical to the CSF for steady sources at high temporal frequencies, such as the 60 Hz refresh rate typical of visual displays.

Many spatiotemporal aspects of the physiological retinal response are less well understood. Clearly, there are inhibitory and reinforcing lateral effects between retinal cells that extend across relatively large portions of the retina. The *Mach band* phenomenon is one common perceptual effect resulting from lateral inhibition across retinal cells. Mach bands are light or dark narrow bands that are perceived near the border of two juxtaposed fields, one field being darker than the other [26]. The bands are the result of inhibitory signals sent across the retinal neural network in complex ways that work to emphasize regions of contrasting luminosity [16]. The perceptual effects of other lateral retinal signals are less clear.

The function of an entire class of retinal cells with extremely long reaching dendritic fields, *amacrine* cells, remains completely unknown. However, the fact that they respond with light stimuli to photoreceptors has been confirmed, and the receptive field associated with an amacrine cell is coextensive with its dendritic field [16]. Further, these cells tend to have vastly overlapping dendritic fields, and their synaptic connections seem to link a wide variety of retinal cell types, including other amacrine cells, ganglion cells, bipolar cells, and horizontal cells. This points to the possibility of very long distance lateral effects. Referring to global visual perceptual phenomena generally believed to arise in cortical processing areas, Rodieck speculates regarding amacrine cells:

"But because the long (distance) processes of amacrine cells provide potential mechanisms for extensive interaction throughout the entire extent of the retina, there appears to be no reason to reject the idea that such phenomena have a retinal origin" [16].

In summary, human sensitivity to spatial frequencies is described by the contrast sensitivity function. While temporal factors do affect spatial perception, these two domains are separable at high temporal frequencies. The minimum possible size for a retinal image of a point source is approximately 0.5 arcminute of visual angle for an emmetropic eye under diffraction

limited conditions. Additionally, the minimum possible discrete sampling element in the retina covers approximately 0.5 arcminute of visual angle. These limits equate to a spatial cut-off frequency of one cycle per arcminute, or 60 cycles per degree visual angle. Small exit pupil RSD's cannot approach these human resolution limits due to optical diffraction limitations, but RSD's with exit pupils near 1.0 mm diameter can provide display resolution equivalent to or exceeding modern computer monitor quality. The line spread function of the human eye predicts the width of an imaged line on the retina for pupil size, and a 1 mm pupil will present a line width of approximately 4.6 arcminutes. Coherent light illumination produces a different optical transfer function than incoherent illumination. In the absence of low frequency noise, coherency enhances low frequency contrast on the retina and limits high frequency resolution commensurate with the degree of coherence. Lateral physiological processes within the retina are poorly understood, but many influence spatial and brightness perception. Amacrine cells make long distance, overlapping connections within the retinal neural network, providing the potential for far-reaching lateral effects across the entire retina. The functions of these cells are not well understood, and the potential perceptual effects of their activations are unknown.

2.2.1.5 Chromatic Considerations

The chromaticity, or color, of visual stimuli indirectly affect brightness and flicker perception as noted in previous sections. Chromaticity has no significant effect on spatial perception beyond phenomena that are explained by related luminous efficiency differences and contrast effects. Color perception has been exhaustively explored with monochromatic sources and with the comparison of monochromatic and polychromatic sources, and the body of literature is remarkably consistent. The tristimulus and opponent process theories of color vision each are well developed and have extensive experimental support. Strong evidence exists in both psychological and physiological literature for separate and essentially independent neural channels for chromatic and luminous information within the visual system. As such, no extensive discussion of chromaticity will be offered since its relevance to the visual perception of RSD's is minimal and since absolutely no evidence in literature or observation points to anomalous color perception with RSD's. The interested reader is directed to LeGrand (1968) or Wyszecki (1982) [18, 26].

However, one aspect of laser-based RSD chromaticity is unique and worthy of comment. As compared to conventional displays or RSD's using non-lasing sources, laser-based RSD's may offer a broader display color gamut and richer, more saturated colors. The laser emissions are monochromatic, providing the greatest possible color saturation for each color utilized in a three-color display system, such as the original VRD. In accordance with accepted color theory, widely differentiated monochromatic sources can provide a wider range of resultant colors by combination than can less saturated sources [26]. Although this difference may be small depending upon the compared displays, it is a unique advantage of the laser-based RSD.

2.2.1.6 Pupil Response

Numerous examinations of the pupillary response to retinal illumination are present in literature, but the data are not cohesive. This is because many variables affect pupil response, and because little effort has been made to coordinate experimental conditions among research efforts. Further, the individual variation in pupil response is large, making precise quantification difficult. Still, because of the unique viewing geometry of small exit pupil RSD's, an exploration of pupil response as applied to this display concept is prudent.

Pupil diameter varies with several factors, including retinal illumination level, size, shape, and retinal position of stimuli, retinal adaptation state, accommodation (for focal distances under one meter), psychological arousal, pharmacological conditions, and individual experience. However, retinal illumination level is, by far, the most significant and influential factor. Generally, in bright conditions the pupil is constricted, and in dim conditions the pupil is dilated. Typical maximum and minimum pupil diameters are 7 mm and 2 mm, respectively. After the onset of a change in luminance conditions, the pupil may go through mild oscillations before settling on a new diameter, indicating perhaps a damped feedback mechanism within the visual system [18].

Figure 2.17 plots eye pupil size as a function of scene luminance. These data represent a meta-analysis of six studies and 125 subjects [61]. The range of averages from the six studies is presented for each incremental luminance level, illustrating the wide range of individual differences in pupil size. Also depicted is a curve representing the calculation of the effective pupil size under photopic conditions based upon Jacob's correction for the Stiles-Crawford effect (as discussed in section 2.2.1.2). As the pupil dilates, the Stiles-Crawford effect on luminous

efficiency becomes more pronounced but, since it is related only to cone cell geometry, the effective pupil size curve does not extend into luminance levels associated with scotopic (rod photoreceptor) conditions.

Stanley and Davies (1995) achieved improved prediction of pupil size with a model based upon a measure of corneal luminous flux density, or the product of luminance and the subtended field size of the stimulus [62]. They hypothesized that much of the widely differing results in pupil size studies were due to differences in the size of the adapting fields used by the various studies. In a study of nine human subjects, they derived the model

$$D = 7.75 - 5.75 \left(\frac{(F/846)^{0.41}}{(F/846)^{0.41} + 2} \right) \quad (\text{eq. 2.5}) [62]$$

where D is the pupil diameter in mm and F is the corneal flux density in $\text{cd/m}^2 \text{ deg}^2$. This hyperbolic function was fitted to their data by iteration and graphically seems to account for the vast portion of the variance among the data, although no error calculation was offered. These researchers concluded that the pupil control mechanism is performing simple integration wherein retinal illumination and stimulus area are interchangeable. They limit this conclusion to field diameters of 25 degrees or less, the maximum field size tested in their study. It is also important to note in this study that the natural pupil of the eye was the limiting aperture, so the Stiles-Crawford effect with pupil size is inherent within these data.

Crawford (1936) discovered that illumination of the foveal region of the retina effects pupil response more than identical illumination in the peripheral retinal areas. Constriction of the pupil is generally less for illumination restricted to the periphery than for illumination on the fovea [63]. As with pupil size in general, this effect is highly variable among individual observers.

The effect of luminance on pupil size varies somewhat depending upon whether the observer is viewing a scene monocularly or binocularly [64]. Across the photopic luminance range, pupil diameter is typically smaller when both eyes are used to view a stimulus. The difference may be as much as 1.75 mm in the central regions of the curve of figure 2.17.

Accommodation and vergence can also have a significant effect on pupil size, although this effect is restricted to viewing distances of one meter (accommodation of one diopter) or less [61]. As the accommodation distance decreases inside of one meter, the pupil constricts as much as 50 percent.

DeLauney (1949) measured the probability density functions of pupil diameters at various luminance levels and found normal distributions of pupil diameters at luminance levels equated with the middle range of pupil sizes (3 mm - 6 mm). At lower and higher luminance levels, skews toward smaller and larger diameters, respectively, developed in the distributions, as would be expected as the maximum and minimum pupil size is achieved at the extremes of luminance levels [65]. For the photopic range of luminances, normally distributed pupil diameters may be assumed in the population except near the natural boundaries of pupil size.

In summary, retinal illumination level has the largest influence on pupil size, but many other factors contribute and produce wide individual variability. Pupil size typically ranges between 2 mm and 7 mm diameter, and a sigmoid function coarsely approximates the pupil's response to luminance changes. Models considering the flux density of luminous energy entering the eye seem to offer good prediction ability independent of stimuli field size variables. Binocular viewing generally causes decreased pupil size as compared to equivalent monocular viewing, and strong accommodation causes the pupil to constrict. Foveal illumination causes greater pupil constriction than peripheral illumination. In the photopic luminance range, pupil diameters in a population are normally distributed except near the upper and lower limits of natural pupil size.

2.2.1.7 Accommodation Response

The human accommodation response is commonly referred to as focusing the eyes. It is achieved through changes in the shape of the lens of the eye that are affected by small intraocular muscles termed the *ciliary bodies*. The changes in lens shape effectively alter the refractive power of the eye to achieve a focused retinal image across a broad range of focal distances. The accommodation response may be autonomic, or may be placed under conscious control. Under autonomic conditions the reaction time to complete an accommodation from the onset of a stimulus is approximately 0.3 seconds [66]. The optical, neurological and physiological processes that facilitate accommodation control are poorly understood.

Under visual stimulus conditions devoid of detail, such as darkness or a completely homogeneous luminous field, the eye achieves a *resting state* of accommodation that varies with individuals. Leibowitz and Owens (1978) determined a mean resting state accommodation of

1.52 diopters (diopter = 1/focal length in meters) with a standard deviation of 0.77 diopters for 220 college aged subjects [67].

Campbell, Robson, and Westheimer (1959) identified oscillations in accommodation that occur persistently when sufficient scene detail is available. Low frequency oscillations in the range of $>0 - 0.5$ Hz dominate the accommodation activity. Higher frequency oscillations with an amplitude that may exceed 0.5 diopter are superimposed on the low frequency oscillations in the range of $0.9 - 2.5$ Hz [68]. These researchers found that the low frequency fluctuations increase in amplitude with small pupils. Others have replicated these findings [13, 69]. The high frequency fluctuations do not change in amplitude with pupil size, and they have been nearly perfectly correlated with the ocular pulse [70].

Stark and Atchison (1997) confirmed the effects of pupil size on both the low and high frequency oscillations [71]. Their findings support the theory of Gray, Winn, and Gilmartin (1992) that the low frequency oscillations are involved in the accommodation control process, perhaps by seeking a maximum contrast on the retina [72]. In this theory, oscillations in accommodation would periodically mildly defocus the retinal image, causing a reduction in image contrast. A feedback mechanism would maintain accommodation between these contrast "stops." Stark and Atchison speculate that when a small exit pupil is employed and a large depth of field results, the oscillations of accommodation must necessarily increase in amplitude to achieve defocus and the reduced image contrast of the stops. Additional psychophysical research examining the effect of image contrast, image quality, and image luminance supports this theory [72, 73].

In summary, the neurophysiology of accommodation is poorly understood. However, the behavior of the system is well documented. With insufficient spatial detail, accommodation achieves a resting focus near 1.5 diopters. With sufficient spatial detail, low frequency oscillations between $0 - 0.5$ Hz occur. These oscillations increase in amplitude when a small pupil is imposed on the eye [71]. Theorists suggest that these oscillations are associated with the process of accommodation control whereby the visual system constantly seeks an accommodation providing the maximum retinal contrast. It is notable that no literature discusses the potential of fatigue of the ciliary bodies with long term viewing of very small pupil imaging systems.

2.2.2 Retinal Scanning Display Considerations

Some unique characteristics of retinal scanning displays warrant closer review in light of their relationship to human visual system characteristics. Of particular interest is the geometry of RSD light rays entering the eye, the spatiotemporal character of the scanning beam's spot image on the retina, and the issue of beam and scanned field coherency.

An RSD creating a small exit pupil in relation to the entrance pupil of the eye is a *Maxwellian view* system, after noted physicist James Clerk Maxwell who first documented such a method of illuminating the retina in his effort to maximize the light reaching the retina from a prismatic source of monochromatic light [74]. Figure 2.18 depicts the optical arrangement for Maxwellian view. A small source is imaged by a lens into the entrance pupil of the observer's eye. When focusing on the lens, or an aperture adjacent to the lens, the observer sees the lens as uniformly illuminated [75]. With a sufficiently small image, or display exit pupil, all of the light enters the eye and the entrance pupil of the eye is no longer the limiting aperture. Rather, the display exit pupil becomes the limiting aperture. The scan of the RSD, as described in sections 2.1.1 and 2.1.2, creates a Maxwellian view geometry by directing the scanning beam through a common spatial position that is placed coincident with the entrance pupil of the observer's eye. Obviously, the RSD view is varying in the spatial and temporal domains with the beam scan, unlike Maxwell's original static design.

The Maxwellian view display geometry must be considered in terms of its effects on the visual system. A collimated beam entering the eye will be focused (within the limits discussed in section 2.2.1.4) onto the retina by the eye's optics. With the assumption that the beam diameter is small (1 mm or less), and that the beam enters the eye near the center of the eye's entrance pupil, the incidence angles of light rays to a retinal photoreceptor aperture plane will be very near normal. Hence, the Stiles-Crawford effect that causes reduced luminous efficiency with large photoreceptor incidence angles is dramatically reduced in significance. A 1 mm pupil with monochromatic illumination near 630 nm (red) will transduce light with approximately 95% the maximum possible efficiency [26]. This fact applies to the entire scanned retinal area when a small exit pupil RSD is properly viewed. It should be clear that the same optical geometry and implications for Stiles-Crawford apply to any Maxwellian view system, scanning or static.

Practically all literature regarding pupil size as a function of luminance level reports data with natural viewing, allowing the eye's pupil to be the limiting aperture. Historically, models of

pupil size under Maxwellian view conditions have been of little practical value and largely ignored. Pupil response to retinal illumination under Maxwellian view conditions may be expected to differ from the response under natural viewing conditions due to the difference in phototransduction efficiencies. The response may be expected to change with the size of the Maxwellian image, or with RSD exit pupil size, since the significance of the Stiles-Crawford effect will vary with the extent of entrance pupil coverage.

As previously introduced, the natural response of the eye's pupil to retinal illumination by Maxwellian view will have no attenuating effect on the illumination. One of the visual system's adaptation mechanisms is thereby circumvented. However, under augmented viewing conditions in which an RSD image is presented simultaneously with naturally viewed imagery, the pupil's response to changes in Maxwellian view illumination (or to natural view illumination changes) will modulate only the natural view illumination. This fact has some small consequences for contrast of the RSD image with the naturally viewed image in augmented display modes.

As compared to most current electronic visual displays, the RSD presents the retina with a unique spatiotemporal signature. Because the source of retinal illumination is a scanning beam, rather than an energized region of phosphor or a persistently illuminated liquid crystal, there is little physical persistence of the RSD display image. The difference can be characterized in terms of the time associated with the illumination of the retina by a single display pixel. For CRT phosphors, phosphorescence is dependent upon phosphor type and refresh rate, but may extend over long periods, usually on the order of tens of milliseconds [76, 77]. The RSD's pixel persistence is a function of scan speed and the size of the scanning spot imaged on the retina. The VRD scans its Gaussian laser spot across a given retinal position in approximately 40 nanoseconds [78]. Thus, for any given pixel, a typical CRT provides physical illumination of retinal photoreceptors for a duration 10^6 times that of the VRD. However, phosphor luminance is not constant during its pixel display time, and it typically falls exponentially following a rapidly achieved peak excitation. Still, considering the Talbot-Plateau law (section 2.2.1.2), the luminance of the VRD must be substantially greater than that of the CRT for conditions of equivalent luminosity. This dictates a significantly different spatiotemporal delivery of luminous power to the retina with the RSD.

Early cursory observations of the VRD seemed to indicate a reduced sensitivity to flicker and enhanced brightness as compared to a typical CRT (Thomas Furness, 1998, personal communication). Kelly, Pryor, Viirre, and Furness (1998) reported reduced flicker perception

with the VRD by factors as great as 9.4, as measured by flicker detection threshold contrast with the method of adjustment [79]. Observations of both Maxwellian view RSD's and expanded exit pupil RSD's engineered by a commercial enterprise provided results conflicting with those of Kelly, et.al. (1998) (John Lewis, Microvision, Inc., 2000, personal communication). It is unclear whether an anomalous visual response results from the unique spatiotemporal stimulus of the VRD, although little in literature supports the prediction of such an unusual temporal effect.

Coherent illumination has been shown to affect the perception of spatial frequencies, as compared to the normal condition of incoherent light (section 2.2.1.4). However, the conditions under which these effects have been measured are with expanded beam steady coherent fields and not with scanned coherent beams. In the former case, the expanded beam acts as a large plane wave that may preserve coherence across the visual field. It seems likely that in the latter case, the scanning operation of an RSD will degrade the level of coherence, as it applies to the scanned field, to a degree that the spatial perceptual effects of coherence are insignificant. Two aspects of coherency are considered: temporal coherency and spatial coherency.

Temporal coherence is the degree to which emitted wave packets have the same phase and speed. Within a coherent laser beam, all wave packets are in phase, with the oscillations of their electric component temporally synchronized [80]. Transmission speed is obviously equal under most circumstances and is not a factor here. Consider any position on the retina within the RSD scanning field. As the beam sweeps across this position during partially overlapping line displays and subsequent frame refreshes, the probability of maintaining precise synchrony of wave packet phases at this position is extremely low. Further, as the beam moves across the retina, even immediately adjacent positions will absorb waves with variable phases as the electromagnetic wave naturally propagates. Thus, it reasons that the temporal coherence considered across the *scanned field* is severely disrupted, while the coherence of the beam itself is preserved.

Spatial coherence is the degree to which the wave packets exhibit identical frequency, direction, and polarization [80]. Clearly, the frequency of the laser energy in an RSD is preserved. Similarly, it seems reasonable that the polarization vectors of the scanned light will not be significantly altered. However, the direction of propagation obviously changes during the scanning operation. Again, as applied to the scanned field, the spatial coherence must be disrupted by the highly variable propagation vector. While the beam is still considered coherent at any given instant in time, the spatial coherence of the overall field cannot be preserved.

The loss of coherence is apparent in the VRD and VRDE image presentations by a lack of laser speckle and by the absence of diffraction fringes about imperfections in the optical path -- phenomena typical with coherent light. Thus, the limiting factor in displaying spatial frequencies with RSD's emitting coherent or incoherent light is the width of the imaged line on the retina, as discussed in section 2.2.1.4. (The temporal bandwidth associated with the modulation of pixels along a scan line must also be considered in display resolution, but this issue is not related directly to visual system coupling and is not addressed in this dissertation.)

2.2.3 Arrayed Small Exit Pupil Display Considerations

As introduced in section 1.2, arrays of small exit pupils positioned about the entrance pupil of the eye seems a viable method of preserving the optical advantages offered by extremely small exit pupil RSD displays while preserving the desirable large pupil coupling area (effective exit pupil area) of more conventional displays. Key to this concept is maintaining a single small exit pupil coupled to the eye's entrance pupil at any time. If multiple exit pupils enter the eye simultaneously, the effective limiting display aperture is multiplied in area and the optical advantages of the small pupil are commensurately degraded. Additionally, depending upon the characteristics of the multiple images delivered to the retina by separate exit pupil displays, the image quality may be degraded as well. These issues are now explored in more detail to provide the reader background and rationale for the subsequent exploration of the arrayed exit pupil concept.

2.2.3.1 Rationale for Arrayed Small Exit Pupil Displays

Small exit pupil displays are generally considered to be undesirable due to the difficulty in maintaining alignment, or *coupling*, with the eye's entrance pupil. Familiar cases of this problem include simple telescopes, binoculars, and microscopes where precise coupling between exit pupil and eye pupil is required to avoid significant vignetting or complete loss of image capture. Given a wide field of view display, simply rotating the eyes to scan the image with central vision will cause decoupling of the pupils. Further, many envisioned applications for RSD's require head- or helmet-mounted display scenarios and may include operational environments with significant motion or vibration. Maintaining precise pupil coupling under such conditions is an impractical

goal. As eye pupil size is not a well controlled parameter, increasing the effective display exit pupil area is the only practical method for maintaining pupil coupling and image capture. However, small exit pupils offer significant optical and power advantages that make them highly desirable for RSD implementation. Thus, a design conflict exists with the engineering of RSD's. Both large and small exit pupils have highly desirable characteristics. Implementing arrays of small exit pupils allows the display designer to reap the advantages of both large and small exit pupils, but this technique also introduces new engineering challenges.

The advantages of a large exit pupil area are clear. The observer does not need to keep his eye in a precise location to view the entire image. As the eye moves about within the exit pupil area due to scanning rotations or eye-display relative motion, some of the light of the large exit pupil will enter the eye and yield an image. The flux density that reaches the retina for imaging will be modulated by the eye's entrance pupil so long as the entrance pupil remains within the larger exit pupil area. From a bio-optical perspective, these conditions are not significantly different from natural viewing. Retinal illumination will be determined by the luminance of the display and the area of the eye's entrance pupil. The depth of field of the image will be relatively small, as determined by the limiting aperture of the eye's pupil. Typically, the display will be collimated near optical infinity for distant viewing comfort and convenience. The light from the exit pupil that does not enter the eye is wasted, absorbed or reflected by the iris, sclera, and surrounding tissues.

This display scenario is typical for many head- and helmet-mounted optical devices. The larger exit pupil allows substantial display-eye relative motion without loss of image capture, as required by many envisioned RSD applications. A typical scenario for RSD implementation is in military aircraft cockpits. This highly dynamic environment is fraught with vibration, high accelerative forces, and rapid head movements by aircrew members. Less demanding envisioned applications of RSD's include use by low-vision patients to improve visual navigation while walking. Each case offers unique problems in maintaining pupil coupling, and each case may be solved primarily by the implementation of an expanded exit pupil area. However, expanding RSD exit pupil area is not a trivial engineering feat, particularly with polychromatic light.

Small exit pupils of 1 mm diameter or less offer two highly desirable advantages. First, the depth of field produced by small exit pupils is quite large, providing an image that is in focus even with the very large accommodation changes typical with an augmented view display. Second, the vast majority of light from the small exit pupil enters the eye for retinal image

formation, making the display highly energy efficient. No light energy is wasted outside the eye as in the expanded pupil case. Thus, small exit pupils provide the opportunity for improved display optical utility and energy efficiency.

The exit pupil of an RSD may be expanded by diffractive optical multiplication. That is, many iterations of a small exit pupil may be created from a single converging beam scan and arranged in a plane for viewing. This has been demonstrated at HITL with the laser based VRD by using a custom designed two-dimensional diffraction grating placed in the optical path of the scanning beam. The grating produces a Fraunhofer diffraction pattern at any given position of the scan, and the diffraction patterns converge at multiple locations beyond the grating to produce multiple converged exit pupils. Thus, the exit pupil area is effectively expanded by replicating the exit pupil many times to create an array of small exit pupils. However, this approach has some shortcomings.

First, a pupil array produced in this manner must be monochromatic. The introduction of polychromatic light disrupts the formation of tightly formed exit pupils because diffraction characteristics vary with wavelength. (While it is theoretically possible to engineer a holographic optical element that would produce similar pupil multiplication with polychromatic sources, this has yet to be demonstrated as a viable technique.) Second, the multiple pupils are fixed in separation distance. Typically, the pupils are nearly adjacent with little separation distance in order to avoid any region where a small entrance pupil may decouple “between” two exit pupils and cause a loss of image. Thus, multiple exit pupils are captured utilizing the entire area of the eye’s entrance pupil. This disrupts the optical advantages of the small exit pupil, as the limiting aperture again becomes the area of the eye’s entrance pupil. Additionally, this technique produces exit pupils of variable luminance, with luminance falling as a function of the distance from the central pupil. Finally, this method offers no individual control over exit pupil display content or power status (on/off) – unique advantageous characteristics of proposed arrayed exit pupil designs to be discussed in subsequent chapters.

Fortunately with the diffraction pupil multiplication technique, the vectors of light rays are accurately reproduced in each exit pupil, with only lateral translations. That is, each exit pupil accurately preserves the angle of the scanning beam at each position in the scan pattern. Thus, these multiplied exit pupils have parallel beam scans. At any given scan position, every exit pupil created by diffraction yields a beam at an identical angle relative to the plane containing the multiple pupils (and relative to the entry aperture of the eye). As a result, the

retinal image created by each exit pupil is completely coincident on the retina. Only a single image is perceived by the observer regardless of the number of exit pupils coupled to the eye's entrance pupil. If this were not true, each captured exit pupil would present its image on the retina in a unique position, producing a confusion of multiple overlapping images. This characteristic of scan parallelism is a key consideration in subsequent descriptions of arrayed exit pupil displays, as it is not easily or practically achievable for small head mounted displays by means other than diffraction multiplication.

Even if homogeneous polychromatic multiplication of RSD exit pupils become feasible through optical advances, the fixed pupil separation distances and lack of individual pupil control makes it less than an optimum solution. The optical advantage of large depth of field is lost with multiple pupil couplings and, perhaps more significantly, the energy cost is approximately equivalent to other more conventional display methods due to the waste of light energy that does not enter the eye.

The large depth of field provided with small exit pupil displays is a significant advantage in many envisioned applications of RSD technology. Particularly relevant is the augmented display condition where the naturally viewed world scene is augmented with RSD displayed information. In many applications the observer may be required to accommodate rapidly between near and distant natural view objects. For example, a production floor environment for large systems such as aircraft, watercraft, or automobiles may require a user to alternatively inspect product assembly details at very close range and upcoming or cued assembly parts at a distance. It is not practical to refocus the augmented display for each iterative accommodation change under such conditions. However, a large depth of field display will remain "in focus" for the observer across a very large range of accommodation changes, obviating the need to refocus the display.

This depth of field advantage also applies to many low-vision scenarios in which the user may not have the ability to accommodate well to any visual stimulus from the natural world scene due to damage or loss of optical tissue within the eye. However, study results at HITL indicate that small exit pupil displays can present a well imaged stimulus to the retina of many low-vision patients in spite of substantial damage to the ocular media [81, 82]. The combination of tremendous depth of field and small entry aperture circumvent many optical problems for these individuals. Further, because many low vision users may need large text and symbolic presentations that do not require a high resolution display, very small exit pupils (smaller than 1

mm diameter) that provide very large depth of field and use a tiny portion of the ocular media may be implemented to aid many low vision users.

Small exit pupil displays hold the potential for extraordinary efficiency in power consumption. Since practically all of the light energy of a single small exit pupil display enters the eye for image creation, no energy is wasted in the creation of a large exit pupil area. Consider an array of RSD small exit pupils creating an effective exit pupil area equivalent to a more conventional large exit pupil display. Assume that every exit pupil in the array is always emitting light energy. In essentially every practical case of exit pupil area and eye pupil size, the array of small exit pupils will require less energy to deliver an equivalent level of retinal illumination, and hence, an equivalently bright display. However, this energy advantage is relatively small with constantly illuminated exit pupils.

Consider an alternate design in which only a single exit pupil at a time is luminous within the array of small pupils. That is, the only exit pupil that consumes power and provides retinal illumination is one pupil that is well coupled with the eye's entrance pupil. Further, the "on pupil" is rapidly switched as necessary with eye-display relative motion to maintain a properly coupled small exit pupil at all times. The energy savings under this scenario increase more than an order of magnitude. Examine the following specific example.

A typical head mounted display in military aviation applications requires an exit pupil of approximately 15 mm diameter, or 177 mm^2 . Assume an observer eye pupil diameter of 3 mm, or 7.1 mm^2 . For a conventionally expanded exit pupil display, the percent of the total display energy entering the eye may be estimated by the ratio of the eye pupil area to the exit pupil area. In this particular case, $7.1 \text{ mm}^2 / 177 \text{ mm}^2 = 4\%$. Thus, only 4 percent of the total emitted display energy goes to illumination of the retina.

Given the 3 mm diameter eye pupil, 16 small exit pupils of 1 mm diameter may be arrayed with equal spacing to provide an approximately equivalent effective exit pupil area of about 170 mm^2 . Each exit pupil will deliver 1/16 the total emitted display energy into the eye, or 6.25 %. Thus, even if all arrayed exit pupils are emitting simultaneously, the small exit pupils are more efficient by a factor of 1.5 ($6.25\% / 4.0\%$). If the small exit pupils are switched on and off so that only a single pupil is emitting at any given moment, the energy efficiency of the display expands to 25 times that of the conventional large pupil display (only 4% of the large pupil display total light energy must be emitted by the small exit pupil display to provide retinal illumination equivalent to the large pupil display).

Granted, the theoretical arrayed exit pupil display with switching pupils introduces new display engineering problems. The most significant of these seems to be the optical production of the array of exit pupils themselves. This problem is discussed in subsequent sections, and the visual perception of compromise engineering solutions is the central concept explored in arrayed exit pupil experimentation described in Chapters 7. The problem of coarse eye tracking has been solved with numerous methodologies already, and the architecture of the RSD display may lend itself well to the integration of novel new eye pupil tracking techniques. With currently engineered RSD light emitting diode technology, the issue of switching light sources on and off is trivial.

Thus, in spite of challenging system engineering and integration problems, as well as many unknowns in the realm of human perception and interfacing, the dramatic energy savings alone make the pursuit of arrayed small exit pupil displays worthwhile. Coupled with the optical advantages outlined above, the exploration of this display engineering option is certainly a prudent endeavor. For the human factors engineer, the first exploratory steps should be an investigation of the visual perceptual characteristics of such displays, and consideration of their impact on human interfacing. In this way, a determination may be made early in the developmental process of whether the display will be practical and usable, and whether further pursuit of the concept is prudent. The following section provides additional background information pertinent to the issue of human interfacing with arrayed small exit pupil displays.

2.2.3.2 Considerations in the Optical Geometry of Pupil Coupling and Pupil Array Generation

It may be feasible to use arrays of RSD small exit pupils to preserve desirable optical and power characteristics of small pupils while also providing the observer the equivalent of a large effective exit pupil area for coupling effectiveness. The need for a larger effective exit pupil area than is provided by a singular small exit pupil is driven by the practical fact of eye-display relative motion. However, the ease with which arrays of small exit pupils may be generated is in question. A more detailed examination of optical geometry is necessary, as related to eye-display relative motion and the practical creation of arrayed pupils.

Eye-display relative motion may occur among four dimensions. These are the three dimensions of motion within which the display itself may move relative to a fixed eye position and a fourth dimension of eye rotation relative to the fixed display. With a typical head-mounted

or helmet-mounted display, the dimension of motion affecting the distance between the display and eye is typically well controlled (eye relief distance, or z-axis coupling). More problematic in dynamic environments is vertical and horizontal motion of the display (as observed by the user) caused by rapid head movement or accelerations. This is because typical display mounting hardware can easily employ a rigid structure that provides a relatively consistent eye relief distance, but it is difficult to affix a mounting structure to the human head that completely disallows the structure sliding about on the head laterally. Short of imbedding skull screws, any head-mounted display will move relative to the eye with sufficient accelerative forces applied. Further, while these types of motions may also alter the eye relief distance, well designed mounting hardware keeps these displacements slight. Primary consideration will be given to the geometry of eye rotation and lateral motion.

The simple geometry of eye rotation as it applies to arrayed small exit pupils is illustrated in Figure 2.19. Graphic 'a' depicts the simplest case of a single small exit pupil converging in the plane of the eye's pupil and illuminating the retina (refractive effects of the cornea and lens have been ignored for simplicity). The fovea examines the center of the image. Rotation of the eye about its center allows the fovea to examine a limited angle within the central portion of the image. The limits of rotation for pupil coupling are illustrated with dashed lines extending from the edges of the eye's pupil, passing through the center of eye rotation, and impacting the retina. As illustrated in graphic 'b', attempts to position the fovea beyond these limits will decouple the pupils and cause a loss of retinal imaging. Clearly, the visual angle associated with the rotation limits for coupling varies with eye pupil diameter and with the diameter of the eyeball. Therefore, the portion of the RSD image that may be viewed with central vision is dependent upon the individual observer's eyeball diameter and, more significantly, upon the observer's entrance pupil diameter.

A model of the eye rotation angle that may be affected with a single exit pupil and that maintains full exit pupil coupling with the eye pupil is offered by deWit [5]. This model considers the pupil diameter, corneal refraction effects, and the diameter of the exit pupil. The model assumes an eye center of rotation to pupil plane distance of 8.5 mm. Table 2.2 lists the eye rotation angle limits as determined by deWit for a range of eye pupil diameters with a 1.0 mm diameter exit pupil. The visual angle listed is the entire image angle that may be viewed with central vision (view by fovea) without partially decoupling the pupils and reducing image luminance. See Figure 2.19a for a schematic of the simplified eye rotation limit geometry.

Table 2.2: Estimations of Eye Rotation Limits for Pupil Coupling

Eye Pupil Diameter (mm)	Rotation Limit Visual Angle (deg)
2.0	6.6
2.5	10.4
3.0	14.1
3.5	17.9
4.0	21.5
4.5	25.2
5.0	28.7
5.5	32.3
6.0	35.7
6.5	39.2
7.0	42.5

If partial exit pupil coupling with the eye is considered, the rotation angle limits will expand. Further, lateral relative motion of the eye and display are not considered here. Coordinated combinations of lateral movements and rotations can facilitate central vision viewing of a wider visual angle of RSD display. However, most applications of RSD's do not provide for such lateral relative motion, as the devices will likely be head-mounted with the goal of reducing relative lateral movements to maintain pupil coupling.

Note that for small pupil sizes of 4 mm diameter or less, less than 22 degrees of an image may be viewed with central vision. Pupil sizes of less than 4 mm diameter are very common under photopic luminance conditions, and pupil sizes near 2 mm are common under bright outdoor luminance conditions [61]. These conditions will limit the viewable display area to less than 10 degrees. For typical visual displays, such as computer monitors, a field of view of 20 degrees or more is desirable. A 17 inch diagonal CRT at arm's length viewing distance (60 cm) provides approximately a 28 degree horizontal visual angle display. Thus, eye rotation alone dictates an expansion of the display exit pupil beyond that provided by the single small exit pupil.

An array of small exit pupils will position pupils side-by-side with some intervening space. Figure 2.19, graphic 'c' depicts two exit pupils positioned about the eye's entrance pupil. The right exit pupil is properly coupled while the left exit pupil is decoupled. As the observer

rotates his eye, as in graphic 'd', the right exit pupil becomes decoupled and the left exit pupil becomes coupled. This allows the observer to position his fovea across a wider visual angle within the retinal image. It is easy to envision a similar third exit pupil further to the right to facilitate image capture with eye rotation in that direction. Additionally, similar arrangements of pupils in the orthogonal dimension will produce a planar array of pupils for eye rotations left, right, up, and down. Properly spaced for entrance pupil diameter, any two adjacent exit pupils should provide approximately double the central vision viewing angle of a single exit pupil.

Two additional issues are illustrated in Figure 2.19. Graphic 'e' depicts the condition where image capture is lost due to the entrance pupil being small enough to fall between two adjacent exit pupils. Under this condition, an image will be captured only for each eye rotation position that couples the pupils, either right or left of the depicted rotation position. This is the previously described condition that dictates the close spacing of diffraction multiplied exit pupils. Graphic 'f' depicts the simultaneous coupling of two adjacent exit pupils by a large entrance pupil, resulting in coincident images on the retina (ocular refractive effects are coarsely depicted in this graphic). These two conditions are highly relevant to subsequent display interfacing discussions.

It is easy to extend the geometric considerations of pupil coupling with eye rotations to lateral eye-display relative movement. Again referencing Figure 2.19, it is easy to envision the eye or beam scans "sliding" left or right to couple or decouple pupils, in lieu of eye rotations. With properly separated exit pupils, the scenario of simultaneous decoupling and coupling shown in graphics 'c' and 'd' applies to lateral movements. Still, for any given lateral relationship between beam scans and eye pupil the rotation limits apply, as do the scenarios depicted in graphics 'e' and 'f'.

Consider graphic 'f' of Figure 2.19. This depiction is accurate only as long as the two beam scans creating the two exit pupils are parallel, as described in section 2.2.3.1. If the two beam scans differ in entry angle to the eye, the dual captured images will not be coincident on the retina. A double image will be perceived by the observer. If additional pupils are coupled simultaneously without parallelism, even more confusing image misalignment will be perceived. Figure 2.20 compares simplified parallel and non-parallel scan optical geometries. If diffraction multiplication of exit pupils is not a viable method of creating arrayed small exit pupils due to the limitations described in section 2.2.3.1, the ease with which arrays of pupils may be generated comes into question. Further, if arrayed exit pupil scans cannot practically be made parallel, the

problem of multiple pupil couplings looms large. Fortunately, compromise engineering designs seem to offer potential solutions that may yield viable displays (see section 2.2.3.3).

The production of arrays of parallel scan small exit pupils is difficult without the use of diffractive optics. The problem involves the method of converging multiple beam scans into a tight constellation of exit pupils while maintaining parallel beam scan paths. Although theoretically feasible, achieving this in a small, light weight, head mounted display system has low practicality. Essentially, each exit pupil requires a separate converging optic in parallel with the converging optics of all exit pupils, and with separation distances small enough to match eye pupil diameters. The left side of Figure 2.21 depicts a simplified geometry of this scenario. The array of converging optics quickly becomes unwieldy, particularly for arrays of up to 16 exit pupils. Optical design trade-offs, such as the converging optic aperture, focal length, field of view, lateral pupil separation distance, and eye relief distance, dictate either extremely narrow field displays, impractically wide separation of pupils, or eye relief distances impractically close to the eye's cornea.

These trade-offs may be envisioned using Figure 2.21. In the parallel scan pattern case, it is easy to intuit how a closer spacing of exit pupils dictates smaller aperture optics. Similarly, increased eye relief distance necessitates longer focal length optics and thereby reduces the display field of view. The substitution of reflective optics can help to solve some of these problems, but this introduces other similarly vexing design trade-off problems. Less conventional alternative concepts may ultimately provide beam scan parallelism with a practical optical design and without the disadvantages of diffraction optics, but such designs have not yet been introduced.

In lieu of a separate converging optic for each beam scan, a single converging optic may be used for all beam scans. The right side of Figure 2.21 depicts this scenario's simplified geometry. The single converging optic greatly simplifies potential optical designs, allowing wide field of view imaging, easily producing desired pupil separation distances and providing ample eye relief. Again, it is easy to intuit these geometric considerations by examining the non-parallel scan graphic in the figure. The larger available aperture provides improved field of view with a large focal length and related eye relief distance. The exit pupil separation distances may be adjusted by the lateral separation of the scan mechanisms and by the selected optic's magnification ratio. However, this method dictates that exit pupils be converged from non-parallel beam scans. Thus, any simultaneous coupling of multiple exit pupils will produce

multiple retinal images that are not precisely coincident. This scenario calls for a method of ensuring only singularly coupled pupils at any given time to avoid multiple disjunct retinal images.

Given these considerations, the arrayed exit pupil display design challenge becomes a choice of attempting to solve either the parallel beam scan problem or the problem of simultaneous multiple pupil couplings with non-parallel scans. Depending upon human the visual perceptual characteristics, the latter challenge may well prove to be the more practical and less expensive option. Further, some envisioned solutions to the multiple pupil coupling problem also enable the enormous energy efficiency described in section 2.2.3.1. An elegant common solution to these two problems seems feasible. A description of the generalized display engineering concepts involved will help the reader to interpret subsequent experimentation and results.

2.2.3.3 General Engineering Concepts and Assumptions for Arrayed Pupil RSD's

The geometry of arrayed pupil generation described above and by the non-parallel scan pattern of Figure 2.21 makes some assumptions regarding the future engineering of RSD's that present arrays of small exit pupils. The primary assumption is that it is feasible to use multiple scanning mechanisms to produce multiple exit pupils. Inherent in this assumption is the expectation that mechanisms for scanning light beams will become mass produced, smaller, lighter, mechanically simpler and relatively inexpensive as compared to current methods. Existing scanning methods make the implementation of multiple scanners infeasible for most display applications due to expense, size, weight, and mechanical complexity. However, the assumption of improved, less expensive scanners is perfectly reasonable given recent successes with micro-electromechanical (MEMS) optical scanning devices and with scanning optical fiber systems. Additionally, the assumption may be made that a small number of beam scanning devices can be employed with multiple beams incident to each oscillating reflector at disparate angles. These scan patterns would subsequently be redirected into the converging optic at proper disparate angles to generate the desired array of exit pupils, thereby emulating the simpler optical path depicted in the non-parallel graphic of Figure 2.21. More elegant designs employing customized reflecting optics for scan convergence are also feasible, reducing bulk and weight. Further, clever designs using

electronically repositionable mirror elements may facilitate the generation of multiple exit pupils in an array with a single 2-D scanning component. The engineering options are numerous.

It may also be feasible to opto-mechanically mobilize a single exit pupil to track with the eye's pupil. This scenario reduces the necessity for multiple scanning mechanisms and for synchronization of multiple scanner-modulator systems. However, mechanical systems have the disadvantage of necessitating the movement of optical elements. Further, optically repositioning an exit pupil in a continuous manner introduces other difficulties in maintaining image rectification and positioning on the retina. While it is uncertain what general engineering approach may ultimately be proven viable, arraying small exit pupils seems a strong option.

Two general pupil arraying methods are considered for maintaining a single exit pupil coupled to the eye's entrance pupil at any given time, although one method seems superior to the other. First, the exit pupils may be separated by mechanical or electronic means at distances approximately equal to the eye pupil diameter. In this way, as one exit pupil is decoupled by relative pupil motion, another exit pupil becomes coupled and retinal imaging is contiguous. This scenario is depicted in graphics 'c' and 'd' of Figure 2.19. This will be termed the *coupling method of optimum separation*.

Alternatively, only a single exit pupil that is properly coupled to the eye may be illuminated at any given time. As the eye moves relative to the display, the illuminated exit pupil is extinguished and a more properly coupled exit pupil is activated. This will be termed the *coupling method of switched singularly coupled pupils*.

Clearly, the first alternative assumes persistent illumination of all (or many) exit pupils as well as an opto-mechanical or electromechanical means of adjusting pupil separation distances. The latter alternative assumes independent control of display photon emitters, such as light emitting diodes (LED's), with fixed pupil separation distances. Typically, electronic switching of fixed emitters is a more desirable solution than mechanical manipulation of electro-optical components. Further, given a tightly spaced exit pupil array, the selective illumination of multiple fixed position exit pupils by electronic means can closely emulate mechanical manipulations of exit pupil separation distances. Finally, illuminating only a single exit pupil at a time promotes the previously described high energy efficiency.

Both options assume that the aperture of the eye's pupil may be detected and tracked in real time to dictate adjustments to displayed exit pupils. Eye tracking technology is sufficiently advanced to address this problem. Two examples of current head-mounted eye tracking systems

are offered by Arrington Research and Gesture Central [83, 84]. Small, lightweight infrared emitter-detector systems can provide sufficient resolution and speed to ensure that a good estimation is made of the eye's central pupil position and/or pupil diameter. Only a coarse estimation is required to ensure that pupils remain coupled. Additionally, Tidwell suggests a methodology for integrating eye tracking into the scanning apparatus [85]. Thus, the integration of real time eye tracking and/or measurement into an RSD system seems a sound assumption.

Remaining is the question of human perception of these proposed displays. The primary concern is drawn from the fact that the use of a single converging optic produces non-parallel scans and results in noncoincident retinal images. As the coupled exit pupils change, the retinal image will shift in position instantaneously by some angular extent. The magnitude of this shift is a significant concern for display image quality and visual perception.

The angular image shift between two exit pupil will be a function of the angular disparity between the two converging scans creating the exit pupils. The angle between the converging scans is a function of the scan incidence angles to the converging optic. These incidence angles are directly related to the relative positions of the scanning source, and scanning source separation also affects exit pupil separation distance.

The scenario is perfectly analogous to a simple imaging problem. The converging optic is imaging the effective aperture of the scan sources, and the scan rays are analogous to the diverging rays emitted from any small object being imaged by a lens. The only difference is that the scan's rays are temporally separated, while a normally imaged object's rays are emitted simultaneously and continuously. Thus, the separation of the scan "objects" being imaged affects the separation of the exit pupil "images," as well as the angular disparity between the imaging rays. The question then is whether an arrangement of scanning mechanisms can be fit closely together at distances from the converging optic that are feasible for head mounted display purposes, while simultaneously affecting exit pupil separation distances as small as 2 mm and keeping angular disparity between adjacent scans sufficiently small for human visual perception.

Given the small size of MEM's and optical fiber scanners, very small separation distances between scanning sources are quite feasible. As recently as May 2002, the Microvision corporation announced the production of a 1 mm aperture MEM's scanner on a chip of just 6 mm x 6mm [86]. Thus, even with current technology the center to center separation of scanner apertures arranged in a plane may be as close as 6 mm. With properly arranged reflecting or prismatic elements the apertures may be imaged much closer, even practically adjacent.

Assuming the simple optical case of a 1:1 magnification scan converging optic with 75 mm focal length, the angular disparity between two scans from apertures of apparent 2 mm center to center separation is just 1.5 degrees. This simple estimation of head mounted RSD engineering parameters is coarse, but it illustrates that the maximum angular disparity between adjacent arrayed exit pupil images should be on the order of 1 degree visual angle.

Thus, even using converging optics with small magnification ratios (or large minification ratios; near 1:1), scanning mechanisms may be compactly arranged near the converging optic for head mounted designs. Optical designs are clearly feasible that provide the desired exit pupil separation distances while keeping adjacent image angular disparity near 1 degree visual angle. Still, human perception and acceptance of switched adjacent images of near 1 degree angular disparity is in question.

In summary, the electronic and mechanical engineering challenges associated with the production of arrays of small exit pupils and their coupling to the human eye are not intractable. It seems reasonable to envision an RSD that uses LED's, multiple scanning mechanisms, and a single converging optic to produce an array of separated small exit pupils that may be variably separated and/or individually switched for coupling with the eye's entrance pupil as determined by an integrated eye tracking system. In fact, precisely this type of RSD concept has recently been awarded a U.S. patent [85]. Given that such display systems are feasible, questions remain regarding the human perception of such displays, the response of the visual system, and the acceptability of the display quality offered. If this display concept is rejected due to perceptual anomalies or reduced image quality, further development is moot. If these characteristics are deemed acceptable by human users, detailed knowledge of visual system responses to the display should precede development and aid in design decisions.

2.2.4 Light Metrology Considerations with Retinal Scanning Displays

Much of the new research described in subsequent chapters involves the measurement of light entering the eye in Maxwellian view and natural view conditions. Estimating retinal illumination under these viewing conditions, involving the measurement and comparison of monochromatic and polychromatic sources of very low power, is a complicated matter requiring meticulous control. A focused description of the basic measurement techniques used in this research will avoid lengthy tangential light measurement topics in subsequent chapters that describe new

studies. Readers lacking background in the basic quantifications of light energy and related terminology are referred to International Light's online *Light Measurement Handbook*, to section 1.1 of the *Engineering Data Compendium: Human Perception and Performance*, or to any of a variety of texts on human vision and optics [19, 87].

In quantifying retinal illumination, a unit of convenience, the troland (td), is frequently used by psychophysical researchers. One troland is defined as the retinal illumination provided under the condition where a surface of luminance 1 cd/m^2 is viewed through an entrance pupil of 1 mm^2 . One troland is thus equal to 10^{-6} lm/sr visual angle ($1 \text{ cd} = 1 \text{ lm/sr}$) [75]. The troland value provided by a stimulus is conveniently determined by measuring the luminance of the extended source with any standard instrument and multiplying the luminance by the area of the entrance pupil in units of square millimeters. As visual angle is readily convertible to retinal area for the emmetropic eye, illumination (luminous power per unit area) in units of lumens per square meter may easily be derived from troland. It is important to note that this technique does not make adjustments for the Stiles-Crawford effect. Luminous efficiency corrections for SC-1 may be made using Jacob's equation (eq. 2.3) as discussed in section 2.2.1.2.

The small exit pupil RSD introduces complications to this otherwise simple measurement scenario. First, the RSD exit pupil becomes the limiting entrance aperture for the eye, and it may be quite small. Making precise spatial measurements of a Gaussian profile of such small extent is, at best, inconvenient. Second, the scanning beam of the RSD is not an extended source of luminance readily measured by standard instruments. It does, however, generate a virtual extended image perceptually equivalent to that perceived when viewing an extended surface.

Two general approaches are used to accurately quantify the RSD's retinal illumination. First, assuming the display emits monochromatic light, a measurement may be made of the entire display luminous power by placing the sensor of a standard optical power meter near the exit pupil so that all of the display light falls upon the sensor. An estimate of visual angle must be made in order that a calculation of luminous power per unit visual angle may be performed. Visual angle may be determined by viewing the display in augmented mode, recording the spatial extent of the RSD image on a distant surface, and trigonometrically calculating the solid visual angle subtended. This technique is most accurate for a given individual, but may not represent the emmetropic model eye. Alternatively, the RSD may be allowed to project its image onto a surface for similar angular measurements, although care must be taken to account for error introduced when using a flat projection surface rather than a concave hemispherical one. For

small angles less than 10 degrees, the flat surface introduces negligible error. Further, depending upon the luminance available from the RSD and the ambient conditions, this technique may not provide sufficient display luminance for accurate measurements. It should be noted that in some instances only a relative comparison between two display conditions of equivalent visual angle is necessary. In this case, a simple measure of luminous power is sufficient to calculate comparison ratios.

The second approach is more convenient to implement and also allows broader applicability. This method was developed by Westheimer (1966) [75]. A calibrated Lambertian reflecting surface of reflectance factor, r , is positioned some distance, x , in meters, beyond the position of the Maxwellian image (or RSD exit pupil) that would normally be in the plane of the eye's pupil. The display is projected upon the Lambertian surface. The luminance of the surface, L , in milliLamberts, is then measured with a standard imaging photometer. The retinal illumination, I , in trolands, is calculated as:

$$I(td) = 10^7 L \frac{x^2}{r} \quad (\text{eq. 2.6}) [75]$$

Converting luminance, L , from milliLamberts to the more common metric units of luminance, candelas per square meter, equation 2.6 becomes:

$$I(td) = 3.142 \times 10^6 L \frac{x^2}{r} \quad (\text{eq. 2.7})$$

By this method, accurate and frequent measurements of retinal illumination may easily be made. Further, by using a photometer rather than an optical power meter, the requirement that sources be monochromatic is eliminated. The imaging photometer, by definition and design, measures polychromatic sources with individual wavelength power weighted by the photopic luminous efficiency function, V_λ . Thus, comparisons between various polychromatic and monochromatic sources are facilitated. Stiles-Crawford effects for small pupils are dramatically reduced, but may still be significant in some cases. Jacob's correction may also be applied in this measurement scenario, depending upon conditions.

Westheimer's measurement technique is similar to that involved in the luminance measurement of so-called *flying spot* displays, or laser projection displays. Like the RSD, flying spot displays are characterized by very brief physical persistence of highly luminous pixels. Recently, some problems in using standard measurement devices to measure such displays have been discovered [88, 89]. In particular, some photomultiplier tube (PMT)-based measurement

instruments may not accurately measure luminance of these displays due to momentary saturation of the PMT. This may occur with PMT-based imaging photometers when very bright, very brief lines are scanned across the measurement aperture. Obviously, this scenario is typical of measurements of an RSD by Westheimer's method. Rarer is the scenario that the measurement device may improperly sample and integrate the display luminance over time, resulting in faulty measurements. This may occur with any type of measurement device and is dependent upon many factors, particularly temporal bandwidth limitations. Care should be taken to ensure that measurements of RSD displays by Westheimer's method are accurate. Accuracy may be tested by seeking agreement among multiple instrument types and by tests based upon the standard of perceptual matching [88, 89].

Measurement error of this type was discovered with a PMT-based instrument used in the critical flicker frequency experiment of Chapter 4 and in an initial brightness matching experiment described in Chapter 5. The measurement error was discovered after the completion of a brightness experiment comparing RSD stimuli with polychromatic static stimuli in which unexpected results were obtained. Experimenter tests of the device in comparison with other photometric devices under carefully controlled conditions clearly indicated error when measuring the unique scanning display employed in the experiment. The display was a very rapidly scanning RSD that presented the aperture of the measurement device with temporally irregular illumination by the flying spot of Westheimer's measurement technique. Subsequent analysis by the manufacturer determined that the error was related to improper sampling and integration of PMT output over time due to the inconsistent periodic luminous source. Subsequent experimenter tests showed that manufacturer upgrades to the device rectified the problem. Unfortunately, the brightness experiment results were erroneous and uncorrectable except in the most general manner, dictating a replication of the experiment. Fortunately, the critical flicker frequency experiment results were far less impacted by the small measurement error and valid conclusions were able to be drawn.

2.3 Conclusions from Background and Literature Review Considerations

Many questions remain regarding the visual perception of RSD's and their practical implementation as effective display devices. The primary issues fall into the realms of retinal response factors, opto-physiological factors, and RSD interface engineering considerations for

display interface. A brief review of the pertinent issues in each realm will introduce general experimental concepts and lead to the formation of hypotheses in Chapter 3.

Retinal response to RSD's may be examined in the intensity, temporal, and spatial domains. Based upon the literature, the spatial domain response seems to be well explored and RSD stimulation is not unique in this domain. This domain does not offer promising investigations. However, previous investigations in the intensity and temporal domains have resulted in some contradictory experimental evidence that a unique retinal response to RSD's may occur, particularly as defined by flicker perception and brightness perception. As a first step in the investigation of coupling RSD's to the human visual system, any unique retinal response in the intensity and temporal domains must be validated and quantified. Experimentation in this realm will compare brightness and flicker perception of RSD's to standard visual stimuli in an effort to establish the existence of any unique retinal response. Subsequently, the quantification of any unique retinal response will lead to an investigation its impact on opto-physiological response and/or human-display interface and related engineering considerations.

Literature in the realm of opto-physiological factors offers strong evidence that unique visual system response to RSD's is expected. In particular, the accommodation response and the pupillary response are expected to differ from that with conventional visual displays. The pupillary response is expected to differ primarily due to Stiles-Crawford effects that differ with small pupil stimuli. Experimentation in this realm will endeavor to derive models of pupillary response to both opaque view and augmented view RSD stimuli, with both monocular and binocular RSD display. Such models are desirable as part of a fundamental knowledge base from which intelligent display engineering design decisions may be made. The pupillary response has direct human-display interface impact when considering the implementation of displays with arrays of small exit pupils in which maintenance of proper pupil couplings is critical to RSD perception and image quality.

While the accommodation response is also expected to be unique due to the small exit pupil in Maxwellian view, this phenomenon has been well documented. Although additional research is warranted to investigate the impact of this unique response in terms of display viewing comfort and long-term effects of display use, such investigations are ancillary to the main thrust of this body of research and will not be explored as a part of this effort.

In the realm of RSD interface engineering considerations, the primary concern is with the preservation of small exit pupils in RSD's and their effective coupling with the eye's entrance

pupil. This investigation is a natural progression from the effort to model pupillary response to RSD's, as the pupillary response should be established as a prelude to effective pupil coupling. The optical and power advantages of using small exit pupils also make this investigation an attractive pursuit.

The arrayed small pupil concept is unique in the spectrum of visual display technology. Little study of visual perceptual phenomena under arrayed pupil conditions has been undertaken. Practical engineering constraints seem to lead to arrayed pupil designs that will present noncoincident images on the retina as various exit pupils are individually coupled to the eye. Preliminary estimates indicate that angular disparity on the order of 1 degree visual angle may be expected between adjacent pupil images. The impact of this display method on visual perception of imagery is unexplored. Preliminary investigation in this realm will explore the fundamental perceptual characteristics of this technique to establish its viability as an acceptable display concept.

Additional experimentation will attempt to establish a model of preferred exit pupil separation distance as a function of eye pupil diameter for arrays of constantly illuminated exit pupils. Such a model will provide basic knowledge of perceptual characteristics under these unique conditions and provide answers to human-display interface questions regarding the effective coupling of pupils. Such a model will be particularly applicable to the design of RSD's implementing exit pupil "switching," as described in section 2.2.3.3, by identifying perceptual limitations on maximum exit pupil separation that apply universally with arrayed exit pupil designs. Since arrays with the largest feasible exit pupil separation will provide the greatest effective exit pupil area, human engineering models defining the perceptual limitations and characteristics across the range of exit pupil separation distances will facilitate the design of efficient and effective arrayed exit pupil displays.

As a whole, these investigations will establish the fundamental visual perceptual characteristics with RSD's and provide models of physiological response that are pertinent to display coupling with the human visual system. Further, these explorations will form a base of human factors knowledge from which effective display designs may be derived. Finally, the general display concepts derived from literature and reasoned assertion may provide the impetus for the development of highly effective, highly efficient RSD display technologies that have the potential to be far superior to current display technologies.

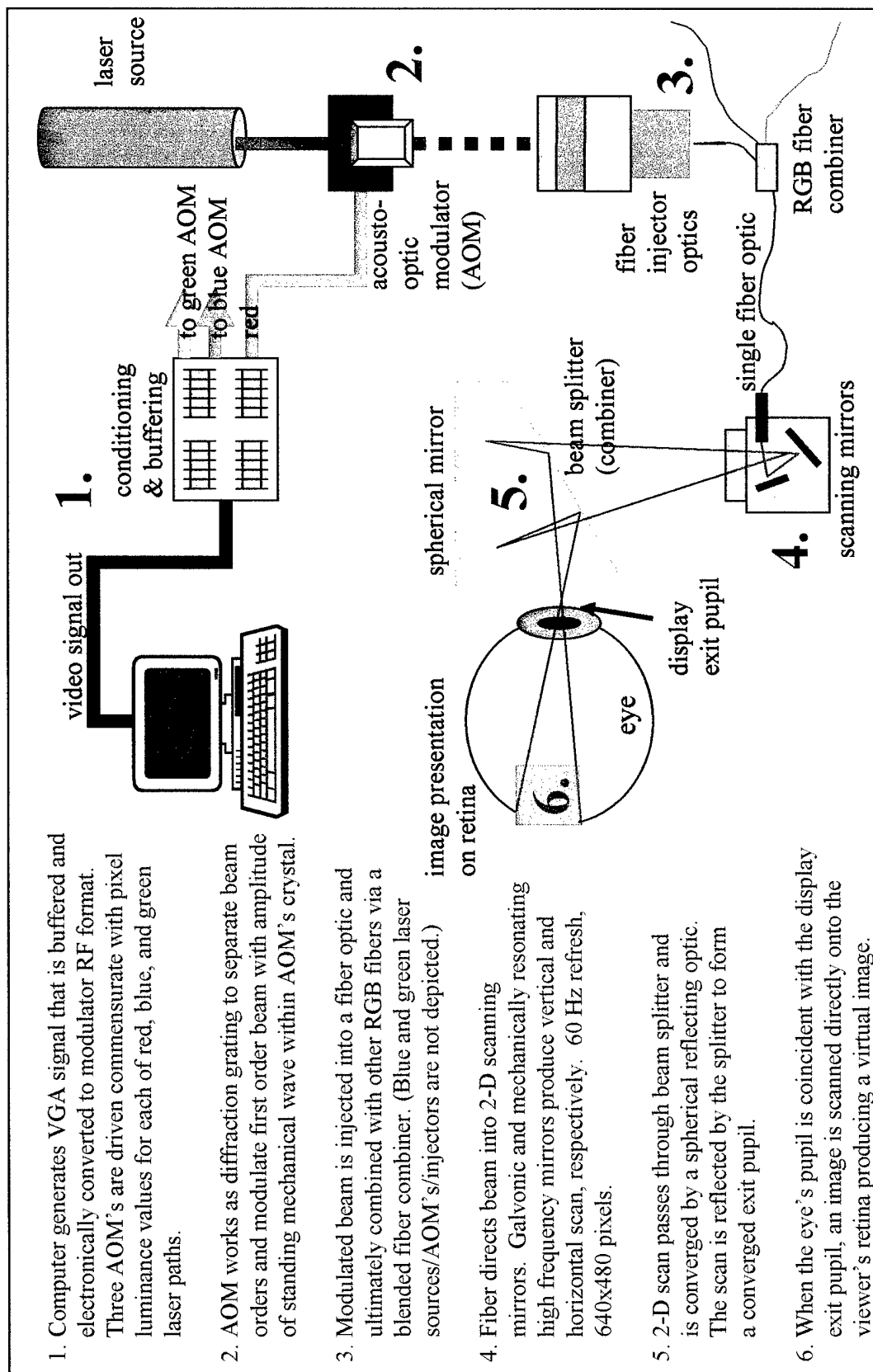


Figure 2.1: Virtual Retinal Display Component Diagram

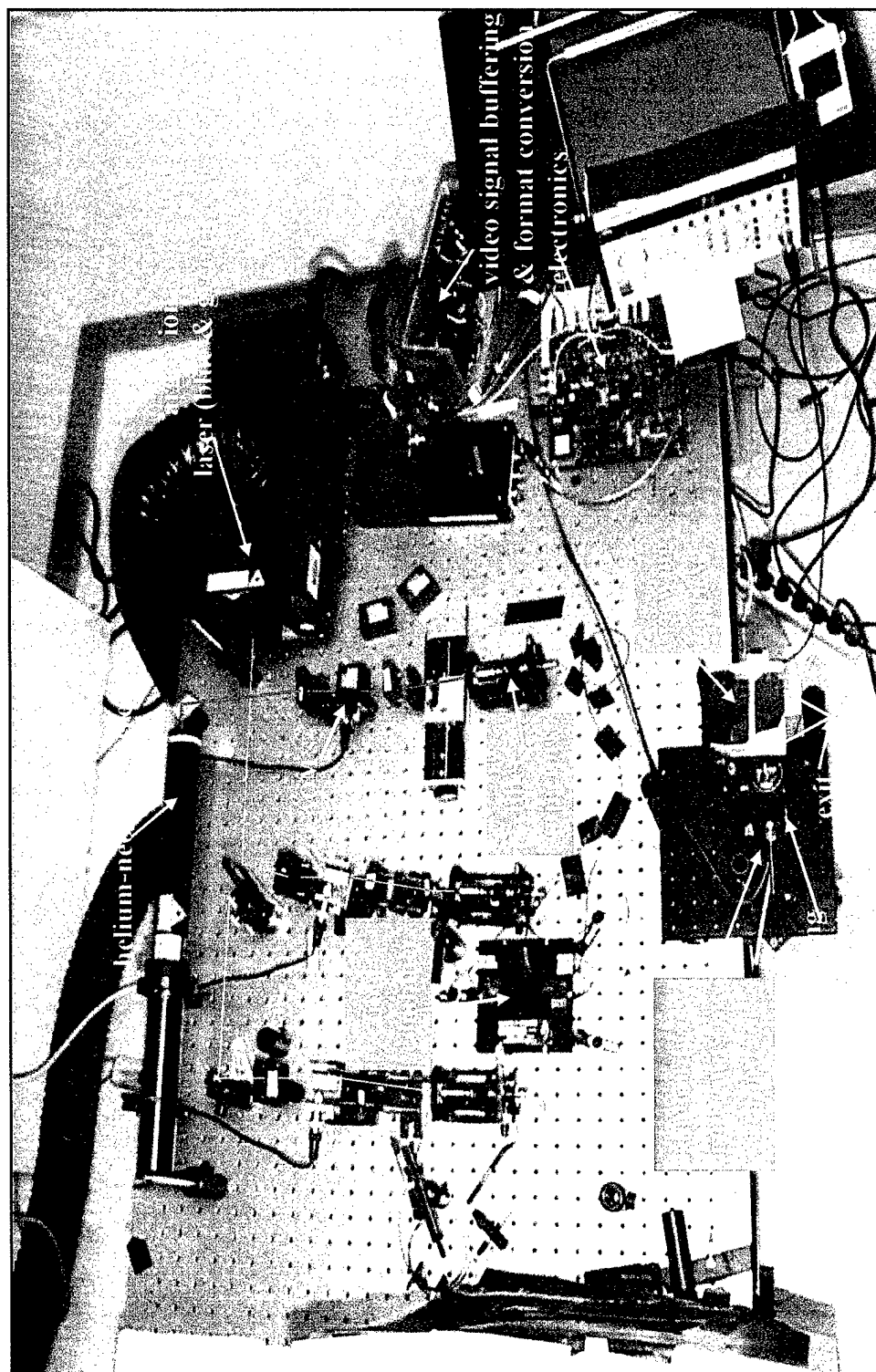


Figure 2.2: Virtual Retinal Display Optical Bench

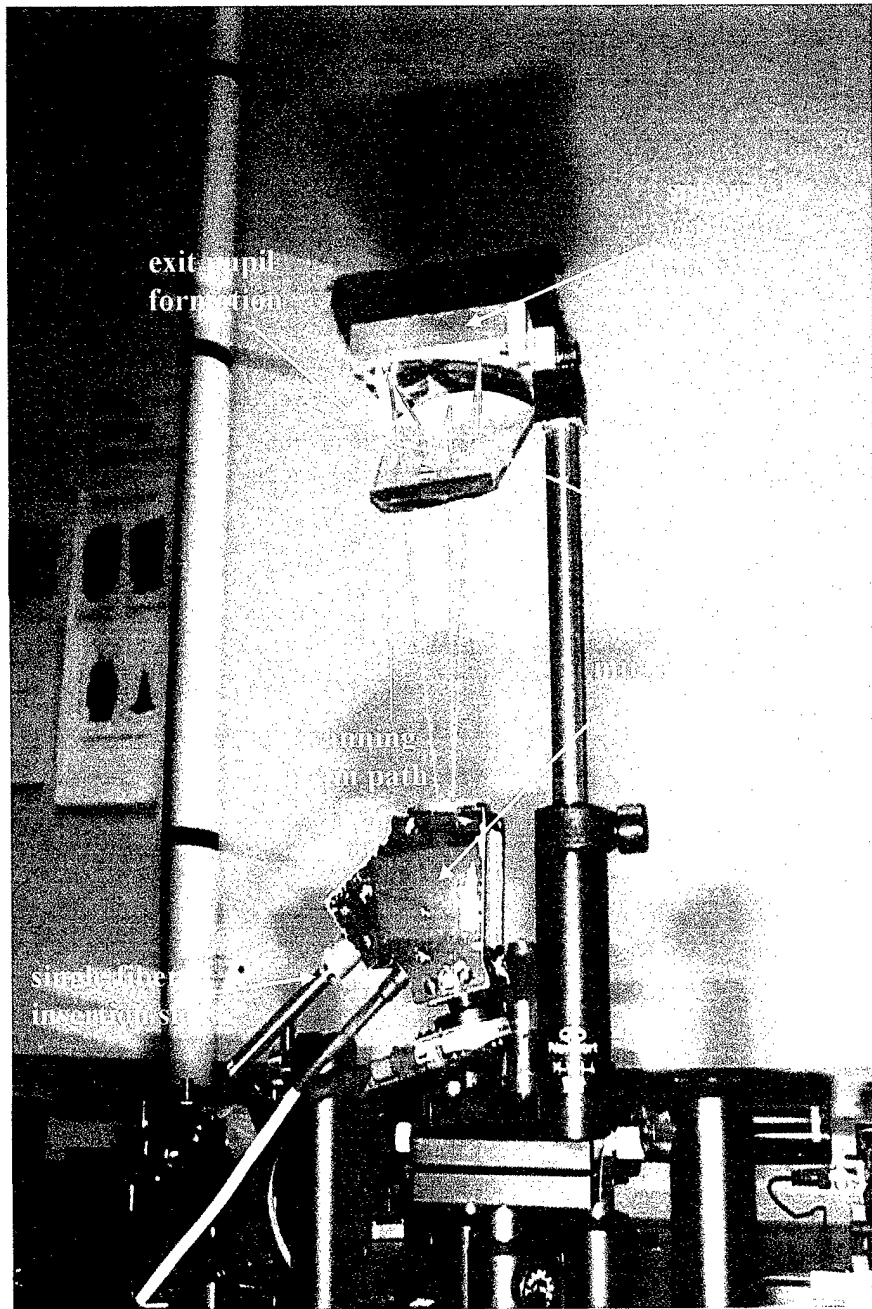
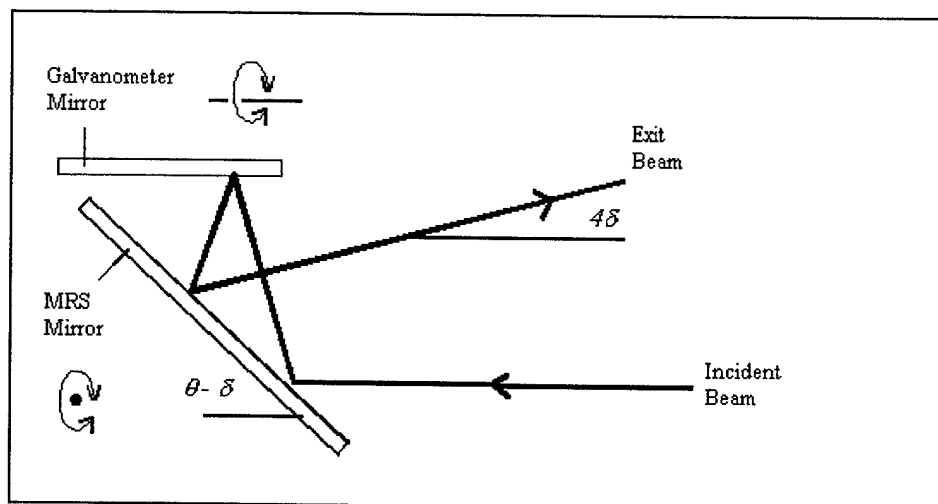
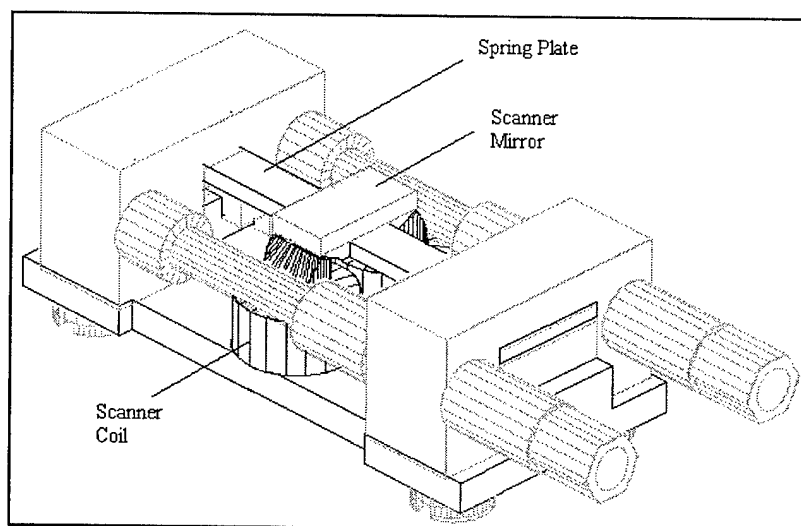


Figure 2.3: VRD Scan Mechanism and Viewing Optics



A. Dual mirror geometry of VRD scanning mechanism.



B. The mechanical resonant scanner (MRS)

Figure 2.4: The VRD Scanning Mechanisms (Tidwell, 1995) [3]

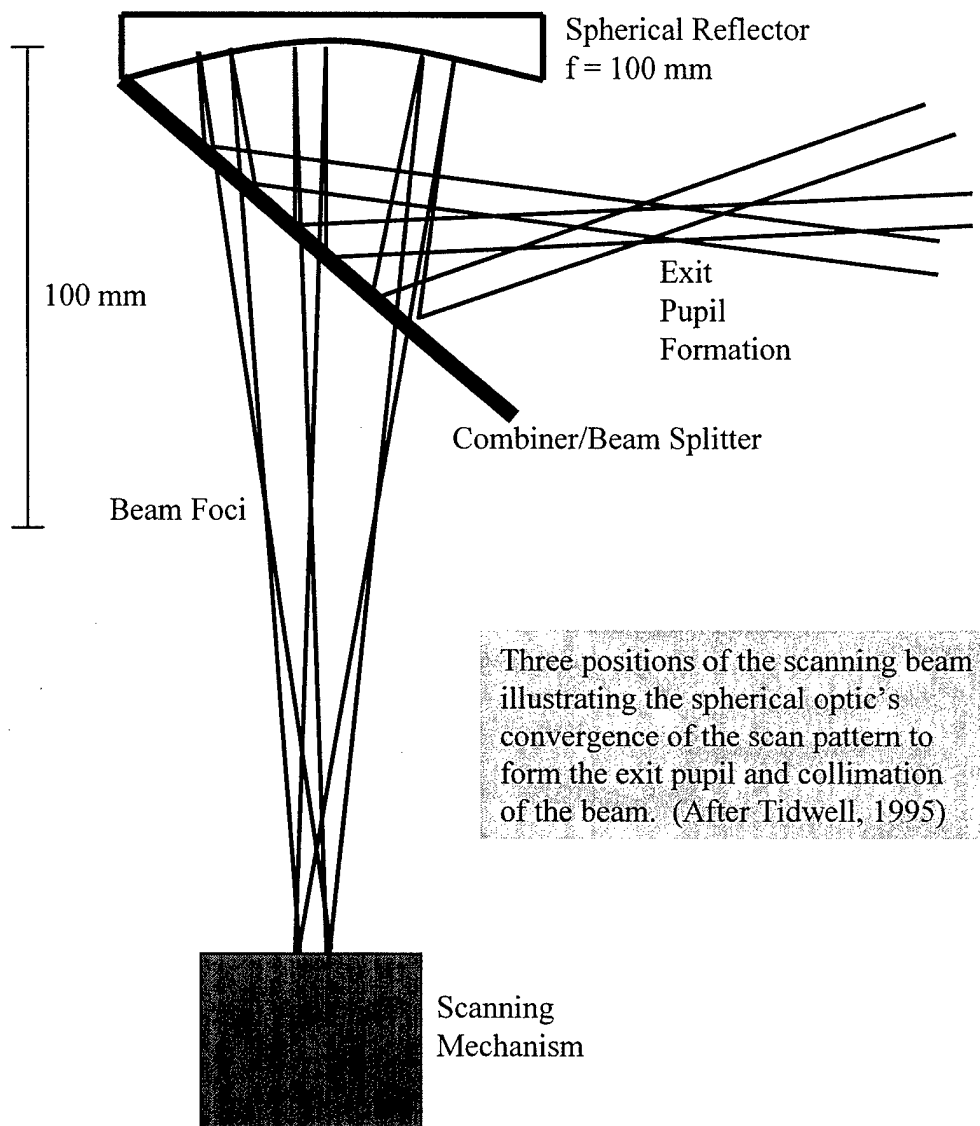


Figure 2.5: Viewing Optics of Virtual Retinal Display

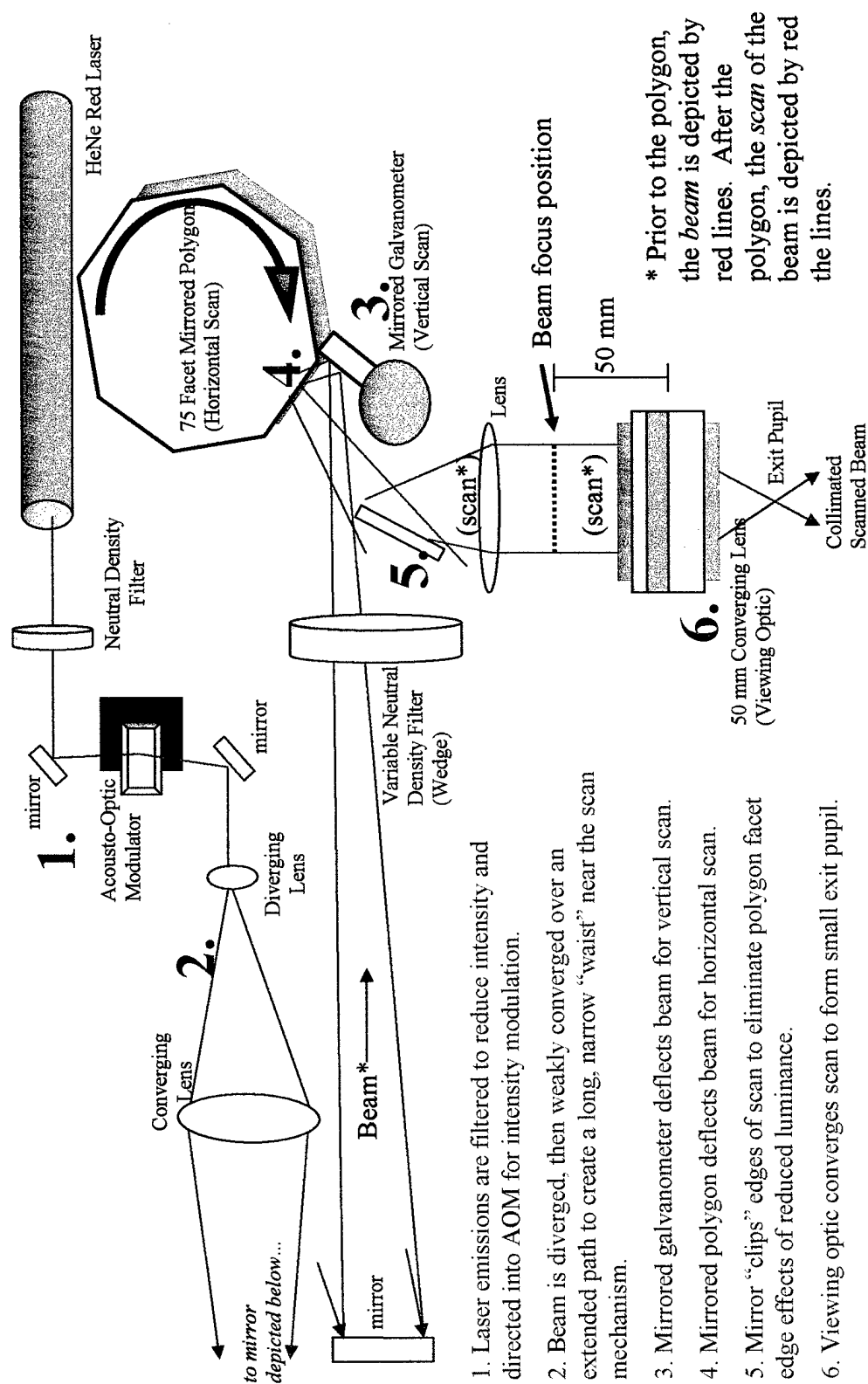


Figure 2.6: VRD Emulator Optical Component Diagram

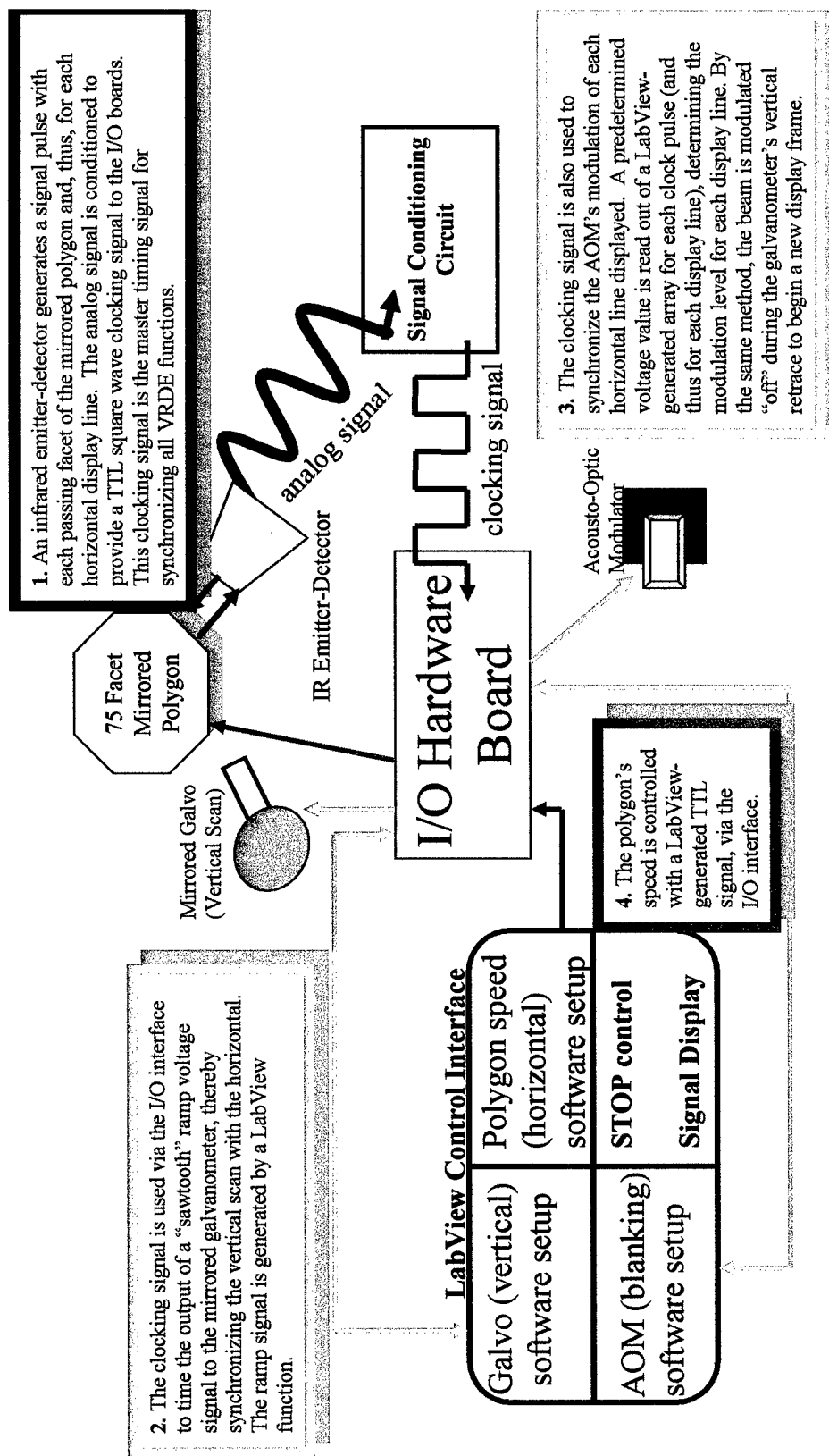


Figure 2.7: Basic VRD Emulator Control Logic Diagram

Arrayed Exit Pupil Emulator. High intensity lamps illuminate apertures in a light stop board. These “windows” are covered with a translucent dispersive filter material. The minified images (12:1) of the windows produce small converged exit pupils for viewing. Window light rays are redirected by mirrors for viewing position convenience, and converging rays are redirected with a beam splitter for augmented view. Exit pupil size, shape, and separation may be adjusted by commensurate changes in the translucent windows. The acetate slide modulates the rays from each window, providing an image within the converged small exit pupil. With small exit pupils of 1 mm diameter or less, the depth of focus is sufficient to provide a sharp image even though the acetate slide is not in the focal range of the lens.

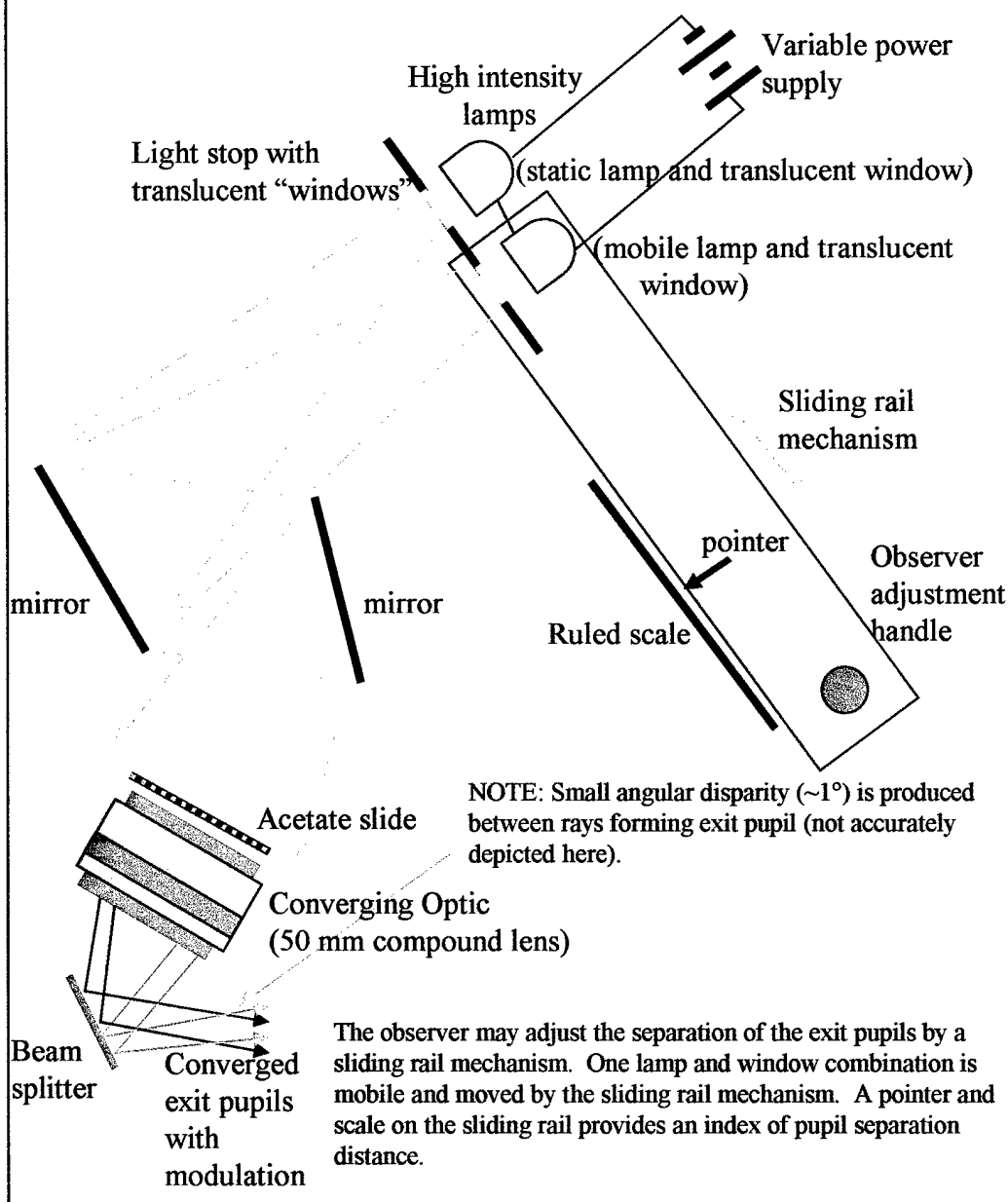
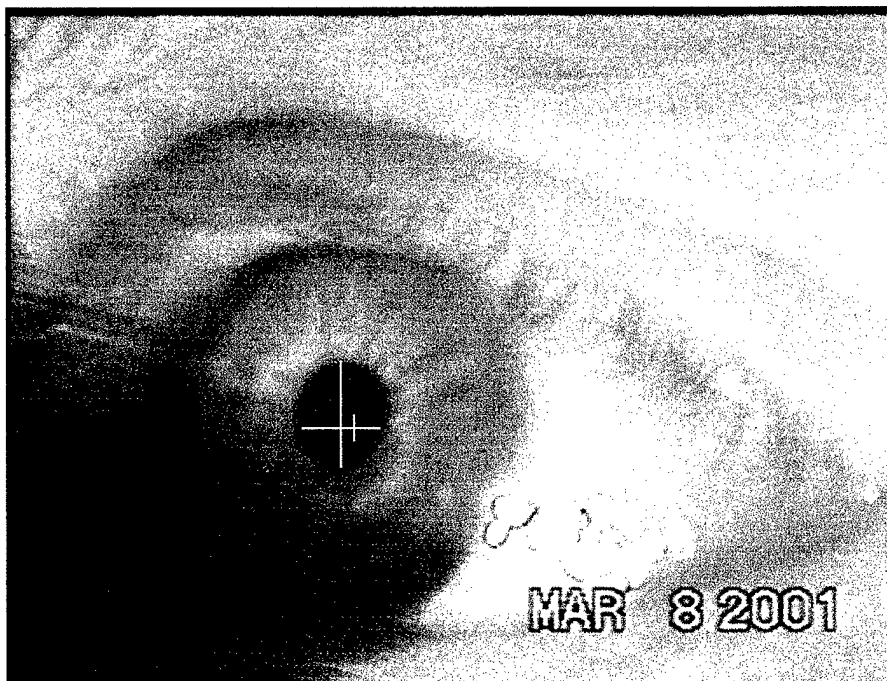


Figure 2.8: Arrayed Exit Pupil Emulator (AEPE)

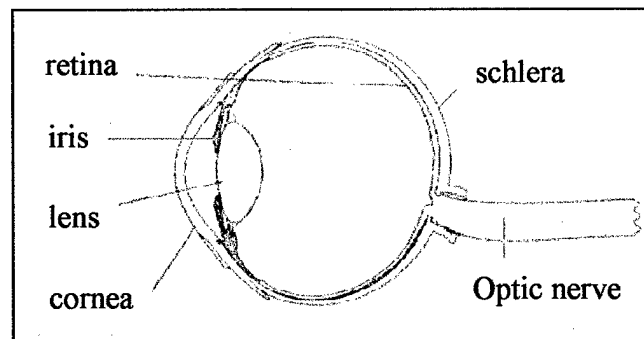


Above: Infrared pupil image under evaluation by pupillometer. Yellow cross is starting position for threshold luminance search routine. White lines connect horizontal and vertical pupil edge positions determined in most recent frame analysis.

Below: Data are written to electronic file in this format.

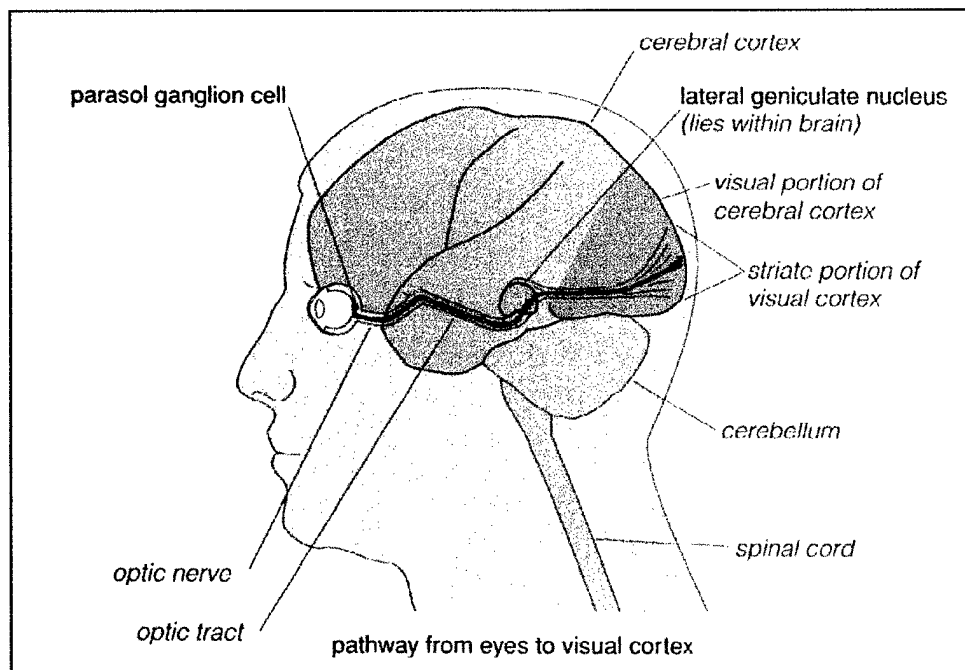
=====		
Demo of Data File		
Frames skipped: 0 Pixels per mm: 22		
Time (ms)	Pixel Diameter	Millimeter Diameter
-----	-----	-----
0	92	4.18
50	93	4.23
160	92	4.18
160	93	4.23
220	93	4.23
330	92	4.18
330	90	4.09
380	89	4.05
440	87	3.95
550	87	3.95
550	86	3.91
650	83	3.77
710	82	3.73
710	82	3.73
760	81	3.68

Figure 2.9: Pupillometer and Output Data



Eye graphic used with permission from Rodieck (1998).

Figure 2.10: Cross Section of Human Eye



Graphic used with permission from Rodieck (1998).

Figure 2.11: Pathways of Neural Signals from the Retina

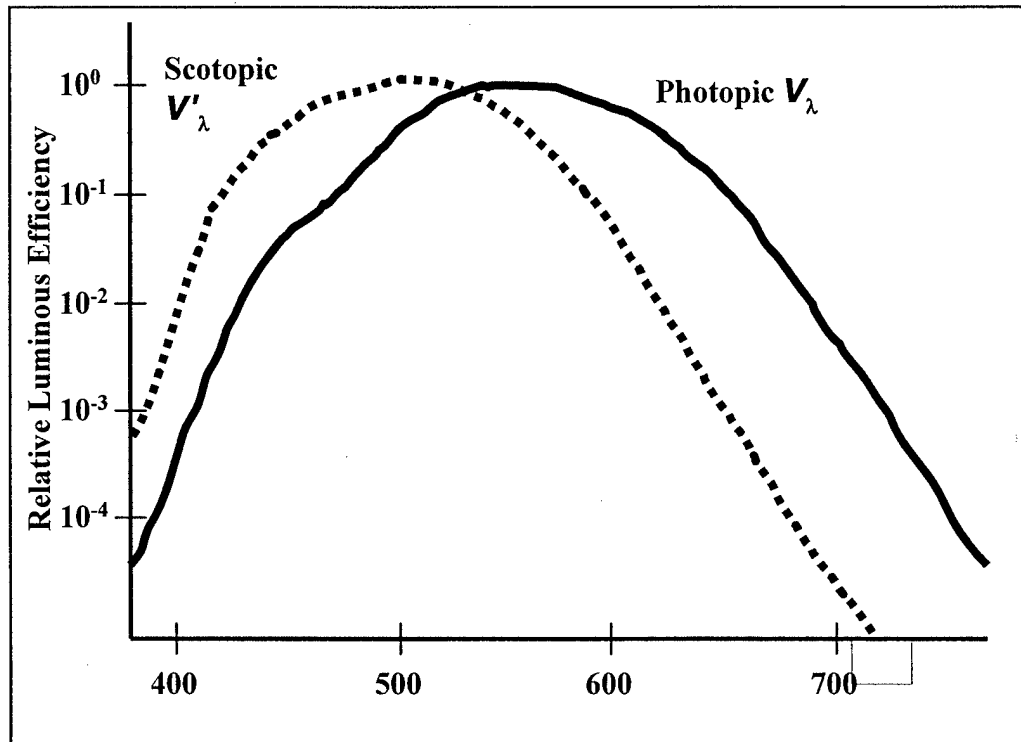


Figure 2.12: Scotopic and Photopic Luminous Efficiency Functions
(after Ryer, 1997)

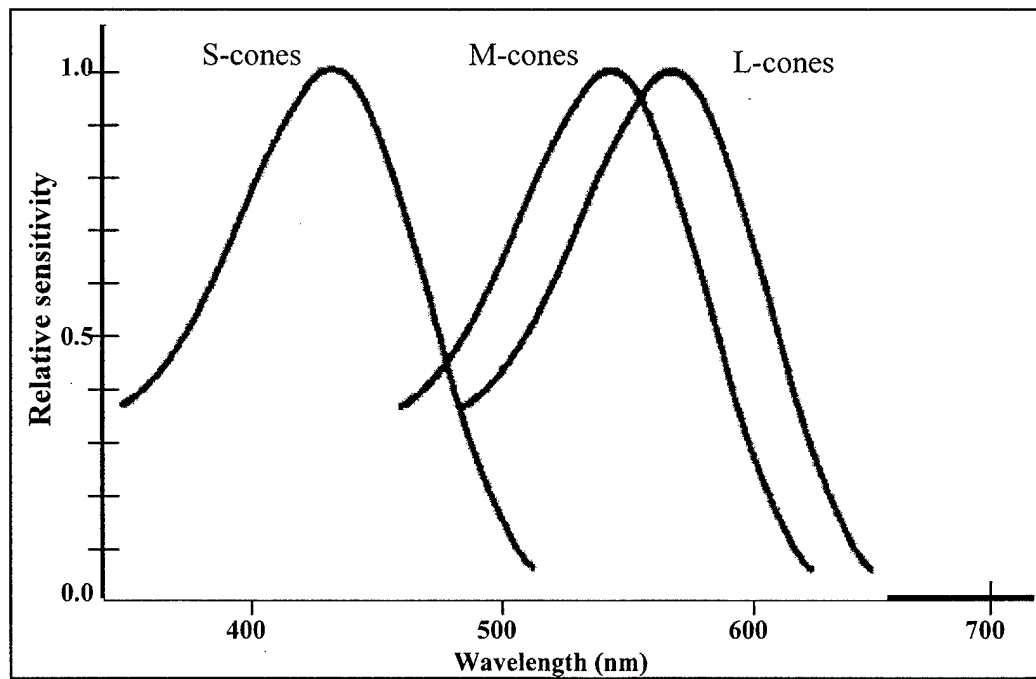
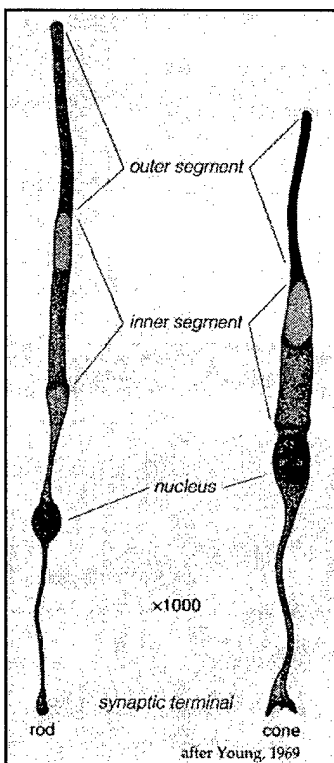


Figure 2.13: Cone Photoreceptor Relative Sensitivities
(after Goldstein, 1999)



Graphic used with permission from Rodieck (1998).

Figure 2.14: Rod and Cone Photoreceptor Cells

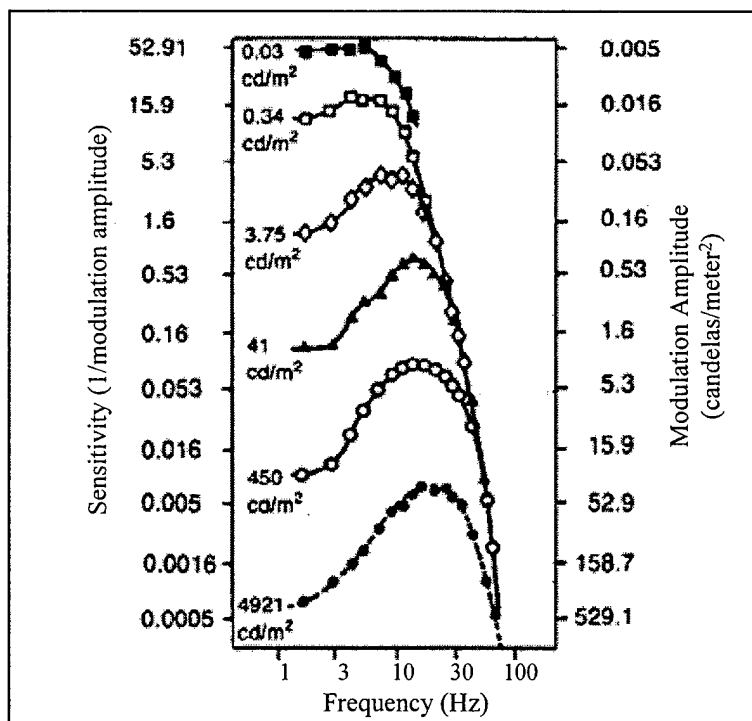


Figure 2.15: Human Sensitivity to Flicker
(from Kelly, 1961)

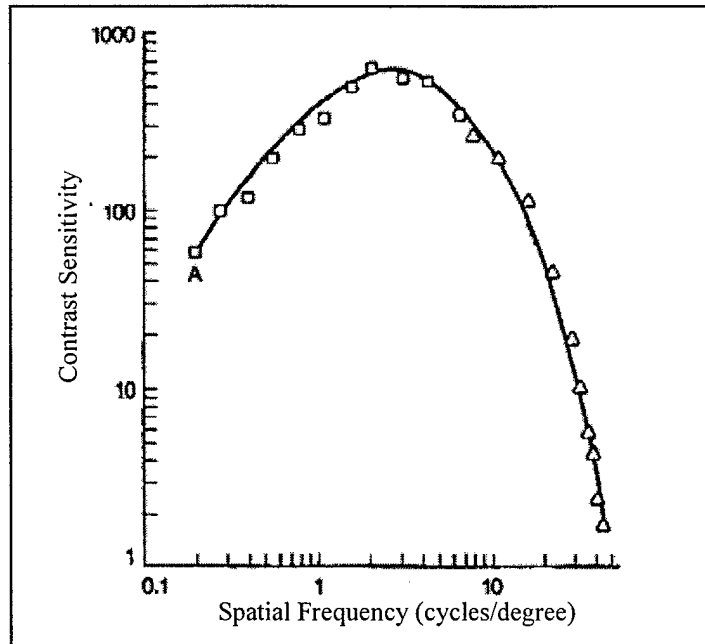


Figure 2.16: Contrast Sensitivity Function
(from Campbell and Robson, 1968)

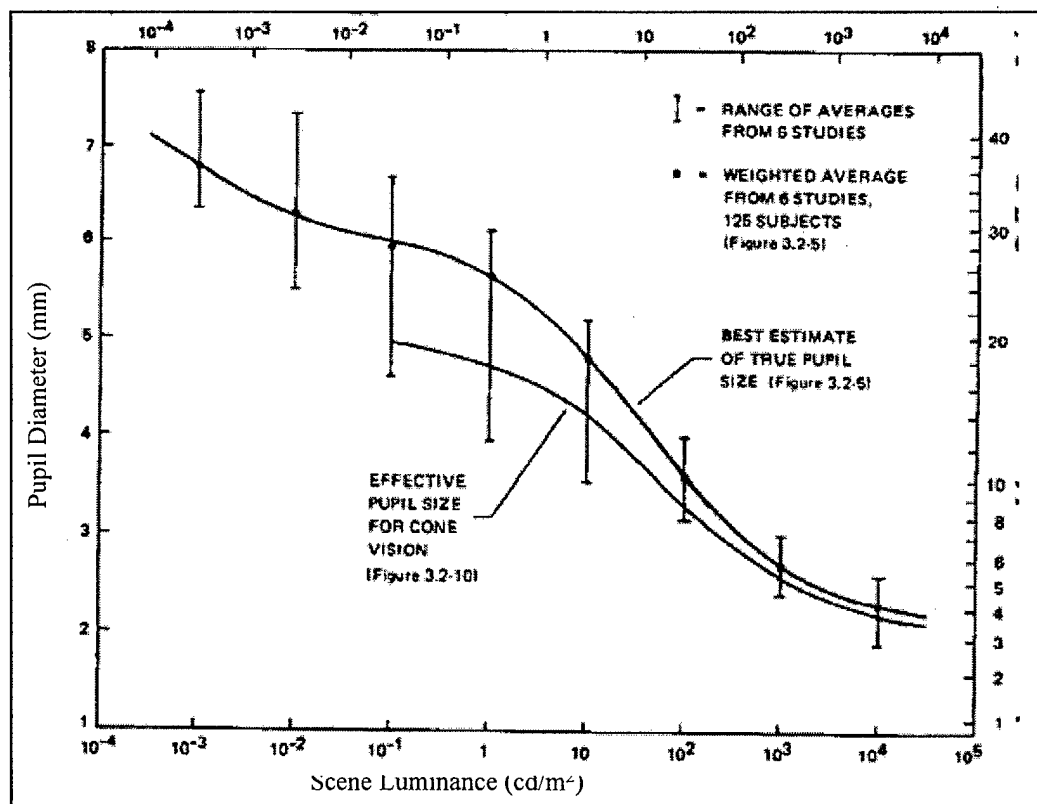


Figure 2.17: Eye Pupil Size as a Function of Scene Luminance
(from Farrell and Booth, 1984)

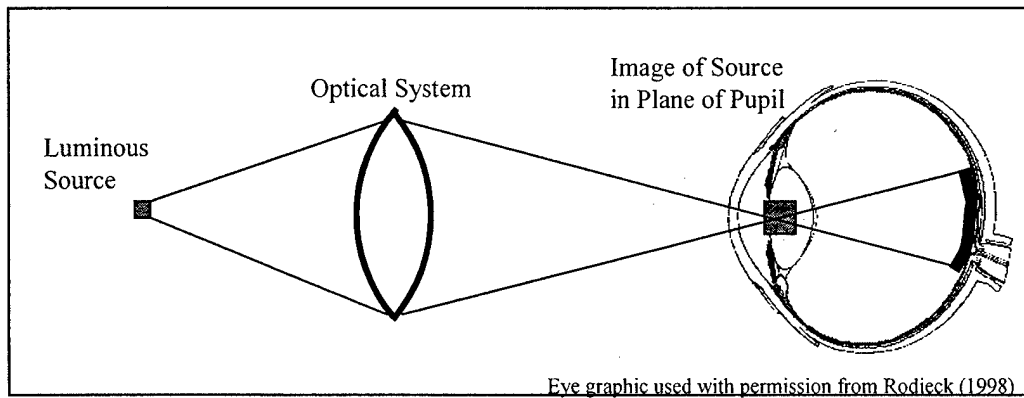


Figure 2.18: Maxwellian Viewing Arrangement
(after Westheimer, 1966)

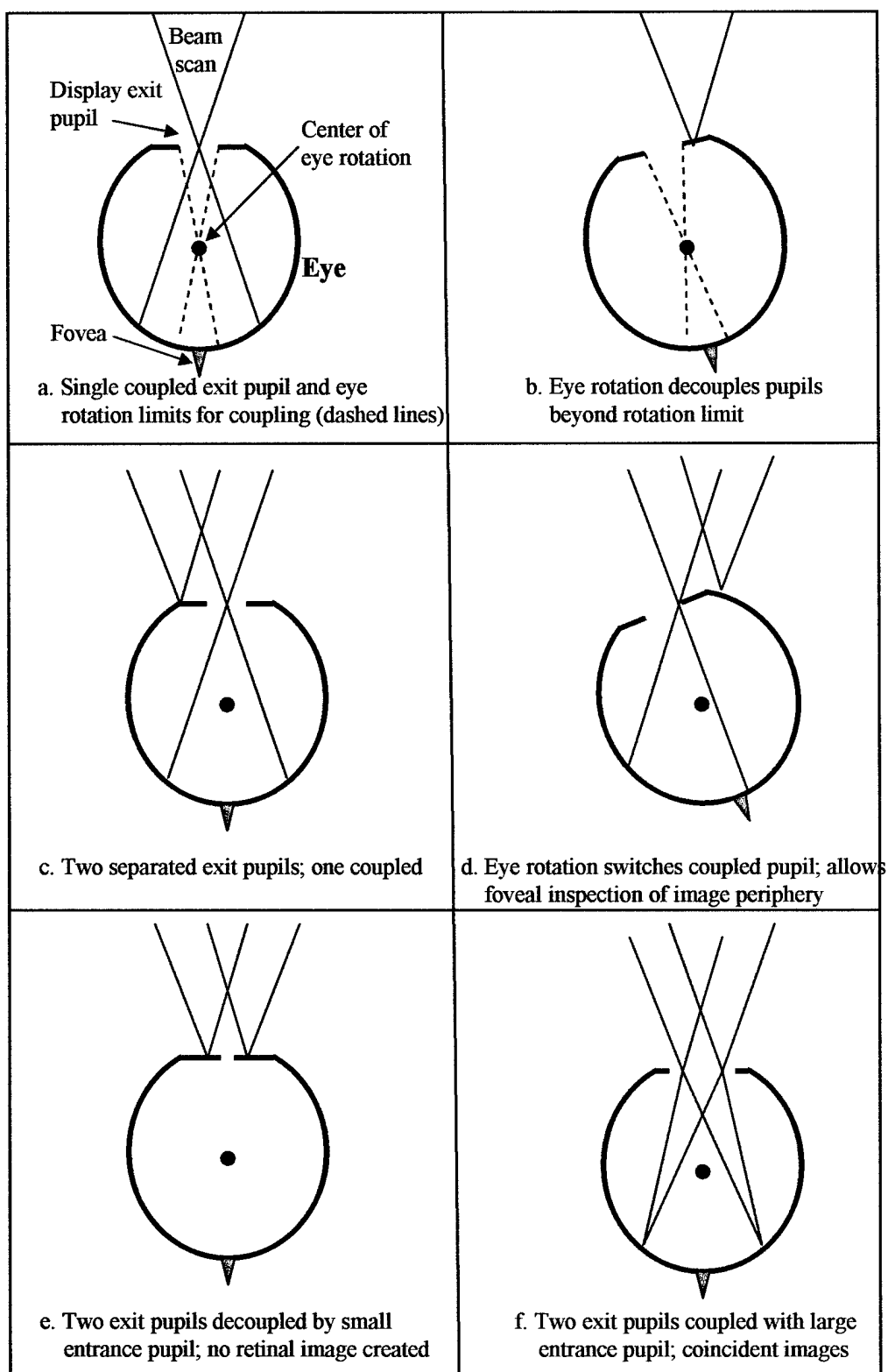
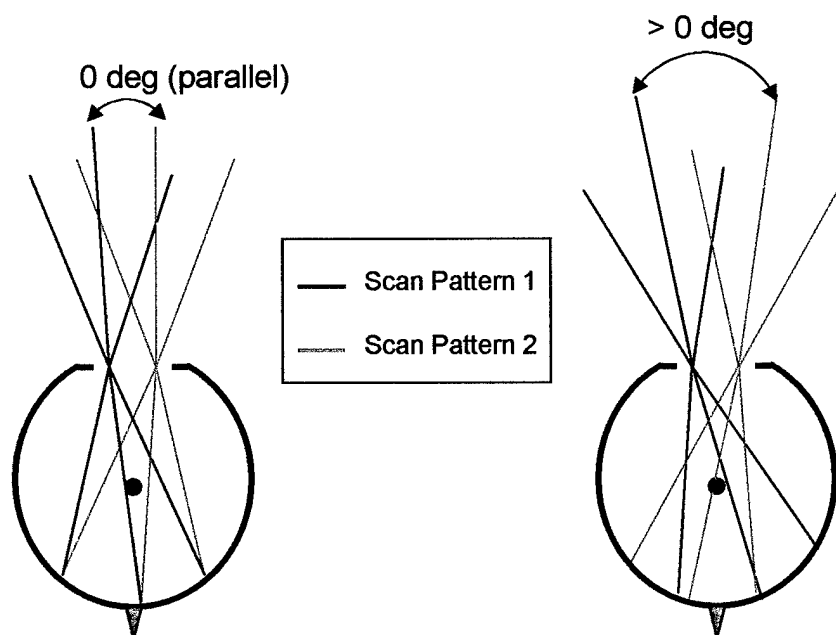


Figure 2.19: Geometry of Eye Rotations with Small Exit Pupils



Parallel Scan: Central scan rays and all matched rays between scans are parallel, resulting in coincident retinal images.

Non-Parallel Scan: Central scan rays and all matched rays between scans are related by an identical angle greater than 0 degrees, resulting in non-coincident retinal images.

Figure 2.20: Simplified Geometry of Parallel versus Non-parallel Beam Scans as Applied to Pupil Coupling

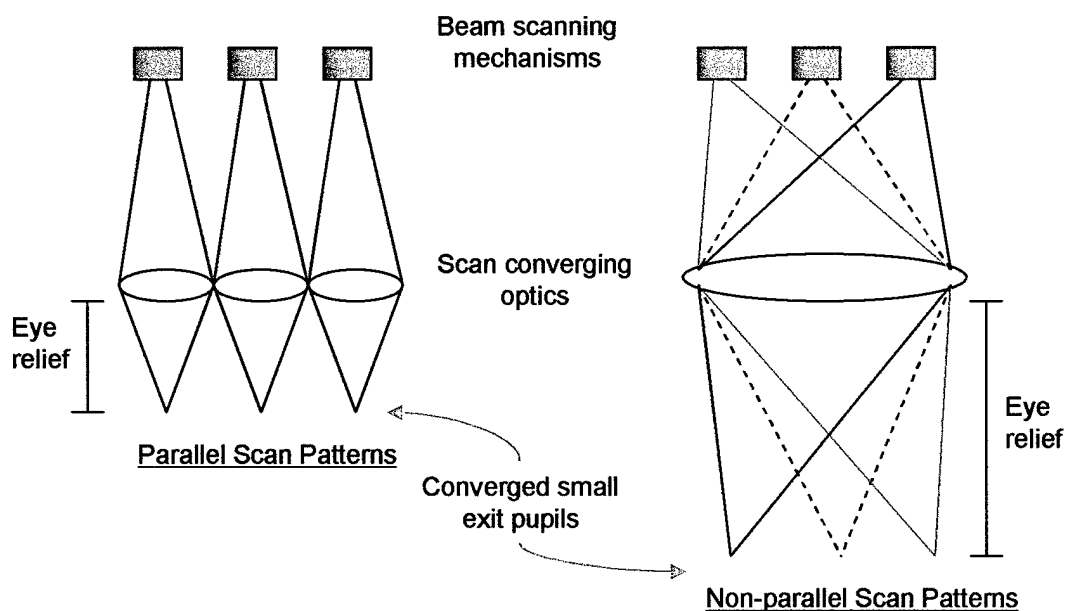


Figure 2.21: Simplified Geometry of Parallel and Non-parallel Beam Scan Generation

Chapter 3: General Hypotheses

This chapter summarizes three major hypotheses, related sub-hypotheses, and additional minor hypothetical effects under investigation. Each hypothesis is described and defended by considering research results from literature, supporting logic, and reasoned assertions. Ancillary topics are also discussed, when relevant. The purpose of this chapter is to specify the theoretical framework within which new research is conducted.

3.1 Hypothesis 1: Retinal response to, and visual perception of, retinal scanning display stimuli is not anomalous.

This hypothesis refutes the findings of Kelly, et. al. (1998) and earlier cursory observations indicating reduced sensitivity to flicker and enhanced brightness perception when viewing the VRD, as compared to perceptions with other conventional display devices [79]. There is insufficient evidence in literature to properly support the proposition of an anomalous retinal response to RSD stimuli, and the flicker sensitivity results of Kelly, et. al. (1998) are subject to question due to relatively poor experimental control and the high variance reported between subjects viewing RSD stimuli. Granted, the physiological workings of the retinal neural network are poorly understood. Rodieck's comments regarding amacrine cell lateral function is but one unknown within the retina's complexity. However, the psychophysical literature offers no perceptual evidence that unique physiological responses are to be expected from RSD stimulation. If this hypothesis is not supported and RSD stimuli are found to produce anomalous retinal responses, current theories of human vision related to brightness perception and temporal perception may require revision to explain the anomalous results. Additionally, such results may have implications for the engineering of RSD's and their interfacing with the human visual system. Research associated with this hypothesis is reported in Chapters 4 and 5.

3.1.1 Sub-hypothesis 1a: Brightness perception of retinal scanning displays is equivalent to that of conventional luminous sources.

This sub-hypothesis specifically refutes early cursory observations of the VRD by Furness, Pryor, and others at HITL (Thomas Furness, 1998, Personal Communication). These observations were

not conducted under controlled experimental conditions, and no accounting for Stiles-Crawford effect or entrance pupil size was made. Further, the observations were made in the low-luminance portion of the photopic range only, as observations were limited by the output power of the original VRD.

Pryor, Nagata, and Viirre (1997) reported perceptual brightness matching data that compared the VRD power output at the exit pupil (in nW) to the luminance of a CRT (in cd/m^2) [90]. While these researchers seem to claim that the VRD is providing an equivalently bright image with much greater efficiency than the CRT, this claim can only be applied to the respective displays' power output and does not address visual system response. These data do not allow proper comparison of retinal response to RSD and CRT stimuli since no estimations of retinal illumination due to the VRD or CRT were attempted.

The investigations of Gilmer (1937), as introduced in section 2.2.1.3, are particularly relevant to this hypothesis [55]. This researcher discovered that the luminosity of a visually fused flickering display is equivalent to that of a constant luminous source (or to that of another visually fused flickering display) when the time averaged luminances of the two displays are equivalent. His data investigated flicker pulses as brief as 8 ns, and flicker frequencies up to 200 Hz. As previously discussed, for a given position on the retina, the exposure time to VRD illumination during each of the 60 Hz frame refreshes is approximately 40 ns. These parameters are well within the range of values investigated by Gilmer, and numerous other researchers since. Given these data, no enhanced perception of brightness with an RSD should be expected, other than that accounted for by the geometry of the RSD stimuli and the Stiles-Crawford effect.

VRD inventor Thomas Furness has speculated that observations of unusual brightness and flicker perception with the VRD may be the result of unique excitation of lateral effects in the retina by the brief and intense impulse function of the RSD combined with the spatiotemporal raster scan and coherent light (Thomas Furness, 1999, personal communication). Enhanced response of the waveguiding photoreceptors to the pulsed coherent energy has also been postulated as a physiological source of these phenomena. Rodieck highlights the response of the broadly reaching amacrine cells to light stimuli on the photoreceptors and supports the possibility of global lateral effects via these cells [16].

This possibility can be positively ruled out only through experimentation, since the response to stimuli of a nature precisely like that of the VRD presented across large section of retina has not been widely reported in literature. However, a vast number of retinal studies, both

psychophysical and physiological, have been conducted with coherent light stimuli. These studies have examined luminous efficiency, flicker perception, photoreceptor electrophysiological response, cortical response to stimuli, and other visual system attributes. The reader is referred to *any* of the voluminous recent literature involving these areas of research. None has reported any anomalous results related specifically to stimulation of the retina with coherent light.

Further, the raster pattern of an RSD is unique only in the extreme brevity of the physical persistence of pixels imaged on the retina and the longitudinal alignment of light rays with photoreceptor cells. Any CRT presents a similar spatiotemporal pattern across a large section of the retina, albeit with longer physical persistence and a wider variety of photoreceptor incidence angles. Further, phosphorescence times are highly variable with phosphor type and refresh rate, and some are quite brief, on the order of microseconds, with the majority of power delivered during the brief initial rapid peak of excitation [76, 91-93]. Thus, the pattern of stimulation provided by an RSD is not entirely unique. Again, no reports are found in literature of anomalous perceptual responses in the comparison of CRT displays to other non-raster or steady luminous sources. For the spatiotemporal pattern theory to be valid, one must assume an effect related to an abrupt threshold of stimulus duration, stimulus intensity, or a combination of both that is not typically crossed by CRT-derived retinal stimuli.

Therefore, given the absence of solid experimental evidence of RSD brightness enhancement, and; given the literature supporting the applicability of the Talbot-Plateau law to RSD stimulation, and; given the absence of literature regarding the effects of coherent light and spatiotemporal patterns on brightness perception; brightness perception of RSD's is hypothesized to be equivalent to brightness perception of conventional luminous sources with equivalent time averaged energy on the retina. Research related to this hypothesis is reported in Chapter 5.

3.1.2 Sub-hypothesis 1b: Flicker perception of retinal scanning displays is equivalent to that of conventional visual displays.

This hypothesis specifically refutes the reports of Kelly, et.al. (1998) of reduced flicker sensitivity with RSD stimuli [79]. These researchers report an average ratio of threshold contrast for flicker detection, VRD/CRT, of 2.0. That is, detection of 30 Hz flicker with the VRD required twice the contrast between bright and dim flickering presentations as did identical detection with a CRT. This study also indicates large variance in detection thresholds between individual subjects with

the RSD. The psychophysical method of adjustment was utilized in this study, and head stabilization for viewing the VRD was accomplished with a chin rest only. Experimental sessions were conducted over a course of several weeks (Dr. John Kelly, 1998, personal communication) [79].

This experiment was conducted with poor experimental controls that may have induced random error and invalidated the results. The psychophysical method of adjustment allows the detection of relatively large effects, but it sacrifices some experimenter control. In this study case, subjects were instructed to make adjustments until flicker was "just perceptible," necessarily leaving the definition of "just perceptible" to the interpretation of each individual subject. While not an invalidating problem, other methods may offer improved experimental control. The study was conducted over a period of weeks, with experimental sessions for same subjects being separated by several days in some cases. This only exacerbated the interpretation problem mentioned above, as individuals vary in performance from day to day [94].

Further, due to mechanical drift inherent in the mounting of optical fibers near the beam injection optics of the VRD (see section 3.1.1), and due to intervening accidental misalignments of the beam injection apparatus, the power output of the VRD was not likely consistent over the long course of this experiment (Dr. John Kelly, 1998, personal communication). This factor certainly introduced increased between subject variance.

Perhaps most significantly, only a chin rest was used to stabilize the position of the head and eye while viewing the VRD. With a chin rest, gross head movements are poorly controlled and may induce severe variability in the position of the VRD exit pupil relative to the entrance pupil of the eye. Given the potential magnitudes of the Stiles-Crawford effect, such variability in relative pupil positions could dramatically increase the variance within and between subjects, invalidating the results. This problem would not significantly affect observations of the CRT that are not in Maxwellian view, but it certainly places into question the mean luminosity of the VRD. Flicker perception is a function of luminosity (section 2.2.1.3), and reduced luminosity conditions require increased contrast for flicker detection. Since head movements are likely to reduce the mean VRD luminosity from the pre-trial maximum level achieved during CRT-VRD brightness match, the effects reported by Kelly may be entirely due to the Stiles-Crawford effect as induced by poorly controlled head motion. The larger variance in VRD data from this study is consistent with this assertion.

The literature does not support the expectation of anomalous flicker sensitivity with RSD stimuli. The results of Brown and de Lange, as mentioned in section 2.2.1.3, indicate that only the fundamental temporal frequency of Fourier transformation has a significant effect on flicker perception. Thus, even though the RSD's temporal signature is a brief Gaussian impulse function rather than a square, sine, or exponential decay function, flicker perception should be essentially equivalent to that of other flickering sources, such as CRT's or square "chopped" sources.

The psychological persistence of brief luminous stimuli (section 2.2.1.3) seems to be the limiting factor in flicker perception. Stimuli of duration less than approximately 0.15 second, even those on the order of nanoseconds, provide the observer with equivalent temporal perception of the stimulus -- that of an instantaneous flash [18]. The luminosity of the stimulus adheres to Bloch's law (section 2.2.1.3). The considerations of the Talbot-Plateau law, as discussed in the previous section, also support this conventional theory. Under the assumptions of these established psychophysical laws, flicker perception of an RSD should not vary from that of conventional flickering luminous sources.

Engineering models intended to predict flicker sensitivity under varying electronic display conditions have been constructed. Farrell (1986) derived a model for predicting CFF of displays [95]. This model, although not intended to apply directly to RSD displays, predicts slightly greater sensitivity to flicker with a VRD-like RSD than with a CRT. This is based primarily on the difference in physical persistence times between the two display types. From the literature, it is unclear whether this model may properly be applied to RSD stimulation at frequencies below true CFF (as in flicker contrast threshold studies), as some function extrapolations must be assumed. However, it seems clear that the model does not predict reduced RSD flicker sensitivity under the conditions typical of RSD-CRT comparison.

Therefore, given the potential errors inherent in previous flicker research with RSD's, and; given that the established psychophysical laws relating to flicker perception do not support anomalous flicker perception of RSD's, and; given that conventional flicker models seem to predict slightly *greater* sensitivity to flicker with RSD stimuli; flicker perception with retinal scanning displays is hypothesized to be equivalent to flicker perception of other standard flickering luminous sources. Research related to this hypothesis is reported in Chapter 4.

3.2 Hypothesis 2: Pupillary responses of the visual system to small exit pupil retinal scanning displays differ from the responses to equivalently perceived conventional displays.

The pupillary response to RSD stimuli will be affected by the increased effective luminance due to the reduced Stiles-Crawford effect. This hypothesized effect is strictly due to the opto-physiological factors of pupil size and the Maxwellian view geometry. Confirmation of this hypothesis and the resulting models of pupillary response will provide information necessary for subsequent engineering of RSD-visual system interface techniques. Specifically, models of pupillary response derived from this research may be used to design coupling methods for small exit pupil displays to the eye. Research related to this hypothesis is reported in Chapter 6.

3.2.1 Sub-hypothesis 2a: For binocular opaque view RSD stimuli and photopic luminance conditions, actual pupil size follows a pupil size function associated with the Stiles-Crawford-adjusted *effective* pupil size.

As described in sections 2.2.1.2 and 2.2.2, a properly coupled Maxwellian view system with a small exit pupil, or pupil plane image size, will increase the efficiency of phototransduction as compared to that of a naturally viewed scene of equivalent corneal flux density. The Stiles-Crawford effect of the first kind is operative in this luminous enhancement. Farrell and Booth (1984) summarized the SC-1 effective pupil size in comparison to actual pupil size, as depicted in figure 2.17 [61]. This curve plots the effective pupil diameter as determined by the actual pupil diameter adjusted by Jacob's effectivity ratio as applied to pupil areas (eq. 2.3, section 2.2.1.2) [39].

If a centrally coupled small exit pupil Maxwellian view system is observed, the efficiency with which phototransduction occurs in the retina is enhanced. That is, substantially more photons will be absorbed by the photoreceptive cells of the retina using a centrally coupled small exit pupil than will be absorbed with an equivalent corneal flux density using the entirety of the eye's entrance pupil. The pupillary control system will respond to the retinal absorption of photons in the normal manner and is not directly influenced by the optical geometry of light impinging on the retina. It will be indirectly affected by this geometry, however, since the photoreceptive cells themselves will respond differentially, depending upon the optical geometry as described by the Stiles-Crawford effect of the first kind.

Therefore, the pupillary control system should respond as a function of the *effective retinal illumination*. Under centrally coupled small exit pupil conditions, the eye pupil should

respond as it does to naturally viewed stimuli of the same *effective retinal illumination*. Thus, for a constant value of corneal flux density, the effective retinal illumination from a centrally coupled small exit pupil Maxwellian view system is greater than the effective retinal illumination of a naturally viewed scene by a factor equal to the effectivity ratio. Retinal illumination is proportional to eye pupil area under natural viewing conditions. Therefore, it reasons that the pupil area determined by the pupillary response system under small exit pupil Maxwellian view illumination should be equal to the pupil area for natural illumination multiplied by the effectivity ratio factor.

By this assertion, the effective pupil size function of figure 2.17 should predict mean pupil diameter of a population viewing RSD stimuli. However, this function was derived from a meta-analysis, is based upon highly variant data, and no precise report of study conditions is provided. As Stanley and Davies assert, much of the variance among such studies may be attributable to differences in the size of the adapting fields used [62]. The derivation of an effectivity ratio-adjusted corneal flux model, based upon the previously introduced work of Stanley and Davies, should provide a better instrument for the prediction of pupil size with RSD stimuli.

Equation 2.5 (section 2.2.1.6) is the iteratively derived function of Stanley and Davies describing pupil diameter as a function of corneal flux density in $\text{cd/m}^2 \text{ deg}^2$. Calculating the pupil area, A , associated with pupil diameter, D , from Stanley and Davies' function, and multiplying this area by the respective effectivity ratio, E , provides a new prediction of pupil area as a function of corneal flux density for a Maxwellian view system with negligible Stiles-Crawford effect:

$$A_{Max} = AE \quad (\text{eq. 3.1a})$$

where A_{Max} is the pupil area under small exit pupil Maxwellian view conditions. Transforming area units in equation 3.1a back to the more convenient units of diameter yields:

$$D_{Max} = \sqrt{\frac{4AE}{\pi}}, \quad \text{or simply,} \quad D_{Max} = D\sqrt{E} \quad (\text{eq. 3.1b})$$

where D_{Max} is the pupil diameter under small exit pupil Maxwellian view conditions. Substituting equations 2.5 and 2.3a for D and E , respectively:

$$D_{Max} = (7.75 - 5.75 \frac{(F/846)^{0.41}}{(F/846)^{0.41} + 2}) \sqrt{1 - 0.0106D^2 + 0.0000419D^4} \quad (\text{eq. 3.1c})$$

Recall that F is the corneal flux density in $\text{cd/m}^2 \text{ deg}^2$ and D is the predicted pupil diameter from the model of Stanley and Davies. The hyperbolic function of equation 2.5 that comprises the first half of equation 3.1c should be substituted for D in calculations. The substituted form of the equation is omitted for brevity.

Figure 3.1 depicts this new model of equation 3.1c along with Stanley and Davies' original function. A coarse comparison between Farrell and Booth's effective pupil size data and this new model is possible by considering the lower end of the photopic range. Under the assumption that Stanley and Davies' 25 degree circular field is the closest in size to the adapting fields included in Farrell and Booth's data, the lower end of the photopic range (approximately 0.1 cd/m^2) must be near $50 \text{ cd/m}^2 \text{ deg}^2$. At this flux density value in the new model (vertical line in figure 3.1), predicted pupil diameter is approximately 5.3 mm. Farrell and Booth's data predict a diameter of approximately 5.0 mm -- only a 6% difference.

Since this new model is based upon previous work conducted under natural viewing conditions of binocularity, and since the factor of monocular or binocular stimulation has a significant effect on pupillary response, this model is directly applicable only to a binocular opaque view RSD scenario. The monocular display condition is discussed subsequently as a separate hypothetical case.

Therefore, given that RSD's are small exit pupil Maxwellian view systems with reduced SC-1 effect, and; given that the Jacobs effectivity ratio is directly applicable to pupil size estimations, and; given that the newly derived model of pupil size for small exit pupil Maxwellian view RSD's coarsely agrees with the data from literature; actual pupil diameter with binocular centrally coupled opaque view RSD stimuli at photopic luminance conditions is hypothesized to follow the newly derived model of effective pupil size (equation 3.1c) that is based upon effectivity ratio adjustments to a corneal flux density model.

3.2.2 Sub-hypothesis 2b: In binocular RSD augmented view under photopic luminance conditions, pupil size is a function of the effectivity ratio-adjusted corneal flux density of the RSD and the luminance of the natural scene.

Under augmented view photopic conditions, the pupillary control mechanism will respond to the combined retinal illumination due to the RSD and the natural scene. The respective influence of each will be a function of the flux density contributed by each. However, with the assumption

that the natural scene is unrestricted and covers approximately 2π steradians of unrestricted binocular view, only the luminance of the natural scene needs to be considered variable for that stimulus. Using the arguments presented in section 3.2.2 above, it follows that augmented view pupil response may be modeled as a family of functions relating pupil diameter to the corneal flux density of the RSD under a range of natural view luminance conditions. Since the natural view will add to retinal illumination and generally reduce pupil size, the augmented view functions are expected to be flatter than that of the new model derived in section 3.2.2, and pupil diameter will be inversely related to natural scene luminance.

As reviewed in section 2.2.1.5, Crawford (1936) discovered that pupil responses to foveal illumination versus peripheral illumination differ [63]. The 2π steradian view of the natural scene in augmented view will add directly to RSD foveal illumination and have strong influence on pupil size. The peripheral portion of the natural view should provide a lesser influence, consistent with Crawford's findings. Stanley and Davies limited their adapting fields to 25 degrees visual angle, so their model is insufficient to predict pupil size with 2π steradian field sizes. Thus, simply summing the retinal illumination effects of the two sources to predict pupil size, as in a corneal flux density model, may produce substantial error. With so little applicable basic literature or data on this topic, attempting to derive more specific theoretical descriptions of these proposed functions is a futile exercise. These new models are best determined empirically with experimental data.

Therefore, given that the augmented view adds to retinal illumination of the RSD, and; given the assumption of unrestricted natural view, and; given the arguments of the preceding related section; pupil size in binocular augmented view photopic conditions is hypothesized to be a function of RSD corneal flux and natural scene luminance, wherein pupil diameter is inversely related to natural scene luminance.

3.2.3 Sub-hypothesis 2c: Under monocular RSD display conditions in both opaque and augmented photopic view, pupil size will follow functions similar in form to the binocular functions, but pupil diameters will be consistently larger than those under similar binocular RSD display conditions.

It has long been established that the eye's pupil will constrict to a greater degree with binocular stimulation than with monocular stimulation [64]. However, literature developing models of

pupil response under monocular conditions is quite scarce. Models of monocular pupil response as a function of corneal flux density, as constructed by Stanley and Davies for the binocular natural view condition, are non-existent. However, with this limited information, a reasoned hypothesis may be made regarding monocular RSD pupil response.

In the opaque viewing case, the stimulation of the observer's visual system will be completely monocular as no background natural view is available to the non-RSD coupled eye. The effective retinal illumination sum of the two eyes will be reduced by half in comparison to the binocular opaque condition. It reasons that in this case the pupil will be significantly less constricted than the binocular case, as the literature clearly indicates. Based upon the work of Reeves, pupils may be expected to be larger by up to 1.5 mm, depending upon photopic luminance levels [64]. Reeves' results indicate a reduced pupil size difference between monocular and binocular conditions at very high photopic luminance levels.

In the augmented view case, binocular stimulation will occur due to the natural view, but the RSD will stimulate only one eye. Thus, the added influence of the RSD to retinal illumination will be reduced, providing a mildly differential illumination to the two retinas. The sum of RSD and natural view illumination on the two retinas will be somewhat less than the sum under binocular RSD conditions, but it will not be dramatically reduced to one-half the binocular sum as in the opaque view case. Thus, a smaller difference in pupillary response between monocular and binocular conditions is expected under augmented view conditions, and the magnitude of this difference should be inversely related to the natural view photopic luminance level. That is, as background natural view conditions brighten, the difference in pupil response due to RSD monocular stimulation should be reduced. At bright photopic levels of background luminance and RSD luminance, the pupil size difference between monocular and binocular RSD stimulation is expected to be near zero. This is consistent with Reeves' findings and with the fact that the effect of RSD stimulation will become proportionately less significant as background luminance increases to both retinas.

As with the binocular augmented view scenario of sub-hypothesis 2b (section 3.2.2), accurately prediction of model results in this case is highly speculative. As in the binocular augmented view case, monocular view models are best determined empirically with experimental data. A family of response curves for monocular conditions should be generated to characterize experimental results across the broad range of photopic RSD conditions and natural view photopic conditions.

Therefore, given that historical models indicate larger pupil sizes for monocular viewing up to 1.5 mm in magnitude, and; given that the opaque view condition presents the most dramatic retinal illumination difference between monocular and binocular conditions, and; given that historical data indicates a reduction in the monocular-binocular view difference with higher photopic luminance levels; pupil size under monocular conditions is hypothesized to be larger than binocular pupil size on the order of 1 mm magnitude for opaque viewing conditions and of markedly smaller magnitudes, inversely related to background luminance, for augmented viewing conditions. This hypothesized estimated difference will be reduced at the extremes of eye pupil diameter near 7 mm and 2 mm due to the physical impossibility of exceeding these natural limits.

3.3 Hypothesis 3: Arrays of small exit pupils are an effective method of preserving the optical advantages of small exit pupil RSD's while offering expanded exit pupil area to the observer.

This hypothesis represents an assertion that multiple separated small exit pupils may be arranged about the entrance pupil of the eye in such a manner that the effective exit pupil area is substantially expanded. Based upon the assertions of section 2.2.3.3, this hypothesis implies that the adjacent exit pupil retinal image disparity on the order of 1 degree visual angle will not significantly disrupt contiguous image perception when exit pupil couplings are switched.

These assertions also imply the separation of exit pupils within the array as a function of eye pupil diameter to promote only single pupil couplings for the preservation of small exit pupil advantages and to minimize the necessity to switch between exit pupils with some display design scenarios. A study of exit pupil separation preference will provide basic modeling information for subsequent display engineering of arrayed pupil concepts. Such a model will describe human observers' preference for the separation of constantly illuminated exit pupils for optimal visual perception of an arrayed pupil display. This preferred pupil separation model, combined with the eye pupil response models proposed in section 3.2, will make available a thorough base of human factors engineering knowledge for the prediction of human interface engineering requirements in the design and implementation of arrayed small exit pupil displays. If this hypothesis is not confirmed, further pursuit of the previously described arrayed exit pupil concepts is unwarranted and alternative engineering concepts may be required for effective coupling of small exit pupil RSD's with the human visual system. Research related to this hypothesis is reported in Chapter 7.

3.3.1 Sub-hypothesis 3a: Arrays of small exit pupils producing retinal images with angular disparity on the order of 1 degree visual angle will not disrupt contiguous image perception by human observers.

Very little literature exists that pertains directly to this new and unique display problem.

Primarily, reasoned assertion and experiential knowledge currently apply well to this problem.

The first consideration is the previously derived estimates for the limits of eye rotation as depicted in table 2.2 in section 2.2.3.2. These estimates suggest that the perception of a 30 degree visual angle display will require at least three exit pupils under small eye pupil conditions if central vision is to be allowed to inspect the entire image (considering eye rotation only in one dimension and ignoring other relative motions). This equates to two opportunities to transition between adjacent exit pupils in an array. As pupil couplings transition among the various adjacent exit pupils in an array, the display image should appear to suddenly shift in position by a small amount. This shift will occur only when transitioning between coupled exit pupils. If lateral eye-display relative motion is well controlled, this shift should occur within the image at a consistent eye rotation position. It follows that each shift will occur consistently for one position of central visual inspection of the displayed image. Clearly, the potential exists for degraded image perception near these shift positions within the image.

However, depending upon image content and visual task, these occasional small image shifts may not be disruptive. The human visual system uses two methods of eye motion, smooth tracking and saccadic motion [16]. Smooth eye motion is employed whenever a moving object is tracked across the visual field. However, essentially all other vision is conducted with rapid saccadic motion [16]. Saccadic eye movements are very rapid "jumps" of the eye from one position to another. This is the type of eye movement used in reading and every other visual task that does not require object tracking. The human visual system has evolved neural functions to help minimize cognitive disorientation that may otherwise occur with such rapid sweeping changes in the visual scene. *Saccadic suppression* is a sensitivity loss that occurs during saccadic actuations in the oculomotor system [17]. Specifically, low frequency spatial sensitivity is temporarily suppressed during saccades, although high frequency sensitivity and color sensitivity do not seem to be affected.

With the exception of visual target tracking tasks, all rotational eye movements will be saccadic. With an arrayed exit pupil display, most tasks that require eye motion across the pupil coupling transition boundaries will use saccadic motion. Since the entire display image will shift with pupil coupling transition, the shift will be a low spatial frequency effect in most circumstances. It is possible that under the majority of arrayed exit pupil display conditions the exit pupil transitional image shift will not be noticeable by the human observer due to saccadic suppression.

Certainly, an observer will notice the shift with a smooth tracking eye motion or if the eye is fixated within a small region of the image near the transition boundary. However, based upon the design concepts discussed in section 2.2.3.3 it seems feasible to design pupil transition or "switching" strategies that will minimize these undesirable effects. Even without such strategies, the regions within the display image that will be disrupted are small and few, and the advantages of using arrays of small exit pupils may well outweigh this minor detractor to image quality.

Therefore, given that pupil coupling transitions should be rare and small, and; given that saccadic suppression reduces low spatial frequency perception; arrayed small exit pupil displays with image disparity on the order of 1 degree visual angle are hypothesized to not cause significant disruption of display image perception.

3.3.2 Sub-hypothesis 3b: The following linear model of preferred exit pupil separation is generally applicable to arrays of small exit pupils about the pupil of the eye:

$$s_{ep} = (m(d_{ep}))p + b(d_{ep}) \quad (\text{eq. 3.2})$$

where s_{ep} is the center-to-center separation of two adjacent exit pupils, d_{ep} is the diameter of the display exit pupil, and p is the diameter of the eye's entrance pupil. The function $m(d_{ep})$ is a slope function to be determined empirically, as is the intercept function $b(d_{ep})$.

This linear model assumes round exit pupils of equal diameter significantly smaller than the diameter of the eye pupil (exit pupil smaller than eye pupil by at least a factor of 2). Exit pupil separation distances are considered to be center to center and no special conditions are imposed on the arrangement or number of exit pupils within an array other than equivalent separation distances among all pupils. This model generally applies to the geometrical considerations of

pupil coupling discussed in section 2.2.3.2 in which all arrayed exit pupils are constantly and equally illuminated.

The model follows the basic slope-intercept form for describing a line. The abscissa of a plot of this function is p , the diameter of the eye pupil. The function $b(d_{ep})$ is the ordinate intercept, determined empirically as a function of exit pupil diameter. The function $m(d_{ep})$ is the slope of the linear model, an empirically derived function of exit pupil diameter. Considering previously discussed geometric factors and human visual perceptual characteristics, hypothetical values for the model variables may be reasonably, if generally, asserted.

The slope of the model, $m(d_{ep})$ should be near unity, implying that the preferred center to center separation of exit pupils is directly influenced by eye pupil diameter. This is reasonable since a perceptual trade-off must necessarily be made by the observer, and the trade off is governed by eye pupil diameter. The trade off involves a balance between the coupling of multiple non-parallel exit pupils versus reduced image brightness due to partial exit pupil coupling. The geometry depicted in the various graphics of Figure 2.19 helps describe the scenario.

In graphics 'c' and 'd,' the exit pupils are separated by a distance approximately equal to the eye pupil diameter. Thus, as the eye rotates, one exit pupil is decoupled and another is coupled at approximately identical eye positions. Clearly, this is an idealized case. The exit pupil has a finite diameter of its own through which the display light must pass to create a retinal image. It is not an infinitely small point position. As the eye rotates or moves relative to the exit pupils, partial exit pupil couplings will occur as exit pupils are coupled and decoupled. In order to avoid a scenario like that in graphic 'e' of Figure 2.19 in which the image is completely lost, the pupils must necessarily be at least partially coupled simultaneously during pupil transitions. This will result in multiple non-coincident retinal images at the eye position where the multiple couplings occur. A partial coupling of an exit pupil will reduce the scanning beam's cross section and its illumination of the retina, thereby reducing the image brightness. So, the observer must make a judgment of the best exit pupil separation distance for image perception by making a trade-off between small regions of non-coincident imaging and reduced image brightness. Clearly, a separation distance that allows decoupling between two exit pupils (graphic 'e' in Figure 2.19) is less desirable than a double image, as no display information at all can be obtained with the absence of an image.

It is important to understand that the only position where this trade-off judgment is pertinent is within the small range of eye-display relative positions where adjacent exit pupils are encountered on opposite sides of the eye pupil. In all other relative positions, only one exit pupil is coupled to the eye and a singular, fully luminous image is presented. Thus, the observer will seek a separation distance that minimizes the region in which multiple pupil couplings occur (increased exit pupil separation) while maintaining enough partial exit pupil couplings to preserve image brightness for perception (decreased exit pupil separation) across this *region of coupling confusion*.

It seems reasonable to expect a consistent portion of partial exit pupil coupling relative to the edge of the eye pupil for all eye pupil diameters. Near the optimum separation distance, each of two adjacent exit pupils will be partially blocked by the edge of the eye pupil (iris) and partially coupled for imaging. Therefore, as the eye pupil changes in diameter, the preferred exit pupil separation distance should change commensurately. A model function of unity slope characterizes this scenario.

However, the Stiles-Crawford effect of the first kind, as described in section 2.2.1.2, may influence preferred exit pupil separation distance. Since phototransduction efficiency is partially a function of eye pupil entry position, the perceived image brightness will decrease significantly when exit pupils are coupled at large radii from the eye pupil center. Thus, when eye pupil diameters are large, the perceived image brightness for eye positions near the region of coupling confusion will be reduced by the Stiles-Crawford factor and by partial pupil coupling.

This may have an effect on the slope of the model function. In order to compensate for the decreased image brightness due to Stiles-Crawford effects in the region of coupling confusion, observers may prefer to allow larger portions of partially coupled exit pupils to enter the eye as eye pupil diameters increase. This must be achieved by positioning the two adjacent exit pupils closer together, relative to the edges of the eye pupil, as eye pupil diameter increases. If this is the case, the slope of the model function will be less than unity. Since RSD image luminance is directly related to coupled exit pupil area, the model slope may be expected to relate increased exit pupil partial coupling areas that are commensurate with decreased phototransduction efficiency as defined by the Stiles-Crawford I function.

Additionally, the model slope may be expected to vary slightly with exit pupil diameter. For equivalent center to center exit pupil separation distance, larger exit pupils will extend nearer to the center of the eye pupil than will smaller exit pupils. Thus, with larger exit pupils, more

photons will pass through the pupil at smaller radii from eye pupil center. The nearer photons pass to the pupil center, the greater their phototransduction efficiency. The result is that Stiles-Crawford I effect will be slightly less significant with larger exit pupils than with smaller ones. Therefore, model slopes may be expected to vary slightly with exit pupil diameter, with smaller exit pupils yielding slopes less than that of larger exit pupils. Therefore, the linear model of exit pupil separation preference depicts slope as a function of exit pupil diameter.

The ordinate intercept of the model ($b(d_{ep})$) may also be expected to vary with exit pupil diameter. As described above, larger exit pupils near the region of coupling confusion will likely extend across a larger portion of the eye pupil than will smaller exit pupils. This allows for a greater separation distance with partially coupled exit pupils than is allowed with smaller exit pupils. As human observers will likely seek to minimize the region producing multiple exit pupil couplings, larger exit pupils provide the opportunity to increase center to center exit pupil separation while still coupling a significant portion of two adjacent exit pupils. Therefore, the ordinate intercept of exit pupil models is also hypothesized to be a function of exit pupil diameter, with larger pupils producing larger intercept values.

Therefore, given that exit pupil separation preference must be determined largely by eye pupil diameter, and; given that the Stiles-Crawford I effect may influence exit pupil separation preference as a function of eye pupil diameter, and; given that exit pupil diameter will affect the magnitude of the applied Stiles-Crawford I effect, and; given that exit pupil diameter will affect the allowable separation of adjacent partially coupled exit pupils; exit pupil separation preference is hypothesized to follow a model of the form described by equation 3.2 into which empirically derived functions will fit for slope and intercept.

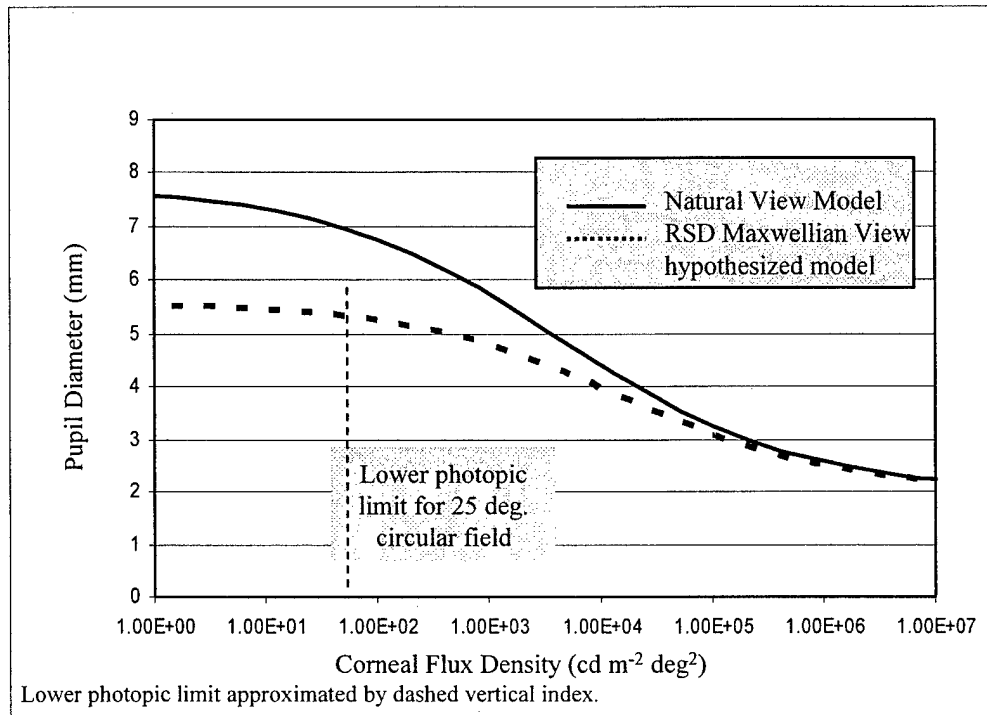


Figure 3.1: Pupil Diameter as a Function of Corneal Flux Density
(after Stanley and Davies, 1995)

Chapter 4: Retinal Response in the Temporal Domain: Flicker Experiments

Two experiments examining human temporal sensitivity to RSD stimuli were the first conducted in this new research thrust. These experiments were selected first because of the interesting results of Kelly, et. al., that warranted replication before additional experimental efforts were attempted [79]. Additionally, flicker perception was one of two retinal response characteristics being investigated in the research, and establishing the nature of the retinal response to RSD stimuli was necessary before planned opto-physiological experiments could be properly designed and conducted.

The first experiment, conducted with Kelly, improved upon his previous VRD flicker study. It compared flicker contrast thresholds of detection for the VRD and a CRT. This experiment refined the earlier effort with stricter experimental control, improved psychophysical methods, and most importantly, the elimination of previously undiscovered systematic error. The second experiment utilized the newly constructed VRD Emulator to compare critical flicker frequency with RSD stimuli to that of a non-scanned, Maxwellian view, flickering source.

4.1 Flicker Contrast Threshold Comparison: VRD vs. CRT

The direct comparison of flicker between an RSD and a conventional CRT display will reveal whether or not the perception of flicker with the RSD is anomalous. CRT displays have a long history of utilization in vision science for stimulus presentation, as their performance is consistent and reliable and their characteristics well documented. Further, the CRT is ubiquitous, so its use as a standard for comparison has practical applicability as well. This experiment compares the flicker contrast threshold of detection between the two types of displays.

4.1.1 Objectives and Hypotheses

The primary objective of this experiment was to contribute to the testing of sub-hypothesis 1b: *Flicker perception of retinal scanning displays is equivalent to that of conventional visual displays.* Testing this hypothesis is one part of testing general hypothesis 1: *Retinal response to, and visual perception of, retinal scanning display stimuli is not anomalous.* Further, the testing of these hypotheses directly addresses the second main objectives of this research effort as

defined in section 1.2: *Explore the temporal domain with RSD's to identify and quantify any anomalous perceptual effects due to retinal response.*

Hypothesis 1b was drawn directly from literature and logical analysis, as discussed in section 3.1.2. Although the previous findings of Kelly, et.al., indicate reduced sensitivity to flicker with the VRD, this result conflicts with conventional theory and is founded on questionable experimental data. A revised and well controlled replication of this experiment was a prudent first step.

In this experiment, the contrast of temporally square stimuli required for flicker to be detected was examined. If the two display devices induce differing visual responses to flickering stimuli, responses that result in differing sensitivities to the flicker, it reasons that a flickering stimulus presented by one display will be more readily visible than the other display presenting an equivalent stimulus. Flicker contrast is the contrast produced between the most luminous and least luminous portions of the temporally varying stimulus, and it may be used as a measure of temporal sensitivity. If the two display devices induce differing temporal sensitivities, the flicker contrast necessary to just detect a flickering presentation should vary between the two displays. Equivalent flicker contrast thresholds of detection indicate equivalent temporal sensitivity.

Based upon the literature concerning Bloch's law, the Talbot-Plateau law, and the work of Brown and de Lange, the visual system is expected to integrate the short duration laser stimuli over a longer time course associated with the integration period of the photoreceptors [18, 45, 46, 53]. As a result, the photoreceptors should have the same time averaged photon absorption over the frame rate of each display when a perceptual luminance match of the two displays is achieved. Consequently, the contrast sensitivity with the two displays should be equivalent.

Concordant with hypothesis 1b, the specific hypothesis for this experiment holds: *The flicker contrast threshold of detection with VRD stimuli will be equivalent to that with CRT stimuli.* This is also consistent with general hypothesis 1, in that no difference in retinal response is expected from the stimuli of the two displays that will induce a perceptual difference in the temporal domain.

4.1.2 Apparatus and Experimental Setup

The bench model virtual retinal display was the primary apparatus used for this experiment. The basic apparatus, as described in section 2.1.1, was augmented with a CRT (EIZO TX-C7; Nanao,

Japan, 120 MHz bandwidth) and a large, first surface mirror to affect stimulus presentations in identical visual space. Figure 4.1 illustrates the augmented setup. When an observer positions his eye at the VRD exit pupil, the VRD image is perceived along with the reversed image of the CRT through the beam splitter and via the 45-degree mirror. By carefully positioning the CRT and mirror, and by making minor adjustments to the horizontal extent of the VRD display, horizontally symmetrical stimuli may be matched in the spatial domain.

The VRD's continuous VGA video signal generated a 640 x 480 pixel image at a frame rate of 60.1282 Hz, non-interlaced. An active video signal splitter provided the same signal to the CRT. Both displays had a horizontal scan rate of 31.5 kHz, and the discrepancy in timing at the left and right edges of the display was not greater than 31.7 μ s. Because of the video digitization process of the VRD, the VRD scan lagged in phase behind the CRT by approximately 4 horizontal lines. The vertical frame rate of the two displays was matched to within 10^{-5} Hz, as measured by a dual channel timer (Phillips 225 MHz timer; Hamburg, Germany).

Figure 4.2 depicts the temporal signature of two "on" modulated VRD pixels separated by a single "off" pixel. The pixels are clearly resolved and have duration of approximately 40 ns. These pixels were recorded near the center of the VRD display, where the MRS sinusoidal scan is fastest. Near the edges of the display, the pixel time extends to nearly twice this value with the slowing sinusoidal scan. The pixels were measured by placing a photomultiplier tube (2.5 ns rise/fall time) at the exit pupil of the VRD during the pixel display. The PMT signal was sampled and stored by a 500 MHz oscilloscope (Tektronix 550; Beaverton, Oregon), and subsequently downloaded to a spreadsheet for analysis and graphing.

At the VRD exit pupil the beam was well collimated. Its profile was essentially TEM_{00} mode, although it was slightly clipped along two opposing edges by the aperture of the MRS mirror. The beam profile was approximately 1.2 x 0.8 mm. These measurements were made using a PMT with 30 μ m aperture mounted on a micrometer stage that allowed precise movement of the PMT across the beam profile. Recordings were again made by oscilloscope.

The CRT had three P-22 phosphors with manufacturer's specified decay times of 1.5 ms and 6.0 ms for red and green, respectively. Measurements under stimulus conditions indicated decay to 1% of maximum luminance in 9.5 ms for red, and 12.0 ms for green phosphors. The $1/e^2$ time constants were 1.4 ms and 1.8 ms for red and green, respectively.

An optical table mount was positioned near the VRD scanning mechanism for a dental impression bite bar. Custom dental impressions for each subject were mounted on an adjustable

bar that was stabilized when the subject's eye was properly positioned at the VRD exit pupil. This apparatus minimized the possibility of head movements during data collection in order to avoid error imposed by the Stiles-Crawford I effect.

An infrared video camera (Sony HandyCam Hi-8) was positioned so that an image of the subject's eye could be recorded from a reflection in the 45-degree mirror, as depicted in figure 4.1. The image of the eye was recorded under stimulus conditions for subsequent measurement of pupil diameter and estimation of retinal illumination from the CRT. A video monitor screen was calibrated in advance of data collection by temporarily mounting a millimeter scale at the exit pupil position and creating a ruled scale from the video monitor image.

4.1.3 Calibrations and Corrections

Prior to experimentation, thorough calibration and testing of the VRD and CRT displays was accomplished. The calibration of display luminance functions was necessary to determine proper levels for contrast presentations in flickering stimuli. An identical calibration was performed in Kelly's previous flicker experiment. Luminance calibration was made with the CRT and VRD. Other tests measured the homogeneity of luminance across the display fields as well as the actual contrasts provided by the displays under stimulus conditions after luminance calibration was completed. The luminance of the displays was also examined over time to ensure consistency throughout the experiment. The calibrations and tests revealed two sources of systematic error apparently uncontrolled in all previous flicker studies at HITL.

4.1.3.1 Luminance Calibration

The video board driving each display provided 256 luminance levels for each RGB output. After a 30 minute warm up period, a photodiode (UDT; Hawthorne, California) with a calibrated photometric filter and lens was positioned near the middle of the CRT face. The filter eliminated infrared wavelengths emitted by the CRT that may introduce error into the calibration. It also weighted the CRT emissions by the photopic luminous efficiency function in accordance with the sensitivity of the retina. The photodiode output was fed into a high-gain transimpedance amplifier, integrated by a tunable 8-pole low pass Butterworth filter (Frequency Devices, Inc.; Haverhill, Massachusetts), then fed into an analog-to-digital board in a PC computer. The output

of the calibration system was low-pass filtered and monitored on-line to ensure total signal integration and to avoid saturation. A custom software program provided homogeneous presentations of the 0 - 255 luminance levels sequentially for each color. The light measurement system output was digitized by the PC board at 5 kHz and averaged over 7 vertical display frames. Zero level offset measurements were also made by blocking the display. Identical calibration measurements were made with the VRD by placing the photodiode at the exit pupil position, although no IR filtering was required and the photometric filter was removed for the monochromatic source. This improved the available signal from the VRD, and amplification adjustments ensured proper integration and saturation avoidance under these conditions. Luminance functions for the 0-255 levels were plotted from these data.

The CRT produced a typical nonlinear luminance output with input voltage, while the VRD's modulators produced a sigmoid function with saturation near the 255 level. Correction of the nonlinearities was implemented with separate software look-up tables for each of the red, green, and blue components of each display type. This methodology allowed the automated selection of the high and low luminance levels from the look-up tables nearest those calculated for the display of flicker contrasts of any desired magnitude and mean luminance.

After luminance calibration, actual display flicker contrasts were measured under stimulus conditions. The photodiode and amplifier used in calibration was routed to the previously described oscilloscope. The photodiode was positioned at the VRD exit pupil for measurement of each display's contrast. A flickering stimulus was presented separately on each display for contrast measurement. The stimulus consisted of a rectangular image, temporally modulated as a square wave at 30 Hz across the entire range of contrast values from 0.05 to 1.0 in steps of 0.05. The high and low luminance values in the flickering stimuli were recorded with the oscilloscope and analyzed in a spreadsheet.

Contrast here is defined as Michelson contrast (c_m):

$$C_m = \frac{L_{\max} - L_{\min}}{L_{\max} + L_{\min}} \quad (\text{eq. 4.1}) [19]$$

where L_{\max} and L_{\min} are the maximum and minimum luminances in the temporal pattern. The CRT produced Michelson flicker contrast values within 0.02 of the target values. However, the VRD Michelson flicker contrasts were systematically low by as much as 0.15, or an actual contrast/target contrast ratio as low as 0.68. These measurements were checked using alternative silicon detectors, alternative amplifiers, and a PMT detector. Identical results were obtained in

each case. The mean stimulus luminance level was properly maintained at the target value, but the high and low luminance values in the flickering stimuli were obviously in error. The plotted error function relating actual contrasts to target contrasts is depicted in figure 4.3. In Kelly's previous flicker study, the actual contrasts were not measured under stimulus conditions. Only the mean luminance levels were tested. Further, systematically low contrast values for the VRD only would produce flawed data indicating higher flicker contrast thresholds for the VRD than for the properly contrasting CRT. Therefore, it was assumed that most, if not all, of the previously reported decreased flicker sensitivity with the VRD was a result of this systematic error in VRD stimuli contrast. Any residual effect after correction of this error would be small.

To date, the source of this calibration error has not been ascertained. An error possibly derived from the nonlinear behavior of the AOM's has been postulated by Kelly, but that theory has not been tested. Detector saturation or system integration error is possible, but subsequent re-examinations reveal no such problems. The contrast targets were adjusted to reflect actual measured contrast values for the conduct of this experiment.

4.1.3.2 Display Homogeneity Tests

A homogeneous luminous display is necessary to make accurate perceptual luminance matches and to properly assess flicker of large visual fields. Both the VRD and CRT were evaluated for luminous homogeneity. Measurements of luminance were made across the displays with single-color fields. Differing methods were necessary to evaluate each of the two displays.

The CRT, being a polychromatic extended source, was measured with an imaging photometer device. A Photo Research (Chatsworth, California) PR-650 spectroradiometer was used to image the CRT from the position of the VRD exit pupil. The maximum luminance change of the CRT across the stimulus field was 6% for red phosphor and 9% for green phosphor. Chromaticity varied negligibly across the display.

The VRD, being a monochromatic Maxwellian view source, was measured again with the oscilloscope and photodiode positioned at the exit pupil. The oscilloscope display was adjusted to depict the power of the laser beam over one frame time. A flat-topped square wave was expected, indicating equivalent laser power from the top to the bottom of the scanned frame. However, the waveform depicted increasing laser power as the scan moved from the top to the bottom of the frame. This vertical inhomogeneity exceeded 25% for the red laser, and 15% for

the green laser. The slope of this waveform was noticed to change if the fiber optic carrying the laser energy was manipulated, and this provided a clue to the source of the inhomogeneity.

As light is carried down a flexible waveguide such as an optical fiber, curves in the waveguide facilitate changes in the polarization vector due to changes in internal reflection characteristics [32]. Manipulations of the optical fiber carrying the VRD's laser light dynamically altered the polarization of the light exiting the fiber. Many types of beam splitters produce polarization effects by which the reflectance-transmittance ratio changes as a function of incidence angle. The beam splitter used in the VRD's viewing optics is such an item. Since the angle of incidence of the scanned beam to the beam splitter changes as the scan is affected, the beam was being differentially reflected and transmitted along the vertical axis of the scan. The magnitude of this effect changed with the varying polarization orientations caused by the optical fiber manipulations.

By securing all of the optical fibers except for a small segment for manipulation, and by then manipulating the unsecured segment by trial and error until a flat response was measured, the inhomogeneity was corrected. The unsecured optical fiber segment was then secured in the proper position to maintain the polarization orientation that reduced the effect to a minimum. This rather inelegant solution proved to be the most practical one, allowing expedient continuation of experimentation. Subsequently, inhomogeneity across the entire VRD display did not exceed 4% for the red laser or 10% for the green laser.

The power across the horizontal extent of the display was checked by changing the oscilloscope display to depict the time of a single horizontal display line and then displaying single lines down the vertical extent of the frame. The horizontal homogeneity was not significantly affected by the polarization effect under stimulus conditions.

It should be noted that this inhomogeneity was previously undiscovered and apparently uncontrolled in earlier flicker studies. The error induced by this inhomogeneity, combined with that of the flawed calibration process, likely accounted for all of the previously reported reduction in flicker sensitivity with the VRD.

4.1.4 Subjects

The purpose of the experiment was disclosed to all subjects, and each gave informed consent. A safety analysis of VRD retinal illumination was previously published detailing the compliance

with related ANSI standards [78]. Seven adult subjects were tested. Four subjects had no previous psychophysical experimental experience. Three were VRD researchers with extensive visual psychophysical experience. Each subject had corrected acuity of 20/20 or better, normal eye alignment, and no known visual defects. Ages ranged from 21 to 46 years. Each subject was tested using the right eye with optical correction, if prescribed. The left eye was covered with an opaque eye patch.

4.1.5 Procedure

The experiment proceeded in two parts: 1) perceptual luminance matching of the CRT and VRD displays, and 2) detection of flickering stimuli under conditions of the perceptual luminance match. As flicker detection is a function of luminosity, it was imperative that subjects accurately match luminous perception of the two displays before flicker detection trials were initiated. Under the assumptions of conventional theory, the perceptual match should provide conditions of equivalent photon absorption by the retina. Thus, estimates of retinal illumination were also made for each subject to ascertain whether this assumption was valid.

4.1.5.1 Perceptual Luminance Match

A rectangular display of 250 horizontal by 300 vertical pixels was presented on both displays simultaneously so that the two presentations were visible in the same space when the eye was positioned at the VRD exit pupil. Adjustments were made in CRT position, mirror angle, and VRD horizontal extent to achieve a precise match in the spatial dimensions of the two rectangular stimuli on the retina. The rectangular region subtended approximately $10.4^\circ \times 10.5^\circ$ visual angle.

Luminance matches were made using a single color on each display. For the red condition, subjects viewed the CRT through a red Kodak Wratten no. 25 filter to make the (x, y) CIE chromaticity coordinates more similar to those provided by the 632.8 nm monochromatic wavelength of the VRD (CRT = 0.697, 0.299; VRD = 0.734, 0.266). Closer color matches between images will promote improved luminance matching since the heterochromatic factor in the matching task is reduced. The green condition produced greater chromaticity difference (CRT = 0.293, 0.607; VRD = 0.052, 0.797). The mean luminance of the CRT was fixed at 8.0 cd/m^2 for red through the Wratten filter, and 39.8 cd/m^2 for green. Natural pupil size

measurements allowed estimates of the mean retinal illumination values in troland (173 td for red and 550 td for green). Artificial pupils were not used to control entrance pupil size with the CRT because vignetting resulted when the two displays were matched in field size. Two subjects with large natural pupil diameters (VG: 6.0 mm and HP: 5.5 mm) viewed the CRT with an additional 0.3 logarithmic unit neutral density filter attenuation due to difficulty in achieving a perceptual match with the VRD within the range of luminances provided by the VRD. Satisfactory perceptual matches were achieved by these two subjects after the CRT was attenuated.

The subject's dental impression bite bar was positioned for proper alignment of the VRD exit pupil with the eye's entrance pupil. Subjective assessment of the brightness of the VRD plus physical examination of relative positions ensured accurate central positioning of the VRD exit pupil within the eye's entrance pupil. The bite bar was fixed in position after adjustments were completed to ensure consistent head and eye position during the entire experiment.

Luminance matches of the two displays were made by heterochromatic flicker photometry (HFP) technique (section 2.2.1.2). A vertical square wave grating of one cycle ($10.5^\circ \times 10.5^\circ$) was presented on both displays simultaneously. The previous alignment procedure ensured that the displays precisely overlapped in visual space. Since both displays were driven by the same video signal, the gratings presented by each display were identical. However, since the CRT was viewed via a mirror, its presentation was reversed horizontally. Hence, the bright half of the single grating cycle from the VRD was positioned on the dim half of the grating cycle from the CRT in visual space, and vice versa. The subject viewed a bright square, one half presented by the VRD and the adjacent half presented by the CRT. Figure 4.4 illustrates the HFP stimuli. The grating was counter phased at 15 Hz, with the bright and dim halves of the grating alternating left and right. The result was a bipartite field of alternating flicker at 15 Hz that the subject could view to accomplish the HFP perceptual match. Contrast was maximized at 99.9% and no background illumination was provided.

The HFP match was accomplished by the subject's adjustment of a variable neutral density filter (wedge) that varied the luminance of the VRD display (Figure 4.1). The subject was instructed to vary the filter until his perception of flicker in the display was minimized. Twenty to thirty trials were conducted per subject, and the mean wedge setting was recorded and used for subsequent flicker detection trials. Standard deviation of the HFP matches varied from 0.21 to 0.02 logarithmic units, but typically was 0.08 log units. Perceptual matches were also made in

side-by-side comparisons of identical static bipartite fields. HFP and side-by-side matches agreed on average to within 0.02 log units and were always within 0.1 log unit.

4.1.5.2 Flicker Detection Trials

Thresholds of flicker contrast were measured separately for each display by a two-alternative forced choice methodology (2AFC). The order of testing with CRT and VRD was randomly selected. A temporally square 30 Hz flickering Gaussian field was the target stimulus with a total spatial extent of $10.4^\circ \times 10.5^\circ$ at 1.2% of maximum contrast level, and $\sigma = 1.8^\circ$, or 43 pixels. The mean luminance of the flickering presentations was held constant. Display luminances were matched in accordance with the filter values determined in the perceptual luminance matching procedure. Subjects fixated on a small dot centered in the Gaussian field to reduce saccadic eye motion that effects flicker detection [18]. The Gaussian stimulus was used in lieu of a stimulus with distinct edges since edge detection is accomplished in the retina by specialized neural circuitry that may influence the detection of flicker and decrease thresholds [16, 23]. Figure 4.5 illustrates two 60 Hz frames of a Gaussian stimulus like that used in this experiment to produce 30 Hz flicker. The background luminance is equivalent to the mean luminance of the flickering Gaussian field.

In the 2AFC technique, subjects viewed two sequenced presentations of 0.5 s duration separated by a 0.5 s blank period for each trial. Randomly selected, only one of the two presentations in each trial was a flickering Gaussian field. The other was a constant field of the same mean luminance as the flickering field. The presentations were generated by a custom software utility that also recorded subject performance. The subject's task was to identify which of the two presentations contained the flickering field and indicate the selection by pressing either the left or the right button on a standard computer mouse (left = first presentation, right = second presentation). Each presentation's start was associated with a brief tone, and the two tones in a trial differed in pitch with the first and second presentations. This helped the subject maintain awareness of the sequencing of the presentations and avoided confusion. The subject self-initiated each trial with a click of either mouse button. A minimum of 30 trials per condition were run for each subject, and contrast conditions were sequenced pseudo-randomly. The 2AFC experiment was conducted with red stimuli only.

In the first experimental session, a subject was presented with up to five different contrast levels spanning a broad range of contrast values. Trials were completely randomized. Subject performance was cursorily analyzed immediately following a session, and an additional session presenting a narrower range of contrast values was typically conducted in order to focus data collection near the subject's threshold level, as determined by the first session's results. Occasionally, a third session was necessary to ensure the threshold was adequately explored. All sessions for all subjects were conducted on the same day without extended breaks between sessions.

As a control condition, flicker thresholds were also measured by the method of adjustment for both red and green conditions for three subjects. These trials were performed either before or after the 2AFC trials, pseudo-randomly. The subject was allowed to vary the contrast of the stimulus using the computer mouse until a 30 Hz flickering Gaussian form was just detectable. The presentation of the Gaussian form, subject contrast control, and data logging were facilitated by the same custom software used in the 2AFC trials. Once the subject had determined a threshold contrast level by mouse actions, a keypad action logged the contrast values into an electronic file on the computer. The same luminance matching conditions determined by the perceptual matching procedure were applied in these trials. A minimum of 30 method of adjustment trials were conducted per condition.

4.1.6 Analysis

In the 2AFC methodology, chance performance is indicated by the 50% correct level of performance in selecting the flickering presentation. Psychophysical performance typically increases from chance as a sigmoid function, such as cumulative normal distribution, with 100% correct performance providing the ceiling of the function. The 75% correct level of performance is defined as the threshold of detection.

Data for each subject were fitted by least squares to a normal cumulative curve relating contrast level to percent correct performance. The 75% correct level as determined by the best fit normal cumulative curve was recorded as the threshold of flicker contrast detection. The thresholds of detection for CRT and VRD of each subject were plotted on a common graph and compared, and the ratios of thresholds between the two displays were calculated and plotted for graphical analysis. The mean threshold across subjects was calculated. The 75% threshold value

was considered as the mean for the cumulative normal distribution, and the standard deviation of the fitted curve was also calculated. Pairwise t-tests of the threshold values were calculated under the assumption that the fitted curve is a close estimate of the true psychometric function.

For the method of adjustment data, mean contrast threshold values were calculated and plotted, along with standard error. Pairwise t-tests were examined within subjects. The mean threshold across subjects was calculated.

Retinal illumination values for the two displays were estimated. The illumination due to the CRT was determined by the product of entrance pupil diameter and display luminance as measured with the PR-650 photometer, and corrected for the SC-1 effect by Jacob's formula [39]. The illumination due to the VRD was determined using Westheimer's method with Maxwellian view conditions (section 2.2.3) and the same PR-650 photometer. The SC-1 effect was considered negligible for the VRD's 1.0 mm diameter pupil size, and no SC-1 correction was made for the VRD. Retinal illumination estimates were examined as ratios of VRD/CRT illumination at the condition of perceptual luminance match.

4.1.7 Results

The range of observed psychometric functions with the 2AFC method is depicted in figure 4.6. Differences in flicker thresholds between the two displays ranged from slightly lower thresholds with the VRD to slightly lower thresholds with the CRT. Subject ST showed very similar psychometric function with the two displays. Contrast thresholds for all subjects are plotted in the upper part of figure 4.7, and threshold ratios of VRD/CRT are plotted in the lower part of figure 4.7. Each individual threshold was within a factor of 1.55 between displays, and four of the seven are clustered very near a ratio of 1.0. The mean ratio of thresholds across subjects was 1.14. Only one subject's (VG) difference was significant (at $\alpha=0.05$) by the t-test.

Thresholds measured by the method of adjustment are plotted in figure 4.8. The top portion of the figure shows the thresholds for the red condition, and the bottom portion plots the green condition thresholds. Again, thresholds were very similar between the two displays. The mean VRD/CRT threshold ratio was 1.03 for red and 1.25 for green. Only one subject (JK) had statistically different thresholds between displays (red condition, $p<0.0001$). The green thresholds are lower than the red due to the higher mean luminance of the green condition. The

thresholds by method of adjustment are also approximately twice that of the 2AFC thresholds -- a common result when comparing the two psychophysical methods.

Figure 4.9 relates the ratio of VRD/CRT retinal illumination to the ratio of VRD/CRT thresholds as determined by the 2AFC method. A strong linear relationship is revealed ($R^2=0.933$; $p<0.001$). This implies that even though all data were collected at each observer's perceptual luminance match by HFP, the actual retinal illumination in some cases was poorly matched, and the VRD/CRT threshold ratio is related to the physical quantity of light on the retina. The dotted line is a prediction by the realized linear relationship that when retinal illumination is physically matched between the displays, the ratio of flicker contrast thresholds should be approximately 1.2. That is, assuming that the VRD/CRT retinal illumination ratio is 1.0 when the two displays are perfectly matched in effective physical energy on the retina, the predicted VRD/CRT flicker threshold ratio indicates a mild reduction in sensitivity to flicker with the VRD. The 1.2 ratio value is close to the 1.14 overall mean value observed in the 2AFC data. However, due to measurement precision considerations discussed in the following section, no firm conclusions may be drawn regarding this small apparent effect.

4.1.8 Discussion and Conclusions

Thresholds for flicker contrast detection are very similar between the VRD and CRT. The lack of physical persistence of the retinal scanning display has no obvious effect on flicker perception, and the integrating functions of the retina seem to operate within conventional theories of temporal perception. Specifically, the findings of Brown and de Lange that only the fundamental temporal frequency is significant to flicker perception at high temporal frequencies, seem to apply to even the uniquely brief and recurring temporal stimulus of the RSD [45, 46].

Of the seven subjects tested, only two exhibited slightly reduced perception of flicker with the VRD (HP and VG), and only one yielded a statistically significant result. It is interesting that the two subjects who showed some reduced VRD flicker sensitivity were the two subjects with large natural pupils for whom neutral density filtering was added to attenuate the CRT display. The resulting low CRT luminance levels (approximately 4 cd/m^2) approach the mesopic range, between photopic and scotopic conditions, where rod photoreceptors begin to activate. Photometry in this range introduces many additional considerations and measurement challenges beyond the scope of this dissertation [96].

However, one pertinent consideration is that the rod photoreceptors are significantly less sensitive to the 632.8 nm wavelength monochromatic light used for the red VRD stimuli than are cone photoreceptors. The CRT's red presentation included a broader spectrum of wavelengths, most being shorter than the VRD's monochromatic source. Literature indicates that substantial differences in critical flicker frequency by wavelength are obtained with luminance levels in the mesopic range [18]. Clearly, differences in sensitivity threshold are also expected. It is possible that these unique low luminance conditions are, at least in part, the cause of the slightly deviant results for these subjects. It is also notable that one of these subjects (HP) did not exhibit similar threshold ratios for the red condition by method of adjustment. In fact, this subject's VRD/CRT ratio of thresholds under the method of adjustment was less than 1.0. It is also notable that these two subjects had the least two values of VRD/CRT retinal illumination ratio, significantly less than unity. That is, the estimated retinal illumination with the VRD was markedly less than with the CRT for these two subjects, as compared to all other subjects whose ratios were near or above unity. Under such conditions a significant reduction in flicker sensitivity would be expected with the VRD.

Additionally, in spite of the use of the dental impression bite bar, some head motion is still possible, particularly over the course of the long and potentially fatiguing experimental sessions associated with the 2AFC methodology. It is possible that the assumption of central entrance pupil alignment of the VRD exit pupil was violated with these two subjects, invalidating their data. In light of the results from the method of adjustment control condition with subject HP, it seems likely that error is the cause. It is also noted that the experimental session with subject VG was the longest of the seven. This subject had particular difficulty achieving a perceptual luminance match between the VRD and CRT (necessitating the first occurrence of the afore mentioned CRT attenuation), and this extended his session to a fatiguing 5.5 hours. Again, under such conditions, the possibility of misalignments between the eye entrance pupil and exit pupil of the VRD increases, along with the potential for error. Discarding the threshold ratios of these two subjects, the mean ratio of the remaining five subjects is .997, indicating nearly exact equivalency between the two displays.

Even considering the results from these two subjects, the slight trend for reduced flicker sensitivity with the VRD is within the limits of expected experimental precision. The homogeneity of the displays was not perfect, and it is notable that the method of adjustment

results for the green condition indicate a larger effect for the VRD. Recall that the level of inhomogeneity present in the green stimuli was 2.0 to 2.5 times greater than for the red stimuli.

It is also noted with the method of adjustment that thresholds are substantially lower for green than for red. This is consistent with the difference in luminance between the two conditions. Flicker detection is improved with higher luminance levels, and the luminance of the green displays was approximately 3 times that of the red.

One unique item of interest is the linear relationship between retinal illumination ratios and flicker contrast threshold ratios. If the assumption of proper entrance pupil alignment of the VRD exit pupil holds, this relationship suggests that for some subjects the luminous efficiency of the VRD stimulus is greater than that of the CRT stimulus. At least, the subjective luminance match for some subjects may have been affected by factors other than physical energies on the retina, and these still warrant investigation. However, the fact that this was not manifested in all subjects in a consistent manner points toward the latter explanation, rather than the former. Additional information will be gathered in brightness matching experiments of Chapter 5 specifically designed to investigate this issue, but the following considerations are likely sufficient to fully explain this small indicated effect.

Because the estimates of CRT retinal illumination are dependent upon eye pupil diameter, and because eye pupil diameter was not monitored throughout the experiment but only during the display brightness matching task, the estimates of CRT retinal illumination may contain some error. Further, the VRD's effective retinal illumination was dependent upon Stiles-Crawford effects of the first kind (SC-1), and minor head movements during the experiment may have induced significant variation in the eye pupil entry position of the VRD's exit pupil. In this case, the effective retinal illumination with the VRD could only decrease from the peak level achieved during the brightness matching procedure. In this case, the reduced effective illumination from the VRD due to SC-1 effects would have contributed to the reduced flicker sensitivity, as flicker detection is degraded by reduced effective illumination of the retina.

Finally, cursory observations comparing the psychological persistence of the VRD and CRT were made under the experimental set-up by two subjects (ST and JK). The temporal integration of stimuli by the retina may be informally measured in a modern replication of the measurement of whirling embers reported by Seguer over 260 years ago [52]. A single raster line on a black background was displayed and stepped up the display field by 4-6 lines per refresh frame. When viewing the display, several lines (3 - 4) are perceived simultaneously even though

only one line is physically displayed per 1/60 second. The number of lines perceived with the VRD and CRT are essentially identical under these conditions. Since the VRD has no physical persistence, the observed effect must be due to the temporal integration by the visual system. Equivalent perception of lines indicates equivalent psychological persistence of the two stimuli of much different physical duration.

In conclusion, this study has shown that 30 Hz flicker contrast thresholds for detection for a retinal scanning display with little image persistence are not different from those of a conventional CRT with substantial phosphor persistence. The shift in VRD flicker contrast thresholds with display luminance is the same as that typical with a CRT. In spite of the vast difference in physical persistence, the psychological persistence of the VRD appears equivalent to that of a CRT. Thus, hypothesis 1b, *Flicker perception of retinal scanning displays is equivalent to that of conventional visual displays*, is supported by these conclusions.

4.2 Critical Flicker Frequency Comparison

The results of the flicker contrast threshold experiment seem to clearly indicate that flicker perception with the VRD is not anomalous. However, contrast thresholds are but one metric in assessing flicker perception. The critical flicker frequency of a display is another flicker perception characteristic that should be investigated to ensure that no effects are overlooked. Thus, as a cross check to the contrast threshold experiment, a brief comparison of CFF was made between an RSD and a temporally square Maxwellian view flickering source.

4.2.1 Objectives and Hypothesis

The primary objective of this experiment was to contribute to the testing of hypothesis 1b: *Flicker perception of retinal scanning displays is equivalent to that of conventional visual displays*. Testing this hypothesis is one part of testing general hypothesis 1: *Retinal response to, and visual perception of, retinal scanning display stimuli is not anomalous*. Further, the testing of these hypotheses directly addresses the second main objectives of this research effort as defined in section 1.2: *Explore the temporal domain with RSD's to identify and quantify any anomalous perceptual effects due to retinal response*.

In this experiment, the critical flicker frequency of a retinal scanning display was measured and compared with that of a non-scanning, standard flickering source. In view of the results of the flicker contrast threshold experiment and the previously reviewed literature, the specific hypothesis for this experiment holds: *The critical flicker frequency for the retinal scanning display is the same as the critical flicker frequency of a non-scanning Maxwellian view flickering source.*

4.2.2 Apparatus and Experimental Set-up

The primary apparatus used in this experiment was the VRD Emulator. The basic configuration described in section 2.1.2 was augmented with a prismatic cube beam splitter, Xenon arc lamp (Oriel Corporation; Stratford, CT), beam chopper, and other optical components as depicted in figure 4.10. The result of the augmented VRDE apparatus was the equivalent presentation of two Maxwellian view displays with coincident exit pupils. One display was the created by the scanning beam of the VRDE, while the second display was the filtered arc lamp.

The VRDE was configured to present a total of 450 laser scan lines as a homogeneous field with vertical line separation subjectively set to the approximate Rayleigh limit. A variable iris placed adjacent to the viewing optic limited the display to circular disks approximately 18° visual angle diameter. The red laser of the VRDE was used throughout his experiment. The beam of the VRDE was well collimated at the exit pupil. Its profile was TEM_{00} , mode. The beam profile was approximately 1.0×1.0 mm (to the $1/e^2$ level). These measurements were made using a PMT sensor with $30 \mu\text{m}$ aperture mounted on a micrometer stage that allowed precise movement of the PMT across the beam profile. Signal recordings from the PMT were made by oscilloscope (Tektronix 550; Beaverton, Oregon) and compiled and plotted with MatLab software.

The VRDE was configured to scan 450 "on" lines and then modulate the laser beam off for a duration equivalent to that required to display the 450 lines. This was accomplished by manipulating VRDE arrays in LabView so that 900 total lines were defined, with the latter 450 lines modulated off by the AOM. The timing of line display is dictated by the clocking of the mirrored polygon IR sensor as described in section 2.1.2. Thus, the 50% duty cycle created by the array configuration would remain constant with variation in the polygon speed and associated frame refresh rate. This would allow subjects to vary the VRDE refresh rate while maintaining

the 50% duty cycle in beam modulation. The VRDE speeds are controlled by LabView software interface on a PC computer.

The xenon arc lamp beam was filtered with a heat glass to eliminate IR energy, then by a 630 nm high pass cut-off filter to approximately match the (x, y) CIE chromaticity coordinates of the monochromatic VRDE display (VRDE = 0.704, 0.290; Xe Lamp = 0.715, 0.282). Neutral density filters were positioned to attenuate the arc's beam prior to the beam's convergence to a focus by a chromatically corrected 50 mm focal length lens. Near the waist, the beam was passed through a spatial filter and then a precision beam chopper (Stanford Research SR-540) to variably flicker the display. The beam chopper consisted of a variable speed rotating disk with alternating field stops and apertures that produced a 50% duty cycle flicker when actuated. The expanded arc beam passed to the prismatic cube beam splitter, and the reflected portion of the beam was converged to a Maxwellian view image by the VRDE viewing optic. Minor adjustments in the beam splitter and other optical components allowed precise alignment of the exit pupils formed by the arc and VRDE, as well as alignment of the spatial extent of the retinal images produced.

An imaging photometer (Photo Research PR-880; Chatsworth, California) was mounted on the optical bench to facilitate display retinal illumination estimates by Westheimer's method with Maxwellian view [75]. Spot measurements made across the field of each display presented on a reflecting standard (LabSper, Inc.; Spectralon USRS-99-010) indicated inhomogeneity in the VRDE of not more than 4%, and not more than 7% in the arc lamp field. A dental impression bite bar mount was positioned in front of the system viewing optic for head and eye stabilization during data collection. The continuous potentiometer control of the arc lamp beam chopper was positioned on the optical bench for easy operation by subjects.

4.2.3 Subjects

The purpose of the experiment was known to all subjects, and each had previously submitted informed consent. A safety analysis of VRD retinal illumination was previously published detailing the compliance with related ANSI standards, and power measurements of the VRDE indicated compliance with the same under normal operating conditions [78]. Three adult subjects were tested. All subjects had psychophysical experimental experience in previous flicker studies. One of these was a VRD researcher with extensive visual psychophysical experience. Each subject had corrected acuity of 20/20 or better, normal eye alignment, and no known visual

defects. Ages ranged from 34 to 49 years. Each subject was tested using the right eye with optical correction, if prescribed. The left eye was covered with an opaque eye patch.

4.2.4 Procedure

The psychophysical method of adjustment was used in this experiment. In nearly dark ambient conditions, subjects viewed the two steady displays simultaneously to ensure proper alignment of the two displays in visual space. The dental impression bite bar was adjusted and fixed after proper pupillary alignment was achieved. The subjects then viewed the 18° homogeneous disk of each display independently with the order of conditions selected pseudo-randomly. The retinal illumination of the two displays was matched by physical measurement. Two levels of retinal illumination were selected for experimentation (1500 td and 150 td).

While viewing the xenon arc display, the subject was instructed to vary the potentiometer control of the beam chopper until the perception of flicker was just detectable. Once the subject was satisfied with the chopper setting, the experimenter noted the chopping frequency from the chopper controller display and recorded it in a spreadsheet as the CFF. Ten trials per condition were conducted.

The procedure while viewing the VRDE was somewhat more involved due to the software interface that was not readily adjustable by subjects attending the bite bar. While viewing the VRDE display, the subject provided sub-vocal (grunts) and hand signals to the experimenter indicating incremental increases or decreases in the refresh rate of the VRDE. With a brief period of coordination and practice, this inelegant procedure was quite effective, although time consuming. Further, the subject was free to relieve himself of the bite bar when necessary to make clarifying comments or to issue specific instructions for adjustments. Once the subject was satisfied with the refresh rate, the frequency was recorded as the CFF by the experimenter in the spreadsheet. Ten trials per condition were conducted.

4.2.5 Analysis

Mean CFF values were calculated for each display and condition and summarized in tabular form. Paired comparisons between display devices were made by t-test.

4.2.6 Results

The CFF of the 50% duty cycle VRDE and 50% duty cycle Maxwellian view xenon arc display were essentially identical. Overall mean values for each condition are summarized in table 4.1:

Table 4.1: Mean critical flicker frequency values

<u>Mean CFF</u>	VRDE	Xe Arc
150 td	38.5	37.1
1500 td	50.1	49.0

No subject showed significant effects between display devices. Mean CFF values for all subjects agreed within 4 Hz. Two subjects (ST and DF) had CFF means agreeing within 1.5 Hz. Standard deviations for all subjects were less than 2 Hz.

4.2.7 Discussion and Conclusions

In light of the previous flicker contrast threshold results, the results of this CFF study are not surprising. The CFF varied as expected with luminance for both displays, and the displays were practically identical in CFF at each luminance level. Although there is a very slight indication of higher CFF with the VRDE, indicating slightly *increased* sensitivity to flicker with the RSD, the trend is extremely small and may be due to error effects. Particularly, the homogeneity of the two displays was not perfect, and small effects of this inhomogeneity are expected. While a minor increase in CFF was also predicted by the extrapolations from Farrell's flicker model, the results are insufficient to reach the conclusion that the prediction was accurate.

Further, discoveries well after the completion of this experiment revealed errors of integration in the measurement of the VRDE display with the PMT-based PR-880 photometer, as described by Boynton and Kelley (see section 2.2.4) [88, 89]. Analyses of the problem with the measurement device indicated that abnormally high variance was present in measurements and that this systematic error also typically resulted in erroneously low averaged readings for the scanning display. Further analyses following corrective actions implemented by the manufacturer revealed that averaged VRDE measurements before the corrections were in error by as much as -0.2 log units, but the mean error was estimated to be near -0.12 log units. Therefore, the matched

retinal illuminations in this CFF experiment were likely in error, with the VRDE retinal illumination being slightly higher than that of the xenon arc due to the photometer's error.

Fortunately, this error is not practically significant in this case. For the experimental conditions, models from literature indicate that a 0.12 log change in display luminance produces a change in critical flicker frequency of just over 1 Hz, and a 0.2 log change in display luminance produces a change of just over 2 Hz [18]. Changes of this magnitude do not impact the statistical results of this experiment. In fact, a slightly higher retinal illumination with the VRDE would explain that displays slightly higher sensitivity to flicker, as hinted by the slightly elevated CFF's. The magnitude of the elevated CFF is consistent with the magnitude of the estimated display luminance difference. Thus, if the estimated corrections in luminance are applied, the results of this experiment indicate an even closer equivalency of the CFF for the two displays.

The 50% duty cycle Maxwellian view arc lamp stimulus is significantly different from either the RSD or CRT stimulus in the spatiotemporal domain. Its persistence is steady during "on" times, not an exponentially decaying function or impulse. The "on" times are a function of the chopping frequency, and were typically 10 - 14 ms in this experiment. There is no raster scan, only a persistent broad field display. In spite of these dramatic spatiotemporal differences, the CFF's were not significantly different.

The Maxwellian view geometry of each display facilitated identical measurement techniques for the two displays. The imprecision associated with illumination estimates derived from natural pupil size is eliminated. With two Maxwellian view systems and coincident exit pupils, no corrections for SC-1 are necessary, further improving the illumination estimates. Additionally, if the entrance pupil and exit pupil alignment is not made precisely, the relative luminous efficiency between the two displays is not affected. Thus, the opportunity for unilateral error due to SC-1 is greatly reduced. Granted, if variable head movements occur between device conditions, an error effect will still be manifested due to SC-1.

In spite of the small photometer error, the retinal illumination for the two displays was well controlled, and no differences were found in flicker perception under closely matched conditions. Differences in CFF would have been expected if one display had been more efficient than the other in affecting phototransduction, or if theoretical flicker-suppressive lateral effects in the retina were activated. The issue of variable luminous efficiency response with the VRDE, as highlighted by the linear relationship between illumination ratios and contrast thresholds in the previous study, seems not to have manifested itself in any recognizable way here.

In conclusion, this study has shown that critical flicker frequency for a retinal scanning display with little image persistence is not different from CFF with a non-scanning Maxwellian view source of equivalent size, shape, chromaticity, and retinal illumination. Thus, hypothesis 1b, *Flicker perception of retinal scanning displays is equivalent to that of conventional visual displays*, is supported by these conclusions.

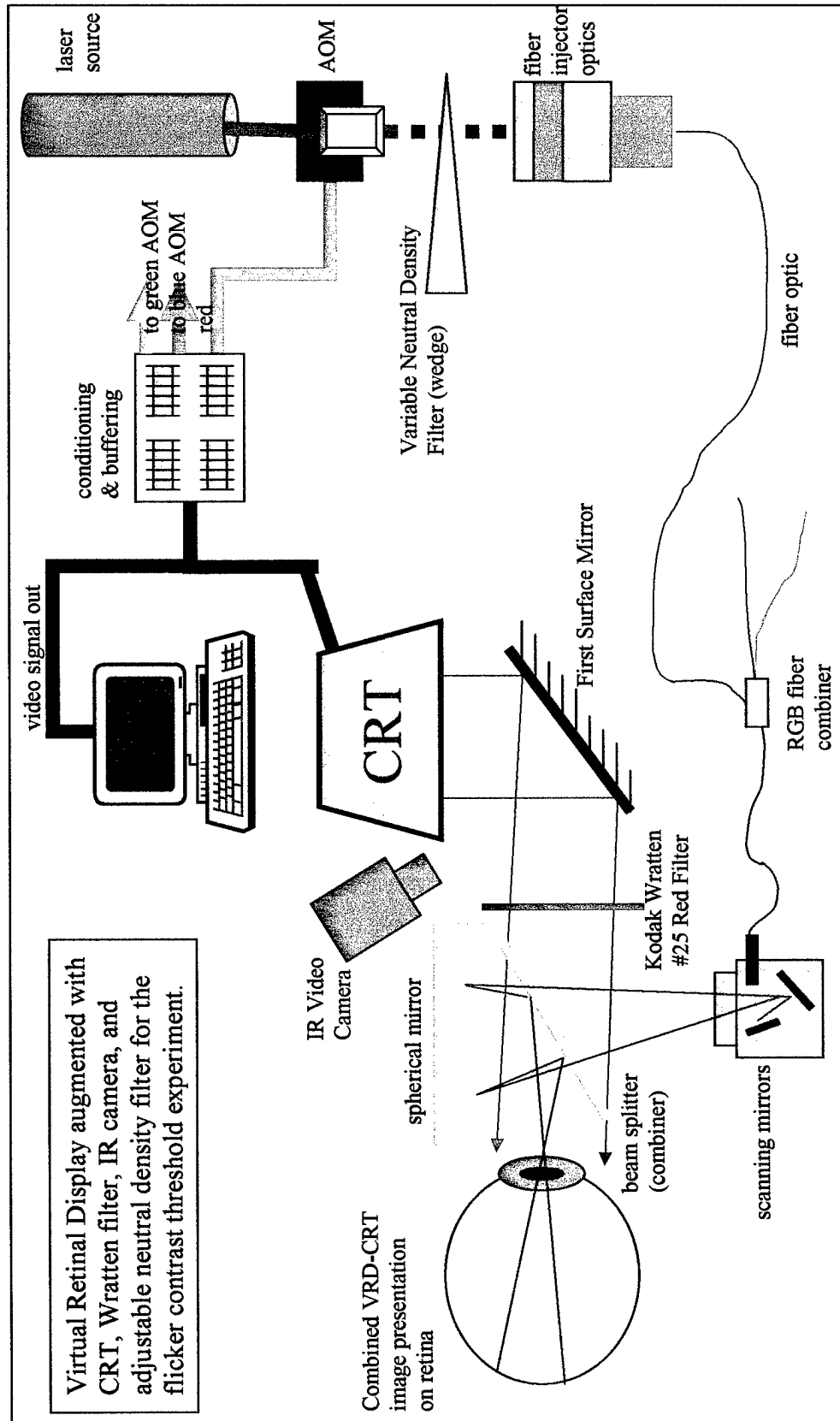


Figure 4.1: VRD Augmented for Flicker Contrast Threshold Experiment

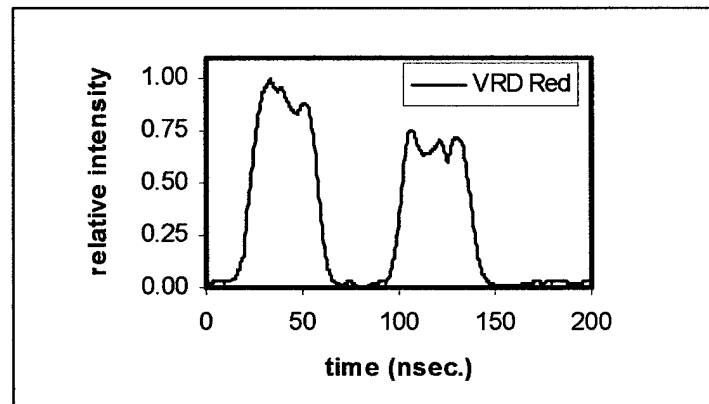


Figure 4.2: Temporal Signature of VRD Pixels

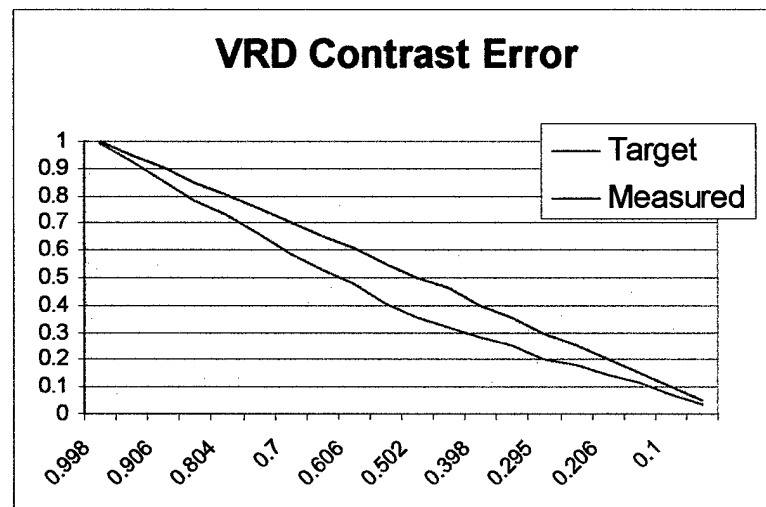


Figure 4.3: Relative Error of Actual Contrasts and Target Contrasts

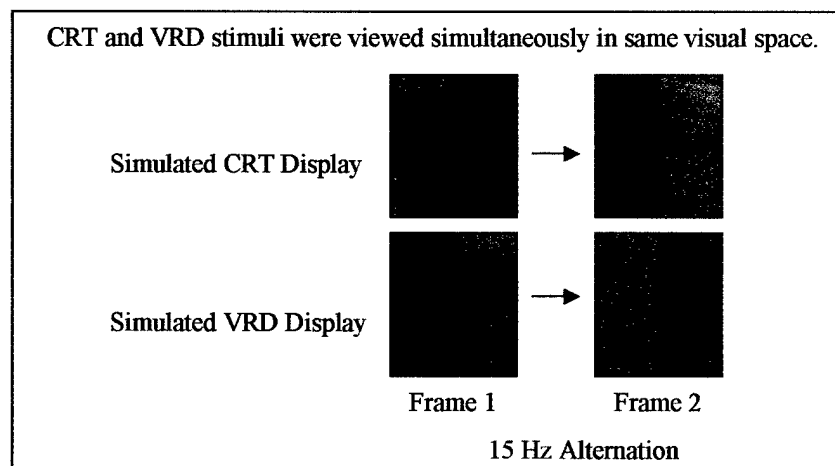


Figure 4.4: Counter Phased HFP Stimuli for Perceptual Luminance Match

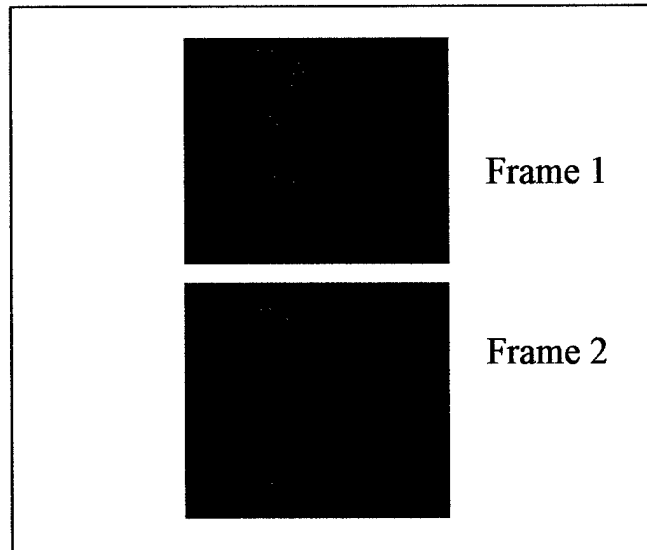


Figure 4.5: Simulated Frames of 30 Hz Gaussian Flicking Stimulus

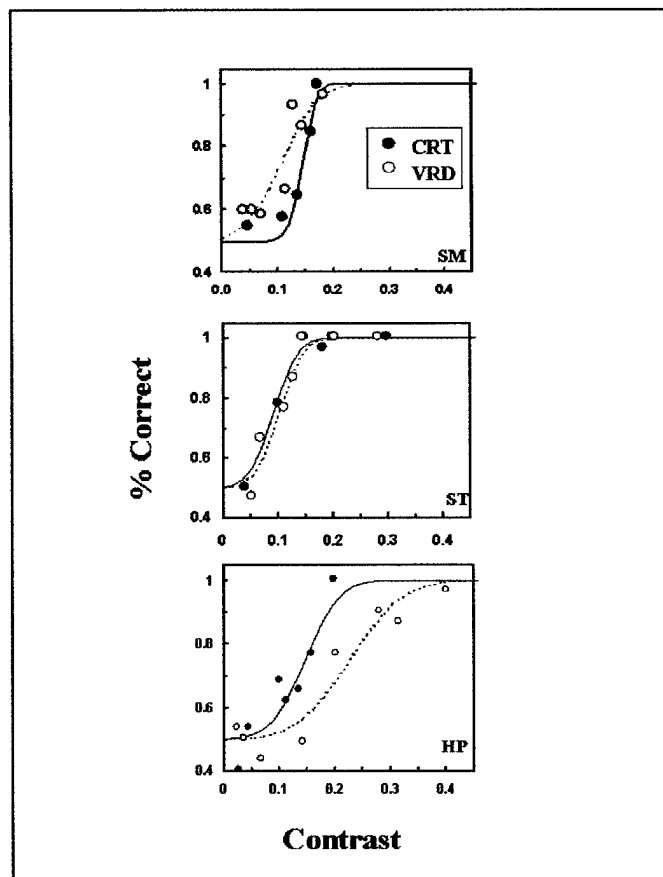


Figure 4.6: Range of Flicker Contrast Threshold Psychometric Functions by 2AFC Method

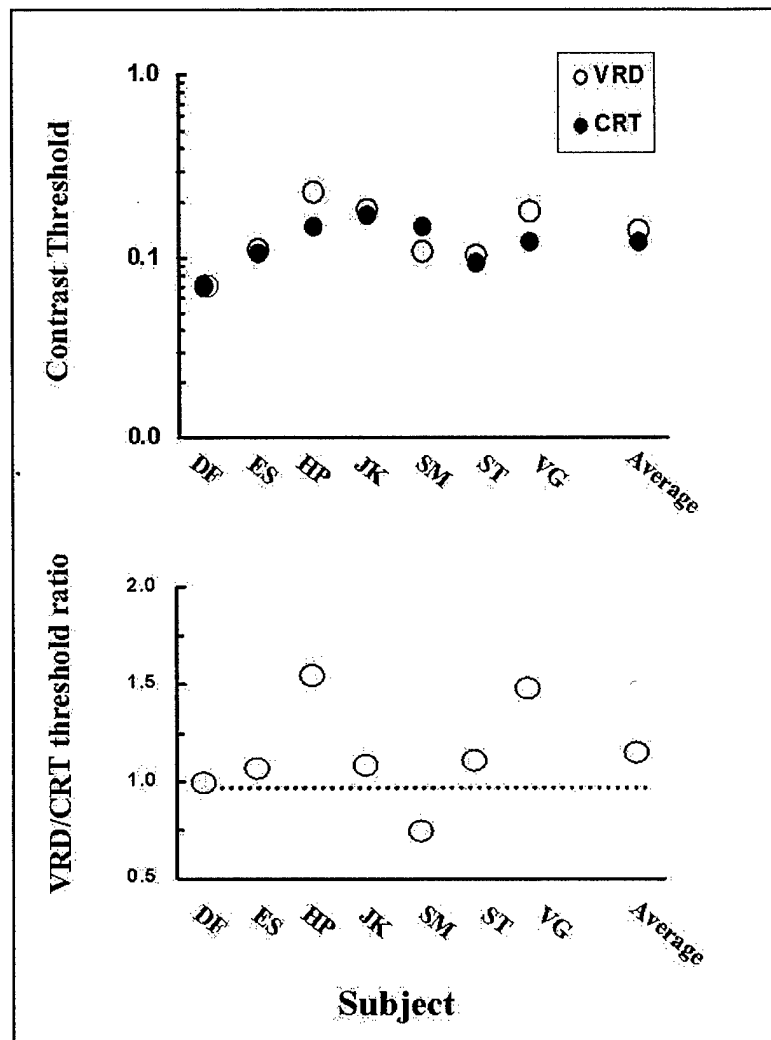


Figure 4.7: Flicker Contrast Thresholds and Threshold Ratios

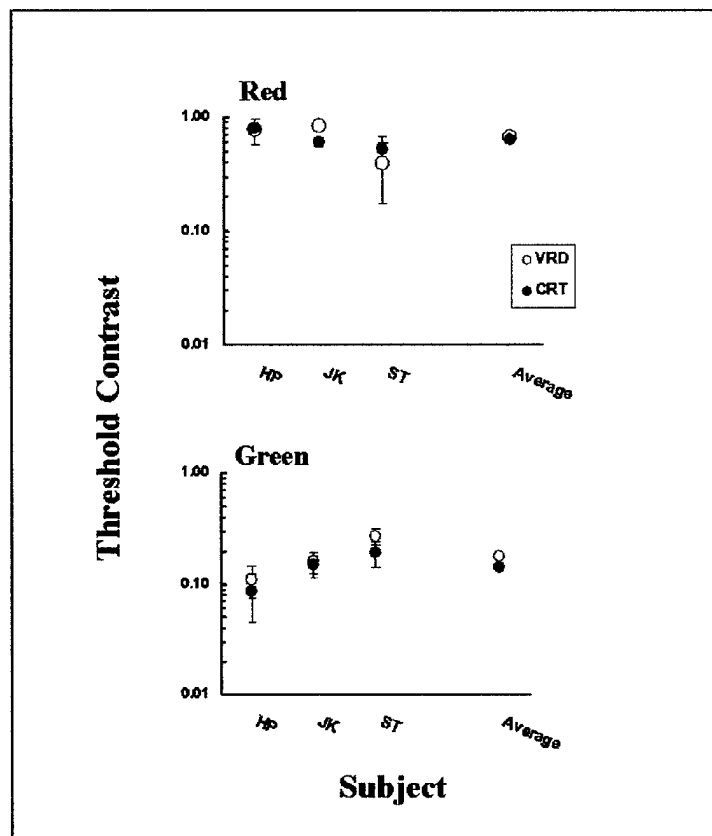


Figure 4.8: Flicker Contrast Thresholds by the Method of Adjustment

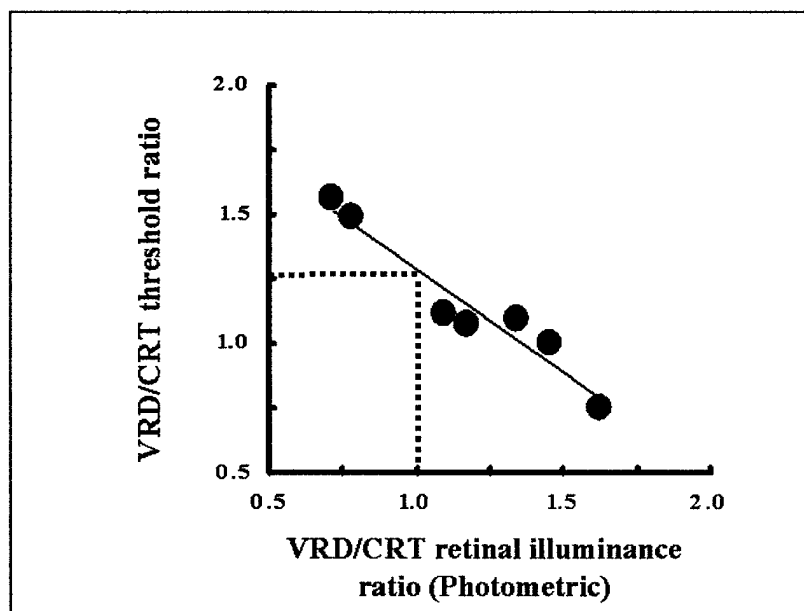


Figure 4.9: Relationship of VRD/CRT Contrast Threshold Ratios to VRD/CRT Retinal Illumination Ratios

VRD Emulator modified for xenon arc lamp Maxwellian view source. The arc lamp beam is filtered for IR, chromaticity, and intensity. The beam is converged, spatially filtered, and temporally chopped. The cube splitter redirects the arc beam coincident with the scan of the VRDE, forming two coincident exit pupils in front of the viewing optic of identical geometry.

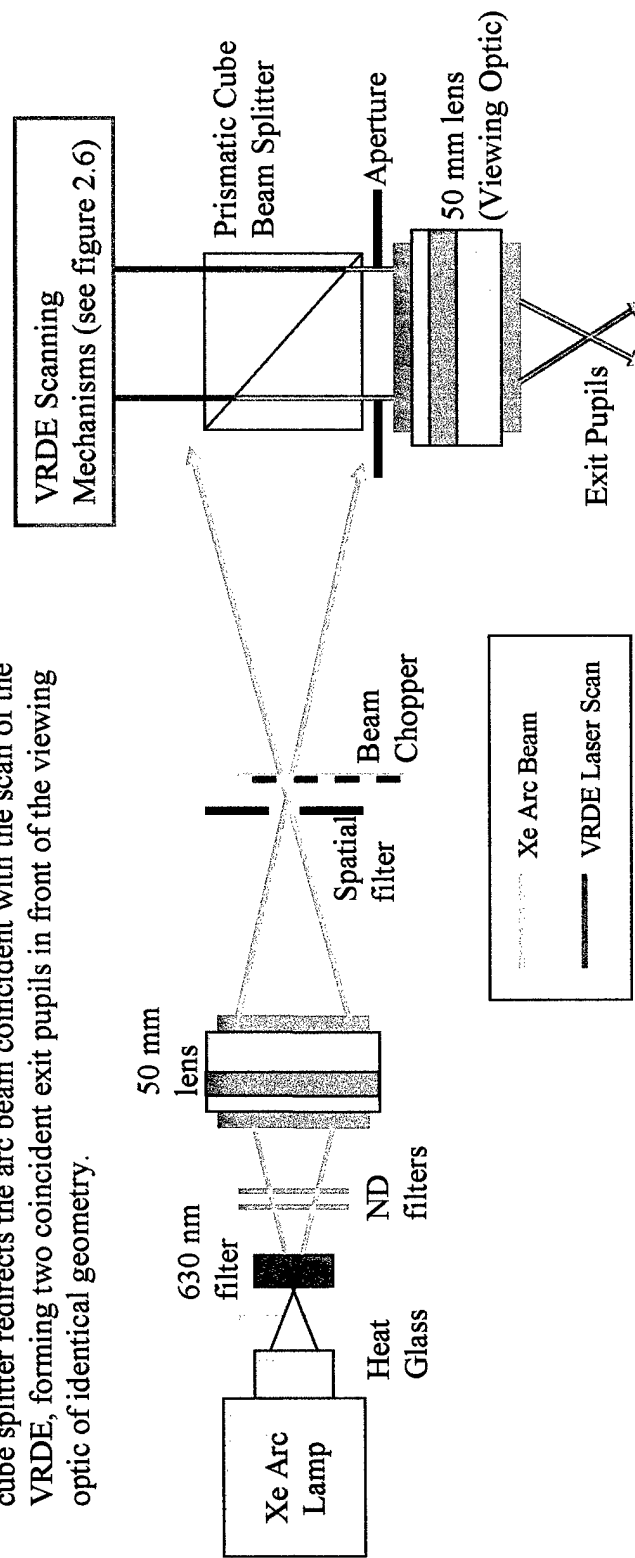


Figure 4.10: VRD Emulator Modified for CFF Experiment

Chapter 5: Retinal Response in the Intensity Domain: Brightness Experiments

As pointed out in the previous chapter describing flicker experiments, some data suggested that luminous efficiency with the RSD may differ from that with non-scanning displays, such as CRT's or other standard sources. Experiments specifically examining brightness with a retinal scanning display are warranted to identify any anomalous responses of the retina in the intensity domain of visual perception.

Two similar experiments were conducted to examine brightness perception. Initially, a comparison was made between the brightness of a Maxwellian view xenon arc display and the VRD Emulator display. In this experiment, subjects made perceptual brightness matches of the two displays by the HFP psychophysical methodology (section 2.2.1.2), and estimates of retinal illumination from the two displays were then made by Westheimer's method of the Maxwellian view (section 2.2.3). Unexpectedly, the VRDE's retinal illumination at perceptual match was measured to be slightly less than that of the xenon arc display (0.08 - 0.18 log units) for all subjects, and the differences were statistically significant. Multiple repeated iterations of the experiment produced essentially identical results.

However, these results were obtained using the PR-880 photometer (PhotoResearch, Chatsworth, California) before the discovery of an integration error in the device (see section 2.2.4 for a detailed discussion). The error was related to improper integration by the photomultiplier tube circuitry and it induced significant error when measuring an irregular periodic source like the VRDE display in this experiment. Subsequent tests revealed consistently low measurements on the order of the obtained effect when measuring an RSD display with the device. In fact, the mean error measurement in experimenter tests of the device was approximately -0.12 log units. Adjusting the experimental results by this mean error value cancelled their significance and resulted in mean values of retinal illumination for the two sources that were within 0.02 log units (5%). This is well within the expected normal human variation for psychophysical measurements.

However, this correction was coarse and these experimental results were invalidated by the measurement error that was unknown at the time of the experiment. Clearly, the small effect was a result of the measurement error, but the correction technique was crude and left the experimental evidence tainted. A conservative approach was taken. Replication of the precise experimental conditions for the sole purpose of corrected measurement of the VRDE stimuli was

deemed to be impractical due to multiple subsequent reconfigurations and changes in the VRDE apparatus. Therefore, this study is not fully reported as the results may be considered ambiguous. However, it is notable that the magnitude of the obtained effect was small and well matched to the magnitude of measurement error with the PR-880 photometer. Therefore, it is asserted that no significant results were actually obtained in the study. It should also be noted that subsequent upgrades to the PR-880 photometer were made by the manufacturer that rectified this problem.

To properly evaluate the retinal response to RSD stimuli in the intensity domain, a new and improved brightness matching experiment was conducted. In lieu of a reproduction of the experiment comparing the polychromatic filtered xenon arc stimulus with the monochromatic VRDE stimulus, an experiment was designed to eliminate the uncontrolled variable of polychromaticity. In this experiment brightness matching comparisons were made between the VRDE and a static source of precisely equivalent chromaticity. That experiment is reported here in entirety.

5.1 Brightness Comparisons of Scanning and Non-scanning Maxwellian Sources

The comparison of brightness due to an RSD and another non-scanning Maxwellian view display that utilize identical luminous sources tested speculation by Furness that the spatiotemporal characteristics of RSD's may enhance luminous efficiency at the retina (Thomas Furness, 1998 and 1999, personal communications). His postulate was based upon prior cursory observation of the VRD's brightness and flicker characteristics and upon the possibility of an RSD-induced spatiotemporal resonance among retinal cells, possibly conducted via amacrine interconnections and potentially incited by the very brief and intense stimulation provided by the VRD.

The use of a Maxwellian view display as a comparison standard controlled variables associated with natural pupil viewing that affect retinal illumination, including the SC-1 effect. Further, it promoted the use of a single common measurement technique for each display type. The use of an identical monochromatic source of illumination controlled the variables of polychromaticity (multiple wavelengths versus a single wavelength source), chromaticity (color), and hue saturation, each of which affects brightness perception [26]. Thus, this comparison isolates the spatiotemporal scan of the RSD as the independent variable much more effectively than did the earlier experiment.

In comparing two different luminous sources by the psychophysical method of adjustment, random variation of 10% is typical among human subjects. Therefore, in all perceptual brightness matching comparisons of displays of equal luminance reported here, a statistically significant deviation in the overall mean luminance ratio of the perceptually matched displays of more than 10% from unity will be considered a practically significant result. Further, variation of more than 10% by any single subject will be considered a practically significant result. While differences of 10% are not sufficient to explain the cursory flicker and brightness observations of the VRD reported by Furness and others, this smaller difference threshold is sufficient to indicate anomalous retinal response to the RSD stimuli.

5.1.1 Objectives and Hypothesis

The primary objective of this experiment was to contribute to the testing of hypothesis 1a: *Brightness perception of retinal scanning displays is equivalent to that of conventional luminous sources.* Testing this hypothesis is one part of testing general hypothesis 1: *Retinal response to, and visual perception of, retinal scanning display stimuli is not anomalous.* Further, the testing of these hypotheses directly addresses the first main objectives of this research effort as defined in section 1.2: *Explore the intensity domain with RSD's to identify and quantify any anomalous perceptual effects due to retinal response.*

Hypothesis 1a was drawn directly from literature, logical analysis, and reasoned assertions. Although some questionable evidence exists in previous VRD research and cursory observations that luminous efficiency with RSD's may differ from that predicted by conventional vision theories, the more plausible explanation is experimental error and the uncontrolled conditions of cursory observation. Specifically, the results of Kelly (1998) and the small potential flicker sensitivity difference discussed in sections 4.1.7 and 4.1.8 leave open the possibility of a small luminous efficiency enhancement with RSD stimulus [79]. However, only precise and thorough scientific investigation will sufficiently expose the truth regarding visual system response to RSD stimuli in the intensity domain.

In this experiment, a comparison of perceived brightness was made between the VRD Emulator's homogeneous scanned field of 632.8 nm laser illumination and an expanded beam, static homogeneous field of 632.8 nm laser illumination. Spatial artifacts typical of coherent

illumination were eliminated from the static laser field by optical methods subsequently described so that brightness perception was not adversely affected.

The reviewed literature by Wald and Brown (1956), Baylor, Nunn, and Schnapf (1987), and Boynton (1979) strongly supports the theory that luminous efficiency is a function of the probability of photon absorption by the photopigments in the photoreceptive cells of the retina [28, 29, 31]. Further, the Talbot-Plateau law seems to indicate that brief temporal stimuli such as that provided by RSD's continues to follow the established rules of temporal integration within the retina with no remarkable enhancement to luminosity [53]. Besides Kelly's erroneous 1998 study, no evidence exists in literature to support anomalous luminosity effects by raster scanning displays of brief persistence [79]. Therefore, if enhancements to luminous efficiency are induced by RSD stimulation of the retina, only a previously undiscovered combined effect of the brief, intense RSD impulse and the large scale scanning across the retina remains to explain such effects. The small possibility of this effect remains, as expressed by Rodieck's questions about the unexplored influences of the far-reaching, interconnecting amacrine cells in the retina [16]. However, such theoretical speculation is insufficient evidence with which to posit an experimental hypothesis.

Concordant with hypothesis 1a, the specific hypothesis for this experiment holds: *At perceptual brightness match, the time averaged retinal illumination due to the VRD Emulator display and Maxwellian view static laser display are equivalent.*

5.1.2 Apparatus and Experimental Set-up

The basic apparatus for this experiment was the VRD Emulator. The basic configuration as described in section 2.1.2 was modified to split the helium-neon laser emissions into two beams and to expand one beam into a static homogeneous field. Additional optical components were added as depicted in figure 5.1.

The VRDE was configured to present a total of 450 laser scan lines as a homogeneous field with vertical line separation subjectively set to the approximate Rayleigh limit. A variable iris placed adjacent to the viewing optic limited the display to circular disks approximately 18° visual angle diameter or less. The red laser of the VRDE was used throughout his experiment as the source of luminance for each presentation. The beam of the VRDE was well collimated at the exit pupil. The beam was TEM₀₀ mode, as determined by the characteristic mode form indicated

in the beam profile, and the beam diameter was approximately 1.0×1.0 mm (to the $1/e^2$ level). The beam profile was made using a PMT with $30 \mu\text{m}$ aperture mounted on a micrometer stage that allowed precise movement of the PMT across the beam profile. Signal recordings from the PMT were made by oscilloscope (Tektronix 550; Beaverton, Oregon), and the conglomerate oscilloscope profiles were merged and plotted as a contour chart using MatLab software to produce the beam profile.

The VRDE laser beam was split with a 50% beam splitter immediately after emission from the laser. The undeflected portion of the beam was directed into the VRDE optics and scanners as previously described. The deflected portion of the beam was routed by first surface mirrors to a lens for expansion. The highly luminous central region of the expanded Gaussian beam was apertured by a subsequent converging lens. The converging beam passed through neutral density filters for attenuation, and the beam was spatially filtered at the focal point to help remove optical artifacts. After the spatial filter, the re-expanded beam was collimated with sufficient spatial extent and directed into a prismatic cube splitter. Each portion of the split expanded beam fell onto rapidly rotating, micro-corner cube retroreflectors. The retroreflected beams were redirected through the cube splitter to a first surface mirror that bent the path toward a second cube beam splitter within the optical path of the VRDE scan. The expanded beam was partially reflected by the cube splitter to be directed into the VRDE viewing optic on a path coincident with the VRDE scan. The VRDE viewing optic converged the expanded beam to form a Maxwellian view image precisely coincident with the exit pupil of the VRDE. As a result, Maxwellian view display fields of equivalent size, shape, and geometry were available for presentation on the retina, one created by the VRDE scan and the second created by a static expanded monochromatic source.

The purpose of the retroreflector arrangement requires some explanation. When viewed directly, an expanded coherent laser beam exhibited spatial patterns due to diffraction effects and speckle. In order to achieve a homogeneous expanded field free of such spatial effects, the coherency of the beam had to be disrupted. As discussed in section 2.2.2, temporal and spatial coherency is disrupted for the RSD scanned field by the scanning action itself, producing a homogeneous display field with no diffraction spatial effects. A method was implemented with the expanded static laser field to disrupt coherency without affecting a scanning pattern in order to allow valid comparisons with the VRDE field. The rapidly rotating retroreflectors (approximately 500 rpm each) serve to disrupt the temporal and spatial coherence of the

expanded beam by randomly scrambling phase relationships and polarization vectors among wave packets. The result was a smooth, homogeneous static display field free of spatial effects.

The homogeneity of each field was measured with a (corrected) PR-880 imaging photometer (Photo Research; Chatsworth, California). Spot measurements made across the field of each display presented on a reflecting standard (LabSphere, Inc.; Spectralon USRS-99-010) indicated inhomogeneity across the VRDE display of not more than 4%, and not more than 8% in the static laser field for field diameters equating to stimulus conditions.

In addition to the optical components, two beam choppers were introduced into the apparatus, one for each display. One chopper was positioned in the VRDE beam path just prior to the scan mechanism (Boston Electronics Corp.; DHC-60). The second chopper was positioned in the static display's beam path prior to beam expansion. Each chopper was electronically controlled by the VRDE computer and LabView software interface. A sequence of discrete voltage levels identified in LabView arrays controlled the position of each chopper. The output of array values was controlled with the clocking signal provided by the mirrored polygon's IR emitter-detector (section 2.1.2) so that chopping of each beam was precisely synchronized with the VRDE display line and frame rates. With properly constructed voltage value arrays, the two display beams were chopped in precise counter-phase to conduct flicker photometry brightness matches.

For HFP brightness matching, the two coincident displays were counter-phased at 15 Hz, as implemented with the beam choppers. The expanded static beam field was displayed as a temporal square wave, while the VRDE accomplished two complete frame refreshes during each of its HFP "on" times. Figure 5.2 depicts an illustration of a typical counter phased signature of the two displays as recorded with an optical sensor and oscilloscope. The VRDE signature appears as a "double humped" trace, as the circular aperture of the display is refreshed twice with scanned horizontal lines.

The light measurement apparatus consisted of an optical power meter (Newport model 1835-C, Newport Corporation, Irvine, California) with analog output routed to a digital sampling oscilloscope (Tektronix 550, Beaverton, Oregon). The power meter was tuned for the 633 nm wavelength of the displays. The oscilloscope was operated in a function integration mode that calculated the area (in ms V) under the displayed waveforms and between repositionable cursors. By placing the power meter detector at the exit pupil position under HFP display conditions, the counter phased waveforms of each display could be independently integrated to provide a

quantification of the optical power entering the eye. This measurement methodology offered excellent precision in making relative comparisons of the display powers. Absolute measures for approximating retinal illumination ranges were made with a (corrected) PR-880 imaging photometer (Photo Research; Chatsworth, California) by Westheimer's method of the Maxwellian view [75].

An adjustable dental impression bite bar was mounted near the VRDE viewing optic. Custom dental impressions for each subject were mounted on the bar that was stabilized when the subject's eye was properly positioned at the mutual exit pupils. This apparatus minimized the possibility of head movements during data collection in order to avoid variation in effective retinal illuminance imposed by the Stiles-Crawford I effect. However, even with small head movements, equivalent SC-1 efficiency factors applied to each display since the exit pupils were coincident.

5.1.3 Subjects

The purpose of the experiment was described to all subjects, and each had previously submitted informed consent. A safety analysis of VRD retinal illumination was previously published detailing the compliance with related ANSI standards, and power measurements of the VRDE indicated compliance with the same under normal operating conditions [78]. Four adult subjects were tested. All subjects had psychophysical experimental experience in previous VRD studies. Two of these were VRD researchers with extensive visual psychophysical experience. Each subject had corrected acuity of 20/20 or better, normal eye alignment, and no known visual defects. Ages ranged from 26 to 39 years. Each subject was tested using the right eye with optical correction, if prescribed. The left eye was covered with an opaque eye patch.

5.1.4 Procedure

The psychophysical method of adjustment with flicker photometry was used in this experiment (section 2.2.1.2). In dark ambient conditions, subjects viewed a static presentation of the two displays to ensure proper alignment of the coincident fields in visual space. The dental impression bite bar was adjusted and fixed after proper pupillary alignment with the exit pupils was achieved. This helped to minimize head movement and eye position variations.

Four conditions were tested for each of the two displays. Two levels of circular field diameter (12° and 3.5°) and two levels of retinal illumination (250 td and 1500 td) were examined. (The maximum field size was limited by the available luminance of the expanded beam as well as the achievable field homogeneity with the expanded beam.) Condition sequences were selected pseudo-randomly. The subjects viewed the 15 Hz counter phased Maxwellian view displays while adjusting a variable neutral density filter (wedge) that modulated the intensity of the VRDE scanning beam. The subject was instructed to adjust the wedge until the perception of flicker in the stimulus was minimized. Once the subject was satisfied with the wedge setting and minimized flicker perception, the experimenter recorded the wedge filter index in a spreadsheet. Several practice trials were run prior to each condition to allow the subject to adapt to the conditions of the new stimulus and to ensure a performance plateau was reached with that adaptation. A minimum of twenty trials were then conducted for each condition.

5.1.5 Analysis

The oscilloscope waveform integration values (in ms V) associated with wedge filter indices was recorded in advance of experimental sessions and spot checked after experimental sessions. The correlated integration values were then used as the dependent measures in analyses. Mean integration values and standard deviations were calculated for each subject, and simple paired comparisons between displays were made by t-test. The ratios of VRD/CRT integration values were calculated and plotted graphically. The integration values were also correlated with absolute illumination estimates as measured with the photometer in units of troland for reporting purposes.

5.1.6 Results

The data as retinal illumination ratios (static display / VRDE) for each subject are summarized in figure 5.3. The mean illumination ratio across subjects for each condition is also depicted. The range of retinal illumination ratios ranged from slightly lower than unity to slightly higher than unity. The ratio means for each condition across subjects are all clustered within 0.016 of unity, and the overall mean ratio was 1.0. As determined by estimates of retinal illumination in troland,

the standard deviation for all subjects and conditions did not exceed 0.052 log units, and was typically 0.035 log units.

Subject RM showed the greatest illumination ratio deviations from unity, with a ratio of just 0.91 in the 3.5° 250 td condition. This subject's mean ratio across conditions was 0.093, indicating reduced illumination from the static field as compared to that of the VRDE at perceptual match. All display comparisons except one (12° 250) for RM were significant. Subject JK showed the greatest ratio deviation above unity at 1.08 for the 12° 1500 td condition, but only that comparison for JK was significant. With a mean ratio across all conditions of 1.04, subject SF showed significant differences between displays for all conditions. This subject had the lowest variance of the four subjects in every condition, and his mean ratio across conditions varied by less than 0.01. This indicates a slightly higher illumination from the VRDE at perceptual match for subject SF. With a mean ratio across conditions of 1.0, subject ST had no significant display comparisons.

5.1.7 Discussion and Conclusions

The mixed results of this experiment represent typical individual differences in visual psychometric function. The fact that the individual differences are centered on the condition of stimuli equality, with variations less than 10% either side of the mean, is a clear indication that the stimuli are well matched physically.

Seven of the 16 display comparisons were statistically significant. However, significance was exhibited both above and below the unity illumination ratio. Given the very low variance of these data, the statistical power in these comparisons was sufficient to resolve the normal psychometric variations among individuals. There is no practical significance in these comparisons. Further, while some significant comparisons were exhibited across conditions for two subjects (RM and JK), there were no clear trends with conditions.

Additional data were collected with one subject (ST) in a pilot study using this apparatus. A bipartite field presenting adjacent hemifields from the two displays was created with non-flickering stimuli. These hemifields were used to make side-by-side brightness comparisons of the scanning and static fields. A broad range of refresh rates of the VRDE was examined, up to 180 Hz. A variety of field sizes were also examined under each refresh rate condition, from 2° to 18°. With each condition, method of adjustment brightness matches were made by adjusting the

wedge filter to vary the intensity of the VRDE display. Repeated trials were conducted in each condition. No significant effects of refresh rate or field size were noted under any conditions.

Therefore, given the variety of results closely clustered about the condition of equality between the displays, and; given the apparent lack of effects due to photopic luminance level or field size, and; given the lack of effects due to refresh rates; the conclusion is reached that no luminous efficiency differences in phototransduction are manifested by the spatiotemporal characteristics of retinal scanning displays. The specific hypothesis for this experiment is confirmed: *At perceptual brightness match, the time averaged retinal illumination due to the VRD Emulator display and Maxwellian view static laser display are equivalent.* Further, this conclusion supports general hypothesis 1a: *Brightness perception of retinal scanning displays is equivalent to that of conventional luminous sources.*

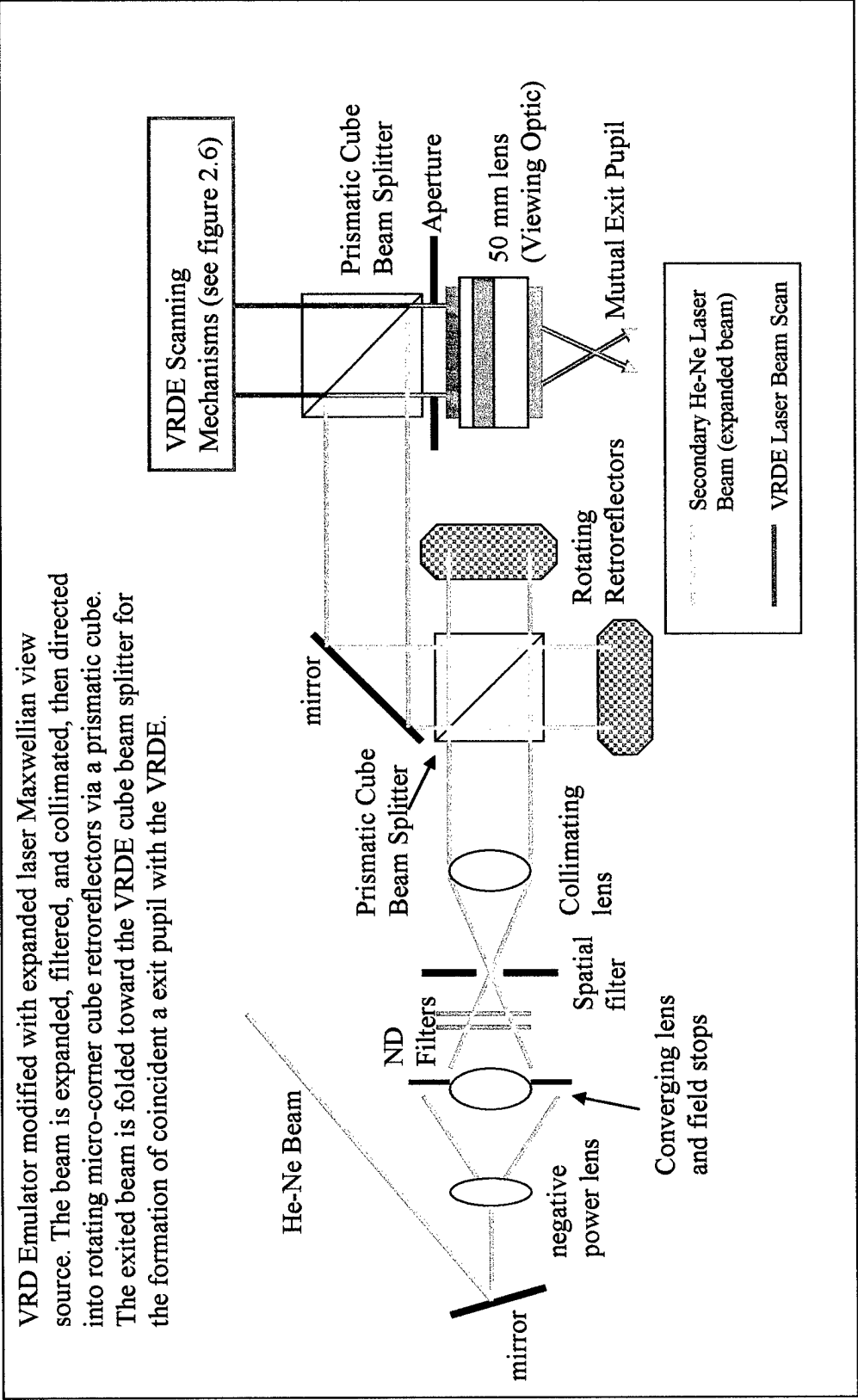


Figure 5.1: VRD Emulator Modified for Brightness Matching Experiment

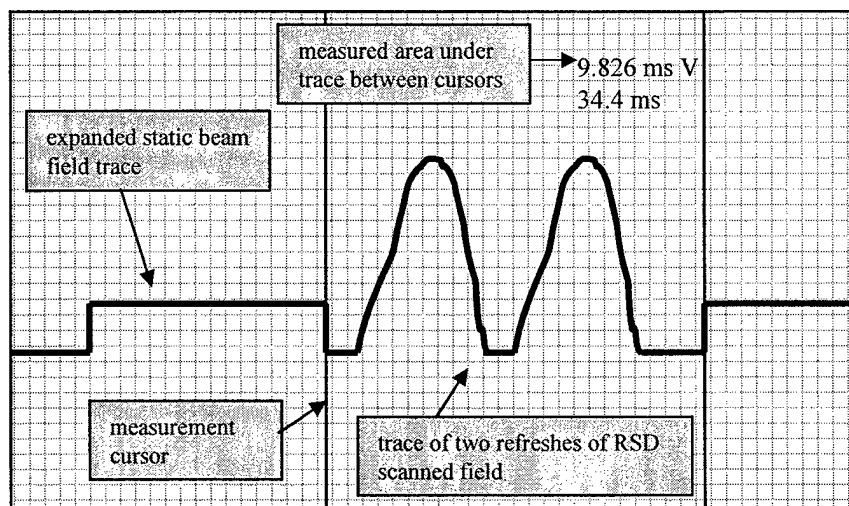


Figure 5.2: Schematic of Typical Oscilloscope Measurement Display for Brightness Matching Experiment Measurements

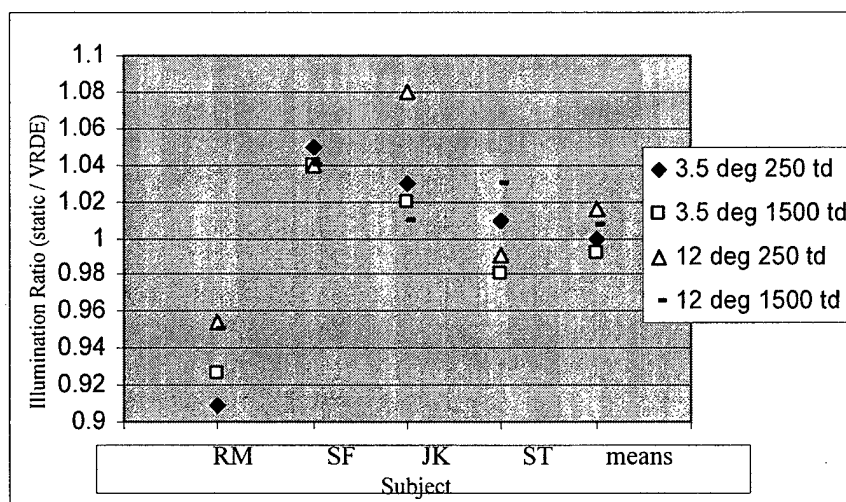


Figure 5.3: Summary of Retinal Illumination Ratios for Brightness Matching Experiment

Chapter 6: Optophysiological Response: Pupillary Response Model Development

A multi-part experiment was conducted to obtain data for the construction of models of human pupillary response to RSD stimulation. The first part of the experiment examined pupil response to binocular and monocular RSD display conditions with opaque, or dark, background.

Subsequent parts of the experiment examined the pupil response to binocular and monocular RSD display conditions in augmented view across a range of background luminance conditions. All data collections were conducted consecutively in unbroken experimental sessions in which each subject participated in all parts. The entire experiment was conducted using the VRD emulator modified to a binocular RSD display arrangement. The results confirmed experimental and general hypotheses, although some unexpected, but explained, findings were obtained. Models of human pupil response were confirmed and empirically derived.

6.1 Objectives and Hypotheses

The general objective of this experiment was to contribute to the testing of hypothesis 2: *Optophysiological responses of the visual system to small exit pupil retinal scanning displays differ from the responses to equivalently perceived conventional displays*. Under this main hypothesis, the testing of three sub-hypotheses are also objectives of this experiment.

- *Sub-hypothesis 2a: For binocular opaque view RSD stimuli and photopic luminance conditions, actual pupil size follows a pupil size function associated with the Stiles-Crawford-adjusted effective pupil size.*
- *Sub-hypothesis 2b: In binocular RSD augmented view under photopic luminance conditions, pupil size is a function of the effectivity ratio-adjusted corneal flux density of the RSD and the luminance of the natural scene.*
- *Sub-hypothesis 2c: Under monocular RSD display conditions in both opaque and augmented photopic view, pupil size will follow functions similar in form to the binocular functions, but pupil diameters will be larger than those under similar binocular RSD display conditions by approximately 1.0 mm.*

The testing of these hypotheses directly supports the third major objective of this body of research: *Explore the pupillary response to small exit pupil RSD's and model the behavior of the pupillary system under RSD stimuli conditions.*

In this experiment subjects were exposed to binocular and monocular RSD stimulation in both opaque and augmented view. The display was affected with small exit pupils directed through the central eye pupils. The subjects' eye pupil images were recorded and subsequently analyzed for pupil diameter measurements. Pupil diameters were examined as functions of RSD corneal flux density (section 2.2.2.5) and background luminance level for both monocular and binocular RSD display.

Based upon the literature regarding the Stiles-Crawford I effect and pupil response, the eye pupil is expected to constrict to a greater extent under binocular RSD stimulation in opaque view conditions than under similar natural view retinal illumination conditions. Concordant with sub-hypothesis 2a, the first specific hypothesis for this experiment holds: *The actual eye pupil diameter in binocular RSD opaque view will follow the Stiles-Crawford adjusted effective pupil size and thereby conform to the function of corneal flux density defined by equation 3.1c in section 3.2.1.*

Based upon the literature regarding pupil response to photopic luminance conditions and the reasoned assertions put forth regarding the combined effects of display and background luminance, pupils are expected to respond as a function of combined background and display luminance under binocular augmented RSD conditions. While no specific mathematical models are hypothesized to define these responses, a family of empirically derived functions is expected to result. Thus, concordant with sub-hypothesis 2b, the second specific hypothesis for this experiment holds: *In binocular augmented view, a family of empirical eye pupil diameter functions will be derived, each with general form similar to the hyperbolic function of equation 3.1c, with pupil diameter inversely related to background luminance by a large effect, and with eye pupil diameter inversely related to RSD corneal flux density by a relatively smaller effect.*

Based upon the literature regarding the comparison of pupil response to binocular and monocular stimulation, pupils are expected to be generally less constricted under monocular conditions than under binocular conditions. The magnitude of this difference is expected to vary with luminance levels. Concordant with sub-hypothesis 2c, the third specific hypothesis for this experiment holds: *Eye pupil diameters with monocular RSD conditions will be larger than eye pupil diameters under binocular conditions of equivalent background and RSD luminance levels, and the magnitude of this difference will range from a maximum of approximately 1.5 mm at the lowest luminance conditions to zero at the greatest luminance conditions.*

6.2 Apparatus, Experimental Setup, and Calibrations

The apparatus used in this experiment was the VRD emulator modified to be a binocular augmented view RSD display. Figure 6.1 diagrams the modified optical arrangement, and Figure 6.2 depicts a photograph of the apparatus. The basic configuration described in section 2.1.2 (Figure 2.6) was extensively modified on the optical path after the mirrored polygon. The scanning beam exiting the polygon was folded and clipped in the horizontal dimension by a first surface mirror in a manner similar to the basic configuration, although the scan was allowed to expand to a greater extent to create a larger effective aperture of approximately 50 mm diameter. A 600 mm focal length converging lens was placed in the scan path to collimate the scan and to gently converge the beam. The long focal length lens provided the greater working distances necessary to expand the scan and to focus the beam at proper locations along the increased lengths of the optical paths.

After scan collimation, the scan was split along two paths, one for each of a subject's eyes. Each scan was folded with first surface mirrors to an elevated platform on the optical bench that held the display viewing assembly. The elevated viewing assembly provided a convenient method of deconflicting the dual optical paths, optical components, and subject anatomy. The two scans were directed so that they would each pass through a dedicated converging lens that was positioned to the temporal side, and slightly behind, each of the subject's eyes. The beam came to a focus at the focal length of the converging lenses (75 mm before the lens) so that a collimated beam was provided for viewing. A beam splitter associated with each scan converging lens folded the converging scan into the subject's eyes, allowing an unblocked view through the beam splitters and affecting an augmented view display.

With the converging lenses positioned slightly aft of eye position, and with other components positioned above or below the viewing elevation, the subject's natural view was almost completely unencumbered. Only a small portion of the converging lenses and a small portion of the elevated platform base were visible in peripheral vision. Additionally, a small first surface mirror used in imaging the eye for data collection was in view approximately 45 degrees right of visual field center for the right eye. This mirror was necessary for the infrared camera to image the eye at an angle that facilitated accurate pupil measurements. At the mirror angle used for imaging, the horizontal and vertical extents of the mirror's image in the field of view were each less than 3 degrees visual angle.

A translucent screen was placed at a distance of approximately 25 centimeters from eye position beyond the viewing beam splitters. This screen was rear illuminated with a bright white light lamp. The lamp was wired to a variable power supply to provide a range of experimenter-defined background luminance levels. The screen and lamp provided a homogeneous white background field for augmented view, and the entire screen was blocked with black felt cloth hung immediately behind the beam splitters to affect opaque viewing conditions.

As discussed in Chapter 2, accommodation affects pupil response when accommodation of more than 1 diopter is required. Clearly, the background screen was closer than the 1 meter distance associated with 1 diopter accommodation. The close distance to the screen was necessary to provide a sufficiently wide background view with good homogeneity of the background illumination. However, the screen provided little, if any, spatial frequency information to promote accommodation at that close range. Instead, a white crosshair, collimated to optical infinity, was provided to guide subjects' accommodation. A small, fine crosshair was painted onto a clear, optical grade glass plate and placed in the right-side optical path at the focal length of the right converging optic (75 mm). The crosshair was front illuminated with a small, variable intensity, white light source. As a result, a well collimated image of the crosshair was superimposed on the visual field of the right eye providing sufficient contrast and spatial frequency cues for accommodation near optical infinity. Further, this crosshair was presented using the large exit pupil of the converging lens (approximately 27 mm diameter) and was not in Maxwellian view. Therefore, no unusual accommodation response resulted to affect pupil response. The variable intensity illumination allowed adjustments for maintaining the apparent crosshair luminance near that of the RSD image and thereby avoiding any significant pupil response effects due to the crosshair.

A variable diameter aperture was positioned in the optical path just before the scan was split into two paths. This affected variable, but equivalently sized, scan patterns for each of the binocular optical paths by which the display field of view (FOV) was manipulated. When the viewing arrangement was properly aligned to a subject's eyes, a fused binocular image of an RSD-imaged disk was perceived with the small white crosshair centrally positioned in the disk. The crosshair appeared in focus when the subject accommodated near optical infinity, and the RSD image similarly appeared in focus with great depth of field. By altering the size of the variable aperture, variable display FOV diameters were presented. By varying the intensity of the RSD laser source, variable RSD luminance levels were presented. By varying the intensity of the

background illumination lamp, variable background luminance levels were presented. Monocular RSD view was affected with an optional light block placed in the left-side optical path prior to the converging lens.

Proper coupling of pupils was affected with a five dimensional adjustment apparatus associated with the left-side viewing assembly. The left-side converging lens and beam splitter were affixed to a sliding rail assembly that allowed horizontal adjustments for interpupillary distance. The beam splitter was adjustable in horizontal rotation about its central axis to adjust scan entry angle to the eye, and it was adjustable in distance from the converging lens to allow forward and aft (z-axis) positioning of the exit pupil position. Finally, the first surface mirrors that folded the scan path were adjustable to manipulate scan angles in the vertical and horizontal dimensions, assisting with fine adjustments necessary to achieving a well fused binocular image.

A custom dental impression bite bar for each subject was positioned between and below the viewing beam splitters on an adjustable base. A lightly padded bar was positioned above the viewing beam splitters as a head rest. The combination of bite bar and head rest helped maintain very consistent eye positions throughout the experiment.

As in previous experiments, an infrared video camera (Sony HandyCam Hi-8) was positioned to image the right eye via the small mirror previously described. The eye images were captured at approximately 45 degrees from normal to the plane of the eye pupil. Pupil response was subsequently measured from these video recordings.

RSD stimuli were varied in intensity using a variable density neutral density filter in the path of the VRDE helium-neon laser beam prior to the scanning mechanism, as depicted in the basic VRDE diagram of figure 2.6. A calibration was made of neutral density filter positions to yield desired values of RSD corneal flux density. A table was constructed relating filter scale values to corneal flux density values, and this table was referenced by the experimenter to affect the range of corneal flux density values in presented stimuli. The calibration was conducted as described in the following section, 6.2.1.

6.2.1 Calibration of Pupillary Response Experiment Stimuli

It was first necessary to derive a method of equating the natural view stimuli of Stanley and Davies' experiment with the Maxwellian view stimuli of the current RSD experiment. Clearly, the goal was to match the retinal illumination resulting from the two different display methods, as

retinal illumination is the primary factor effecting pupil response. Only by equating these two types of visual stimuli could a valid comparison of models be conducted. The method of determining matched stimuli is generally described below, and a detailed description with an example calculation is provided in Appendix B.

To accomplish the equating of display stimuli, values of stimuli luminance in the natural view conditions of Stanley and Davies' experiment were calculated for display fields of view area as square degrees of visual angle (corneal flux density / FOV deg² yields cd/m²). Using these calculated luminance values and the mean eye pupil diameter response of the Stanley and Davies model, calculations of mean retinal illumination in the natural view scenario of Stanley and Davies' experiment were made for selected combinations of field of view and luminance (display luminance x pupil area = retinal illumination). Thus, RSD retinal illumination equivalents to these model-derived natural view retinal illumination estimates would effectively match the display conditions of Stanley and Davies' original experiment, ignoring geometrical considerations of the Maxwellian view and associated Stiles-Crawford I effects.

For each RSD field of view and desired RSD corneal flux density value, an optical power value was derived from the matching retinal illumination value and the solid angle associated with the RSD scan creating the display field of view (retinal illumination as lumens/steradian x scan solid angle in steradians = power in lumens). A simple conversion from lumens to watts was facilitated by the 632.8 nm monochromaticity of the VRDE helium-neon laser. Thus, an easily measurable power value was derived for each RSD experimental display condition of corneal flux density.

Using a Newport optical power meter (model 1835-C, Newport Corporation, Irvine, California), the VRDE display power was measured while the neutral density filter was adjusted. When the calculated power for a specified corneal flux density conditions was achieved, the neutral density filter position was recorded. A tabularized set of neutral density filter positions was created relating filter position to corneal flux density values, providing a simple and accurate method of changing corneal flux density values throughout the experiment. By this calculation and calibration method, RSD stimuli matching the Stanley and Davies' natural view stimuli in retinal illumination were created.

Background luminance in augmented view trials was adjusted with a variable power supply on the background illumination lamp. Background illumination levels were measured from the subject viewing position, through the viewing beam splitters, using a PhotoResearch PR-

880 photometer (PhotoResearch, Chatsworth, California). The power supply was adjusted to achieve the desired background luminance values, and these power supply settings were recorded for reference during the conduct of augmented view pupillary response trials.

6.3 Subjects

The purpose of the experiment was disclosed to all subjects and each gave informed consent. Twelve adult subjects were tested comprised of seven females and five males. Ages ranged from 21 years to 43 years. Each subject had corrected acuity of 20/20 or better, normal eye alignment, and no known visual defects. One subject (SM) had been advised by multiple medical vision professionals that she had an abnormally large pupillary response. Because of this fact, SM's data was subsequently omitted from all summary statistical analyses and model derivations. Eight of the subjects had no previous experience with psychophysical or opto-physiological experimentation. Four subjects were HITL research associates with some experience as subjects for similar types of experiments. Each subject was paid for participation in this study.

6.4 Method and Procedure

This experiment was essentially a univariate $2 \times 4 \times 9 \times 4$ factorial design. The independent variables, ordered by their respective factorial levels reference above, were: monocular/binocular RSD, RSD field of view, RSD corneal flux density, and background luminance. The single dependent measure was pupil diameter. Ten subjects participated in all conditions, consistent with a complete within subjects design. (Two subjects did not receive the highest level of background luminance condition due to reported discomfort, but they received all other conditions.) However, due to experimental limitations, a fully completed within subjects matrix for the 10 subjects was infeasible, resulting in systematic blocks of missing values within the matrix. Specifically, only the two largest levels of RSD field of view were completed with all nine levels of corneal flux density due to safety and display limitations, and the greatest level of background luminance was completed with only one level of field of view. Thus, within subjects analyses were limited to fully completed matrix subsets and were used primarily to check results obtained with the lower powered factorial methods applied to the larger data sets. Based upon previous research in pupillary response the condition effects were anticipated to be large, and the

greater power of the within subjects methods was expected to be unnecessary to discern significant differences. This expectation proved to be accurate.

The experiment proceeded in three parts: 1) alignment of binocular viewing assembly to subject's eyes, 2) data collection with monocular and binocular stimuli in opaque RSD view, and 3) data collection with monocular and binocular stimuli in augmented RSD view. Proper alignment of the apparatus to each individual subject's eye position was critical to the accurate collection of data. Thus, a meticulously conducted alignment procedure was accomplished and thoroughly tested. The alignment procedure was typically carried out on the day prior to data collection due to the extensive time and effort involved. This helped avoid subject fatigue and prohibitively long single session times for subjects. The two data collections were always conducted within a single morning or afternoon session with a brief break between, following a retesting of the binocular display alignment. Each of the three experimental parts is now discussed in detail.

6.4.1 Binocular Display Alignment

Due to the nature of the Stiles-Crawford I effect, alignment of exit pupils through the central eye pupil was critical to the success of this experiment. As such, extreme care was taken to ensure proper coupling of the binocular RSD exit pupils to the eyes' entrance pupils. Pupil coupling alignment and binocular image fusion was thoroughly tested prior to data collection with each subject.

Subjects were first fitted with a custom dental impression bite bar formed with a non-toxic thermal plastic. A detailed verbal and visual briefing about the alignment procedure, testing procedures, and desired fused binocular display appearance was conducted and all subject questions were answered. The bite bar was mounted to its adjustable base on the viewing assembly platform and the subject was instructed to capture the right-side exit pupil with the bite bar enclosed in teeth. The left-side viewing assembly was coarsely adjusted to match left eye position while the right eye had the right-side exit pupil captured.

Once these coarse viewing assembly adjustments were made and while the subject still captured the right-side exit pupil, the head rest bar was adjusted to fit firmly against the subject's forehead. With the background screen assembly removed from the apparatus, the experimenter visually examined the coupling of the exit pupil and eye pupil. Under subdued ambient lighting

conditions, slight specular reflections from the cornea were visible that allowed the experimenter to ascertain the path of the scan into the subject's eye. Additionally, minor eye rotations by the subjects caused the exit pupil to present itself on the iris where its size and form were clearly visible to the experimenter. By carefully examining the exit pupil position and form, making minor adjustments to the subject's head position, and individually fixing each dimension of the bite bar and head rest bar positions, the exit pupil was precisely targeted on the center of the right eye pupil. Subsequently, the subject was directed to rotate eyes left, right, up and down, and to closely estimate the equivalence of the angles at which pupil decoupling occurred by noting the view position within the RSD displayed disk and by noting background scene lateral distances at the position of decoupling. If inequalities were reported, minor adjustments in head position were affected to correct the alignment and achieve precise central pupil coupling.

Following the fixation of the head position for right eye alignment, the left eye viewing assembly was finely adjusted to couple the left-side pupils. Using visual examination procedures similar to those described for the right eye, the experimenter adjusted each dimension of the left-side viewing apparatus to achieve alignment between the left-side exit pupil and the left eye pupil. Once a good left-side exit pupil positioning was achieved, the subject was asked to examine the binocular fusion of the display disk. This was affected by having the subject move the left-side optional light block back and forth repeatedly to "wipe" the left image on and off, allowing accurate comparison with the right image position. Typically, some minor angular adjustment in the scan entry angle to the eye pupil was necessary to achieve well fused disk images. In most cases, the subject was allowed to use turn-screw adjusters on one of the first surface mirrors in the left-side optical path to make these fine adjustments. Once display fusion was reported by the subject, left-side exit pupil position was re-examined for centrality within the eye pupil. Typically, several iterations of exit pupil position adjustment and subject affected fusion tweaking were necessary to achieve a well fused image with proper central pupil coupling.

Following the completion of the left-side alignments, the centrality of the fused image was tested by having the subject again make close estimates of the eye rotation angles necessary to cause decoupling. The desired effect was to have both left and right images decouple simultaneously and with equivalent eye rotation angles in all directions. This indicated dual centralized pupil couplings and well fused images. Further, RSD and ambient lighting conditions were brightened to constrict the pupil near its smallest diameter. The subject was asked to

perform a similar test and to ensure that centralized binocular coupling was well maintained with the small eye pupil diameters.

It is important to note that during the entire alignment procedure the white crosshair image was displayed to the subject. The subject was instructed to focus and fixate on the crosshair during all adjustment procedures, except where eye rotations were required. This maintained consistent eye positions and vergence for the alignment procedure.

This alignment procedure was meticulous and occasionally quite difficult. It was not uncommon for this portion of the experiment setup to consume one and a half hours. For this reason, the alignment was typically conducted on the day prior to data collection sessions. A recheck of proper alignment was conducted immediately before data collection sessions. On two occasions additional minor alignment adjustments were necessary immediately preceding data collection. In spite of the intense manual manipulations required to achieve proper couplings, the procedure and apparatus worked well to ensure properly coupled pupils throughout the data collection sessions. However, in two early cases, accidental subject impacts with the apparatus induced pupil misalignment during data collection, necessitating realignment and repeating the data collection. Subsequent reinforcements to the optical apparatus avoided additional such unfortunate and time consuming incidents. Additionally, three subjects reported decoupling of one exit pupil during the course of the experiment and required minor readjustment of the exit pupil positions to continue data collection. Each of these decoupling reports occurred only during the highest luminance conditions when the eye pupil was constricted to its smallest diameter.

6.4.2 Stimuli and Data Collection in Opaque View

Following the alignment procedure, the background screen assembly was replaced and a large black felt cloth was hung between the viewing beam splitters and the background screen. This blocked the entire background view and affected an opaque view RSD scenario.

The subject was briefed on procedures and had all questions answered before beginning data collection. Several iterations of practice trials were conducted with high ambient light conditions to familiarize the subject with the pace and rhythm of the procedures. Once the subject reported good familiarity with the procedures, a ten minute dark adaptation period was begun. The ambient room lighting was extinguished and the experimental area was sealed behind a black felt curtain in complete darkness. During the dark adaptation period, the experimenter

verbally reviewed procedures with the subject. At the termination of the dark adaptation period, the subject was positioned on the bite bar and head rest. Visual stimuli were then presented to the subject sequentially.

Trials were always presented in tandem, monocular display then binocular display, for every combination of additional conditions. Subjects kept both eye open during all trials. Four levels of RSD field of view (RSD disk image diameter) were presented (5, 12, 20 and 28 degrees visual angle diameter). Within each level of field of view, between five and nine levels of RSD corneal flux density were presented, ranging from 10^2 to 10^6 $\text{cd/m}^2 \text{deg}^2$. With the smallest two RSD fields of view, the greatest RSD corneal flux density levels were omitted due to display power limitations and subject eye safety considerations. Thus, the 5 degree FOV condition was presented with five levels of corneal flux density ranging from 10^2 to 10^4 $\text{cd/m}^2 \text{deg}^2$, and the 12 degree FOV condition was presented with seven levels of corneal flux density ranging from 10^2 to 10^5 $\text{cd/m}^2 \text{deg}^2$. The 20 degree and 28 degree FOV disks were each presented with the full range of nine RSD corneal flux density levels. Between each level of FOV, subjects were again dark adapted for 10 minutes to begin each FOV condition with similarly dilated eye pupils. Field of view disk images were presented in order of diameter, either smallest to largest or largest to smallest, determined pseudo-randomly. A complete listing of RSD stimuli conditions in units of corneal flux density and in equated units of troland and FOV combinations is provided in Appendix A.

Within each level of FOV, the order of RSD corneal flux density presentations was always least to greatest. Once the eye pupils were dilated with the dark adaptation period, incremental constrictions of the pupils were affected by ascending RSD corneal flux density from least to greatest value. This general technique is consistent with numerous previous studies of pupillary response and, in particular, it is consistent with the procedures of Stanley and Davies whose results form the foundation of the current RSD opaque view pupil response model.

For each level of RSD corneal flux density, the subject was tasked to attend to the white crosshair and to request increased crosshair luminance from the experimenter when its contrast with the RSD disk image was insufficient to maintain good focus and fixation. In this way, the fixation crosshair was gradually increased in apparent luminance commensurate with RSD corneal flux density. This method, added to the fact that the crosshair was a very small item in the visual field, eliminated any measurable pupillary effects of the crosshair.

For each individual trial, subjects were exposed to the new condition for several seconds, typically between 10 and 15 seconds. Following this brief adaptation period, an infrared video recording of the right eye was made for several additional seconds, typically between 5 and 8 seconds. The experimenter verbally annotated the video record's audio track with each trial's conditions for subsequent data reduction and analysis. The subject was made aware of the recording period for each trial and was asked to minimize eye blinks during that time. The subject was reminded consistently to maintain visual fixation and focus on the small crosshair at the center of the RSD display disk. Subjects were allowed a brief break of a few seconds "off bite bar" as often as desired, but they were encouraged to maintain viewing position throughout a FOV presentation. Very few breaks were taken within any FOV presentation across all twelve subjects. Longer breaks of ten minutes were incurred between FOV conditions for the dark adaptation period.

Following the completion of all trials for the experimental session, the video tape was analyzed for pupil diameter measurements. Each trial's video recording was digitized and examined with the pupillometer (section 2.1.4). For each trial recording, video analysis of pupil diameter was initiated immediately following the cessation of pupillary oscillations that typically occur upon a change of luminance level. In most cases, the pupil was well stabilized during the recording period, although a few subjects exhibited small, high frequency pupil oscillations throughout their exposure to the RSD stimuli. The mean value of pupil diameter during the recording period was calculated and entered into an analysis spreadsheet as the pupillary response to the trial condition.

In some cases, the infrared image of the eye contained undesirable specular reflections of the RSD scan and/or poor contrast between the pupil and iris that caused the pupillometer to be ineffective and prone to error. The contrast problem was particularly evident with subjects having light-colored irises that are poorer reflectors of infrared energy than dark irises. In these cases, manual measurements of the pupil diameter were made using a video monitor and a ruled scale. In these cases, several measurements of eye pupil diameter were made through each trial's recorded period and the mean measurement value was calculated as the trial condition response. Comparison of test results of this technique with the results of the pupillometer yielded no significant differences and no trends for potential systematic error.

6.4.3 Data Collection in Augmented View

The augmented view data collection session followed the opaque view data collection session after a short break. Procedures were identical to the opaque view procedures with a few significant exceptions necessary with augmented view display.

The black felt cloth was removed from the apparatus to allow an unimpeded natural view of the translucent background screen for augmented view. Subjects were again dark adapted and subsequently exposed to the background luminance level for approximately one minute prior to the initiation of RSD stimuli to allow pupil stabilization with the background luminance. Three levels of background luminance were presented, 10 cd/m^2 , 100 cd/m^2 , and 1000 cd/m^2 . These levels of background luminance coarsely approximated candle lighting, indoor lighting, and shaded or overcast outdoor lighting, respectively. Consistent with the procedure of presenting least to greatest luminance conditions, these three background conditions were always presented in ascending order. Video recording and data reduction procedures were identical to those described in opaque view procedures.

With the 10 cd/m^2 and 100 cd/m^2 levels of background luminance, RSD stimuli were presented in augmented view in a manner and sequence identical to that described in the opaque view procedures of section 6.4.2. With the 1000 cd/m^2 background luminance condition, a smaller set of data were collected with only the 28 degree RSD field of view and with only five levels of corneal flux density. The data collection was limited under this background condition because the high background luminance combined with high RSD luminance was somewhat uncomfortable for subjects and occasionally caused mild retinal saturation effects with extended viewing periods at the highest RSD corneal flux density levels. These effects were exacerbated with smaller fields of view for equivalent corneal flux density levels, as equivalent optical power levels were delivered to smaller retinal area. Further, with this background luminance condition the effects of the lower RSD corneal flux density levels on pupillary response were found to be negligible and not measurable, so a subset of corneal flux density levels were presented with emphasis on the highest levels.

6.4.4 Pupillary Response Pilot Study and Experimental Design Revisions

Following procedures similar to those outlined in sections 6.4.2 and 6.4.3, a pilot study was conducted prior to formal data collections to explore the parameters of pupil response and to ensure experimental procedures were sound. Some unexpected findings dictated changes in the final experimental design and procedures.

The pilot study was conducted with two male subjects of 28 and 39 years of age, both with previous experience as visual psychophysical experimental subjects. In addition to the disk shaped RSD field of view stimuli described in previous sections, circular RSD images ("rings") of various diameters were presented to simulate sparse augmented view display content, such as wire frame graphics or visual display highlighting of natural view objects (see Appendix C). Ring stimuli were selected for convenience in determining retinal illumination levels, to consistently control the angular distance of display elements from the fovea, and to provide generally applicable results. Four levels of ring stimuli ranged in diameter from 5 degrees visual angle to 30 degrees visual angle, and each was approximately 1 degree visual angle in width. During trials the subjects were visually fixated on the white crosshair positioned in the center of each ring stimulus.

The results indicated only a small difference in pupil response means between ring and disk stimuli in augmented view for equivalent levels of RSD corneal flux density, with the trend indicating slightly larger pupil response diameters with the ring stimuli. The trend was reduced in magnitude with increased background luminances. No significant effect was obtained even under the lowest photopic background luminance conditions for all diameters of stimuli. Only when the greatest RSD corneal flux density magnitudes were combined with relatively low background luminance levels and large ring and disk diameters was an unambiguously measurable and statistically significant difference in effect between disk and ring stimuli obtained. However, at these large magnitudes of RSD corneal flux density, the RSD to background contrast was extreme with the ring displays, causing undesirable visual effects of blooming and glare. The conclusion was drawn that under practical RSD augmented view conditions, RSD corneal flux density (and background luminance) is the critical variable for pupil response, independent of basic RSD image form characteristics.

As an ancillary consideration, the inclusion of ring stimuli in all augmented view conditions effectively doubled the duration of the data collection session. Both subjects reported

substantial eye fatigue and general discomfort following the long sessions that continued for a total of more than 4 hours. As the pilot study seemed to indicate that no practical findings would result with the ring stimuli, these stimuli were excluded from the formal experiment. One additionally planned intermediate level of RSD field of view was deleted to further reduce data collection session durations.

The decision to reduce the 1000 cd/m² background luminance trials, as described in section 6.4.3, was also based upon results and subject feedback from the pilot study. Brighter background luminance levels were found to constrict pupil diameters such that RSD flux density had little additional effect. One subject reported retinal saturation effects with extended viewing of the brightest conditions. Thus, a small subset of the originally planned conditions within the 1000 cd/m² background condition was selected for the formal study in order to establish a ceiling effect. An additional level of even higher background luminance was also planned for the pilot study, 5,000 cd/m², coarsely approximating sunlight conditions. However, it rapidly became apparent that no measurable effect of RSD stimulation would result, as subjects' pupil diameters were constricted at or below the normal limit of 2 mm by the background luminance alone. Again, as no practical findings were expected at this level of background luminance, the condition was deleted from the experimental design.

The pilot study findings and the resultant revision of experimental conditions confined the experimental conditions to a set that would clearly yield practically useful results. The final set of experimental conditions is the set described in sections 6.4.2 and 6.4.3. The revisions also reduced the data collection sessions to reasonable durations that avoided severe subject fatigue while maintaining a single morning or afternoon collection period. The sessions were reduced from a duration exceeding four hours to approximately 1.75 hours. With the time necessary for the alignment procedure, subjects dedicated a total of just over 3 hours to the experiment.

6.5 Analysis

Subjects' pupil response data were analyzed using SPSS software version 9.0 for Windows on a PC computer. A factorial analysis of variance (ANOVA) was conducted to examine main effects and interactions of monocular/binocular RSD display, display field of view, corneal flux density, and background luminance using a significance criterion of 0.05. Tukey's Honestly Significantly Difference Test was used to assess all post-hoc pair wise comparisons.

Additional factorial analyses were conducted for each background luminance condition in isolation. Main effects and interactions of monocular/binocular RSD display, display field of view, and corneal flux density were examined within each background luminance condition using a significance criterion of 0.05. Tukey's Honestly Significantly Difference Test was again used to assess all post-hoc paired comparisons. Additional z-tests and the non-parametric Wilcoxon rank-sum test were used to make conditional comparisons with hypothetical model predictions.

A regression analysis was conducted using an Excel spreadsheet to compare mean pupillary response values for opaque view conditions with the hypothesized pupillary response model of section 3.2.1. Model-explained variance as the Pearson product (R^2) in the data was calculated, and conditional comparisons were made. Graphical plots of various data depictions were made with an Excel spreadsheet to visually illustrate results and to depict the resultant family of functions describing pupillary response across the range of experimental conditions.

6.6 Results

Significant results were obtained throughout the analysis as main effects, interaction effects, and paired comparison effects. The results also provided detailed information for the development of empirical models of human pupillary response to small exit pupil RSD stimulation. Results are now reviewed as a conglomerate set and as subsets defined by background luminance condition.

All ANOVA summary tables present the effect source degrees of freedom (df), mean squares value (MS), mean squares error (Error), the F statistic (F) and the significance (p) value. All post-hoc paired comparison tables present the mean value of pupil diameter within table cells for the associated condition, and these tables depict homogeneous subsets in columnar form to indicate non-significant groupings. The significance (p-value) of each homogeneous subset grouping is provided at the bottom of each group's column.

6.6.1 All Background Luminance Conditions Results

Considering all background luminance conditions, main effects were exhibited for each of the independent variables of monocular/binocular RSD display, RSD field of view, RSD corneal flux density and background luminance. Each of these main effects was significant to $p < .001$. Significant interactions were obtained for background x monocular/binocular RSD ($p < .001$), for

background x corneal flux density ($p < .001$), and for background x RSD field of view ($p = .013$). The ANOVA summary of significant results is presented in Table 6.1 below.

Table 6.1: ANOVA Summary of Significant Pupil Response Effects (all background conditions considered)

Source	df	MS	Error	F	p
Monocular/binocular	1	45.405	45.405	65.975	<.001
RSD Field of view (FOV)	3	5.470	16.409	7.948	<.001
Corneal flux density	8	31.446	251.572	45.692	<.001
Background luminance	3	251.197	753.591	364.994	<.001
Background x monocular/binocular	3	18.803	56.408	27.321	<.001
Background x corneal flux density	20	8.605	172.100	12.503	<.001
Background x FOV	6	1.847	11.083	2.684	.013

Significant effects were obtained with paired comparisons for all background luminance level comparisons, each with $p < 0.001$. Homogeneous subsets of background luminance by pupil diameter are displayed in table 6.2.

Table 6.2: Homogeneous Subsets of Background Luminance by Mean Pupil Diameter

Background Luminance	N	Subset (by Tukey HSD)			
		1	2	3	4
1000 cd/m ²	110	2.444			
100 cd/m ²	688		3.217		
10 cd/m ²	716			3.754	
Opaque view	716				4.651
Significance		1.000	1.000	1.000	1.000

Significant effects were obtained with pair-wise comparisons of RSD field of view when considering all data across background luminance conditions. Differences in pupil response were obtained between the 5 degree FOV and both the 20 and 28 degree FOV conditions. The 12 degree FOV and 28 degree FOV conditions were significantly different. Homogeneous subsets of RSD field of view by pupil diameter are displayed in table 6.3, with means for groups.

Table 6.3: Homogeneous Subsets of RSD Field of View by Mean Pupil Diameter

RSD Field of View	N	Subset (by Tukey HSD)		
		1	2	3
28 degrees	740	3.689		
20 degrees	639	3.811	3.811	
12 degrees	504		3.887	3.887
5 degrees	347			3.965
Significance		.086	.456	.440

It should be noted that within each background luminance condition, only the 10 cd/m² background condition yielded significant results among RSD fields of view. These comparisons are detailed in section 6.6.3. The comparisons depicted in Table 6.3 indicate effects considered across all background luminance levels.

Significant effects were obtained with paired comparisons of corneal flux density. Differences in pupil response were obtained in all comparisons with the following exceptions: no significant differences were obtained between any immediately adjacent pair of corneal flux density levels and no significant differences were obtained among the lowest three levels of corneal flux density. The results are summarized as homogeneous subsets of corneal flux density by pupil diameter in table 6.4 on the following page. Again, the reader is reminded that these results are collapsed across all background luminance conditions.

A summary graphical plot of pupil diameter means is depicted in Figure 6.3. The means are collapsed across the RSD field of view variable, depicting subjects' mean pupil diameters as a function of corneal flux density for each condition of monocular/binocular RSD and background luminance condition. Curves are color coded and shape coded to group monocular/binocular RSD pairs and to distinguish pairs by background luminance condition.

6.6.2 Opaque View Background Condition Results

Examining the subset of data for opaque view conditions only, main effects were exhibited for the independent variables of monocular/binocular RSD display and for corneal flux density. Each of these two main effects was significant to $p < .001$. No main effect of RSD field of view was obtained ($p = .847$). No significant interactions were obtained. The ANOVA summary of significant results is presented in Table 6.5 on the next page.

Table 6.4: Homogeneous Subsets of RSD Corneal Flux Density by Mean Pupil Diameter

RSD Corneal Flux Density ($\text{cd/m}^2 \text{ deg}^2$)	N	Subset (by Tukey HSD)			
		1	2	3	4
1×10^6	161	3.055			
5×10^5	162	3.181			
1×10^5	212		3.497		
5×10^4	235		3.551		
1×10^4	284			3.821	
5×10^3	306			3.824	
1×10^3	284				4.113
5×10^2	281				4.204
1×10^2	305				4.305
Significance		.780	.999	1.000	.235

Table 6.5: ANOVA Summary of Significant Pupil Response Effects (opaque view conditions only)

Source	df	MS	Error	F	p
Monocular/binocular	1	120.630	120.630	136.725	<.001
Corneal flux density	8	51.140	409.121	57.963	<.001

Significant effects were obtained with paired comparisons of corneal flux density within the opaque view conditions. Adjacent RSD corneal flux density conditions were found to be not significantly different, except for the lowest two pairs ($1 \times 10^2 \text{ cd/m}^2 \text{ deg}^2$ and $5 \times 10^2 \text{ cd/m}^2 \text{ deg}^2$), which were significant. All other paired comparisons of RSD corneal flux density were significant. The results are summarized as homogeneous subsets of corneal flux density by pupil diameter in table 6.6, with subset means displayed.

A linear regression analysis was made to compare data with the hypothesized model of binocular RSD pupil response described in section 3.2.1. By the Pearson product, 95.3% of data variance was explained by the hypothesized model ($R^2=.953$). Graphical plots of the model compared with experimental data means and with Stanley and Davies' original model are presented in Figure 6.4, along with a linearized model and experimental data means comparison in Figure 6.5 (subject SM omitted; see section 6.3). In each graphic, data are plotted as pupil

Table 6.6: Homogeneous Subsets of RSD Corneal Flux Density by Mean Pupil Diameter (opaque view conditions only)

RSD Corneal Flux Density (cd/m ² deg ²)	N	Subset (by Tukey HSD)							
		1	2	3	4	5	6	7	8
1 x 10 ⁶	161	3.323							
5 x 10 ⁵	162	3.506	3.506						
1 x 10 ⁵	212		3.843	3.843					
5 x 10 ⁴	235			4.106	4.106				
1 x 10 ⁴	284				4.472	4.472			
5 x 10 ³	306					4.671	4.671		
1 x 10 ³	284						5.116	5.116	
5 x 10 ²	281							5.310	
1 x 10 ²	305								5.956
Significance		.961	.422	.750	.303	.936	.095	.945	1.000

diameter means collapsed across RSD field of view. Standard error bars are depicted on mean experimental values in the function of RSD corneal flux density.

Comparisons by z-test of pupil diameter means collapsed across RSD field of view with model predictions obtained statistically significant differences with three levels of RSD corneal flux density. Significant results were found with the lowest level of RSD corneal flux density (10² cd/m² deg²) and with the greatest two levels of RSD corneal flux density (5 x 10⁵ and 1 x 10⁶ cd/m² deg²). It should be noted that the statistical assumption of population distribution normality is violated when pupil diameter is near the natural upper and lower diameter limits. Parametric statistical comparisons in these regions of pupil response may be invalidated with violation of the normality assumption.

Graphical plots of pupil diameter means collapsed across RSD field of view for binocular RSD view with opaque background condition are incorporated into Figure 6.3 (SM omitted; see section 6.3). The binocular RSD view opaque background data were fitted with an exponential function that provided a better fit to the experimental data than the hypothetical model. The exponential model yields an R² value of 0.996 and is of the form

$$P=7.7684e^{-0.1653x} \quad (\text{eq. 6.1})$$

Where p is the mean eye pupil diameter in millimeters and x is RSD corneal flux density in $\text{cd/m}^2 \text{ deg}^2$.

Graphical plots of pupil diameter means by subject, collapsed across RSD field of view, are presented in Figure 6.6a for binocular conditions in opaque view. Curves are color coded to distinguish individual subject responses while depicting the range envelope across subjects. The range of mean pupil diameters across RSD corneal flux density levels averaged 2.71 mm. Omitting subject SM due to her unusually large pupil response (see section 6.3), this average range was only 1.95 mm.

Graphical plots of pupil diameter means collapsed across RSD field of view for monocular RSD view with opaque background condition are also incorporated into Figure 6.3. The monocular RSD view opaque background data were fitted with a linear function that provided a best fit to the experimental data. The linear model yields an R^2 value of 0.998 and is of the form

$$P=-0.6134x+7.4284 \quad (\text{eq. 6.2})$$

where p is the mean eye pupil diameter in millimeters and x is RSD corneal flux density in $\text{cd/m}^2 \text{ deg}^2$.

Graphical plots of pupil diameter means by subject, collapsed across RSD field of view, are presented in Figure 6.7a for monocular conditions in opaque view. Curves are color coded to distinguish individual subject responses while depicting the range envelope across subjects. The range of mean pupil diameters across RSD corneal flux density levels averaged 3.27 mm. Omitting subject SM due to her unusually large pupil response (see section 6.3), this average range was only 2.38 mm.

6.6.3 Background Condition 10 cd/m^2 Results

Examination of the subset of data for 10 cd/m^2 conditions only revealed main effects for the independent variables of monocular/binocular RSD display ($p=.016$), for RSD field of view ($p<.001$), and for corneal flux density ($p<.001$). No significant interactions were obtained. The ANOVA summary of significant results is presented in Table 6.7 on the following page.

Table 6.7: ANOVA Summary of Significant Pupil Response Effects (10 cd/m² background conditions only)

Source	df	MS	Error	F	p
Monocular/binocular	1	4.637	4.637	5.880	.016
RSD field of view	3	8.345	25.034	10.582	<.001
Corneal flux density	8	4.485	35.884	5.688	<.001

Significant effects were obtained with paired comparisons of RSD field of view within the 10 cd/m² background luminance condition. Differences in pupil response were obtained between the 5 degree FOV and 28 degree FOV conditions, as well as between the 12 degree and 28 degree FOV conditions. Homogeneous subsets of RSD field of view by pupil diameter are displayed in table 6.8, with means for groups. This small effect is the only significant FOV effect revealed within any background luminance condition.

Table 6.8: Homogeneous Subsets of RSD Field of View by Pupil Diameter (10 cd/m² background conditions only)

RSD Field of View	N	Subset (by Tukey HSD)	
		1	2
28 degrees	212	3.933	
20 degrees	216	3.734	3.734
12 degrees	168		3.684
5 degrees	120		3.572
Significance		.330	.167

Significant effects were obtained with paired comparisons of corneal flux density within the 10 cd/m² background luminance condition. Significant differences were found with the following comparisons of RSD corneal flux density (in cd/m² deg²): 1×10^2 with both 1×10^6 and 5×10^5 , 5×10^2 with both 1×10^6 and 5×10^5 , 1×10^3 with 1×10^6 , and 5×10^3 with 1×10^6 . The results are summarized as homogeneous subsets of corneal flux density by pupil diameter in table 6.9.

Table 6.9: Homogeneous Subsets of RSD Corneal Flux Density by Pupil Diameter (10 cd/m² background conditions only)

RSD Corneal Flux Density (cd/m ² deg ²)	N	Subset (by Tukey HSD)		
		1	2	3
1 x 10 ⁶	47	3.327		
5 x 10 ⁵	47	3.472	3.472	
1 x 10 ⁵	71	3.577	3.577	3.577
5 x 10 ⁴	72	3.723	3.723	3.723
1 x 10 ⁴	96	3.741	3.741	3.741
5 x 10 ³	96		3.801	3.801
1 x 10 ³	96		3.871	3.871
5 x 10 ²	95			3.927
1 x 10 ²	96			3.934
Significance		.108	.140	.263

Graphical plots of pupil diameter means collapsed across RSD field of view for binocular RSD view with 10 cd/m² background condition are incorporated into Figure 6.3 (SM omitted). A linear function was fit to the means by least squares yielding the model:

$$p = -0.180x + 4.35 \quad (\text{eq. 6.3})$$

where p is the mean eye pupil diameter and x is RSD corneal flux density. The resultant R^2 value was 0.946. However, these data were best fit by a 2-degree polynomial function as:

$$p = -0.0308x^2 + 0.0696x + 3.8992 \quad (\text{eq. 6.4})$$

that yields $R^2 = 0.982$.

Graphical plots of pupil diameter means by subject, collapsed across RSD field of view, are presented in Figure 6.6b for binocular conditions with 10 cd/m² background luminance. Curves are color coded to distinguish individual subject responses while depicting the range envelope across subjects. The range of mean pupil diameters across RSD corneal flux density levels averaged 2.77 mm. Omitting subject SM due to her unusually large pupil response (see section 6.3), this average range was only 1.45 mm.

Graphical plots of pupil diameter means collapsed across RSD field of view for monocular RSD view with 10 cd/m² background condition are incorporated into Figure 6.3 (SM

omitted). The best fit linear function for these data yielded the model:

$$p = -0.1451x + 4.5377 \quad (\text{eq. 6.5})$$

where p is the mean eye pupil diameter and x is RSD corneal flux density. The resultant R^2 value was 0.899. However, these data were best fit by a 2-degree polynomial function as:

$$p = -0.0344x^2 + 0.1336x + 4.0301 \quad (\text{eq. 6.6})$$

that yields $R^2 = 0.982$.

Graphical plots of pupil diameter means by subject, collapsed across RSD field of view, are presented in Figure 6.7b for monocular conditions with 10 cd/m² background luminance. Curves are color coded to distinguish individual subject responses while depicting the range envelope across subjects. The range of mean pupil diameters across RSD corneal flux density levels averaged 3.18 mm. Omitting subject SM due to her unusually large pupil response (see section 6.3), this average range was 2.91 mm.

6.6.4 Background Condition 100 cd/m² Results

Examination of the subset of data for 100 cd/m² conditions only revealed main effects for the independent variables of monocular/binocular RSD display ($p = .005$) and for corneal flux density ($p < .001$). No main effect of RSD field of view was obtained. No significant interactions were obtained. The ANOVA summary of significant results is presented in Table 6.10 below.

Table 6.10: ANOVA Summary of Significant Pupil Response Effects (100 cd/m² background conditions only)

Source	df	MS	Error	F	p
Monocular/binocular	1	3.683	3.683	7.962	.005
Corneal flux density	8	2.588	20.468	5.530	<.001

Significant effects were obtained with paired comparisons of corneal flux density within the 100 cd/m² background luminance condition. Significant differences were found with the following comparisons of RSD corneal flux density (in cd/m² deg²): 1×10^2 with both 1×10^6 and 5×10^5 , 5×10^2 with both 1×10^6 and 5×10^5 , 1×10^3 with both 1×10^6 and 5×10^5 , 5×10^3 with 1×10^6 , and 1×10^4 with 1×10^6 . The results are summarized as homogeneous subsets of corneal flux density by pupil diameter in table 6.11.

Table 6.11: Homogeneous Subsets of RSD Corneal Flux Density by Pupil Diameter (10 cd/m² background conditions only)

RSD Corneal Flux Density (cd/m ² deg ²)	N	Subset (by Tukey HSD)		
		1	2	3
1 x 10 ⁶	45	2.851		
5 x 10 ⁵	45	2.934	2.934	
1 x 10 ⁵	69	3.053	3.053	3.053
5 x 10 ⁴	69	3.148	3.148	3.148
1 x 10 ⁴	92		3.224	3.224
5 x 10 ³	92		3.274	3.274
1 x 10 ³	92			3.320
5 x 10 ²	92			3.360
1 x 10 ²	92			3.398
Significance		.190	.081	.066

Graphical plots of pupil diameter means collapsed across RSD field of view for binocular conditions with 100 cd/m² background condition are incorporated into Figure 6.3 (SM omitted).

A linear function was fit to the means by least squares yielding the model

$$p = -0.145x + 3.71 \quad (\text{eq. 6.7})$$

where p is the mean eye pupil diameter and x is RSD corneal flux density. The resultant R^2 value was 0.972. However, these data were best fit by a 2-degree polynomial function as:

$$p = -0.0107x^2 + 0.0581x + 3.5502 \quad (\text{eq. 6.8})$$

that yields $R^2 = 0.979$.

Graphical plots of pupil diameter means by subject, collapsed across RSD field of view, are presented in Figure 6.6c for binocular conditions with 100 cd/m² background condition. Curves are color coded to distinguish individual subject responses while depicting the range envelope across subjects. The range of mean pupil diameters across RSD corneal flux density levels averaged 2.11 mm. Omitting subject SM due to her abnormally large pupil response (see section 6.3), this average range was 1.60 mm.

Graphical plots of pupil diameter means collapsed across RSD field of view for monocular conditions with 100 cd/m² background condition are incorporated into Figure 6.3 (SM omitted). A linear function was fit to the means by least squares yielding the model

$$p = -0.145x + 3.71 \quad (\text{eq. 6.9})$$

where p is the mean eye pupil diameter and x is RSD corneal flux density. The resultant R^2 value was 0.972. However, these data were best fit by a 2-degree polynomial function as:

$$p = -0.0127x^2 + 0.0283x + 3.6099 \quad (\text{eq. 6.10})$$

that yields $R^2 = 0.983$.

Graphical plots of pupil diameter means by subject, collapsed across RSD field of view, are presented in Figure 6.7c for monocular conditions with 100 cd/m² background condition. Curves are color coded to distinguish individual subject responses while depicting the range envelope across subjects. The range of mean pupil diameters across RSD corneal flux density levels averaged 2.40 mm. Omitting subject SM due to her abnormally large pupil response (see section 6.3), this average range was 1.34 mm.

6.6.5 Background Condition 1000 cd/m² Results

Within the 1000 cd/m² background luminance condition, no significant main effects or interactions were obtained. With this background condition, data were collected for 10 subjects with only the 28 degree RSD field of view and for five levels of corneal flux density, including: 1×10^2 , 5×10^3 , 5×10^4 , 5×10^5 , and 1×10^6 cd/m² deg². (see sections 6.4.3 and 6.4.4).

Graphical plots of pupil diameter means for binocular conditions with 1000 cd/m² background condition are incorporated into Figure 6.3. A linear function was fit to the means by least squares yielding the model

$$p = -0.074x + 2.69 \quad (\text{eq. 6.11})$$

where p is the mean eye pupil diameter and x is RSD corneal flux density. The resultant R^2 value was 0.938. However, these data were best fit by a 2-degree polynomial function as:

$$p = -0.0155x^2 + 0.051x + 2.4728 \quad (\text{eq. 6.12})$$

that yields $R^2 = 0.993$.

Graphical plots of pupil diameter means by subject are presented in Figure 6.6d for binocular conditions with 1000 cd/m² background condition. Curves are color coded to distinguish individual subject responses while depicting the range envelope across subjects. The range of mean pupil diameters across RSD corneal flux density levels averaged 0.94 mm.

Subject SM, who had abnormally large pupil response, was not presented the 1000 cd/m² background luminance condition and is thus omitted from these results.

Graphical plots of pupil diameter means for monocular conditions with 1000 cd/m² background condition are incorporated into Figure 6.3. A linear function was fit to the means by least squares yielding the model

$$p = -0.0644x + 2.6705 \quad (\text{eq. 6.13})$$

where p is the mean eye pupil diameter and x is RSD corneal flux density. The resultant R^2 value was 0.904. However, these data were best fit by a 2-degree polynomial function as:

$$p = -0.0179x^2 + 0.0796x + 2.422 \quad (\text{eq. 6.14})$$

that yields $R^2 = 0.999$.

Graphical plots of pupil diameter means by subject are presented in Figure 6.7d for monocular conditions with 1000 cd/m² background condition. Curves are color coded to distinguish individual subject responses while depicting the range envelope across subjects. The range of mean pupil diameters across RSD corneal flux density levels averaged 0.94 mm. Subject SM, who had abnormally large pupil response, was not presented the 1000 cd/m² background luminance condition and is thus omitted from these results.

6.7 Discussion and Conclusions

The results of this experiment strongly support the asserted experimental hypotheses. The opaque view pupil diameter response generally followed the Stiles-Crawford adjusted hypothetical model, with some minor deviations near the extremes of pupil response. A family of pupil diameter response curves resulted from augmented view data, each similar in form and affected primarily by background luminance and secondarily by RSD corneal flux density. A strong effect due to monocular or binocular RSD display was noted that was inversely related to luminance conditions. As the experimental hypotheses were supported, so were the asserted sub-hypotheses and the general hypothesis number 2. *Opto-physiological responses of the visual system to small exit pupil retinal scanning displays differ from the responses to equivalently perceived conventional displays.* Each experimental hypothesis, applicable results, and implications are now discussed in more detail.

6.7.1 Binocular Opaque View RSD Model of Pupil Response

The first experimental hypothesis held: *The actual eye pupil diameter in binocular RSD opaque view will follow the Stiles-Crawford adjusted effective pupil size and thereby conform to the function of corneal flux density defined by equation 3.1c in section 3.2.1.* This hypothesis is well supported by results reported in section 6.6.2.

The graphics of Figure 6.4 visually summarize the support of this hypothesis. The mean pupil response values across subjects for each RSD corneal flux density level are collapsed across the field of view variable, as no significant differences were obtained among FOV levels in the opaque viewing condition. This is identical to the construction method of Stanley and Davies' original model from which the hypothesized model was derived. Their model was constructed with the original intent of predicting pupil response in natural view conditions independent of stimuli size, or field of view. As such, it is a construct of subject responses collapsed across varied fields of view.

The main effect of corneal flux density and the associated paired comparisons clearly indicate differences across the spectrum of conditions. Although many immediately adjacent corneal flux density pairs were not statistically significant, this does not detract from the model's validity as a predictive tool.

Graphical analysis clearly depicts the data closely following the hypothesized model, deviating significantly only at the extremes of pupil diameter response. As a comparison, Stanley and Davies' original model is also depicted, and the deviation of the data from that foundational model is stark. By regression analysis, the hypothetical model explains more than 95% of the variance in experimental data. While the small deviations from the model warrant explanation, the hypothesized model is generally validated by these data.

The significant deviations from the model, while unanticipated, are not surprising. First, as discussed in section 2.2.1.5, the population of human pupil diameters is not normally distributed near the upper and lower limits of natural pupil response. A skew develops in the population distribution near these extremes. Parametric statistical analyses assume a symmetric normal population distribution. Since this assumption is violated by the skewed population distribution near the extremes of natural pupil response, the parametric tests used to make the comparisons between model and data may be invalid. Suitable non-parametric statistical methods for the comparison of a singular model value with a sample distribution are not well developed,

as knowledge of the non-normal population distributions must be assumed from sample distributions. However, the non-parametric Wilcoxon rank-sum test may be applied with the assumption of a pupil model sample distribution of multiple values each equivalent to the model prediction, and thus, with zero variance. By this method the Wilcoxon rank-sum test is a non-parametric analog to the parametric z-test. Applying this non-parametric test also yields significant results at the greatest two levels of corneal flux density ($p < .001$ and $p = .017$). Clearly, a significant difference exists between model and data for these corneal flux density levels that warrants an explanation outside of statistical considerations. It is possible that some systematic experimental error affected the results.

Potential sources of experimental error existed that may have affected pupil response in a systematic way, particularly at the high luminance portion of the stimuli spectrum. First, the Stiles-Crawford I effect is known to promote peak sensitivity near the center of the eye pupil. However, true peak sensitivity with SC-1 varies widely in pupil entry position among individuals. Applegate and Lakshminarayanan (1993) performed a thorough investigation of this phenomenon and found peak SC-1 sensitivity entry positions more than 2.0 mm from the geometric pupil center, with deviations of 1.0 mm to 1.5 mm very common [97]. It is quite reasonable to assert that VRDE exit pupils were not precisely coupled to the exact SC-1 peak sensitivity positions for subjects, as this exact pupil entry position cannot be ascertained without extensive and elaborate individual subject visual testing. It is also reasonable to postulate that the VRDE exit pupils did not remain perfectly coupled to the central eye pupil for the entire duration of the experiment due to minor subject head movements and possible mechanical slippage of the head stabilization apparatus over the course of the 2 hour sessions. Thus, the disparity between exit pupil position and SC-1 peak sensitivity position may well have exceeded 2 mm in some cases.

If the exit pupils were not precisely coupled to the peak SC-1 sensitivity position in the eye pupils, a reduction in effective retinal illumination would have resulted as compared to that assumed by the hypothetical model. The effect would have induced increased pupil diameters as compared to the diameters that would have resulted from the perfectly SC-1 peak-coupled pupils assumed by the hypothetical model. Further, it reasons that this error effect would be most noticeably revealed at small eye pupil diameters where the integrated SC-1 effect across the eye pupil is small and phototransduction efficiency of the natural view is relatively high. Under these conditions the Jacobs' effectivity ratio is small and any reduction in RSD effective retinal illumination due to off-peak coupling will have a proportionally larger effect on the ratio. At

large eye diameters where the effectivity ratio is large, the minor off-peak reduction in effective retinal illumination should have a proportionally smaller effect and not induce a large change in eye pupil diameter.

This explanation is generally consistent with the experimental data, but the estimated magnitude of the off-peak SC-1 effect is insufficient to fully explain the significantly different results with the highest RSD corneal flux density levels. At pupil entry distances 2 mm from SC-1 peak sensitivity, the effective illumination is approximately 70% of the peak effective illumination. Thus, the effective RSD corneal flux density would be 0.70 the RSD corneal flux density assumed by the model. Thus, for the highest RSD corneal flux density level of 1×10^6 $\text{cd/m}^2 \text{deg}^2$, the effective flux density analog would be approximately 7×10^5 $\text{cd/m}^2 \text{deg}^2$ with the 2 mm coupling disparity. At this level of corneal flux density, the hypothetical model predicts a pupil diameter of 2.55 mm, a value that remains significant from the experimental data at the $\alpha=.05$ significance level by both parametric and non-parametric statistical methods.

To achieve a result that is not significant at the $\alpha=.05$ level, it is necessary to assume an SC-1 off-peak distance that results in an effective corneal flux density analog approximately 0.55 that of the 1×10^6 $\text{cd/m}^2 \text{deg}^2$ level, or 5.5×10^5 $\text{cd/m}^2 \text{deg}^2$. This magnitude of effectivity ratio reduction is achieved with pupil couplings approximately 2.5 mm from SC-1 peak sensitivity position. It is feasible that pupil coupling errors of this magnitude occurred in some subject cases, but not likely in a majority of cases because pupil decoupling would have occurred for most subjects. Further, these levels of postulated reduction in effective corneal flux density provide results that are barely non-significant and do not closely approximate the mean experimental values obtained. Nevertheless, some smaller off-peak pupil couplings clearly took place in the experiment, contributing to the data deviations from the pupil response model at high levels of corneal flux density.

Another explanation for the model deviations is much more probable than the extreme off-peak couplings that would be necessary to manifest the observed deviations, and it would have a synergistic effect with off-peak pupil coupling. If central pupil coupling errors were induced due to initial visual alignment deficiencies or due to minor head movements by subjects and mechanical slippages of the head stabilizing apparatus, it is possible that at small eye pupil diameters only a partial coupling of pupils occurred in one or both eyes. That is, if alignment error was induced in the course of the experiment, only part of a display exit pupil may have entered the eye pupil as the eye pupil became constricted to the smallest diameters. Clearly this

would reduce the effective retinal illumination presented at the highest corneal flux density levels and would result in relatively larger pupil diameters. At lower corneal flux density levels where the eye pupil was large, such partial couplings would be much less likely to occur. Thus, an inherent experimental bias against small pupil response exists under this scenario, inducing error as an increased pupil diameter response at the highest levels of corneal flux density. Additionally, partial pupil decoupling would not be clearly apparent to the subject who was viewing a fused binocular image that frequently changed in apparent brightness over the course of the session. Thus, subject reports of partially decoupled pupils should not be expected.

A synergistic effect with SC-1 off-peak coupling would also occur under this scenario. Given that the mean pupil diameter at the highest corneal flux density level was just under 2.9 mm, and given that the display exit pupil diameter was just over 1.0 mm, a relative movement of approximately 0.9 mm between exit pupil and eye pupil would have induced some partial pupil decoupling. If partial decoupling occurred, off-peak coupling SC-1 effects and reduced RSD retinal illumination effects would simultaneously increase in magnitude and reduce the effective retinal illumination in a multiplicative manner. This synergy would result in a substantially larger effect on pupil response than either factor alone.

As a hypothetical example, assume the average eye pupil diameter for the highest corneal flux density condition (2.88 mm), and assume a relative disparity between the central eye pupil and the exit pupil center of 1.5 mm that also induces a disparity between SC-1 peak sensitivity position and exit pupil center of 2.5 mm. By the SC-1 sensitivity function, the effective flux density will be reduced to 0.55 the peak position magnitude. The partially coupled pupils reduce the light entering the eye by approximately one-half the fully coupled magnitude. The resultant effective retinal illumination is then only 0.275 the magnitude of the value assumed by the hypothetical model. For the highest corneal flux density conditions this equates to an effective flux density of $2.7 \times 10^5 \text{ cd/m}^2 \text{ deg}^2$. At this level, the model predicts a pupil diameter response of 2.78 mm, nearly equivalent to the observed mean experimental value of 2.88 mm and far from a statistically significant difference given the observed variance. Thus, an average relative head motion by subjects of just 1.5 mm over the long course of the data collection session could easily induce error resulting in the significant differences observed with high levels of corneal flux density in the opaque view condition.

During the course of the experiment, three subjects reported pupil decoupling in one eye under high corneal flux density conditions with greatly constricted eye pupils. Minor adjustment

of exit pupil positions was necessary to continue data collection. These incidents point to the fact that the head stabilization apparatus, while providing good stabilization for most subjects, was not perfect. Even when tightly biting on the dental impression bite bar and with forehead pressed firmly into the head rest, subjects were able to make very small movements of the head. Although inadvertent, such relative motions certainly occurred with regularity over the long duration of data collection sessions. Post experimental analyses of eye pupil video records revealed small changes in eye position with most subjects. While no extensive quantitative analysis of the magnitude of these relative movements was undertaken, a random sampling of 25 measurements seems to coarsely agree with the hypothetical estimates previously discussed. Sample relative eye position changes ranged from 0 mm to 3.0 mm with a mean value of 1.4 mm. It is logical to conclude that the deviations from the hypothetical model at high corneal flux density levels can be attributed to this systematic experimental error.

However, this error does not explain the single deviation from the model at the low end of the corneal flux density conditions. Small magnitudes of coupling error with large eye pupil diameters should not induce a large effect on pupil response. No additional uncontrolled variables have been exposed. Procedural error or uncontrolled variables do not seem to be the source of this result. One possible explanation involves the transition of retinal photoreceptors in use at lower luminance levels.

It is possible that the corneal flux density model for predicting pupil response begins to fail near the mesopic range of luminance. It is more likely that the model begins to fail in the mesopic range under the specific conditions of this experiment. In the mesopic range of luminance, between photopic and scotopic ranges, the rod retinal photoreceptors begin to become active. Upon their activation at lower luminance levels, rod response to visual stimulation begins to affect pupil response. The question arises: Did differences exist between the stimuli presented by Stanley and Davies and the stimuli presented in the current experiment that may have invoked a different retinal response only with the initiation of rod photoreceptor activation and thereby cause deviations from the model predictions? In retrospect, the answer is clearly yes.

Stanley and Davies presented polychromatic white light disk stimuli in the development of their model, while the current experiment presented monochromatic red stimuli of 632.8 nm wavelength. Under normal photopic conditions of equivalent stimuli luminance, chromaticity has a very small affect on the luminance channel of visual perception and, thus, a negligible affect on pupil response [18]. However, this condition changes when rod photoreceptors become involved

in retinal response at lower luminance levels associated with the mesopic and scotopic ranges of luminance. Examination of the scotopic luminous efficiency function (V'_λ ; see section 2.2.1.2) reveals that rod photoreceptors are highly sensitive to the shorter wavelengths of the visible spectrum, but relatively insensitive to the longer wavelengths. The photopic and scotopic functions are quite different in chromatic sensitivity.

The stimuli in each experiment were measured under photopic luminance assumptions, quantitatively relating the stimuli and associated retinal response under purely photopic conditions. However, because of the difference in photopic and scotopic sensitivity functions, the stimuli and retinal responses do not maintain the same quantitative relationships when the retina begins to respond under mesopic conditions that begin to invoke the scotopic rod receptors. Therefore, Stanley and Davies' broadband white light stimuli provided relatively strong stimulation to the rod photoreceptors under low corneal flux density conditions causing the pupil response in their model to be mildly constricted. The 632.8 nm long red wavelength stimuli of the current experiment did not provide similar rod stimulation under low luminance conditions. Thus, the rod response was likely of much smaller magnitude in the low luminance condition with long wavelength light than the hypothetical model assumed because the hypothetical model was derived from the model of Stanley and Davies. Because of the wavelength sensitivity shift that begins in the mesopic luminance range, the effective retinal illumination in the current experiment was less than the model assumed, and low corneal flux density pupillary response yielded larger pupil diameters than predicted by the hypothetical model.

Thus, it is quite reasonable that an insufficiently controlled experimental variable produced a systematic bias against small pupil diameter response at high levels of corneal flux density, thereby causing the significant deviations from the hypothetical model. Additionally, retinal spectral sensitivity changes under low luminance conditions coupled with chromatic differences between the stimuli used in the development of the two models make deviations from the hypothetical model an expected phenomenon under the lowest levels of corneal flux density. Therefore, given that the majority of the data clearly support the model and, given that the significant deviations have been logically attributed to experimental error and disparate stimuli, the first experimental hypothesis is confirmed with an added conditional clause: *Under conditions where RSD exit pupils are well coupled to the SC-1 peak sensitivity pupil entry position, the actual eye pupil diameter in binocular RSD opaque view follows the Stiles-*

Crawford adjusted effective pupil size and thereby conforms to the function of corneal flux density defined by equation 3.1c in section 3.2.1.

Clearly, most practical applications of head-mounted RSD's will induce pupil coupling error similar to, or more severe than, that occurring in this experiment. As such, significant deviations from the hypothesized model will occur under luminance conditions that induce highly constricted eye pupils. It is also likely that in some cases narrow spectrum RSD light sources may be used near the red portion of the visible spectrum that will induce deviations from the model under low luminance conditions similar to those revealed by these experimental results. With these practical considerations in mind, it is reasonable to suggest that the exponential model of binocular RSD opaque view, defined in section 6.6.2 and closely fitting experimental results, is a more suitable tool for estimating pupil response to RSD stimulation under applied conditions. However, the engineer should consider anticipated user and environmental conditions as compared to experimental conditions, and utilize both models intelligently.

6.7.2 Binocular Augmented View RSD Models of Pupil Response

The second experimental hypothesis held: *In binocular augmented view, a family of empirical eye pupil diameter functions will be derived, each with general form similar to the hyperbolic function of equation 3.1c, with pupil diameter inversely related to background luminance by a large effect, and with eye pupil diameter inversely related to RSD corneal flux density by a relatively smaller effect.* This hypothesis is strongly supported by the results reported in sections 6.6.3 through 6.6.5.

Figure 6.8 graphically depicts the resultant binocular RSD family of empirical functions (extracted from the summary Figure 6.3). The plots depict subject mean pupil diameters collapsed across field of view as a function of RSD corneal flux density for each background condition (SM omitted; see section 6.3).

The binocular augmented view functions clearly depict pupil response inversely related to background luminance. The effect is quite consistent across the range of RSD corneal flux density levels for binocular augmented view. The reported interaction between background luminance and RSD corneal flux density is evident primarily in the comparison of opaque view to augmented view functions. This artifact is discussed more fully in section 6.7.4. As

hypothesized, a smaller inverse relationship is evident with RSD corneal flux density and pupil response.

In opposition to the hypothesis, the hypothesized hyperbolic form is not well represented in the binocular augmented view results. Rather, the functions appear very nearly linear and were closely fit with linear models and best fit with polynomial degree 2 models. The models are summarized in table 6.12 below, where p is pupil diameter in millimeters and x is RSD corneal flux density in $\text{cd/m}^2 \text{ deg}^2$. Some of the flattening of these functions is likely due to the previously described pupil coupling error, since the higher RSD corneal flux density means are likely larger than they would be with perfectly SC-1 peak position coupled pupils. The background luminance also seems to have imposed a flattening of the hyperbolic function at lower RSD corneal flux density levels. Examination of the slopes of the linear models provides an indication of additional small interaction effects between background luminance and RSD corneal flux density.

Table 6.12: Models of Binocular Augmented View Pupil Response

Background Luminance	Linear Model	Linear R^2	Polynomial Model	Polynomial R^2
10 cd/m^2	$p = -0.180x + 4.35$	0.946	$p = -0.0308x^2 + 0.0696x + 3.8992$	0.982
100 cd/m^2	$p = -0.145x + 3.71$	0.972	$p = -0.0107x^2 + 0.0581x + 3.5502$	0.979
1000 cd/m^2	$p = -0.074x + 2.69$	0.938	$p = -0.0155x^2 + 0.051x + 2.4728$	0.993

The range and variance of pupil response diameters in binocular augmented view varied with background luminance condition. Figure 6.6 compares the background luminance conditions in binocular RSD view with plots of subject means collapsed across field of view and depicted by individual subject. The range of mean responses is easily inferred from these plots with each of the background luminance levels, and it generally decreases with increased background luminance. Modeling the variance of these data will provide a method for estimating the statistical variation to be expected about a mean pupil diameter for a known background luminance condition.

The standard deviation of subjects' mean pupil diameters was calculated for each RSD corneal flux density level within each level of background luminance. The mean of these standard deviation values was then calculated for each background luminance condition and

plotted as in Figure 6.9. These derived values are mean values of standard deviation among subject mean pupil response diameters across all RSD corneal flux density levels. An R^2 value of 0.990 resulted with the linear model:

$$\sigma = -0.0997L + 0.6283 \quad (\text{eq. 6.15})$$

where σ is the standard deviation among subjects' means and L is the logarithmic value of background luminance in cd/m^2 . Subject SM, due to her abnormally large pupillary response (see section 6.3), was omitted from these model data.

Using the previously described models of pupil response and the model of subjects' means variation described here, estimates of mean pupil response and variance may be determined under a wide variety of binocular RSD implementation conditions. As noted with the binocular opaque view models of pupil response, these models of binocular augmented view pupil response contain inherent pupil coupling error that certainly must have affected pupil response at the high end of the RSD corneal flux density spectrum. However, such coupling error is also inherent in most envisioned applications of head mounted RSD's. As such, these models are asserted to be valid for statistical prediction under most applied RSD scenarios.

6.7.3 Monocular versus Binocular RSD View Pupil Response

The third experimental hypothesis held: *Eye pupil diameters with monocular RSD conditions will be larger than eye pupil diameters under binocular conditions of equivalent background and RSD luminance levels, and the magnitude of this difference will range from a maximum of approximately 1.5 mm at the lowest luminance conditions to zero at the greatest luminance conditions.* This hypothesis is well supported by the results reported in sections 6.6.1 through 6.6.5.

A comparison of monocular and binocular RSD results is incorporated into Figure 6.3 for all background luminance conditions. As reported in the individual background condition results, the effect of monocular/binocular RSD view was significant within all background conditions except the 1000 cd/m^2 background. In agreement with the hypothesis, monocular RSD pupil response consistently produced larger diameters than did binocular RSD conditions, and the magnitude of the difference is clearly inversely related to background luminance level. The mean magnitude of the differences across RSD corneal flux density levels is summarized in table 6.13.

Table 6.13: Monocular Versus Binocular RSD View Pupil Response Difference

Background Luminance Level	Mean Value of Pupil Diameter Difference
Opaque View Background	0.875 mm
10 cd/m ²	0.327 mm
100 cd/m ²	0.145 mm
1000 cd/m ²	0.013 mm

These values are plotted in Figure 6.10 and best fit with a 2-degree polynomial function as:

$$\delta = 0.104L^2 - 0.589L + 0.8592 \quad (\text{eq. 6.16})$$

where δ is the monocular-binocular RSD eye pupil diameter difference in millimeters and L is the logarithm of background luminance in cd/m². This polynomial fit results in $R^2=0.988$.

The hypothesized maximum magnitude of the monocular/binocular RSD effect is not fully supported by these results. A z-test of the 1.5 mm hypothesized estimate of maximum effect and the monocular/binocular difference values obtained in opaque background conditions is significant to $p<.0001$. Further, an inference from the stated hypothesis was that the magnitude of the monocular/binocular response difference would be significantly reduced with higher levels of RSD corneal flux density. This hypothetical inference is not supported, as no interaction of monocular/binocular RSD and RSD corneal flux density was obtained within any of the individual background luminance conditions. A test of the hypothesized minimum magnitude of the monocular/binocular RSD effect at the 1000 cd/m² background obtains statistically significant results for the hypothesized zero value, but there is little practical significance to this result.

Other notable differences resulted between monocular and binocular RSD conditions with regard to the range and variation in subjects' mean pupil response diameters. A mean value of the range of mean pupil response diameters was calculated for each background luminance condition for both monocular and binocular RSD view conditions. (The average of the ranges associated with mean pupil response for each level of RSD corneal flux density was calculated.) A mean value of standard deviation for each background luminance condition was similarly calculated. (The average was taken of the standard deviations associated with the mean pupil response in each level of RSD corneal flux density.) Figure 6.11 depicts these comparisons. It

should be noted that subject SM, due to her abnormally large pupillary response (see section 6.3), was omitted from the data presented here.

In each comparison, the binocular RSD condition yields a more linear function in which the range or variation decreases with background luminance. In each comparison, the monocular condition yields a sigmoidal function in which the opaque view condition is slightly less variable than the 10 cd/m² condition. Although the binocular range function is somewhat sigmoidal, it is diametrically out of phase with the monocular range function. The binocular standard deviation function is very linear, while the monocular case is again sigmoidal. Generally, the range and variation are greater for the monocular condition.

The differences in the forms of these functions indicate that the human population distributions of pupil responses may be quite different depending upon monocular or binocular RSD conditions. As such, models of variation in monocular and binocular view are prudent to develop, and they will utilize different mathematical forms. A linear model of binocular RSD view standard deviation was presented in section 6.7.2 that incorporated opaque and augmented results. A polynomial model of monocular RSD standard deviation is presented in section 6.7.4 that incorporates augmented view results only.

6.7.4 Monocular View RSD Models of Pupil Response

Monocular RSD's may be employed in some applications. As such, the following mathematical models of monocular RSD view pupil response are presented as aids in RSD design and engineering decision making. These models mirror the binocular RSD view pupil response models previously presented.

The monocular RSD family of pupil response functions is presented in Figure 6.12 (extracted from Figure 6.3). The plots depict subject mean pupil diameters collapsed across field of view as a function of RSD corneal flux density for each background condition in monocular RSD view (SM omitted; see section 6.3). As with the binocular data, these monocular data clearly depict pupil response inversely related to background luminance. Again, the reported interaction between background luminance and RSD corneal flux density is evident primarily in the comparison of opaque view and augmented view functions. A small inverse relationship is obtained between RSD corneal flux density and pupil response diameter.

As with the binocular data, the hypothesized hyperbolic form is not well represented in monocular data. The data are well fitted with linear models. Again like the binocular results, second order polynomial functions provide the best fit to the augmented view data. These models, linear and polynomial, are summarized in table 6.14 below. As with previously established convention, p is pupil diameter in millimeters and x is RSD corneal flux density in $\text{cd/m}^2 \text{ deg}^2$.

Table 6.14: Models of Monocular Augmented View Pupil Response

Background Luminance	Linear Model	Linear R^2	Polynomial Model	Polynomial R^2
Opaque	$P=-0.6134x+7.4284$	0.998	Not applicable	N/A
10 cd/m^2	$p=-0.1451x + 4.538$	0.899	$p=-0.0344x^2 + 0.1336x+4.0301$	0.982
100 cd/m^2	$p=-0.145x + 3.710$	0.972	$p=-0.0107x^2 + 0.0581x+3.5502$	0.979
1000 cd/m^2	$p=-0.0644x + 2.6705$	0.904	$p=-0.0179x^2 + 0.0796x+2.422$	0.999

The range and variance of pupil response diameters in monocular augmented view varied with background luminance conditions, as presented in section 6.7.3. Figure 6.7 compares the background luminance conditions in monocular RSD view with plots of subject means collapsed across field of view and depicted by individual subject. The range of mean responses is easily inferred from these plots with each of the background luminance levels, and it generally decreases with increased background luminance. Modeling the variance of these data will provide a method for estimating the statistical variation to be expected about a mean pupil diameter for a known background luminance condition in monocular augmented view.

The standard deviation of subjects' mean pupil diameters was calculated for each RSD corneal flux density level within each level of augmented view background luminance. The mean of these standard deviation values was then calculated for each background luminance condition and plotted as in Figure 6.13. These derived values are mean values of standard deviation among subject mean pupil response diameters across all RSD corneal flux density levels within each background luminance level. Utilizing the monocular RSD augmented view results, an R^2 value of 1.0 resulted with the polynomial model:

$$\sigma = 0.1811L^2 - 0.9831L + 1.6994 \quad (\text{eq. 6.17})$$

where σ is the standard deviation among subjects' means and L is the logarithmic value of background luminance in cd/m^2 . This model applies only to augmented view conditions of background luminance between 10 cd/m^2 and 1000 cd/m^2 . Again, subject SM was omitted from the results from which this model was derived due to her abnormally large pupillary response (see section 6.3).

The models of monocular pupil diameter response, coupled with this model of variance in the subjects' means, provides a method of estimating the statistical characteristics of pupil response to be expected under a variety of monocular RSD implementation conditions. As previously noted with binocular models, these monocular models contain inherent pupil coupling error that certainly must have affected pupil response at the high end of the RSD corneal flux density spectrum. However, such coupling error is to be expected in head-mounted applications of RSD's. As such, these models are asserted to be valid for prediction under most applied monocular RSD scenarios.

6.7.5 Consolidated General Discussion and Conclusions

Table 6.15 summarizes all asserted models for binocular and monocular RSD view by background luminance level. These models were derived without incorporation of data from subject SM who had an abnormally large pupillary response (see section 6.3). In all cases p is pupil response diameter in millimeters, x is RSD corneal flux density in $\text{cd/m}^2 \text{ deg}^2$, σ is the mean standard deviation of subjects' pupil diameter means across RSD corneal flux density levels, L is background luminance in cd/m^2 , and δ is pupil diameter difference in millimeters. The best fit mathematical form has been used for each case.

Some additional interesting practical implications may be derived from consideration of overall experimental results. These include topics related to general conclusions from the results, interactions among the experimental data, and the practical application of derived models. First, it is clear that with small exit pupil RSD's in Maxwellian view the human pupil response will differ from the pupil response under natural viewing conditions. Generally, the pupil will be more constricted than under natural viewing conditions that equate to the luminance profiles provided by RSD or RSD plus natural view. It is also clear that, as cited in previous literature, the human pupillary response has a broad range and is highly variable among individuals (see section 2.2.1.6). However, it is evident that the range of responses is substantially

Table 6.15: Summary of All Asserted Pupil Response Models

Binocular RSD	Background Luminance	Model	R²	Form
pupil diameter	opaque	$P=7.7684e^{-0.1653x}$	0.996	exponential
pupil diameter	10 cd/m ²	$p=-0.0308x^2 + 0.0696x + 3.8992$	0.982	polynomial
pupil diameter	100 cd/m ²	$p=-0.0107x^2 + 0.0581x + 3.5502$	0.979	polynomial
pupil diameter	1000 cd/m ²	$p=-0.0155x^2 + 0.051x + 2.4728$	0.993	polynomial
std deviation	0-1000 cd/m ²	$\sigma=-0.0997L + 0.6283$	0.990	linear
Monocular RSD	Background Luminance	Model	R²	Form
pupil diameter	opaque	$P=-0.6134x + 7.4284$	0.998	linear
pupil diameter	10 cd/m ²	$p=-0.0344x^2 + 0.1336x + 4.0301$	0.982	polynomial
pupil diameter	100 cd/m ²	$p=-0.0107x^2 + 0.0581x + 3.5502$	0.979	polynomial
pupil diameter	1000 cd/m ²	$p=-0.0179x^2 + 0.0796x + 2.422$	0.999	polynomial
std deviation	10-1000 cd/m ²	$\sigma=0.1811L^2 - 0.9831L + 1.6994$	0.990	polynomial
Monoc/Binoc Difference				
	0-1000 cd/m ²	$\delta=0.104L^2 - 0.589L + 0.8592$	0.988	polynomial

reduced under augmented RSD view conditions with moderate to high levels of photopic background luminance.

With the corneal flux density quantification of RSD stimuli, the RSD field of view variable (FOV) had very little effect within individual levels of background luminance. Stanley and Davies' foundational corneal flux density pupil response model was derived specifically to circumvent effects of stimuli field of view and, therefore, was similarly derived from results collapsed across various fields of view. Only within the 10 cd/m² background condition was a significant comparison obtained, and only two homogeneous subsets resulted from these comparisons representing differences between each of the two smallest fields of view and the largest. This is an important consideration since the derived pupil response models utilize mean pupil diameter values collapsed across FOV, and since greater utility of the models is possible if RSD FOV is not a factor in estimating pupil response. Still, application of the newly derived models should be properly limited to RSD scenarios with fields of view between 5 degrees and 28

degrees visual angle, although small extrapolations to wider fields of view may be reasonable in some circumstances.

Clearly, monocular versus binocular RSD view has a marked effect on pupil response. Not only did the monocular RSD view induce larger pupil diameters as compared to binocular RSD view, the range of responses was increased with monocular view and the variation among data was substantially different between the two RSD ocular conditions. These results all seem to indicate a complex difference in visual system response between the two conditions, as well as a difference in the distribution of the human population's responses.

As an ancillary observation, the dynamics of pupil response were observed to be quite different between these two conditions. With binocular view, the pupil response was essentially stable for most subjects. With monocular RSD view the pupil response was frequently oscillatory, occasionally inducing large variations in pupil diameter within a single trial. While no systematic quantification of these oscillations was undertaken, cursory measurement of the more extreme instances of this phenomenon obtained ranges exceeding 2 mm diameter. Interestingly, many subjects reported strong occurrences of binocular rivalry with monocular RSD viewing conditions. This rivalry caused the RSD image to fade in and out of prominence in visual perception. It is not likely coincidental that a correlation seemed to develop over the course of the data collections between reports of the binocular rivalry symptoms and the exhibition of highly dynamic pupil response. Again, no formal systematic quantification of these phenomena was made as the discoveries evolved piecemeal over the conduct of the experimental sessions, and the suspected correlation in these phenomena was realized *post hoc*. Nevertheless, this potential effect may have significant practical implementation ramifications for RSD's (and other monocular displays).

Interestingly, the interaction between background luminance and RSD corneal flux density resulted primarily from differences between opaque and augmented backgrounds. Further, the opaque background condition produced more constricted pupils at high levels of RSD corneal flux density than were obtained under identical conditions with the 10 cd/m² background luminance (see Figure 6.3). The experimental error discussed in section 6.7.1 does not seem to provide an explanation of this result since the augmented functions are all similarly formed at the high end of the RSD corneal flux density spectrum for all background conditions, and the interaction is clearly evident across all RSD corneal flux density levels. If the interaction was solely due to the experimental error associated with poor pupil coupling it would be manifested

only at the highest levels of RSD corneal flux density and the remaining portions of the functions would be more parallel.

Instead, this interaction seems to indicate a unique pupillary response with opaque view stimuli as compared with augmented view stimuli. This is not completely unexpected, as the opaque view conditions stimulated only a relatively small portion of the central retina compared to the augmented view conditions that stimulated the entire retina with background luminance. As discussed in section 2.2.1.5, stimulation of the foveal region of the retina has a stronger effect on pupil response than peripheral retinal stimulation, and many factors affect pupil response, including the size, shape, form and perceptible dynamics of visual stimuli. As compared to the central retinal stimulation of the opaque view conditions, a small moderating effect on pupil constriction seems to have resulted with stimulation of the entire retina in augmented view. Although a difference in chromaticity also existed between the white light background field and the red HeNe laser stimuli of the RSD, literature indicates that this has only a very minor effect on pupillary response, particularly as compared to overall retinal illumination effects and even to retinal image position effects [18].

Design efforts to produce small exit pupil displays that maintain well coupled pupils may reference the pupil response models herein to ascertain general engineering parameters required to accommodate the pupil response of a targeted population segment. The pupil response models may be employed to estimate the mean pupil diameters to be expected for various combinations of background luminance conditions and display corneal flux density. The models of pupil response variation may be used to obtain estimates for the statistical spread of pupil responses to be expected among the population of users, and display parameters may be engineered to accommodate a targeted statistical population range of pupil response.

If these models are to be used in the manner described, the question of their applicability to real world scenarios must be addressed. These models were constructed under artificial laboratory conditions. The RSD stimuli were homogeneous static images, not heterogeneous dynamic images as would be expected with many applications. The RSD image was a contiguous image and not a sparsely populated text and wire frame image like that required by many augmented view display scenarios. Small experimental error in pupil coupling was present throughout the data collections. Thus, can these models accurately apply to real world scenarios?

First, the laboratory conditions were necessary to exert a sufficient level of control over variables to achieve consistency in results for reliable comparisons among conditions. However,

as far as the human visual system is concerned, the stimuli were just as valid as any real world stimuli. Granted, few real world scenarios call for large, contiguous, homogeneous static field images, but equivalent levels of RSD corneal flux density were shown to provide practically equivalent pupil response across a broad range of display fields of view. Further, the pilot study using ring image stimuli obtained no practical differences in pupil response between ring and disk stimuli at RSD corneal flux density levels reasonable for comfortable contrast with the background luminance. Therefore, the models should not be susceptible to significant error due to these factors of image content density and form.

The fact that the RSD stimuli were static rather than dynamic may have some merit as a criticism. Image dynamics have been shown to influence pupil response, as has image content. However, the range of possible image dynamics and content is practically unlimited, and selecting sub-categories of image dynamics for this foundational study would not have been a prudent decision. Rather, this variable is better considered in a separate study if it proves to be a significant issue.

The fact that some pupil coupling error is inherent within these models does not seem to invalidate their practical utility, but rather enhance it. It is not reasonable to expect perfectly coupled pupils to be maintained with head mounted displays. The position of the exit pupil within the eye pupil will change in an essentially random manner under most user conditions. Further, the simple act of scanning around an RSD image with eye rotations changes the pupil coupling alignment. As in the experiment, the extent of the coupling error must be limited by the size of the eye pupil itself. Therefore, the magnitude of coupling error with relatively small eye pupils inherent in the experimental data may reasonably be expected to approximate that obtained in real world scenarios.

However, under larger pupil conditions increased pupil coupling errors may be expected. While these will have a lesser effect on pupil response in RSD augmented mode for the reasons detailed in section 6.7.1, deviation from the model may be expected with larger eye pupils and large coupling error. However, in a practical analysis, if coupling errors of large magnitude are allowed with large eye pupils, the utility of the head mounting and pupil alignment apparatus will be severely limited when environmental conditions dictate more constricted eye pupils. This issue is convolved with the issues of multiple exit pupil presentations reviewed in Chapter 2 and examined experimentally in a Chapter 7. As noted in Chapter 2, practical engineering solutions seem to be feasible to ensure accurate maintenance of pupil couplings with small exit pupil

displays. As such, large coupling error should be minimized as a significant source of model deviations.

Considering the experimental results and the confirmation of experimental hypotheses, the following general conclusions are drawn regarding the general hypotheses introduced in Chapter 3. General hypothesis 2a is confirmed within previously discussed limitations of peak SC-1 coupling alignment: *For binocular opaque view RSD stimuli and photopic luminance conditions, actual pupil size follows a pupil size function associated with the Stiles-Crawford-adjusted effective pupil size.* General hypothesis 2b is confirmed: *In binocular RSD augmented view under photopic luminance conditions, pupil size is a function of the effectivity ratio-adjusted corneal flux density of the RSD and the luminance of the natural scene.* General hypothesis 2c is confirmed: *Under monocular RSD display conditions in both opaque and augmented photopic view, pupil size will follow functions similar in form to the binocular functions, but pupil diameters will be consistently larger than those under similar binocular RSD display conditions.* These conclusions support the confirmation of the overarching general hypothesis 2: *Pupillary responses of the visual system to small exit pupil retinal scanning displays differ from the responses to equivalently perceived conventional displays.*

Given the confirmation of these hypotheses, the models derived herein are asserted to provide close estimates of the human pupil response to be expected under a wide variety of small exit pupil RSD application scenarios. While no model is perfect, and always subject to a vast number of unique exceptional conditions, these models represent the best estimates currently available in the burgeoning field of RSD engineering.

As described in Chapter 2, the future of RSD engineering will likely include designs implementing arrays of exit pupils to increase effective exit pupil area for improved human-display coupling. Such arrayed exit pupils should help to maintain good central pupil coupling alignment, enhancing the accuracy of the derived pupil response models. Further, arrays of exit pupils must be created with some logical separation distance between adjacent exit pupils, and the optimal distance must clearly be at least a partial function of eye pupil diameter. The pupil response models derived here provide information about human pupil response necessary to anticipate engineering requirements for such display concepts. However, additional investigation of human preference and performance with arrayed exit pupils will provide additional insight prerequisite to display design. The explorations and experiment of Chapter 7 represent an initiation of such an investigatory process for arrayed small exit pupil RSD's.

The VRDE collimated scan was split into two paths, each folded to a converging lens of 75 mm focal length and 60 mm aperture. Beam splitters folded the converging scans to form two exit pupils for binocular display viewing in augmented view. The lens-splitter combinations were elevated above the other optics and scan paths to avoid path and component spatial conflicts.

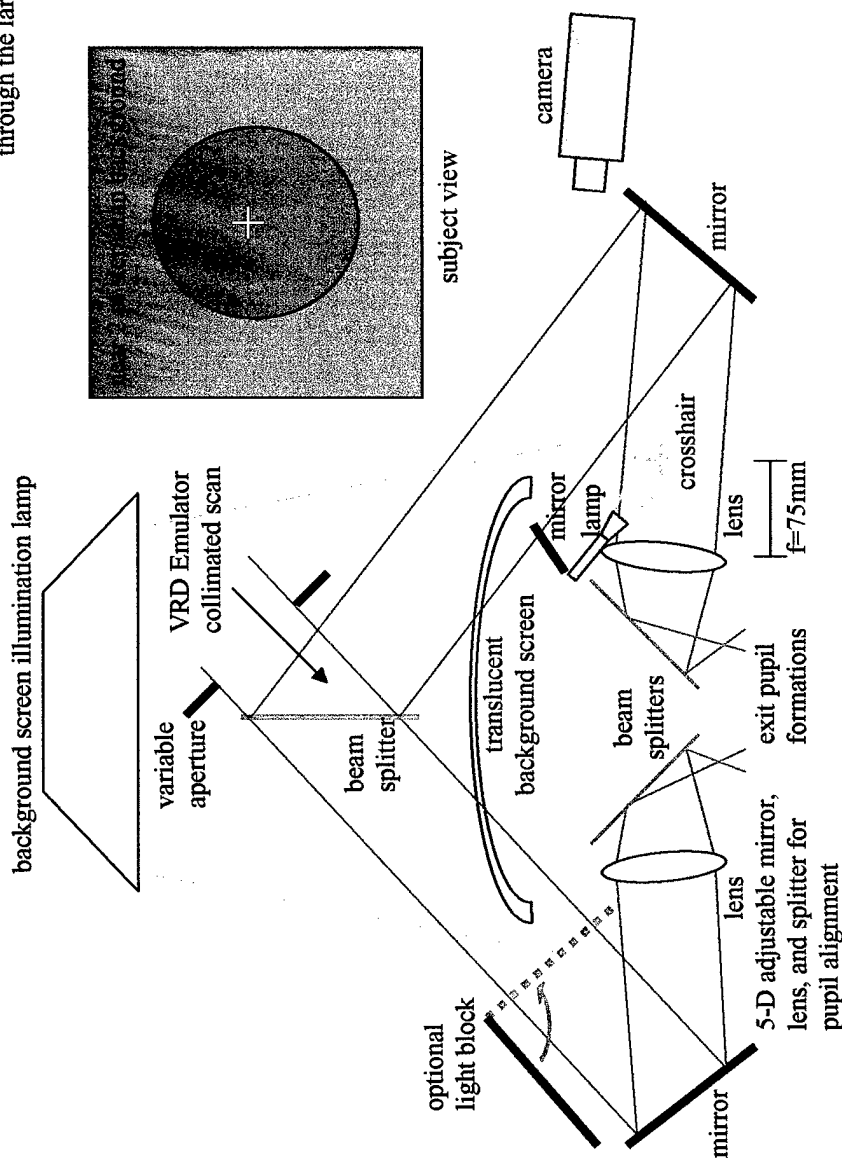


Figure 6.1: VRD Emulator Binocular Display Arrangement

In the right side optical path, a front illuminated narrow white crosshair was positioned at the focal length of the converging lens. This was affected with a clear glass plate and a painted crosshair. Thus, an image of the crosshair collimated to optical infinity was provided to subjects through the large exit pupil of the converging lens.

A translucent background screen was rear-illuminated with a white light lamp and positioned so that it provided a near 2-pi steradian background scene for augmented view. The lamp luminance was varied to provide different background luminance levels.

An infrared video camera recorded images of subjects' right eyes via a small mirror near the right beam splitter.

The left side mirror-lens-splitter assembly was adjustable in five dimensions to allow accurate pupil coupling for all subjects. A dental impression bite bar and forehead rest (not depicted here) were used to stabilize eye positions throughout the study.

The fused binocular view appeared as a red disk with a small white crosshair at the center. A variable diameter aperture in the path just before the scan split allowed changes in display disk diameter. The background was the naturally viewed scene of the translucent screen with variable luminance, or a blackened background for opaque view.

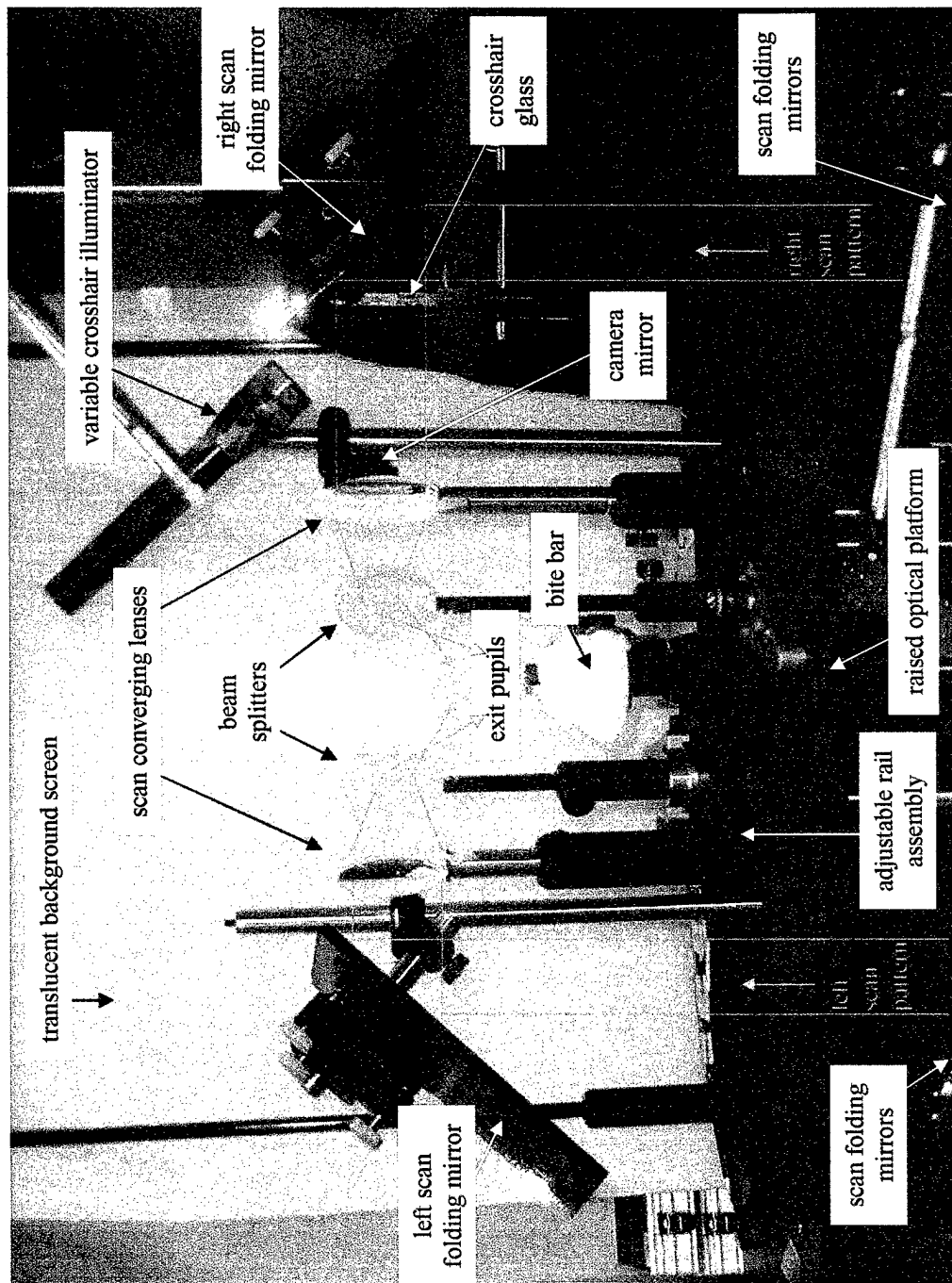


Figure 6.2: Augmented Photograph of VRD Emulator Binocular Display Arrangement

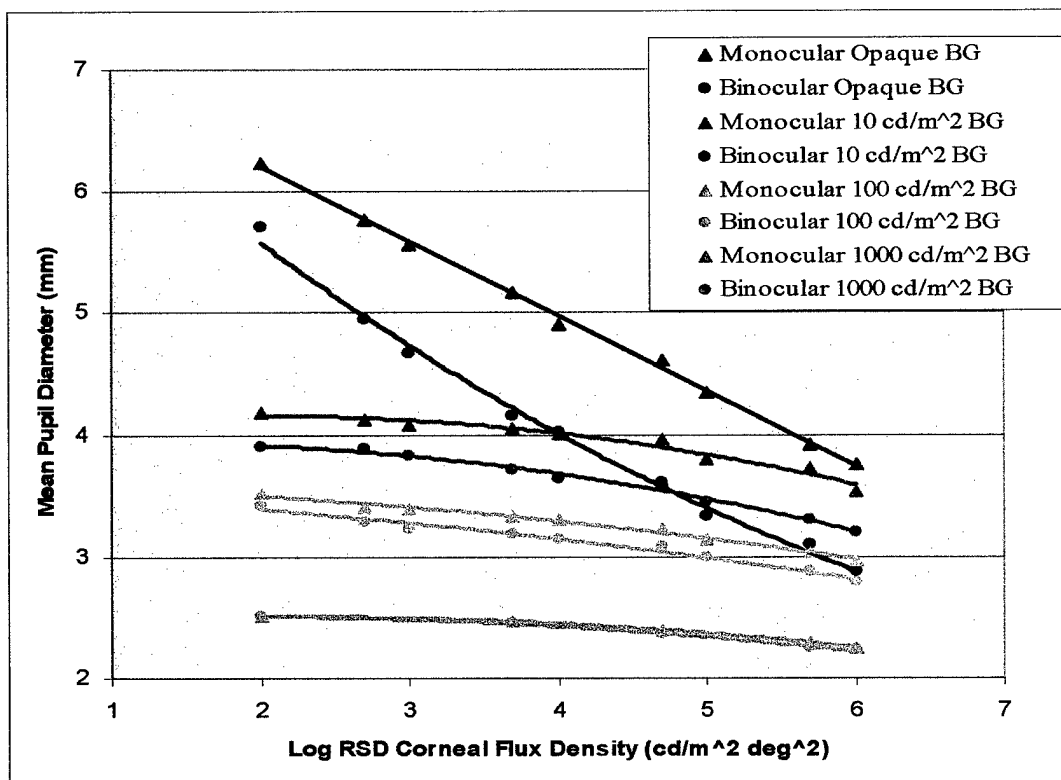


Figure 6.3: Summary of Subjects' Mean Pupil Responses

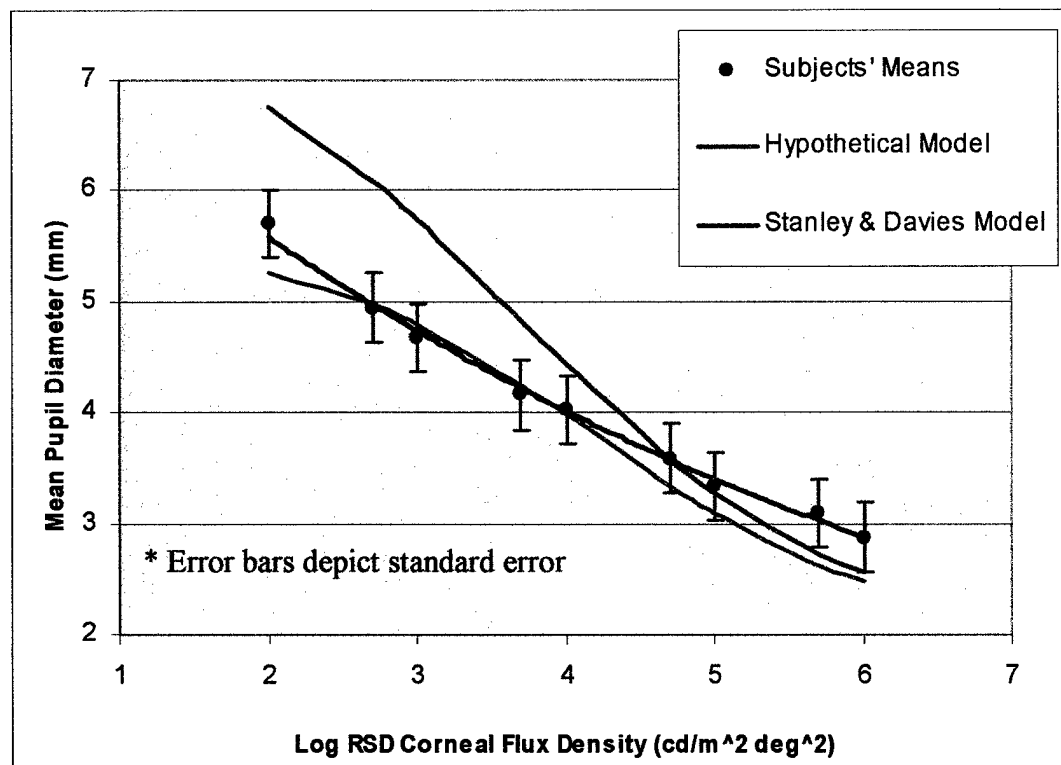


Figure 6.4: Comparison of Results with Pupil Response Models

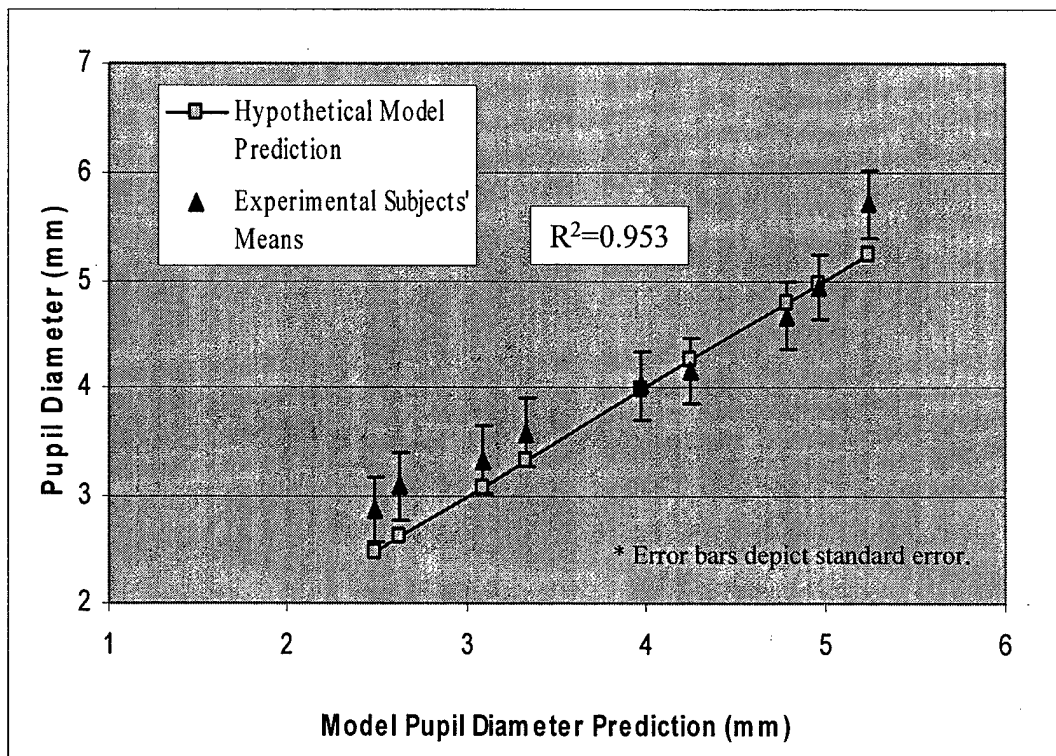


Figure 6.5: Linear Comparison of Results with Hypothetical Model

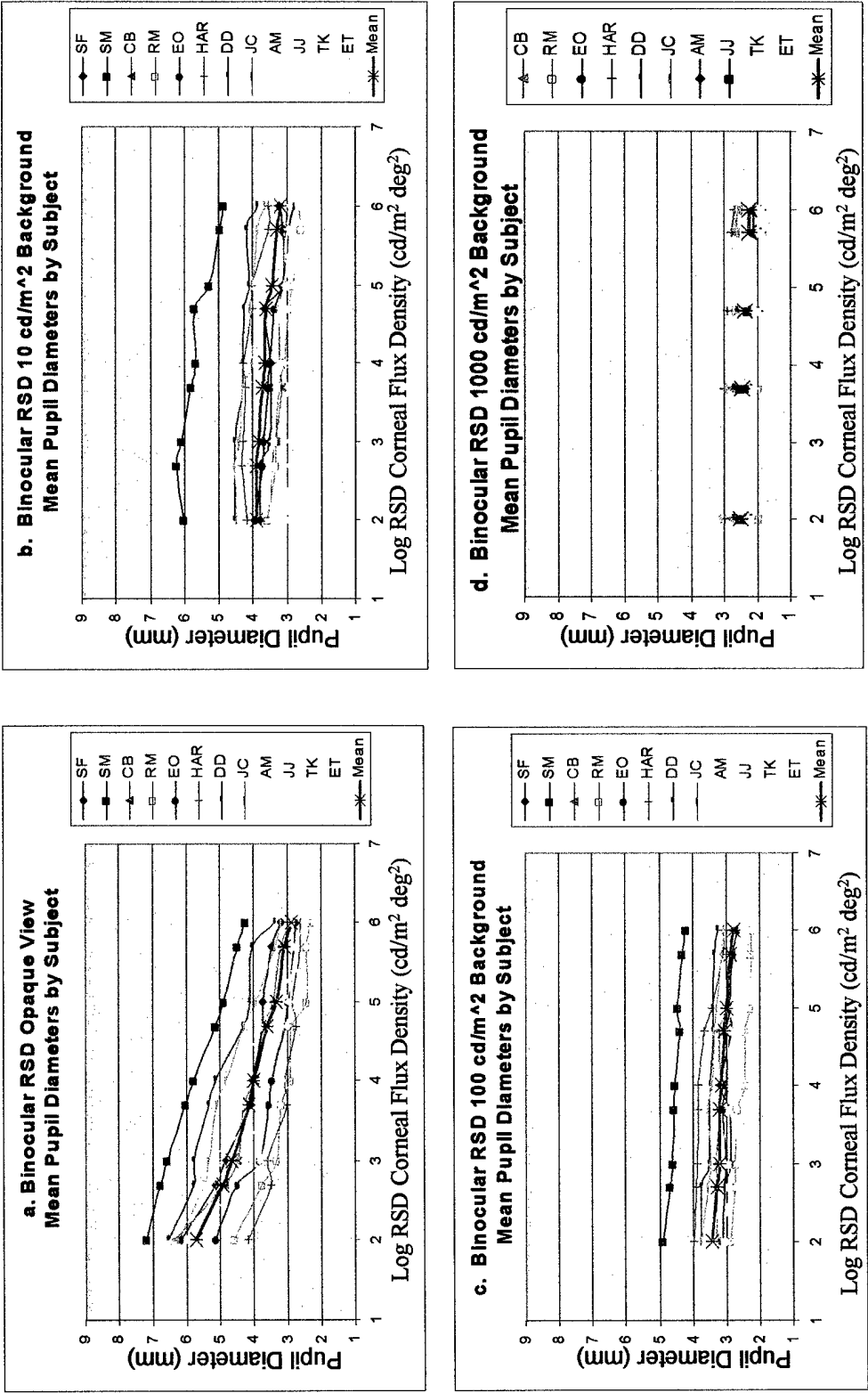


Figure 6.6: Comparison of Binocular RSD Mean Pupil Response by Background Luminance and Subject

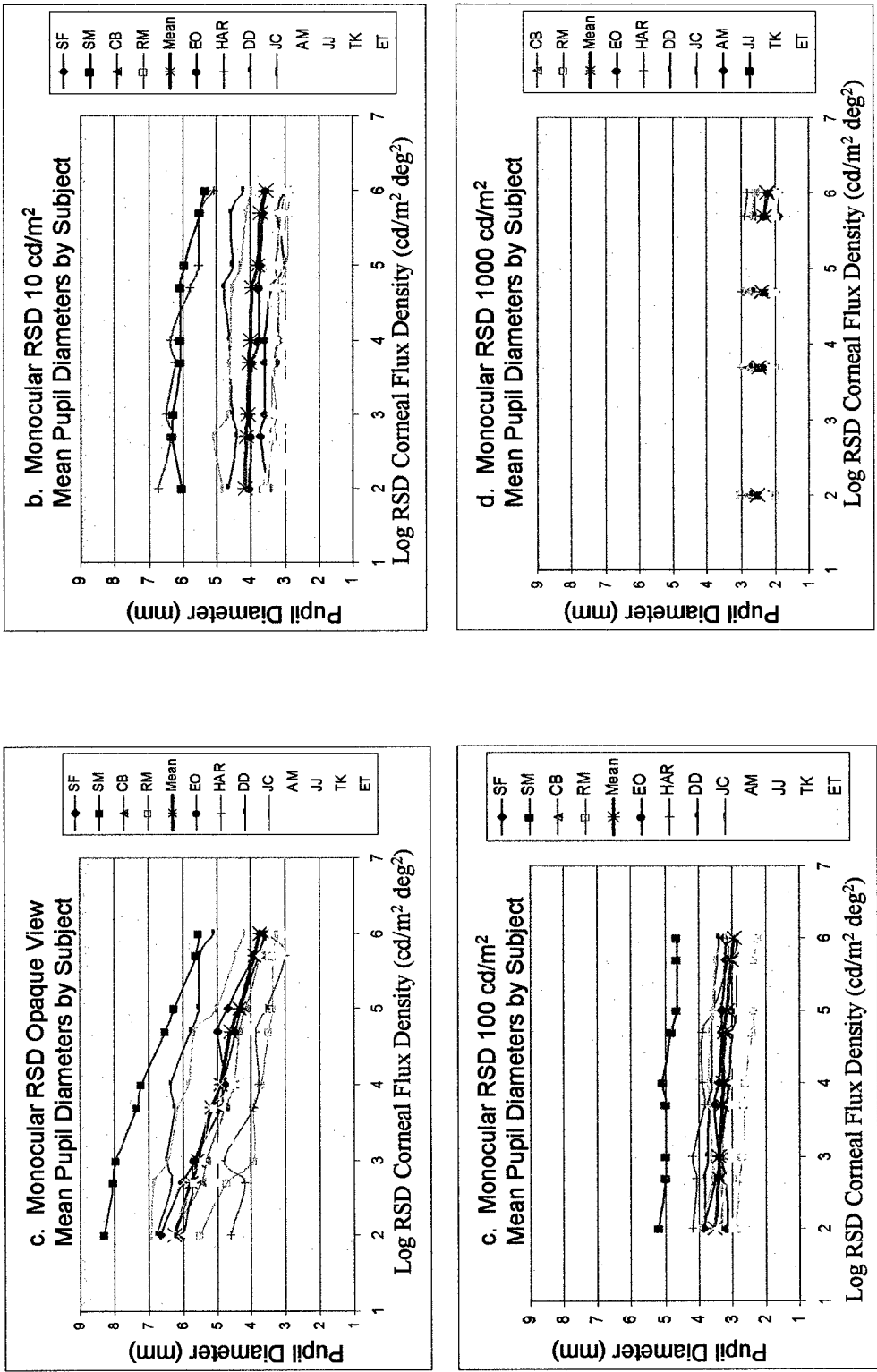


Figure 6.7: Comparison of Monocular RSD Mean Pupil Response by Background Luminance and Subject

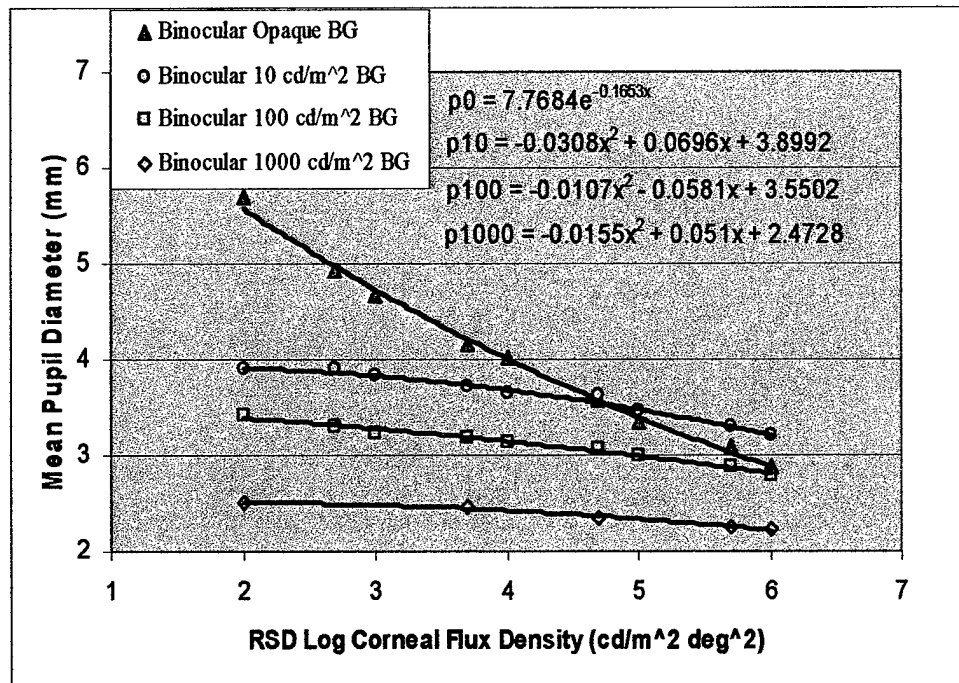


Figure 6.8: Binocular RSD Family of Pupil Response Functions

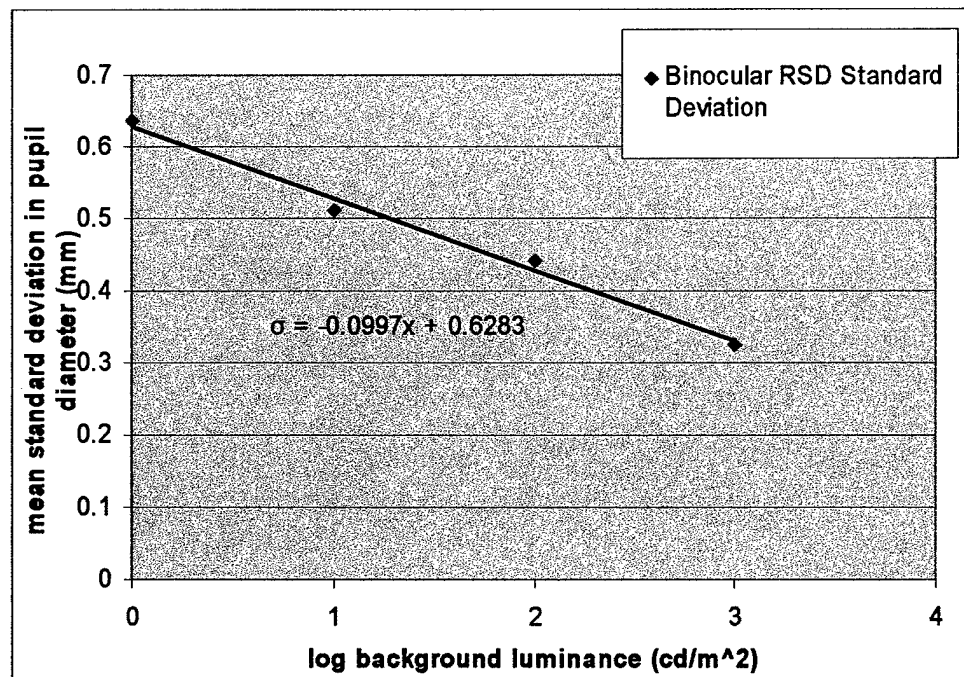


Figure 6.9: Binocular RSD Standard Deviation with Background Luminance

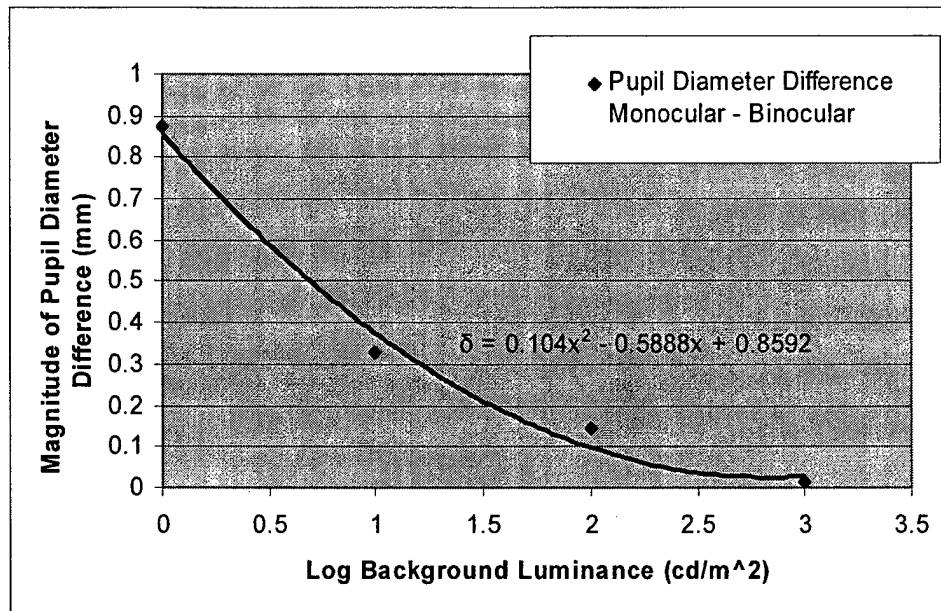


Figure 6.10: Pupil Diameter Difference, Monocular RSD – Binocular RSD

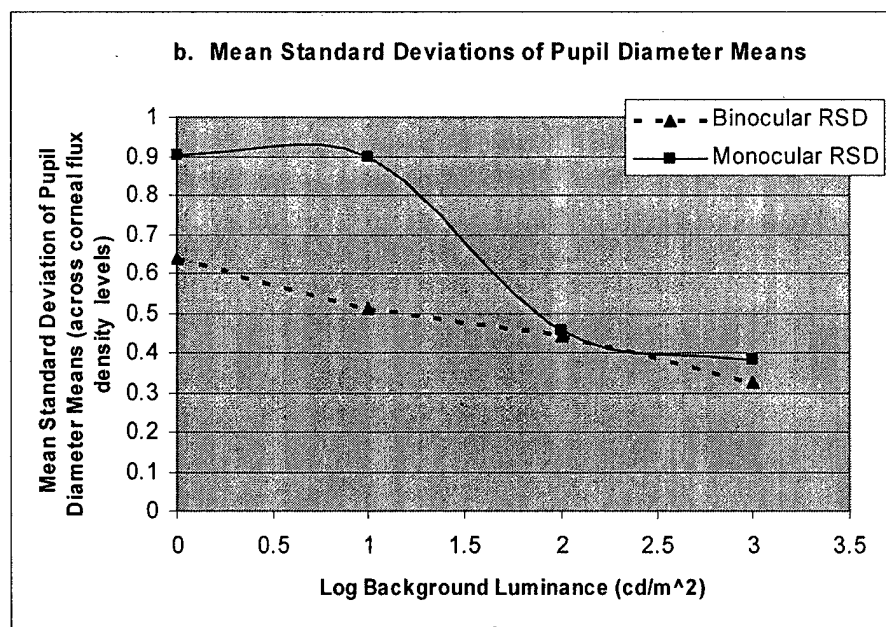
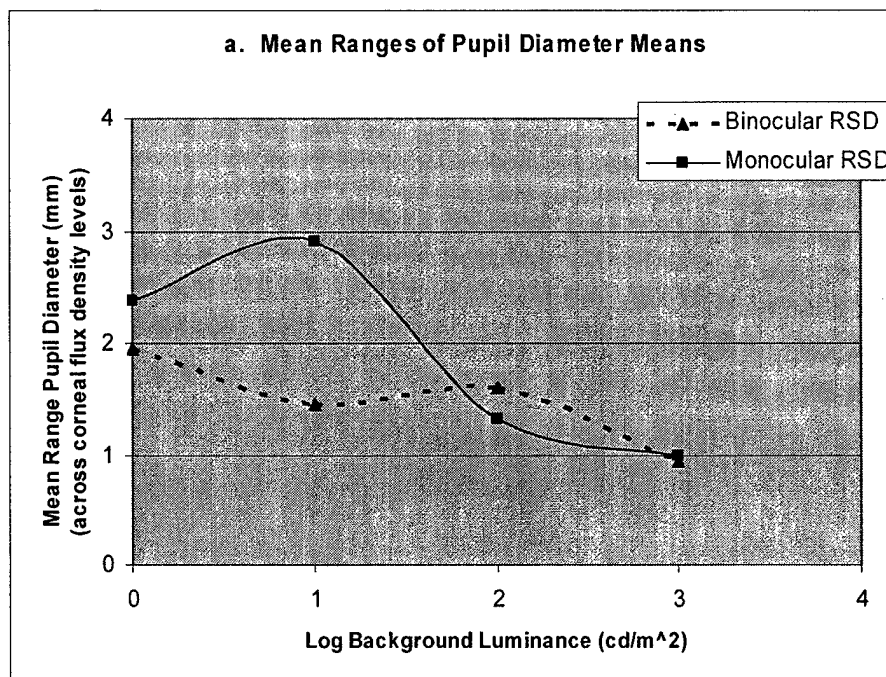


Figure 6.11: Mean Range and Standard Deviations of Pupil Diameter Means, Monocular versus Binocular

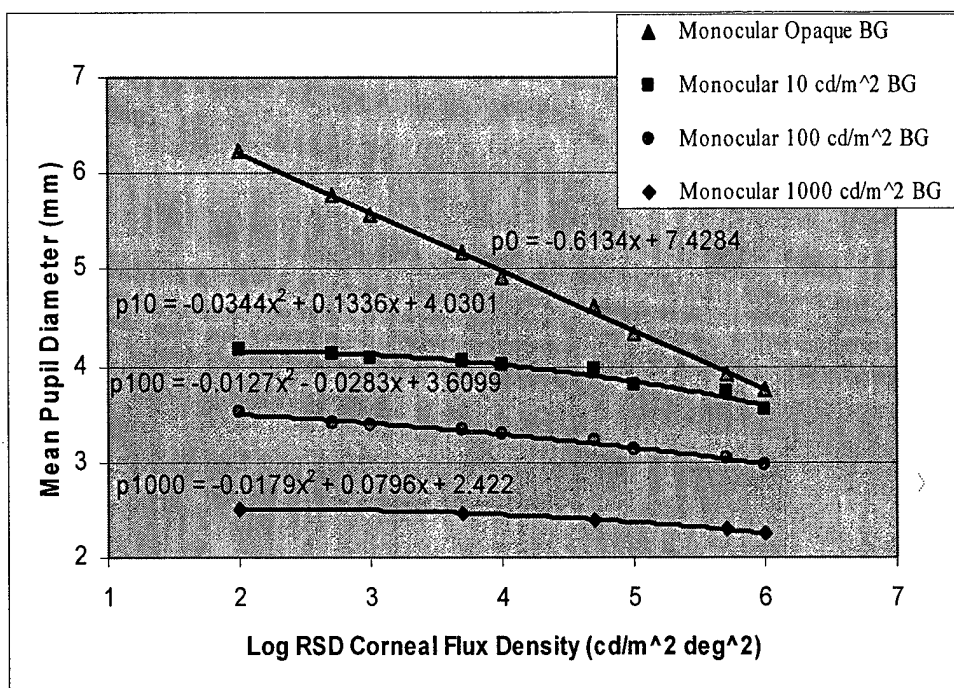


Figure 6.12: Monocular RSD Family of Pupil Response Functions

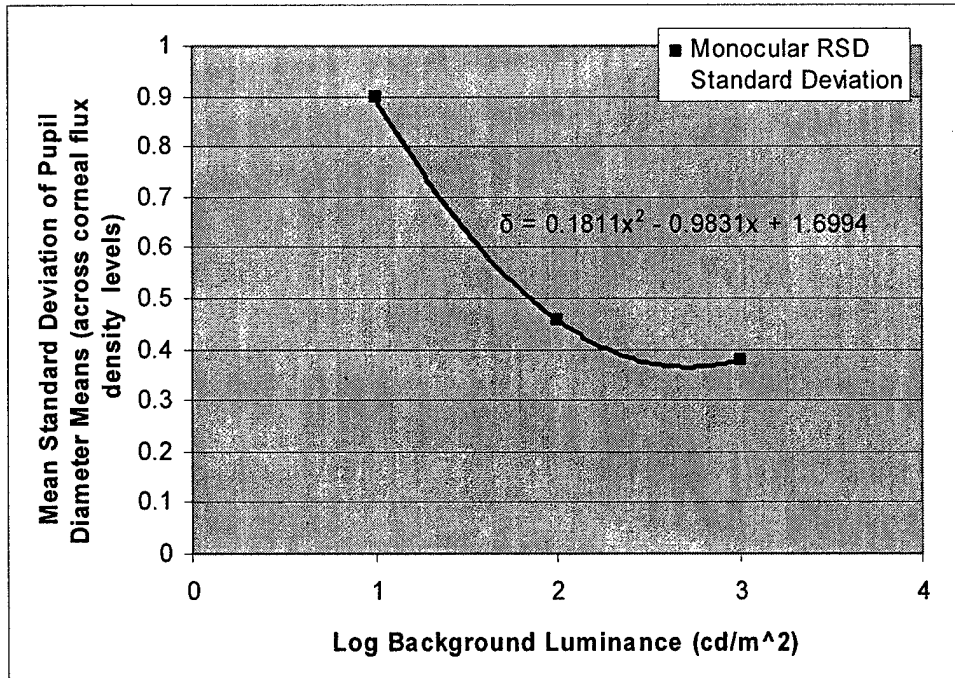


Figure 6.13: Monocular RSD Standard Deviation with Background Luminance

Chapter 7: Small Exit Pupil Arrays: Concept Explorations and Exit Pupil Separation Preference Experiment

The reasoned assertions of section 2.2.3 and its subsections lead to the conclusion that RSD's utilizing arrays of small exit pupils are a logical next step in the evolution of RSD technology. Indeed, as a remarkable coincidence and with no foreknowledge by this author, the U.S. Patent Office awarded a patent for precisely such an RSD display concept within only a few days of this writing [85]. This new patent incorporates eye tracking technology, as advocated in section 2.2.3.3, to facilitate exit pupil "switching" and maintain only a singular small exit pupil actively coupled to the eye at any time. The advantages of such display systems are too attractive to ignore. Arrayed small exit pupil RSD's will certainly be designed and produced for a wide variety of applications in the near future. As posited in section 2.2.3.1, understanding the human interface implications of this display concept is a prudent first step to design and engineering.

An exploration of the arrayed exit pupil concept was undertaken to investigate basic visual perceptual characteristics with an arrayed pupil display. Observations were made with various types of display content and exit pupil formations. An experiment was also conducted to empirically derive a model of optimum/maximum exit pupil separation distance for arrayed small exit pupils. This model is envisioned to provide designers information about the optimum exit pupil separation distance as a function of eye pupil diameter and exit pupil diameter for arrays that are constantly illuminated. Alternatively, the model will provide information regarding the maximum desirable exit pupil separation distance as a function of eye pupil diameter and exit pupil diameter for exit pupil arrays using switched singularly illuminated exit pupils. These concepts of exit pupil separation are fundamental to designing effective and efficient methods for implementing arrays of small exit pupils.

7.1 Basic Explorations of Arrayed Small Exit Pupil Concepts

An exploration of the basic concepts associated with arrayed small exit pupil displays was undertaken using a novel, but simple, optical apparatus. The exploration investigated the basic visual perceptual characteristics of the display concept and assessed its viability as a usable visual display. Unique visual perceptual characteristics were revealed and additional novel display concepts were conceived. The arrayed small exit pupil display concept was determined to be

viable and useable, and worthy of further investigation and development. The general hypothesis 3 was confirmed: *Arrays of small exit pupils are an effective method of preserving the optical advantages of small exit pupil RSD's while offering expanded exit pupil area to the observer.*

7.1.1 Objectives and Hypotheses

The primary objective of the arrayed pupil exploration was to examine basic human perception of the display concept. Of particular interest was the effect on visual perception of the coupling of exit pupils created from beam scans that were not of parallel geometry and did not register coincident images on the eye's retina. As introduced in section 3.3.1, saccadic suppression was hypothesized to mask the transitional effects on image presentation during exit pupil coupling transitions for the majority of visual tasks. Only tracking tasks and static viewing very near the position of coupling confusion were hypothesized to readily reveal the image "jump" from one angular position to the next. Thus, these explorations informally tested the sub-hypothesis 3a: *Arrays of small exit pupils producing retinal images with angular disparity on the order of 1 degree visual angle will not disrupt contiguous image perception by human observers.*

In addition to the evaluation of the basic perceptual effects of exit pupil coupling transitions, the effect of display content density during pupil transitions was of interest, as was the perception of displays that were available only at specified eye rotation positions. That is, the perception of displays that coupled to the eye only when the eye was rotated to a limited specific region of the available eye rotation angle. Finally, the disruptive perceptual effects of z-axis coupling error were examined, in which the converged exit pupil was not coincident with the plane of the eye's entrance pupil.

This exploration directly supports the fourth major objective of this body of research: *Explore interface engineering options for preserving the advantages of small exit pupil display with arrays of small exit pupils and model human preference for basic arrayed pupil display characteristics.* Additionally, the results of this exploration contribute to the fifth major objective of this body of research: *Derive human factors engineering guidelines for implementing RSD's with arrayed small exit pupils.*

7.1.2 Apparatus

The basic apparatus used for explorations was the Arrayed Exit Pupil Emulator (AEPE) described in section 2.1.3 and depicted in Figure 2.8. For some initial observations, the two-window light stop was replaced with variously windowed stops affecting various exit pupil quantities, sizes, shapes, and relative positions. In these cases, a single large lamp was used to illuminate all translucent windows.

7.1.3 Observers

The primary observer for initial arrayed pupil display evaluations was the author. Additional observations for confirmation of effects were made by three HITL researchers with extensive experience in visual display design and visual perceptual experimentation. All observers were males between 36 and 53 years of age.

7.1.4 Procedures

The exploration procedures were initially informal observations that were incrementally refined into formal observations and later formulated into the human subjects experiment described in section 7.2. After constructing the AEPE, the author used the apparatus to examine various arrayed exit pupil conditions. These conditions included arrays of 2 to 5 exit pupils, arrays of round, rectangular, and square exit pupils, arrays presenting dense display content, arrays presenting sparse display content, two-pupil arrays of variable separation distance, two-pupil arrays of identical content but different chromaticity, "switched" exit pupils, and arrays with imposed coupling error in the z-axis of alignment.

The simple general methodology was to construct the required translucent windows and stops for the desired exit pupil characteristics, view the resulting display with various modulating acetate slides, and assess the display's qualities and characteristics. Following selected observations and assessment by the author, additional observers were called upon to make independent observations and assessments regarding specified display characteristics. These additional observer assessments were summarized and recorded.

7.1.5 Results and Discussion

The results of observations clearly indicate that the concept of arrayed small exit pupils is viable for most envisioned applications of RSD's. The visual perceptual effects of exit pupil transitions with non-parallel beam scans were not significant detractors. The hypothesized masking effect of saccadic suppression was clearly observed under many conditions. A description of the general visual perceptual effects is followed by observational results with specific conditions.

When viewing the AEPE display with a singularly coupled exit pupil, the slide-modulated image was clearly presented (given sufficiently small exit pupil area for large depth of field). Except for the absence of distinct RSD scan lines that are frequently detectable with the VRD and VRDE, no perceptible differences in display imagery were noted as compared to a true RSD image. The unique qualities of the arrayed exit pupil display become obvious only with the presentation of more than one exit pupil.

7.1.5.1 General Perceptual Characteristics and the Region of Coupling Confusion

With two exit pupils simultaneously presented, the perception of the display depends greatly upon the separation distance between the two exit pupils. With a separation distance greater than the diameter of the eye pupil, the effect is as follows:

Rotating the eye so as to view the background scene "between" the two exit pupils allows no coupling of pupils and no image presentation to the retina. When the eye is rotated toward one of the exit pupil positions and coupling is achieved, the image suddenly appears in augmented view. As the eye continues to rotate in the same direction, the image is scanned by central vision until pupil decoupling again occurs at the opposite side of the eye pupil at which point the image disappears from view. As noted in section 2.2.3.2, the angular extent of the image available to central vision is a function of pupil diameter. Rotating the eye back in the opposite direction again couples and decouples the same exit pupil, and continued rotation may then couple with the adjacent exit pupil, reinstating the image in view.

Under these conditions, the observer may note a slight difference in the portion of the image available to central vision with each of the two adjacent exit pupils. A typical scenario with a small eye pupil and large field of view RSD will allow the observer to centrally view only one third of the image immediately left of image center using one exit pupil and only one third of

the image immediately right of image center using the adjacent exit pupil. While the remaining portions of the image are visible in peripheral view in each case, the attempt to centrally view these parts of the image will result in pupil decoupling and a loss of image. The effect is disquieting to the observer.

With two simultaneously presented exit pupils of lesser separation distance, simultaneous coupling of the two exit pupils is possible. Under this condition, a double image is perceived, one presented by each exit pupil. Obviously, if the exit pupils are not immediately adjacent, some eye rotations will cause the decoupling of one exit pupil while maintaining coupling with the other. A typical scenario under these conditions has the observer seeing a confusion of dual non-coincident RSD images when looking at the central portions of the display, but seeing a clear singular image when central vision is directed to the extremities of the image. Again, only a portion of the image is clearly perceptible using central vision with either of the two exit pupil couplings, causing the observer some frustration.

A compromise separation distance exists between the two conditions described above in which the exit pupils are separated by a distance approximately equal to the diameter of the eye pupil. With such a separation distance, one exit pupil is decoupled just as another is coupled, providing good continuity of a singular image and allowing the entire image to be viewed with central vision via multiple sequenced exit pupil couplings. Under the condition where the exit pupil separation distance is near the eye pupil diameter, the problematic conditions previously described are still applicable, although the angle of eye rotation through which the effects are noticed is appreciably smaller.

As noted in section 2.2.3.2, the finite size of the exit pupil precludes a perfect exit pupil separation distance scenario where one exit pupil decouples precisely as an adjacent exit pupil couples. Instead, the observer perceives a small angular extent through which a double image is perceived and that may be reduced in brightness due to partial dual exit pupil couplings. If the exit pupils are separated more distantly, less opportunity for dual images exists, but less exit pupil area is coupled and a dim image results near the coupling transition eye rotation position. If the exit pupils are more narrowly separated, the image maintains high brightness, but a double image is perceived over a wider area of eye rotation. The region of eye rotation through which this dilemma occurs has been termed the region of coupling confusion (section 3.3.2).

Observations were made using the two exit pupil adjustable apparatus of the AEPE as depicted in Figure 2.8 in which the observer adjusted the separation of the exit pupils. The visual

perceptual characteristics of the region of coupling confusion changed commensurate with exit pupil separation distance, as expected. The observer was able to achieve a good compromise separation distance that was judged to maintain display brightness with a minimum of dual image visual area. Making this judgment became more difficult as the angular extent causing dual exit pupil capture was reduced, as finding and fixating on the small region of coupling confusion became more challenging. It became necessary for the observer to affect deliberate, slow, step by step visual observations across sub-elements of display content to find the region of coupling confusion. Rapid eye movements across the scene that affected exit pupil switching did not readily expose the region, nor were the image position jumps obvious. This is attributed to the hypothesized effect of saccadic suppression. Only a deliberate slow scan or step by step fixations across the image promoted the detection of the region of coupling confusion and the associated image position change. Once the region of coupling confusion was identified by the observer and its image position was noted for the current exit pupil separation distance, subsequent identifications of the region were more readily achieved by fixating near the noted image position.

Typically, once the observer had achieved an optimum exit pupil separation distance for his eye pupil diameter, the region of coupling confusion caused a narrow curvilinear disruption across the image when the eye rotation position allowed the partial coupling of both exit pupils. It is important to understand that the disruption was a manifestation across the entire image for an extremely narrow range of eye rotation positions, and the range of eye positions were manifested as a curvilinear pattern through the image. No actual line or curve was perceived within the image. The disruption was perceived only at a specific position of central vision in the image. That is, scanning slowly across the image revealed no disruption until a specific image position was placed in central vision at which point the disruption would appear across the entire image. When central vision was moved away from that image position, the disruption again disappeared. For exit pupils separated horizontally as in the AEPE apparatus, the disruption position pattern ran vertically through the image and was manifested only when a proper and precise central vision fixation position was achieved in the horizontal dimension. This manifestation will now be termed the arrayed pupil *boundary disruption*.

Depending upon the precise separation distance and the dynamics of eye pupil oscillations, the boundary disruption was manifested as one of the two perceptual phenomena previously described. With greater separation distance, the boundary disruption became a linear

“hole” or “trough” in the contiguous image. Thus, as the observer slowly scanned across the image, the image would suddenly be lost entirely through a small range of central vision fixation positions within the image. Alternatively, with lesser separation distance, the boundary disruption was a linear region of central vision fixation positions at which the entire image became a doubled disjunct presentation.

The extent of the boundary disruption and the region of coupling confusion are partly functions of exit pupil diameter. For a given pair of adjacent partially coupled exit pupils positioned diametrically on opposite edges of the eye pupil, eye rotation in the direction of one exit pupil will cause the edge of the eye pupil to pass across that exit pupil until it is fully coupled to the eye and the diametrically opposed exit pupil is completely blocked by the iris (decoupled). The region of coupling confusion is defined by the eye rotation angular extent through which at least partial coupling is affected for both exit pupils. Clearly, for equivalent center to center separation distance of exit pupils in an array, the angular extent of eye rotation through which partial coupling will be affected is directly proportional to exit pupil diameter. Therefore, smaller exit pupils inherently produce smaller regions of coupling confusion and smaller boundary disruption perceptual artifacts.

7.1.5.2 Display Content Density and Saccadic Suppression

Some perceptual differences were noted with differences in display content. In particular, the density of display content seemed to influence these differences, although display type and display density were frequently confounded in these observations, as was the setting of the optimum exit pupil separation distance. The perceptual differences were manifested as differences in the level of difficulty identifying the boundary disruption and the associated image positional change. Generally, with high density information content such as paragraph style text or combinations of images and wrapped text, observers rarely noticed the image position change, but had relatively little difficulty finding the boundary disruption position when asked to identify it. With sparsely populated content, such as wireframe diagrams combined with short, small text tags, observers more readily noticed the image position change, but had a relatively difficult time finding the boundary disruption position when asked to identify it. It is important to reiterate that the position change effect and the boundary disruption effect were not judged to be significant detractors and were rarely noticed without a deliberate attempt at identification. Still, judged

relatively, the two conditions of image content density clearly resulted in perceptual differences. Examples of the modulation stimuli used in these observations are presented in Appendix C.

After adjusting exit pupil separation to a position judged to be optimum for minimizing boundary disruption effects, the observers reported on their perceptions of the display. In a typical reading task in which a densely populated paragraph of white letters was presented in augmented view against a darker contrasting background, all three observers reported an inability to detect the pupil coupling transition when scanning the text at normal reading speeds. As noted in the formulation of hypotheses, reading is affected with saccadic eye motion, and saccadic suppression reduces low spatial frequency sensitivity. The large field of view paragraph of dense text clearly provided some low frequency stimuli, but high frequency stimuli must also have been present. Still, the perception of its positional change with exit pupil coupling transitions was effectively suppressed with reading saccades.

In a similar task in which observers viewed a still frame of a news agency web site combining high density text and large block graphics and images, similar difficulty was had in identifying the positional change associated with exit pupil coupling transitions. The scanning of such a combination image is likely conducted with very similar saccadic eye movements, yielding similar results to the pure reading task. Additionally, the block images and diagrams, as well as the dense text around them, were low spatial frequency stimuli, facilitating saccadic suppression.

However, when viewing a sparsely populated wireframe diagram that contained simple graphics of orthogonal lines and short text tags or numerical displays, the image positional shift associated with exit pupil coupling transitions was more readily apparent to the observers, although the other effects of the boundary disruption were of little significance. In fact, observers reported extreme difficulty in locating the exact position of the boundary disruption within the sparsely populated imagery in spite of easily detecting the image position shift. Two possible explanations for the positional shift perceptual differences are posited.

First, it is reasonable to assume that the wireframe diagram content does not constitute a sufficiently low spatial frequency stimulus to capitalize on the suppressive effects associated with saccadic eye motion. Thus, the positional shift is clearly detectable with pupil transitions. Alternatively, the sparse content of a particular geometry may have aided visual detection. In this particular case, the wireframe diagram presented long graphic lines across the visual field that were not in the proximity of additional graphics or text. Such long, linear structures may have induced a visual task for scanning along the lines that was more akin to visual tracking tasks that

do not utilize saccadic motions. If this was the case, no saccadic suppression would have been enacted by the visual system. Possibly, a combination of these two explanations was responsible for the enhanced sensitivity to the boundary disruption's positional change characteristic.

It seems clear that the difficulty reported with identifying the exact location of the boundary disruption is related to the density of image content. With the densely populated text image, high frequency disruptions were clearly affected all across the image at the position of coupling confusion. Once the general region of the disruption was identified, it was relatively easy for observers to narrow the search and make fine adjustments to the separation of exit pupils since the disruption was visibly affecting text, regardless of the position in the image. However, with the low density content of the wireframe image, little image content was available for the observation of the disruption. Thus, it was much more difficult for observers to pinpoint the location of the disruption within the scene.

7.1.5.3 Miscellaneous Additional Observation Results

Several additional comparisons were made by observation. These include the observation of exit pupils of various shapes, exit pupils with differing chromaticity, and the switched illumination of singularly coupled exit pupils.

Exit pupils for RSD's will not always be round. Depending upon the source of illumination, square or rectangular pupils are likely. As such, observations with square and rectangular pupils of various sizes were made. No clear differences due to shape among any of the similarly sized exit pupils were expected, and none were observed.

As a method of assisting observers with the task of identifying the position of the boundary disruption within the scene when displaying two exit pupils, one translucent window in the AEPE apparatus was covered with a Kodak Wratten filter (yellow number CC40Y) for a set of observations. As a result, the image displayed with the filtered exit pupil was tinted slightly. Observation of the display under these conditions induced an interesting visual effect in addition to aiding the observers with locating the position of the boundary disruption.

With the text image, the text was normally white, as modulated by the slide. When reading across a line of text with the filter positioned on one exit pupil, the text color of the entire image changed from white to yellow as a line was read, left to right. Although the application of such a technique seems of little practical value, it points to the possibility of displaying different

information with different exit pupils in an arrayed pupil display. Clearly, such an arrangement would not be desirable for expanding exit pupil effective area, but alternative display concepts may utilize this general idea. This concept is discussed more fully in section 7.3.

A simple arrangement for affecting switched singularly coupled exit pupils was added to the AEPE apparatus. This was essentially a properly sized rotating light block that covered one of the two translucent windows at a time. By rotating the light block, either of two exit pupils could be presented in isolation, and rapid switching of the two exit pupils was affected. This was intended to coarsely emulate the postulated switched singularly coupled exit pupil display concept described in section 2.2.3.3.

After setting a proper exit pupil separation distance, that distance was closed slightly to ensure complete capture of either exit pupil. While viewing the display, the light block was rotated back and forth to cause alternative capture of single exit pupils. With a fixed gaze, the positional change was obvious when switching the coupled pupil. When employing saccadic eye motions in a normal reading task, the positional changes were much less noticeable, although the effect was not identical to saccadic suppression observed with the constantly illuminated pupils set at optimum separations. Sensitivity to the positional changes seemed to be slightly greater than with the previous observation's conditions and somewhat inconsistent in the occurrence of effects.

Although no further testing of this concept was conducted, it is posited that the slightly greater sensitivity to positional change was essentially a statistical phenomenon. Under the earlier conditions, eye motion was surely involved 100 percent of the time that pupil coupling changes were made because the eye motion itself caused the coupling change. Under the later switched exit pupil emulation, the pupil coupling changes were not induced by eye motions and were not necessarily affected simultaneously with eye motions. Saccadic eye motions are rapid starts and stops in the changing of eye position. Thus, in the case where eye motion was not causing the changed pupil couplings it is likely that the coupling changes were occasionally made while eye motion was stopped between individual saccades. In this case, the saccadic suppression would not be fully activated during the exit pupil coupling change and the sensitivity to positional change would be less suppressed. Further, this phenomenon would be essentially random, accounting for the observed inconsistency of effects.

It is also notable that with the switched singularly coupled exit pupil no boundary disruption was evident. This was expected, as only a single exit pupil was coupled at any given

instant and provided no opportunity for double imagery to be presented on the retina. Essentially, the switched singularly coupled exit pupil scenario changes the nature of the region of coupling confusion, or potentially eliminates it completely, depending upon the specific implementation of exit pupil switching logic. The image positional change associated with pupil coupling transitions remains, however.

7.1.5.4 Visual Perceptual Effects of z-Axis Pupil Coupling Error

The properly coupled RSD exit pupil will converge in or very near the plane of the eye pupil. This proper z-axis pupil coupling is critical to the avoidance of undesirable effects with both singular small exit pupil RSD's and arrayed small exit pupil RSD's. However, with arrayed pupil displays that seek to utilize the full extent of available eye pupil diameter, z-axis pupil error coupling induces unique visual effects near the region of coupling confusion.

With a single small exit pupil, z-axis coupling error will be manifested as a vignetted display. The magnitude of the z-axis error that produces vignetting is a function of RSD field of view, as wider field of view displays present a cone of scanning rays with a shorter optical waist. Because the exit pupil is created by a converging cone of light rays, any relative z-axis positional error between the eye entrance pupil and display exit pupil will cause the cone of rays to converge either before (-z-axis) or after (+z-axis) the plane of the eye pupil. In either case, if the error is sufficiently large or the eye pupil sufficiently small, the iris of the eye will begin to block rays of light from entering the eye. Vignetting of the image occurs because selected light rays representing a subset of the image are completely blocked by the iris. If the exit pupil is well coupled with ray convergence occurring in the plane of the eye pupil, partial pupil coupling will partially block *all* light rays, resulting in reduced retinal illumination overall, but a portion of each ray will reach the retina resulting in the presentation of the entire image.

The precision with which z-axis coupling must be maintained is partly a function of the display field of view. A wide field of view RSD has a rapidly converging cone of scanning light rays and, thus, a converged waist that rapidly expands in the z-dimension. The z-axis coupling must be well maintained to avoid vignetting effects. A narrow field of view display has a less severely converging scan pattern and, thus, a "longer" waist that is more tolerant of z-axis coupling error. Figure 7.1 graphically depicts these various scenarios and subsequent geometrical

considerations. Additionally, deWit offers a model of z-axis error for the prediction of vignetting with RSD field of view for singular exit pupil displays [4, 5].

With arrayed small exit pupils near the region of coupling confusion, exit pupils are near or on the edge of the eye's iris. If the exit pupil is not well coupled on the z-axis, vignetting will occur instead of a reduction in retinal illumination. When this condition was observed with a pair of adjacent arrayed exit pupils with the AEPE apparatus, a unique perceptual experience was obtained.

The two images presented by the disparate exit pupils were seen to partially overlap with central vision inspection. With central vision inspection within the overlapping region, double image perception was observed. Outside of the overlap region, singular image perception was observed. The extent of the overlap was directly related to the exit pupil separation distance. The pattern of the overlapping region was that of two overlaid circular images, each partially overlapping the other to jointly form an ovoid shaped area. As with the boundary disruption, the overlapping ovoid region was observed within only a limited eye rotation angle. Thus, a full (or slightly vignettted) singular image was observed with the coupling of either exit pupil alone, but the overlapping region of dual imagery was observed as the central vision position moved across the image into the region of coupling confusion. Additionally, the curvature of the overlapping image region seemed to vary with lighting conditions, being more tightly curved with greater luminances.

This observation is easily explained by the coupling geometry of the condition. With z-axis pupil coupling error, each exit pupil is simultaneously vignettted by the eye iris in the region of coupling confusion. As such, two vignettted images reach the retina. Because of the reversal of imagery by the optics of the eye, the edges of each image that are affected by iris vignetting overlap on the retina about the center of the combined pupil presentations. This results in the ovoid shaped region where double imagery is perceived with central vision inspection. Further, the curvature of the ovoid overlapping region is a function of eye pupil curvature. Thus, smaller pupils that result from brighter luminance conditions increase the curvature of the ovoid region. By examining the simple geometry presented in Figure 7.1, it is easy to intuit that the overlapping double image region expands with reduced exit pupil separation distances. Increased exit pupil separation distances reduce the double image region but increase the severity of vignetting. The result is a substantial degradation of image perception in either case.

7.1.6 Conclusions

Sub-hypothesis 3a is confirmed: *Arrays of small exit pupils producing retinal images with angular disparity on the order of 1 degree visual angle will not disrupt contiguous image perception by human observers.* This conclusion is based upon the reported observations, specifically the observations that under many conditions the positional change and boundary disruption associated with exit pupil transitions were not noticeable. This conclusion also supports general hypothesis 3: *Arrays of small exit pupils are an effective method of preserving the optical advantages of small exit pupil RSD's while offering expanded exit pupil area to the observer.*

Although the boundary disruption was identifiable with a deliberate visual search, it did not significantly disrupt image perception or significantly degrade image quality. Similarly, although the image positional change was detectable, particularly with high spatial frequency or sparsely populated display content, it did not offer a significant degradation of image perception. Thus, the concept of arrayed exit pupils presenting non-coincident imagery of small angular disparity is judged to be a viable concept.

Display content, content density, and visual task will largely determine the magnitude of the perceptual effects associated with pupil coupling transitions, either by optimal separation distance or by switching singularly coupled exit pupils. The primary perceptual characteristic influencing these factors is saccadic suppression. There seems to be no perfect solution, with each scenario of imagery characteristics and pupil transition strategies offering trade-offs in visual perceptual advantages and disadvantages. Still, with these minor perceptual imperfections, the degrading effects are minor and do not negate the previously introduced advantages of the display concept.

One potential source of image degradation, particularly with arrayed pupil displays of wide field of view, is z-axis pupil coupling error. This type of coupling error becomes particularly disruptive to image perception when the optimum exit pupil separation method of coupling transitions is employed. However, even with switched singularly coupled exit pupils, significant image perception degradation may occur by vignetting. Careful display head mounting engineering designs will be necessary to help avoid this condition.

Given that the switched singularly coupled exit pupil method is a feasible concept that utilizes eye pupil tracking and/or pupil measurement technologies, numerous scenarios are

conceivable for the implementation of control logic to calculate the timing and conditions for affecting pupil coupling transitions. While it is recommended that this avenue of research be explored to develop models of human perception and performance with various control logic scenarios, such an expansive undertaking is beyond the scope of the present body of research. As an alternative foundational step, the concept of pupil coupling transition by optimum pupil separation is now examined with the empirical development of a preliminary model of human preference for the optimum pupil separation distance.

7.2 Optimum Exit Pupil Separation Distance Preference Experiment

A human subjects experiment was conducted to empirically derive a model for the prediction of the optimum exit pupil separation distance as determined by observer preference. A hypothesized model format was introduced in section 3.3.2 with the optimum exit pupil separation defined as a function of eye pupil diameter and exit pupil diameter. The model format was based on reasoned assertions derived from literature regarding human visual perceptual characteristics, from knowledge of RSD stimuli characteristics, and from previous RSD experimental results. Five human subjects were tasked to observe a display comprised of two exit pupils and to adjust the separation of the exit pupils until they judged the separation to be the optimum for the minimization of exit pupil coupling transition visual effects. Eye pupil diameter and exit pupil separation distance were recorded and analyzed. Results supported the experimental and general hypotheses, and model components were empirically derived.

7.2.1 Objectives and Hypotheses

The primary objectives of this experiment were to validate the hypothesized form of a model of human preference for the optimum exit pupil separation distance for effective pupil coupling transitions and to empirically derive the model components. These objectives are embodied in sub-hypothesis 3b that is tested with this experiment: *The following model of preferred exit pupil separation is generally applicable to arrays of small exit pupils about the pupil of the eye:*

$$s_{ep} = (m(d_{ep}))p + b(d_{ep}) \quad (\text{eq. 3.2})$$

where s_{ep} is the center-to-center separation of two adjacent exit pupils, d_{ep} is the diameter of the display exit pupil, and p is the diameter of the eye's entrance pupil. The function $m(d_{ep})$ is a function to be determined empirically, as is the function $b(d_{ep})$. The testing of this hypothesis supports the fourth and fifth major objectives of this body of research: 4. *Explore interface engineering options for preserving the advantages of small exit pupil display with arrays of small exit pupils and model human preference for basic arrayed pupil display characteristic*; and 5. *Derive human factors engineering guidelines for implementing RSD's with arrayed small exit pupils*.

The hypothesized model is of a linear form with variables of eye pupil diameter and exit pupil diameter. It assumes round exit pupils smaller than the pupil of the eye by a factor of 2 or greater and array elements to be of equivalent separation distances. The model asserts that the optimum exit pupil separation is primarily a function of eye pupil diameter. Two imbedded functions of exit pupil diameter were empirically derived, one representing the slope of the overall linear model ($m(d_{ep})$) and the other representing the ordinate intercept ($b(d_{ep})$). As described in section 3.3.2, these imbedded functions were hypothesized to change significantly with exit pupil diameter due to expected Stiles-Crawford I variability with exit pupil diameter and due to expected partial pupil coupling area variability with exit pupil diameter.

Each of the imbedded functions was estimated with a linear equation for a limited range of exit pupil diameters between 0.5 mm and 1.0 mm. Although examination of a greater range of exit pupil diameters would likely have revealed non-linear functions, particularly with SC-1 effects, this short range was practical for most envisioned applications. Larger exit pupils will sacrifice desired optical advantages while the tiny aperture of smaller exit pupils will significantly deteriorate the resolution and quality of the RSD image (see section 2.2.1.4). (Additionally, smaller exit pupils of smaller diameter scanning beams begin to induce significant deleterious visual perceptual effects due to interruption of beams by floating matter within the humors of the eye and due to unbalanced eye tear film [98].)

7.2.2 Apparatus and Experimental Setup

The monocular apparatus for this experiment was the Arrayed Pupil Emulator (AEPE) as described in section 2.1.3 and as depicted in Figure 2.8. The adjustable translucent windows of

the AEPE were configured to create pairs of adjacent round exit pupils of either 0.5 mm diameter or 1.0 mm diameter, interchangeable by the experimenter. The sliding rail mechanism allowed the observer to manipulate the separation of these two exit pupils.

A stationary ruled scale coupled with a pointer on the sliding rail mechanism allowed easy measurement of the separation of the exit pupils. The ruled scale was used as an index that was calibrated to exit pupil separation distances. This calibration was accomplished using a table-mounted magnifying reticle to directly measure exit pupil separation distances by visual inspection. The precision of the reticle measurements and the ruled scale increments allowed significant digit quantification of the separation distances to 0.01 millimeter (the hundredth place being the first estimated digit).

The acetate slide used to modulate the displayed image depicted a paragraph of white text, as presented in Appendix C. The paragraph image covered a visual angle of approximately 30 degrees horizontal by 24 degrees vertical. The apparatus was configured with a viewing beam splitter to affect an augmented view display.

The background natural view scene was of a lightly colored wall at approximately 3 meters distance. A high intensity white light lamp illuminated the background wall with variable intensity, as adjusted by the experimenter. The augmented view was unencumbered, offering a nearly 2-pi steradian natural field of view.

An optical/infrared video camera was mounted out of the subject's view, and a small first surface mirror was mounted 45 degrees from center display view to provide a reflected image of the subject's right eye to the camera. This allowed the video recording of the subject's pupil for subsequent measurement and analysis without significantly encumbering the natural field of view. This also provided a method of monitoring each subjects' pupil response during the course of the experiment.

A custom dental impression bite bar was created for each subject and mounted below the viewing beam splitter with a five dimensional adjustable bracket. An adjustable position padded forehead rest was mounted above the viewing beam splitter. The bite bar and head rest provided head and eye position stabilization throughout the experiment. These stabilizers were positioned so that the emulated RSD display was always presented to the subject's right eye.

7.2.3 Subjects

The purpose of the experiment was disclosed to all subjects and each gave informed consent. Five adult subjects were tested, 3 males and 2 females. Ages ranged from 26 years to 40 years. Each subject had corrected acuity of 20/20 or better, normal eye alignment, and no known visual defects. All of the subjects had previous experience with psychophysical or opto-physiological experimentation, as each had participated in at least one previous RSD experiments within this body of research. Three subjects were HIT Laboratory research associates with ample experience as subjects in visual psychophysical experiments related to RSD research. Each subject was paid for participation in this study.

7.2.4 Methods and Procedure

For the purposes of statistical comparisons between conditions, this experiment was a 2 x 1 factorial within subjects repeated measures design. For the purposes of deriving model functions, exit pupil separation distance was simply examined as a covariate with eye pupil diameter, and best fit linear functions were determined, as appropriate.

Two levels of the independent variable exit pupil diameter were presented (1.0 mm and 0.5 mm) with two conditions of the variable eye pupil diameter. Because each subject's eye pupil response was different and varied slightly over time, no consistent values for the two levels of eye pupil diameter were feasible between subjects or even within the same subject. Rather, gross changes in eye pupil diameter were affected by changes in background scene luminance. The experimenter strove to simply obtain a relatively small pupil diameter and a relatively large pupil diameter for each subject within a range of approximately 2 mm to 5 mm. As such, the eye pupil diameter variable should be formally considered as a *subject* variable that is uncontrolled, and this experiment should formally be considered a correlational study.

However, this design is unique in that a dependent variable may be declared that is a valid and consistent ratio scale measurement as a function of eye pupil diameter and exit pupil separation distance. This *pupil delta* variable, representing the difference between eye pupil diameter and exit pupil separation distance, provided a dependent measure allowing consistency of comparisons across all eye pupil diameters. Thus, even though the subject variable of eye pupil diameter was uncontrolled, a consistent ratio scale comparison was made with this derived

dependent measure that was valid irrespective of eye pupil diameter. As such, valid within subjects comparisons between levels of exit pupil diameter were made across eye pupil diameters. Comparisons between the highly varied "levels" of eye pupil diameter have no formal definition and were not proper.

The subject was briefed on the purpose of the experiment and was provided a detailed verbal description of the visual perceptual phenomena that would be experienced. Using drawings and verbal descriptions, the experimenter explained the region of coupling confusion and the pupil coupling transition image shift. The experimenter explained the optimum exit pupil separation distance, defining it as the preferred separation distance by the subject that maintained good image brightness while minimizing the effects of the boundary disruption. The experimenter provided procedural suggestions to assist the subject with expeditiously identifying the boundary disruption.

The subject was right-eye aligned to the AEPE display, and the dental impression bite bar and head rest were positioned for maintenance of head and eye position. The alignment was accomplished so that the two exit pupils were centered vertically on the eye pupil and so that normal eye rotation allowed the coupling of each exit pupil even when widely separated. The subject was allowed to manipulate exit pupil separations and view the display while the experimenter monitored exit pupil positions relative to eye pupil position via the optical/infrared video camera and monitor. In this way, the experimenter was able to infer the visual experiences of the subject and explain the various phenomena commensurate with their occurrences. Figure 7.2 depicts a captured image of a subject's eye with exit pupils illuminated.

After the subject was familiar with the visual environment of the display, several practice trials were conducted to familiarize the subject with the pace and procedure of the trials. Following practices, the display and background luminances were set for initial experimental conditions and data collection trials were initiated.

For each trial, the experimenter randomly offset the position of the AEPE's sliding rail mechanism, inducing a random separation distance of the two exit pupils. The subject was then tasked to adjust the separation distance using the sliding rail mechanism until the optimum exit pupil separation was achieved. Upon setting an exit pupil separation distance, the subject issued a sub-vocal signal indicating trial completion. The experimenter verbally annotated the audio track of the video tape with trial identification information and recorded the ruled scale setting of

exit pupil separation distance in an electronic spreadsheet. For each condition a minimum of ten trials were conducted with each subject.

The two levels of exit pupil diameter were pseudo-randomly ordered in presentation. The two quasi-levels of eye pupil diameter, grossly affected with background luminance changes, were also pseudo-randomly ordered. The luminance level of the naturally viewed background was measured with a PhotoResearch PR-880 photometer (PhotoResearch, Chatsworth, California), and the retinal illumination due to the AEPE display was estimated by Westheimer's method using the same PR-880 photometer, as described in section 2.2.4.

Throughout the data collection periods, the experimenter monitored the relative positions of eye pupil and exit pupils for each trial via the video camera and monitor, as depicted in Figure 7.2. Since a true 2-D array of exit pupils was not being presented, but rather only a pair generically representing any two adjacent exit pupils in an array, it was possible for the exit pupils to not be maintained at positions directly across the eye pupil diameter. That is, significant vertical rotation of the subject's eye would cause the horizontally adjacent exit pupils to not be positioned diametrically across the pupil. This condition would have induced significant error, as decreased exit pupil separation distances would have been necessary to achieve the region of coupling confusion across a chord of the eye's circular pupil rather than across the diameter. The experimenter instructed the subjects to read lines positioned higher or lower within the display paragraph in order to affect minor adjustments in vertical eye position that ensured diametrical positioning of the exit pupils with respect to the eye pupil during the judgment of optimum exit pupil separations.

7.2.5 Analysis

Analyses were conducted with SPSS for Windows 9.0 on a PC computer and with Microsoft Excel. Using the derived dependent measure, *pupil delta*, an analysis of variance was conducted to examine the main effect of exit pupil diameter. A regression analysis was made of center to center exit pupil separation distance and eye pupil diameter for each exit pupil condition. Pearson products were calculated and a linear best fit function was determined by least squares for each set of exit pupil condition data. Graphical plots of data were constructed by exit pupil condition sets depicting exit pupil separation distance as a function of eye pupil diameter.

Using the two slope values of the linear best fit functions for each of the exit pupil condition data sets, a linear function describing the change in slope with exit pupil diameter was determined. Similarly, using the two ordinal intercept values of the linear best fit functions for each of the exit pupil condition data sets, a linear function describing the change in ordinal intercept with exit pupil diameter was determined. These two linear functions were substituted into the form of the hypothetical model of optimum exit pupil separation to complete its empirical derivation.

As a brief validation of the models of pupil response derived by the experiment of Chapter 6, predictions of eye pupil diameter response were made under the display conditions of this experiment. Predictions derived by graphical interpolation from the pupil response models were compared with measured pupil response diameters. A regression analysis was performed and the Pearson product was calculated as a measure of model prediction accuracy.

7.2.6 Results

The results of the effect of exit pupil diameter on exit pupil separation distance are summarized by the plots of Figure 7.3. These plots depict all individual data points of exit pupil center to center separation distance as a function of eye pupil diameter for each of the two exit pupil diameter conditions. Best fit linear functions are depicted for each data set, along with the respective linear equation and R^2 calculation. Table 7.1 summarizes the fit linear equations, where s_{ep} is the center-to-center separation of two adjacent exit pupils and p is the diameter of the eye's entrance pupil.

Table 7.1: Best Fit Linear Functions to Exit Pupil Separation Data

Exit Pupil Diameter (mm)	Best Fit Linear Function	R^2
0.5	$s_{ep} = 0.8296p + 0.2838$	0.905
1.0	$s_{ep} = 0.8925p + 0.4637$	0.825

(eq. 7.1)

(eq. 7.2)

Strong effects were obtained for both eye pupil diameter and exit pupil diameter, each yielding $p < .001$. The effect of exit pupil diameter is graphically evident from the vertical separation of the best fit linear functions depicted in Figure 7.3. The mean values of pupil delta

(eye pupil diameter minus center to center exit pupil separation distance) were -0.08 mm with the 1.0 mm diameter exit pupils and 0.33 mm with the 0.5 mm diameter exit pupils.

Fitting linear functions to the slope values and to the ordinate intercept values obtained in the best fit linear functions for each of the two exit pupil conditions yields the equations of Table 7.2, where d_{ep} is the exit pupil diameter, $m(d_{ep})$ is the function determining slope values of the exit pupil separation best fit functions, and $b(d_{ep})$ is the function determining intercept values of the exit pupil separation best fit functions.

Table 7.2: Linear Functions Fitting Slopes and Ordinate Intercepts of Pupil Separation Functions

Source Values	Linear Equation	
slope values	$m(d_{ep}) = 0.1258 d_{ep} + 0.7667$	(eq. 7.3)
intercept values	$b(d_{ep}) = 0.3598 d_{ep} + 0.1039$	(eq. 7.4)

Inserting these function estimates for slope and intercept into the hypothesized model form yields an empirical model for estimating the preferred optimum pupil separation distance as determined by exit pupil diameter and eye pupil diameter:

$$s_{ep} = (0.1258 d_{ep} + 0.7667)p + 0.3598 d_{ep} + 0.1039 \quad (\text{eq. 7.5})$$

where s_{ep} is the center-to-center separation of two adjacent exit pupils in millimeters, d_{ep} is the exit pupil diameter in millimeters, and p is the diameter of the eye's entrance pupil in millimeters.

Eye pupil response diameter predictions estimated from the monocular pupil response models derived in Chapter 6 are compared with measured pupil responses in Figure 7.4. The abscissa represents the axis of model prediction pupil diameter and the ordinate is measured pupil diameter response. Data points are depicted in comparison with the various models' "perfect prediction" diagonal line. Regression analysis yielded $R^2 = 0.82$, indicating good prediction performance. Although no proper examination of the variance prediction models could be made with these data, the range of measured values is approximately equivalent to the smallest range found in the pupil response study conditions (1000 cd/m² background condition). Additionally, the measured values seem well centered about the prediction line. These data were derived from a small subset of display and background conditions. The backgrounds ranged from 0 cd/m² (opaque view) to 700 cd/m². The display corneal flux density estimates were more restricted due

to the conditional needs of the exit pupil separation experiment, ranging from approximately $2.33 \times 10^4 \text{ cd/m}^2 \text{ deg}^2$ to $9.22 \times 10^4 \text{ cd/m}^2 \text{ deg}^2$.

7.2.7 Discussion and Conclusions

The results strongly support the form of the hypothetical model of optimum exit pupil separation distance. Evidence of each of the hypothesized effects described in section 3.3.2 was obtained. Therefore, sub-hypothesis 3b is confirmed: *The following model of preferred exit pupil separation is generally applicable to arrays of small exit pupils about the pupil of the eye:*

$$s_{ep} = (m(d_{ep}))p + b(d_{ep}) \quad (\text{eq. 3.2})$$

where s_{ep} is the center-to-center separation of two adjacent exit pupils, d_{ep} is the diameter of the display exit pupil, and p is the diameter of the eye's entrance pupil. The function $m(d_{ep})$ is a function to be determined empirically, as is the function $b(d_{ep})$.

As anticipated, the greatest effect on exit pupil separation resulted from eye pupil diameter. The change in exit pupil separation distance was almost directly proportional to the change in eye pupil diameter, resulting in linear best fit equations with slopes near unity. However, as hypothesized, the slopes of these functions were slightly less than unity and they varied with exit pupil diameter.

Such deviations from unity were posited in section 3.3.2 as hypothesized effects of the Stiles-Crawford I phenomenon. It was also asserted that the slope deviations from unity were expected to indicate increases in the coupled area of partially coupled exit pupils commensurate with changes in phototransduction efficiency as dictated by the SC-1 efficiency function. That is, for a partially coupled exit pupil, the pupil area actually entering the eye should increase as eye pupil diameter increases at a rate that consistently compensates for the reductions in phototransduction efficiency due to SC-1 effects. To check this hypothesized effect across the range of eye pupil response diameters, ratios of the coupled areas of the exit pupils may be compared with ratios of SC-1 efficiency for various eye pupil diameters. Since, in the homogeneously luminous exit pupil case, pupil area is directly proportional to retinal illumination, similar ratios support the assertion that the increased coupling area of the partially coupled exit pupil was compensating for the reduced effective retinal illumination due to SC-1

effects. Dissimilar ratios indicate additional or different factors influencing exit pupil separation function slopes.

The 1.0 mm exit pupil results were examined in this manner. For several selected pairs of eye pupil diameters, ratios were calculated for SC-1 phototransduction efficiencies using the SC-1 function as determined by Moon and Spencer [40]. The exit pupil center position, relative to the center of the eye pupil, was used as the radius for SC-1 efficiency calculations. Additionally, using the empirically derived best fit linear equation from the 1.0 mm exit pupil condition to determine exit pupil separation distance and eye pupil diameter, and using standard geometric formulae for area calculations, ratio estimates were calculated for the partially coupled exit pupil areas entering the eye. (These were estimates since, in the geometric calculations, the curvature of the eye's pupil was approximated as a straight line for simplicity. The calculation was made as the area within the circle between a chord and its enclosed arc. In this case the chord was defined by the edge of the iris, a curved edge. However, since the eye pupil diameter was typically much larger than the exit pupil diameter, the approximation of this curve as a linear chord did not induce significant error.)

Table 7.3 summarizes the comparison of SC-1 efficiency ratios and coupled pupil area ratios for the 1.0 mm diameter exit pupil. The efficiency ratios and area ratios are remarkably closely matched across the range of comparisons, supporting the assertion that the increased pupil coupling area preferred with increased eye pupil diameters is due to subjects' compensating for reduced image brightness caused by SC-1 effects.

Table 7.3: Comparison of SC-1 Efficiency Ratios to Coupled Pupil Area Ratios for the 1.0 mm Exit Pupil Condition

eye pupil diameters for comparison	ratio of SC-1 efficiencies	ratio of coupled exit pupil areas
5.0 mm : 2.2 mm	1.65	1.53
4.0 mm : 2.2 mm	1.30	1.34
3.0 mm : 2.2 mm	1.12	1.15
5.0 mm : 3.0 mm	1.50	1.33
4.0 mm : 3.0 mm	1.18	1.16

An identical comparison of ratio values with the 0.5 mm exit pupil diameter condition yields the values of table 7.4. More disparity results between ratio comparisons than with the 1.0 mm exit pupil condition, but the obtained comparisons are still closely matched and support the assertion. Further, due to the smaller size of the exit pupils, it was certainly more difficult for subjects to make the very fine adjustments in the separation distances that would affect image brightness in the region of coupling confusion. Thus, greater error is expected than in the 1.0 mm exit pupil case. It should also be noted that with the 0.5 mm exit pupil condition, the mean exit pupil separation distance with eye pupils of 4.5 mm diameter and larger resulted in the condition that the entire exit pupil was coupled.

Table 7.4: Comparison of SC-1 Efficiency Ratios to Coupled Pupil Area Ratios for the 0.5 mm Exit Pupil Condition

eye pupil diameters for comparison	ratio of SC-1 efficiencies	ratio of coupled exit pupil areas
4.4 mm : 2.0 mm	1.44	1.73
4.4 mm : 3.0 mm	1.29	1.27
3.0 mm : 2.0 mm	1.12	1.36
3.6 mm : 2.2 mm	1.21	1.44

The slopes of the exit pupil separation equations were also hypothesized to decrease with decreased exit pupil diameter. This was expected, again for SC-1 considerations. As the exit pupil separation distance was defined as center to center separation, larger exit pupils extended further toward the central region of the eye pupil where phototransduction efficiency is increased. Thus, when smaller exit pupils are presented that do not extend as far toward the central eye pupil, SC-1 effects are more significant than with the larger exit pupils, given equivalent center to center separation distances. As a result, a more significant adjustment in exit pupil separation distance was necessary with small exit pupils to compensate for SC-1 reductions in effective retinal illuminance. The results generally support this assertion, with the slope of the 0.5 mm exit pupil best fit equation being smaller than the 1.0 mm best fit slope, 0.8296 versus 0.8925, respectively (see Figure 7.3).

The ordinate intercepts of these equations were also hypothesized to change with exit pupil diameter. This assertion was based not only on the expectation of slope changes with exit

pupil diameter, but also due to geometrical considerations related to exit pupil coupling. With larger exit pupils, the opportunity to separate the exit pupils while maintaining some coupled area is greater than with smaller exit pupils. With smaller exit pupils, extended separation may produce an exit pupil boundary disruption in which the image is completely lost for some range of eye rotation positions. Similar separation with larger exit pupils does not result in image loss. Thus, larger exit pupils may be separated to a greater extent than smaller exit pupils at the optimum separation distance, resulting in a change in the ordinate intercept of the best fit linear equations. Evidence of this effect is clear from the vertical separation of the two best fit functions. The intercepts differ with the 0.5 mm exit pupil intercept being less than the 1.0 mm intercept, 0.2838 versus 0.4637, respectively.

Given the evidence for each of the hypothesized effects from which the general form of the hypothesized model was derived, the form of the model is clearly validated. The internal consistency of data and hypothesized effects lends support to the empirically determined nested functions for the hypothesized model's slope and ordinate intercept. As such, the empirically derived equation 7.5 (section 7.2.6) is asserted to be a valid model for the estimation of the optimum exit pupil separation distance, as determined by human preference, for affecting arrayed exit pupil transitions by the separation method.

However, this preliminary model makes several assumptions about the nature of the exit pupils that may be violated by some RSD designs, leading to opportunities for additional research. In particular, the luminance of exit pupils in this study was essentially homogeneous. The round exit pupils were equally luminous throughout the disk shaped aperture. This characteristic is generally consistent with some envisioned RSD luminance sources, but inconsistent with others. For example, the luminance profile of the original VRD used in earlier experiments in this body of research is a Gaussian form. Gaussian forms are quite common for many sources, particularly for gas lasers. Light emitting diode sources may produce other beam profiles that approximate Gaussian or other profiles that are not homogeneous.

The perceptual nature of the exit pupil boundary disruption must be partly a function of the exit pupil luminance profile. Since the observer seeks to maintain image brightness while minimizing the effects of the boundary disruption, luminous variability across the exit pupil diameter will induce variability in image brightness as a function of the exit pupil luminous profile. Thus, two exit pupils of differing luminous profiles must induce differing functions of

image brightness with exit pupil separation distance, ultimately generating differing functions of optimum exit pupil separation distance.

As an example, consider a Gaussian beam profile that produces a Gaussian exit pupil aperture. The greatest portion of light energy passes near the center of the aperture, while the flux density near the periphery of the aperture is significantly reduced in accordance with the Gaussian function. This is in stark contrast to the homogeneous exit pupil in which the entire aperture is equiluminous. Consider the partially coupled case in which the iris blocks one half of the exit pupil area (ignoring small effects of iris curvature). In both the Gaussian and homogeneous exit pupil case, one half of the flux density of the exit pupil will enter the eye. However, as the exit pupils are separated further, the flux density entering the eye from the Gaussian formed exit pupil will be reduced at a greater rate than with the homogeneous exit pupil. Alternatively, as the exit pupil separation distance is closed, the flux density entering the eye from the Gaussian exit pupil will increase at a more rapid rate than with the homogeneous exit pupil. Thus, image brightness will operate as two distinctly different functions of exit pupil separation, yielding distinctly different functions of optimum separation distance.

The example discussed above is similar to the comparison of two homogeneous exit pupils of differing diameters. The small homogeneous exit pupil is analogous to the Gaussian form exit pupil since small changes in separation distance will have a more profound effect with the smaller exit pupil than with a larger exit pupil. Therefore, as compared to a homogeneous exit pupil of similar diameter, the changes in the optimum separation distance function for a Gaussian form exit pupil should be similar to the functional changes obtained with smaller diameter homogeneous exit pupils. That is, slope and intercept should decrease with the Gaussian exit pupil, although perhaps not as precipitously as with the smaller homogeneous exit pupil. Clearly, the rates of change in these functions will vary with the precise Gaussian form. Broader, more gently tapering Gaussian forms will induce separation functions more like large homogeneous exit pupil functions, while narrow, steeply tapered Gaussian forms will result in functions more like small homogeneous exit pupil functions.

Another less significant issue not examined closely in this experiment is the condition where a region of coupling confusion is achieved with three equidistant exit pupils in a 2-D array. While the region of coupling confusion may be expected to provide slightly different perceptual disruptions from the two exit pupil case, it does not seem reasonable that the separation distance between exit pupils should be altered by this fact. If the optimum exit pupil separation distance

was slightly altered due to image brightness and boundary disruption considerations at the precise eye position associated with the region of coupling confusion for three equidistant exit pupils, a perceptual change would be manifested in the two exit pupil case that may cause undesirable effects. As the geometry of equidistant element arrays dictates that the two exit pupil regions of coupling confusion are twice as common as the three exit pupils cases, such an adjustment does not seem prudent.

As a final consideration with the empirically derived model, it seems that some applicability may be made to the transition method of switched singularly coupled exit pupils. While some perceptual effects of the boundary disruption do not apply to the switched singularly coupled exit pupil scenario (multiple imagery, image loss), certainly the effects of changing image brightness and image position do apply. The SC-1 considerations and partially coupled exit pupil considerations discussed previously in this section must apply as well to image brightness obtained with the switched exit pupil method of affecting coupling transitions. Therefore, it seems reasonable that the model of equation 7.5 may be utilized to identify the maximum exit pupil separation distances that should be provided by any arrayed small exit pupil display for a given eye pupil diameter, regardless of pupil coupling transition method. Exceeding these separation distances with any method of pupil coupling transition will induce noticeable artifacts in RSD imagery perception near the region of coupling confusion.

Determining this maximum desirable exit pupil separation distance may have significant implications with regard to the perception of arrayed exit pupil displays. Clearly, engineering of arrayed pupil displays will seek to minimize the visual effects associated with the transitioning of exit pupil couplings. The primary method of minimizing these effects may be to minimize the necessity for coupling transitions to occur. This requires careful consideration of the relationship between display field of view and estimates of the maximum eye rotation angles for maintenance of exit pupil couplings, as described in section 2.2.3.2 and summarized in table 2.2. By maximizing exit pupil separation distances, the necessity to transition pupil couplings is minimized, and the opportunity for the perception of visual effects of the boundary disruption is minimized. Thus, the model of equation 7.5 may be generally applicable in identifying absolute maximum separations for all methods of exit pupil coupling transition.

In conclusion, the empirical model of optimum exit pupil separation distance is asserted to be valid in form and content. It is further asserted to be generally applicable for the determination of maximum separation distances for arrayed exit pupil displays. Still, this model

is preliminary and limited in its applicability to various exit pupil luminance profiles. Additional research is warranted to refine and expand this model and to explore additional factors influencing human perception of arrayed display exit pupil transitions. The results and conclusions reached here have succeeded in supporting the fourth and fifth major objectives of this body of research: *4. Explore interface engineering options for preserving the advantages of small exit pupil displays with arrays of small exit pupils and model human preference for basic arrayed pupil display characteristic; and 5. Derive human factors engineering guidelines for implementing RSD's with arrayed small exit pupils.*

7.3 Additional Arrayed Small Exit Pupil Observations and Explorations

Following the experiment of section 7.2, additional informal observations and explorations were undertaken by the author. These included the observation of a large 2-D array of small exit pupils under conditions of optimum separation distance for eye pupil diameter, the observation of different imagery displayed via different, widely separated exit pupils, and considerations of the applicability of this research to a recently awarded U.S. patent for an arrayed small exit pupil RSD.

Using the AEPE apparatus, an array of ten exit pupils of 0.5 mm diameter was presented. This was accomplished with a single light block panel pierced with a static array of ten round translucent windows of equal separation distance and rear illuminated with a single high intensity lamp. The center to center separation distance between any adjacent pair of exit pupils was made to be 3 mm, and the resulting dimensions of the effective exit pupil area were approximately 10 mm x 7 mm. The array of exit pupils was arranged as depicted in Figure 7.5.

The display was presented in augmented view, identical to the arrangement described in the experiment of section 7.2. The AEPE display luminance was held constant, but the background luminance was varied by the observer to affect changes in eye pupil diameter. By adjusting the background luminance, the observer was able to closely match his eye pupil diameter to the separation distance of the exit pupils, thereby affecting an optimally separated array of exit pupils for coupling transitions by separation. The eye pupil diameter and display field of view conditions dictated the use of a minimum of three exit pupils in the horizontal dimension for eye rotation motion, and two exit pupils in the vertical dimension. Additional exit pupil transitions were affected with lateral motion of the head and eye.

The observer modulated background luminance to achieve an optimally separated exit pupil condition with the 3 mm fixed separation exit pupil array. After the optimum separation adjustment was judged satisfactory, an eye pupil measurement was made. This singular datum agreed well with the optimum pupil separation model prediction. The 0.5 mm exit pupil model predicts that a 3.0 mm exit pupil separation will be optimum with an eye pupil diameter of 3.3 mm. The observer's eye pupil was measured to be 3.1 mm.

Under optimum separation distance conditions, the array of exit pupils provided an excellent expansion of effective exit pupil area. As observed with the previous observations of two exit pupil presentations, the boundary disruptions near regions of coupling confusion were noticeable with deliberate effort to observe them, but they did not significantly detract from the perception of the image. With normal saccadic eye motions, the disruptions were masked just as in the two exit pupil condition. Generally, the perception was of a single contiguous image presented via a large exit pupil display.

The observation of boundary disruptions of three simultaneous exit pupils was difficult to make as a very precise gaze position had to be maintained, and minor eye pupil oscillations affected changes in the capture of all three partial exit pupils. However, the effects were not substantially different than with the two exit pupil case. With careful observation the boundary disruption was observed to be comprised of three disjunct images, rather than two, as obviously expected. The disruption seemed to manifest within a very small region of the display image that was shaped coarsely as a triangle. Again, this is expected, as dictated by the geometry of three exit pupil partial couplings. Also noted about the three exit pupil boundary disruption were small regions of two pupil boundary disruption, oriented as roughly linear regions emanating in each of three directions from the small three exit pupil disruption region. These observations are consistent with the geometry of the pupil couplings, as may be inferred from Figure 7.5.

An observation was made using two widely separated exit pupils and a modulating acetate slide with different imagery depicted on either side. By carefully manipulating eye pupil diameter and the separation of two presented exit pupils, the distinct visual information on either side of the acetate slide was made to be viewable with central vision using only one of the two exit pupils. That is, rotating the eye to couple one of the exit pupils allowed the central visual inspection of only the left half of the image, while rotating to couple with the other exit pupil allowed central visual inspection of only the right half of the image. By further implementing manually switched light blocks over each of the two halves of the acetate slide, an emulation was

created of an RSD presenting different information via different exit pupils. In this type of RSD scenario, switching between display options is affected with a simple rotation of the eye.

While the emulation was a simple mock-up of an actual multi-display RSD, this proof of concept was compelling. In augmented view, the straight forward gaze direction was completely unencumbered by the RSD, allowing a completely natural view. When RSD information was desired for display, an eye rotation approximately 20 degrees right affected the coupling of an exit pupil displaying text information that was easily read. A return to a straight forward gaze removed the display from view. Alternatively, an eye rotation approximately 20 degrees left coupled a second exit pupil for the display of imagery related to the text. After only a few minutes of observation, this method of alternating between the natural view and the two related displays seemed comfortable and entirely natural. Of course, the angular values cited here for switching displays may be varied, as may the dimension of eye rotation. Although not specifically observed, vertical separation of information by similar methods may be more effective in many scenarios, keeping the central vertical and entire horizontal visual scene unencumbered for natural viewing. These issues suggest additional research opportunities for exploration of multiple display RSD interfacing and information formatting under various task scenarios.

To date, the RSD's utilizing multiple separated exit pupils to present different imagery via each separate exit pupil have not been developed. However, given that arrayed exit pupil RSD's are feasible, a natural progression in display evolution leads to independent modulation of exit pupil light sources for the presentation of different imagery by different exit pupils. While alternative optical designs will be necessary to properly orient these display exit pupils for selective coupling with the eye, such designs are not radical departures from currently implemented systems. The computational and electro-optical engineering challenges are easily answered with current technology. Only inspiration and technological pull are needed to initiate such display developments.

Clearly, the inspiration has begun. A U.S. patent has recently been awarded for the arrayed small exit pupil RSD concept [85]. Although the display patent depicts various design embodiments, each embodiment seems to call for a singular optic for the convergence of multiple exit pupils, just as described in section 2.2.3.2. Although advocating this optical technique, the patent does not address the issues of human visual perception that arise with this implementation and its resulting non-parallel beam scans. This body of research applies directly to the practical

implementation of the patented display designs, and perhaps it will help to circumvent what otherwise may be considered a visual perceptual roadblock to further arrayed pupil RSD development.

7.4 Conclusions

In conclusion, the exploratory and experimental results strongly support general hypothesis 3: *Arrays of small exit pupils are an effective method of preserving the optical advantages of small exit pupil RSD's while offering expanded exit pupil area to the observer.* This display design concept offers unique and attractive advantages in optical qualities, power consumption, and human interface implementations. The visual perceptual anomalies inherent with the design do not appear to significantly detract from image quality and interpretation, and techniques are feasible to reduce or eliminate the impact of the perceptual anomalies. Clearly, further exploration of the arrayed small exit pupil display concept should continue, and development should be pursued.

The explorations and experiment described in this chapter provided some interesting insights into the perception of arrayed small exit pupil displays. Many of the perceptual characteristics were predicted by hypotheses, based upon reasoned assertions and analyses of the optical geometry associated with the display concept. Other display characteristics and display interface concepts were revealed or envisioned only with the observation and evolution of the AEPE apparatus and the analysis of resulting observational data. Through this evolving, iterative process of display design, observation, and evaluation, the fourth major objective of this body of research was successfully completed: *Explore interface engineering options for preserving the advantages of small exit pupil display with arrays of small exit pupils and model human preference for basic arrayed pupil display characteristics.*

Basic human factors engineering and display interface guidelines for arrayed pupil displays were deduced from the results and analyses of these observations and experiments. These guidelines are detailed in Chapter 8 and generally concern the overall design of arrayed pupil displays, spacing of pupil array elements, the reduction of exit pupil boundary disruption effects, and display concepts for additional research and investigation. As such, the fifth and final major objective of this body of research was successfully completed: *Derive human factors engineering guidelines for implementing RSD's with arrayed small exit pupils.*

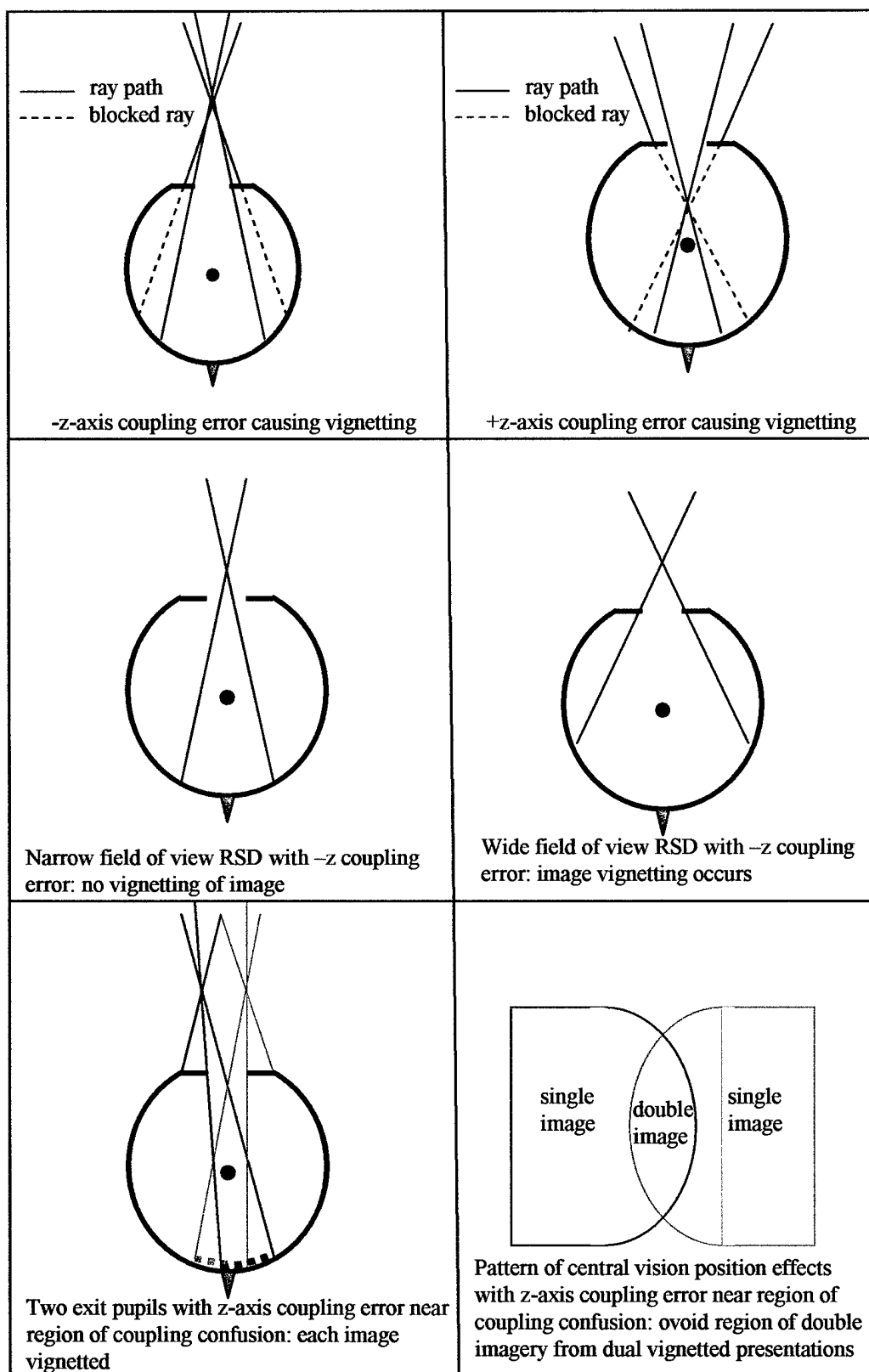


Figure 7.1: Geometry of z-axis Pupil Coupling Error

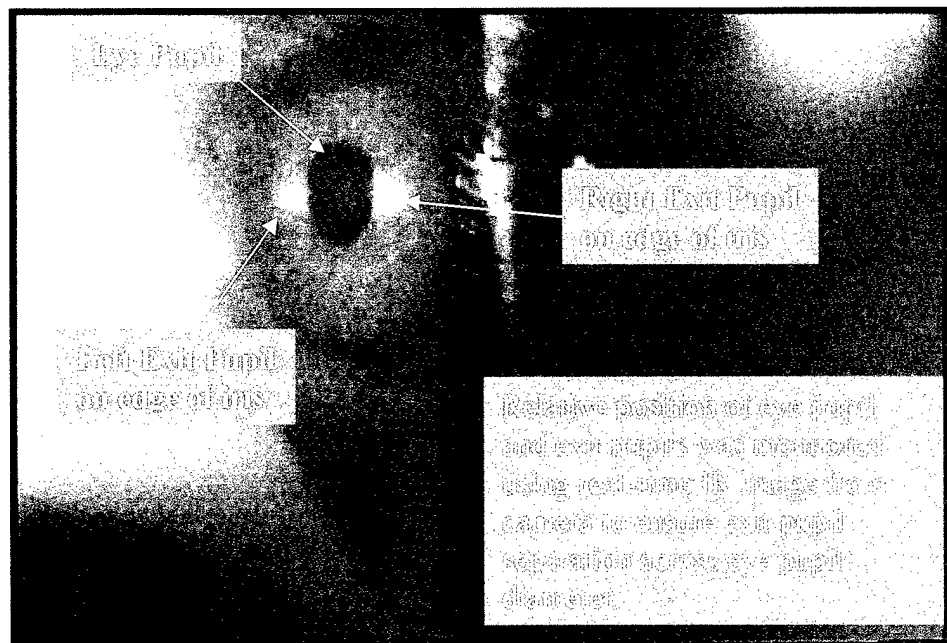


Figure 7.2: Infrared Image of Subject Eye During Arrayed Exit Pupil Separation Experiment

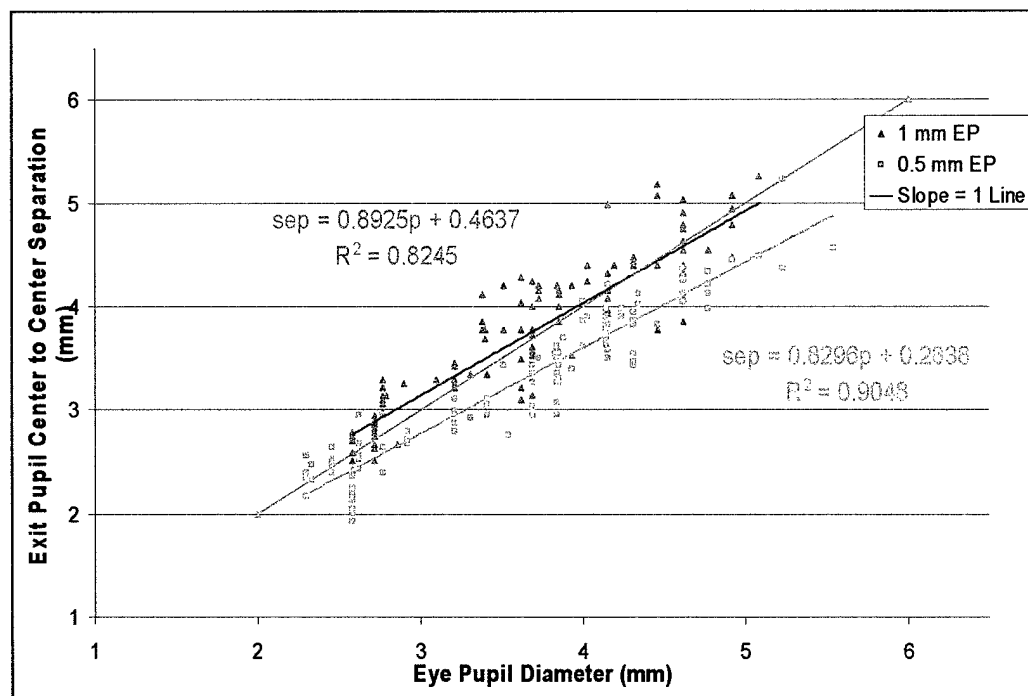


Figure 7.3: Pupil Separation Preference Study Summary Results

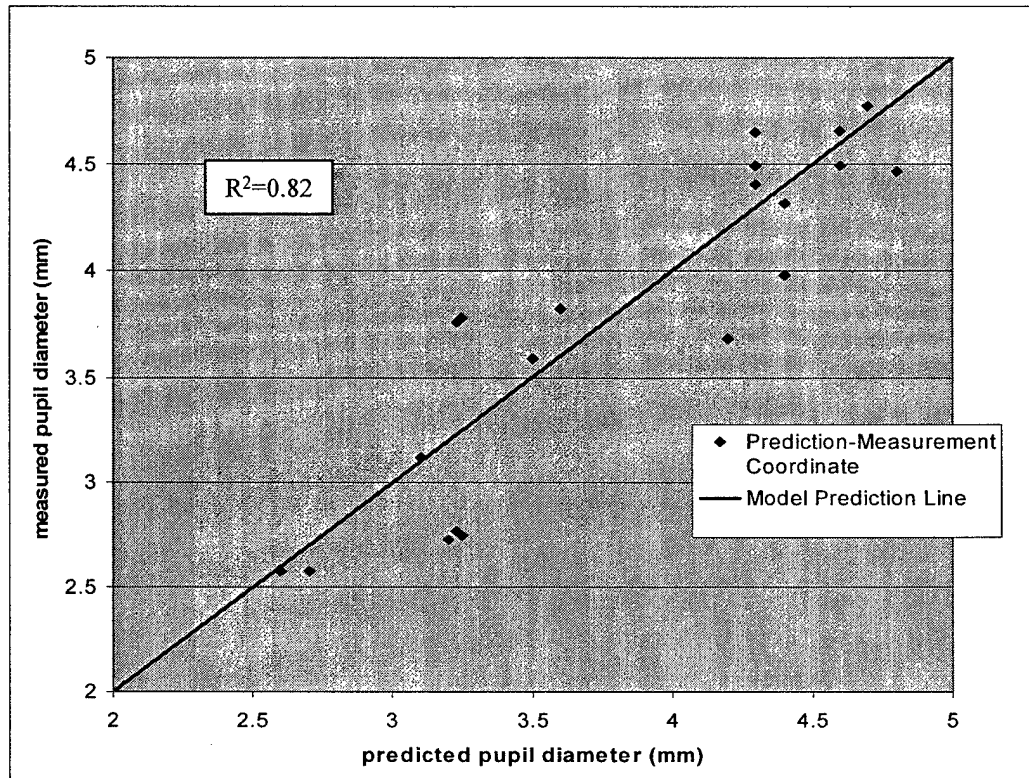


Figure 7.4: Eye Pupil Diameter Measurements Compared with Pupillary Response Model Predictions

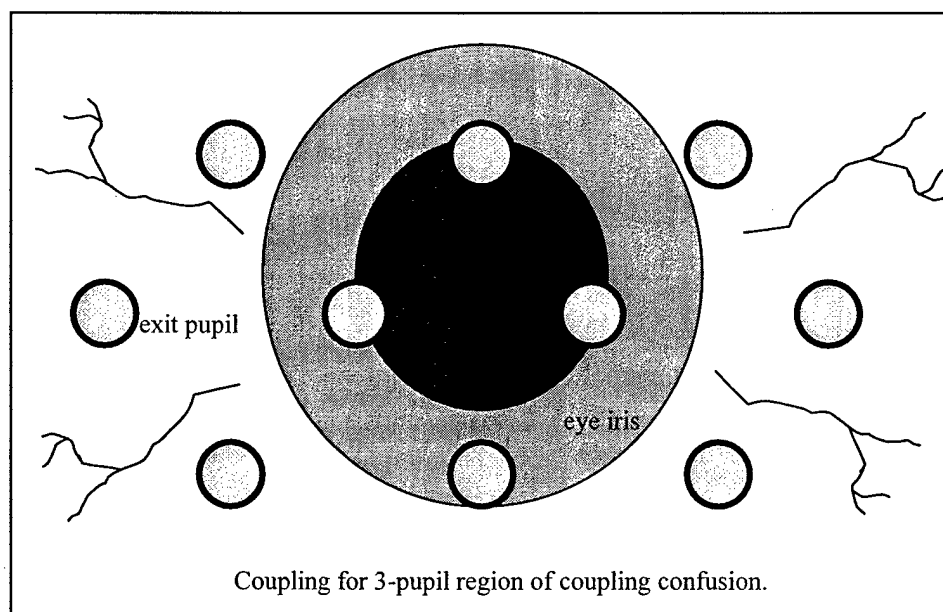


Figure 7.5: Illustration of 10 Exit Pupil Array Presented About Eye Pupil

Chapter 8: General Discussion and Conclusions

This body of research represents a broad effort to investigate the visual perceptual characteristics associated with the human use of retinal scanning displays and to identify means of effectively coupling retinal scanning displays with the human visual system. This effort has necessarily been a multidisciplinary undertaking, incorporating tenets and explorations of perceptual psychology, vision science, human neurophysiology, physics, optics, electrical engineering, and mechanical engineering, all fused within the systems engineering perspective of the human factors engineer. Within this multidisciplinary framework, the overarching goal has been to discover and evaluate methods of improving the human interface with the new and evolving visual display technology of the retinal scanning display. This effort has achieved that goal through the completion of five major research objectives.

Each of the five major objectives of this body of research has been successfully completed through a combination of experimental hypothesis testing, structured observation, and literature review. In this chapter each objective is restated and followed by a summary of the significant findings and implications associated with each. Recommended human factors guidelines are compiled for arrayed exit pupil display implementation. Recommendations for additional research are presented, along with additional RSD interface concepts.

8.1 Visual Response in the Intensity Domain

The first major objective was stated as: *Explore the intensity domain with RSD's to identify and quantify any anomalous perceptual effects due to retinal response.* This objective was supported by both the flicker experiments of Chapter 4 and the brightness experiments of Chapter 5. The general finding was that no significant perceptual anomalies in the intensity domain were induced by RSD stimuli.

This finding implies that the brightness perception of RSD stimulation is consistent with conventional theories of visual perception of luminous sources. Specifically, the experimental evidence indicated that with equivalent time averaged illumination of the retina RSD stimuli were perceived equal in brightness to standard non-scanning luminous sources. While some small but significant differences were obtained in the flicker contrast threshold comparison experiment that

seemed to point toward unique RSD-induced characteristics of brightness perception, these differences were inconsistent and readily attributed to experimental error.

The subsequent studies of brightness perception described in Chapter 5 formally disproved the existence of any unique visual response in the intensity domain to RSD stimulation of the retina. The first experiment compared the monochromatic RSD stimulus to the polychromatic stimulus of a filtered arc lamp. A small effect was noted, but this was subsequently attributed to error in the measurement device. Coarse corrections to these results seemed to indicate that no significant effect was obtained. A revised second experiment eliminated the uncontrolled variability in chromaticity of the earlier experiment by using identical laser sources for comparisons, one static and one scanned by the VRDE. The combination of a highly accurate measurement technique and a statistically powerful experimental design yielded some statistically significant results. However, the results were mixed in effect direction and were well within the expected range of normal human variation, centered about equality. Additional comparisons of static and scanned sources with increased scanning rates and display sizes yielded no noticeable differences. Therefore, no practically significant results were obtained and RSD stimuli were shown to induce no anomalous retinal responses in the intensity domain.

While these findings seem unremarkable, they formally disproved notional concepts about novel RSD retinal stimulation and enhanced visual perception that were based upon cursory observations and erroneous experimental data [79]. Further, in unique and fundamental research such as this, it is prudent to make very few assumptions about the characteristics of a poorly understood complex system like human vision. These findings provided a firm and unambiguous foundation for subsequent investigations within this body of research involving opto-physiological and perceptual phenomena associated with the coupling of RSD's to the human visual system. As no anomalous retinal response was indicated, models of human opto-physiological response and subsequent display interface concepts may soundly be based upon normal retinal response characteristics reported in literature. These findings also provide similar footing for follow-on research in the realms of vision science, perceptual psychology, and display engineering.

In addition to these findings, these studies facilitated the development of unique display apparatuses and experimental techniques that may be utilized in future endeavors across disciplines. Specifically, the development of the VRD Emulator provides a unique capability for

stimulating the retina that may be used in a variety of experimental scenarios. Indeed, the VRDE was utilized subsequently within this body of research for multiple experiments and observations. Further, the method developed in the monochromatic brightness matching experiment for reducing the spatial and temporal coherence of a laser source to match the coherency disruption affected by the RSD is a novel concept. This technique should prove useful for any experiment requiring monochromatic visual stimuli that do not induce the optical effects and related visual artifacts typical with coherent sources. Also within the monochromatic brightness matching experiment, a technique was developed to precisely measure and compare the luminance of an RSD with a static luminous source within the context of a flicker photometry experiment. This novel approach may have direct applicability to future flicker photometry experiments that present any scanned, periodic, or temporally modulated visual stimuli.

Considering the results of the brightness matching experiments and observations, and considering the results of related aspects of the flicker experiments, the first major research objective was successfully accomplished. No anomalous retinal response was revealed and unique new experimental techniques were developed.

8.2 Visual Response in the Temporal Domain

The second major objective was stated as: *Explore the temporal domain with RSD's to identify and quantify any anomalous perceptual effects due to retinal response.* This objective was supported by the flicker contrast threshold experiment and critical flicker frequency experiment of Chapter 4. The general finding was that no significant perceptual anomalies in the temporal domain were induced by RSD stimuli.

This finding implies that the temporal perception of RSD stimulation is consistent with conventional theories of visual perception of temporally refreshed or flickering luminous sources. Specifically, the experimental evidence indicated that human sensitivity to temporal flicker with RSD stimuli is not different from sensitivity to temporal flicker with conventional or non-scanned stimuli. The experimental evidence supports this indication with both flicker contrast comparisons and critical flicker frequency comparisons. Although some small differences were obtained with two subjects in the flicker contrast threshold comparisons, these differences have been reasonably attributed to experimental error. No similar differences were obtained with comparisons of critical flicker frequency.

The flicker experiments of Chapter 4 formally disprove existence of any unique visual system response in the temporal domain to RSD stimulation of the retina. The first experiment compared flicker contrast sensitivity using the VRD with flicker contrast sensitivity using a typical CRT display. This difficult, two-alternative forced choice experiment yielded a very small effect with the VRD of reduced flicker sensitivity. However, this effect was entirely attributable to two subjects whose visual stimuli were necessarily reduced in luminance, as compared to all other subjects, due to difficulty in achieving stimuli brightness matches. Further, because of these difficulties, the data collection sessions for these two subjects were substantially extended and likely induced significant visual fatigue not experienced by the other subjects. Additionally, comparisons made with alternative techniques by these two subjects contradicted their results obtained with the 2-AFC method. Therefore, the 2-AFC results of these two subjects are highly questionable, and the remaining subjects' data indicate equivalent flicker contrast sensitivity with the CRT and VRD. Still, even with the inclusion of these two anomalous subjects' data, only a small difference in sensitivity was obtained, and that difference may reasonably be attributed to experimental factors other than retinal response. Clearly, no large effect, if any, is induced by the RSD stimuli in terms of flicker contrast sensitivity.

The second experiment compared critical flicker frequency of an RSD with a non-scanning Maxwellian view stimulus of similar chromaticity. No significant effects with CFF were obtained. The CFF's of the two displays were nearly identical frequencies. This result was obtained in spite of the dramatic difference in the duty cycle and temporal-spatial characteristics of the two displays. These results further confirmed the results of the contrast sensitivity experiment and led to the final conclusion that no anomalous retinal response in the temporal domain results with RSD stimulation.

As with the brightness studies, these findings may seem unremarkable. Also like the brightness studies, they formally disproved notional concepts about novel RSD retinal stimulation and reduced flicker sensitivity that were based upon cursory observations and erroneous experimental data (Thomas Furness, 1998, personal communication) [79]. In fact, the author's preparation for the conduct of the flicker contrast sensitivity experiment was the catalyst that led to his discovery of systematic error in the previous flicker experiments that had motivated speculation about novel retinal responses to the VRD. It was prudent to thoroughly test these hypothesized novel effects with well controlled experiments to firmly establish their existence or absence.

As a result, a firm and unambiguous foundation was established in the domain of temporal retinal response from which subsequent investigations of opto-physiological and human interface phenomena could be launched. As no anomalous retinal response was indicated, models of human opto-physiological response and subsequent display interface concepts may soundly be based upon normal retinal response characteristics reported in literature. Further, non-scanning RSD emulation displays may be utilized in subsequent experimentation without fear that unique scanning display retinal effects will invalidate results obtained with more conventional display apparatuses.

Considering the results of the flicker contrast sensitivity experiment and the critical flicker frequency experiment, the second major research objective was successfully accomplished. No anomalous retinal response in the temporal domain was revealed.

8.3 Human Pupillary Response with Small Exit Pupil RSD's

The third major objective was stated as: *Explore the pupillary response to small exit pupil RSD's and model the behavior of the pupillary system under RSD stimuli conditions.* This objective was directly supported by the pupillary response experiment described in Chapter 6. The general finding was that human pupillary response to retinal stimuli from small exit pupil RSD's differs from human pupillary response to naturally viewed stimuli.

As detailed in Chapter 6, the eye's pupil is generally more constricted with small exit pupil RSD stimuli than with natural view stimuli. The eye's pupil is more constricted with binocular RSD stimuli than with monocular RSD stimuli. Pupillary response in RSD augmented view is strongly affected by background luminance as an inverse relationship and also inversely related to RSD corneal flux density by a weaker effect. The population variance in pupillary response with augmented view is inversely related to background luminance. The specific findings were characterized with empirical models of pupil response under opaque view and augmented view conditions with both monocular and binocular RSD stimuli. Ancillary empirical models of pupillary response variance and monocular-binocular response difference were also derived.

The findings of this experiment and the resulting family of models represent the first documented examination of the unique pupillary response to small exit pupil RSD's. The hypothesized model of binocular opaque view response was firmly based on established pupillary

response models and well documented characteristics of human visual function. The development of the remaining models, particularly the augmented view models, was unprecedented in literature. The derived family of models will provide fundamental human response predictions for the engineering of RSD displays that must maintain precise coupling with the eye's pupil.

Specifically, the implementation of these models will provide the display designer with estimates of the mean pupil diameter to be expected among display users for a wide range of environmental and RSD conditions. Additionally, these models facilitate estimations of the variation of pupil diameter to be expected among the population, providing the display designer with statistical information necessary to target display parameters within desired population percentiles. Estimation of binocular display pupillary response may also be predicted from monocular results, or vice-versa.

As discussed in detail in section 6.7.1, the pupillary response models were derived with some random coupling error from the precise SC-1 peak sensitivity pupil position, and this was manifested significantly only with small eye pupil diameters. This error was due to the fact that each individual's SC-1 peak sensitivity position varies by as much as 2 mm from pupil center, and due to the practical inability to maintain perfect head stability over the long course of the experiment. This may somewhat reduce the value of these models for the vision science community.

However, in retrospect, the inclusion of this random error seems a fortuitous advantage for the practical application of these models. Applied RSD scenarios will typically utilize head mounting apparatuses that will not provide perfect pupil coupling. Further, the magnitude of the coupling error must be self-limiting by eye pupil diameter and by practical display considerations. Thus, the random error inherent in the models is bracketed within magnitudes to be expected in the vast majority of applications. While not idealized SC-1 peak sensitivity models with separate error quantifications, the models maintain practical and statistical viability for the prediction of means and variances among the human population. The limited pupil response model validation performed in parallel with the exit pupil separation experiment of Chapter 7 yielded encouraging results for the viability and robustness of the models.

Considering the general findings and specific results of the pupillary response experiment, and considering the family of models empirically derived from data, the third major

research objective was successfully completed. The pupillary response to small exit pupil RSD stimulation was thoroughly characterized and mathematically modeled.

8.4 Arrayed Small Exit Pupil Displays

The fourth major research objective was stated as: *Explore interface engineering options for preserving the advantages of small exit pupil displays with arrays of small exit pupils and model human preference for basic arrayed pupil display characteristics.* This objective was directly supported by the arrayed exit pupil display exploration and arrayed exit pupil separation experiment of Chapter 7. The general findings were that the concept of arrayed small exit pupil displays is viable and does not significantly impact RSD image perception, and that human preference for exit pupil separation distance is a function of both eye pupil diameter and exit pupil diameter. A mathematical model of arrayed exit pupil separation distance preference was empirically derived and unique arrayed display concepts were explored.

Two primary methods of affecting exit pupil coupling transitions were explored. The first method was by the optimum separation for eye pupil diameter of constantly illuminated exit pupils to allow natural eye motions to affect coupling transitions. This was the primary method investigated in this research. The second method was by switching exit pupil illumination on or off, depending upon eye pupil position, so that only a single illuminated exit pupil was coupled at any given time. The subsequent discussions refer to the optimum exit pupil separation method unless otherwise indicated.

The exploration of the arrayed exit pupil concept revealed several unique perceptual characteristics of arrayed pupil displays. The most notable characteristics were produced in the region of coupling confusion, the region of eye rotation positions where multiple adjacent exit pupils are at least partially coupled to the eye pupil. The boundary disruption, a perceptual artifact associated with exit pupil coupling transitions in the region of coupling confusion, was manifested as a small region of central vision inspection within the perceived RSD image where either doubled imagery or a loss of imagery was experienced. Boundary disruptions of various size, shape, and character were manifested depending upon the relationship between the exit pupil separation distance and eye pupil diameter, and depending upon the number of partially coupled exit pupils in the region of coupling confusion. Additionally, the angular extent of the boundary disruption (and the region of coupling confusion) was determined to be directly related to exit

pupil diameter. Thus, the magnitude of these visual artifacts may be reduced with the implementation of smaller diameter exit pupils.

With optimized separation of the exit pupils, the boundary disruption appeared only within a very small range of eye rotation positions, and a deliberate effort by the observer was typically required to identify the boundary disruption. Most frequently, and particularly with rapid saccadic eye motions, the boundary disruption was not perceived by the observer. This finding lends strong support to the viability of the arrayed pupil display concept.

Also associated with the region of coupling confusion and coinciding with the boundary disruption was a shift in image position on the retina caused by the inherent non-parallel alignment of adjacent exit pupil beam scans. The visual perceptual phenomenon of saccadic suppression dramatically reduced the perception of this image shift with common visual tasks such as reading or scanning about an image. This effect was most evident with densely populated or low spatial frequency display content. With sparsely populated or high spatial frequency display content, the image shift was more evident to the observer with scanning inspections about the image.

With the pupil coupling transition method of switched singularly coupled exit pupils, the artifacts of the boundary disruption were circumvented since only a single exit pupil was illuminated at any time. However, the related image shift was still manifested with this method of coupling transitions. Observations revealed that perception of the image shift may be somewhat more evident to the observer with this coupling transition method because transitions may be affected when the eye is not in motion and saccadic suppression is not operational. Clearly, this is dependent upon characteristics of the switched exit pupil control logic and system response performance. Switched pupil systems may be designed to ensure coupling transitions are affected during eye movements, thereby reducing the perception of the image shift.

Applicable to each coupling transition method is the problem of z-axis coupling error. This error in converged exit pupil alignment with the plane of the eye pupil may cause substantial image vignetting. With arrays of exit pupils, uniquely patterned visual perceptual artifacts occur with z-axis error near the region of coupling confusion. The effects are substantially disruptive to image perception. This coupling error is exacerbated with wide field of view RSD's.

A model was empirically derived for the preferred optimum separation of exit pupils for coupling transitions. The hypothesized general form of this model was validated by experimental results, and components of the model were empirically derived from subject data. The model

provides predictions of the optimum arrayed exit pupil separation distance as a function of eye pupil diameter and exit pupil diameter. The model is envisioned to provide prediction of the optimum exit pupil separation distance for the minimization of boundary disruption artifacts, and it may be employed for prediction of the absolute maximum exit pupil separation with the switched singularly coupled exit pupil method of coupling transition.

The exit pupil separation experiment findings indicated that eye pupil diameter was the primary variable affecting optimum separation distance. The impact of reduced phototransduction efficiency by the Stiles-Crawford I effect induced small changes in exit pupil separation distance inversely related to eye pupil diameter. Exit pupil diameter was found to have a substantial effect on separation distance due to considerations of the Stiles-Crawford I effect and due to geometrical considerations related to pupil size and partial couplings.

Large arrays of optimally separated exit pupils were observed to provide excellent effective display exit pupil area without significant disruption of image perception. Additionally, the presentation of multiple emulated RSD images, each presented by a unique exit pupil at a unique eye rotation position, was explored as a potential display concept. The arrangement facilitated the alternation of various augmented view display presentations using natural eye rotation movements while maintaining an uncluttered forward gaze natural view. The concept demonstration was a compelling illustration of the future potential of arrayed small exit pupil displays.

These findings and models provide the display designer and engineer the fundamental display characteristics and tools necessary for the prediction of arrayed pupil RSD interface parameters and requirements. Combined with the pupillary response models, excellent prediction capability is available for estimating an expected range of eye pupil diameters across a wide range of conditions and for estimating the arrayed exit pupil separation distances that will minimize visual perceptual artifacts.

Considering the results of the exploration of arrayed small exit pupil display concepts, and considering the results of the exit pupil separation experiment, the fourth major research objective was successfully completed. The arrayed small exit pupil display concept was proven to be a viable approach to preserving the small exit pupil while providing expanded effective exit pupil area, and human preference for arrayed small exit pupil separation distance was successfully mathematically modeled.

8.5 Human Factors Engineering Guidelines for Arrayed Small Exit Pupil RSD's

The fifth major research objective was stated as: *Derive human factors engineering guidelines for implementing RSD's with arrayed small exit pupils.* This objective was supported primarily by the arrayed exit pupil explorations and exit pupil separation experiment of Chapter 7. Additional support for the derivation of recommendations was provided by the pupillary response experiment of Chapter 6. Indirect foundational support for this objective was derived from the retinal response experiments of Chapter 4 and Chapter 5. The general findings related to this objective extend throughout the body of this dissertation and are compiled here. Suggested guidelines were derived directly from the results and findings of experiments and explorations and, in some cases, were logically inferred from literature, observations, and research findings. Specific guideline recommendations follow, with pertinent discussion and references to specific sections of this dissertation added as required.

1. *To preserve the optical advantages of the small exit pupil RSD, arrayed exit pupils should be of a diameter near 1.0 mm.* The advantage of large depth of field described in sections 1.1 and 2.3.1 is well preserved with exit pupils of this diameter. If the depth of field advantage is not of significant concern for the particular application, larger exit pupils will offer advantages such as improved central vision accessible field of view for a single coupled exit pupil.

As cited in section 7.2.1, exit pupils of diameters significantly less than 1.0 mm may induce undesirable optical effects that impact image quality. The primary cause of these effects is diffraction limitations on image resolution by which image quality drops markedly with exit pupil diameters below 1.0 mm diameter (see Table 2.1 section 2.2.1.4). Additionally, scanning beam interactions with floating matter in the ocular humors. Extensive RSD observations by the author confirm these reported effects, especially with scanning coherent beam exit pupils of diameters 0.5 mm or less. However, the implementation of exit pupils of diameters less than 1 mm offer other desirable advantages in the case of arrayed exit pupils and, depending upon display content, may not induce significant visual artifacts.

Specifically, as noted in section 7.1.5.1, the extent of the boundary disruption with arrayed exit pupils is directly related to exit pupil diameter, with smaller exit pupils reducing the extent of the disruption. Thus, for arrayed pupil RSD's that utilize the optimum exit pupil separation method of affecting coupling transitions, smaller exit pupils are advantageous in the

effort to minimize the boundary disruption effects. Further, if the RSD image content is sparse, such as a wire frame image and/or brief text labels, the visual effects of ocular floater shadowing on the RSD image is markedly reduced. However, the resolution of displays with exit pupils near 0.5 mm diameter will be reduced (see Table 2.1 section 2.2.1.4). Under limited conditions of sparse display content and low resolution requirements, the implementation of exit pupils near 0.5 mm diameter may be viable.

For most purposes, however, arrayed RSD exit pupil diameters near 1.0 mm will essentially eliminate ocular floater artifacts and provide excellent depth of field. Further, with the implementation of the switched singularly coupled exit pupil method of coupling transitions, concerns about boundary disruption effects with these larger exit pupils (except for image shift) is alleviated.

2. Active exit pupils in arrayed small exit pupil RSD's should be separated by equivalent distances. For constantly illuminated exit pupils with the coupling transition method of optimum exit pupil separation, the geometry of pupil coupling dictates equidistant separations. Clearly, only one optimum separation distance is applicable for eye pupil diameter at any given time. With the switched singularly coupled exit pupil transition method equal separation is not dictated by coupling transition geometry. Still, it reasons that at any given time a single maximum exit pupil separation distance can apply, and the maximum effective exit pupil area will be affected most efficiently (with fewest coupling transitions) with maximally separated exit pupils. Therefore, equivalent separation distances among active exit pupils in an array are prudent, regardless of coupling transition method. This guideline applies to exit pupils of equivalent shape and size with separation distances measured center to center.

3. Exit pupil arrays should be designed for a targeted range of the user population in accordance with available models of human pupillary response, optimum exit pupil separation, and with consideration for RSD field of view. Designs for arrayed exit pupil RSD's should be optimized for the targeted tasks, environments, and user populations. Although a "generic" universally applicable arrayed exit pupil RSD design may be feasible and highly desirable, it should be designed with the statistical models of human pupillary response in mind to avoid the expense and waste of over-engineering. As with most visual display technology, RSD's will typically be designed to fit a specified user, task, and environment. As examples, an arrayed exit

pupil RSD for augmented view implementation in a fighter aircraft cockpit will have very different interfacing requirements and implementation options than an opaque view RSD designed for a low vision patient to use for urban pedestrian navigation. Each of these will have different interface requirements than an optionally opaque or augmented arrayed pupil RSD targeted for interactive video entertainment. The models of human pupillary response and optimum exit pupil separation distance derived in this body of research are recommended as preliminary models for arrayed small exit pupil RSD design and engineering consideration.

As an aid in integrating these models and RSD design considerations, Figure 8.1 is offered. This plot depicts the two best fit linear functions for the relationship between eye pupil diameter and optimum exit pupil separation distance along with a scaled reference to the estimated angular field of view accessible by central vision with a single coupled exit pupil. This plot integrates Figure 7.3 with field of view accessibility estimates derived as in table 2.2 (section 2.2.3.2). Once an eye pupil diameter or range of diameters has been derived from the RSD pupillary response models, the plot of Figure 8.1 is entered on the abscissa. Moving up to the desired exit pupil diameter function, estimates of the optimum exit pupil separation distance may be determined on the left ordinate scale. From the same position, estimates of the field of view available by central vision inspection with a single exit pupil may be made on the right ordinate scale associated with the selected exit pupil function. The quantity of optimally separated exit pupils required to provide full RSD field of view inspection by central vision (with eye rotation only) may be calculated by dividing the RSD field of view by the referenced single exit pupil field of view value and rounding up to the nearest integer. Additional relationships among eye pupil diameter, optimal exit pupil separation, and accessible RSD field of view may also be assessed.

4. *To minimize the visual artifacts associated with exit pupil coupling transitions and to realize the maximum advantages from arrayed exit pupil RSD's, display designs should affect exit pupil coupling transitions by the method of switched singularly coupled exit pupils.* Clearly, as discussed in section 2.2.3.1 and section 7.1.5.3, the method of the switched singularly coupled exit pupil has distinct advantages over other arrayed exit pupil concepts. These include remarkable reductions in power requirements as compared to more conventional displays of equivalent exit pupil area and the avoidance of most visual artifacts associated with the exit pupil

boundary disruption. Thus, if engineering and economic considerations allow, the primary method of transitioning exit pupil couplings should be by switched singularly coupled exit pupils.

If switched singularly coupled exit pupils are deemed infeasible for a particular application, the method of optimum exit pupil separation distance should be implemented to affect exit pupil coupling transitions. If feasible, pupil diameter sensing and automated adjustment of pupil separation distances should be implemented. Otherwise, a simple user adjustable control of exit pupil separation distance should be provided. As a last option, static exit pupils may be affected in an array with the best estimated optimum separation distance for anticipated environmental conditions. This last option is likely to be unusable for most envisioned applications, but it may offer a relatively inexpensive augmented display option for environments with very bright ambient luminance conditions where the variation in human pupillary response is extremely low across a significant range of the population.

5. To minimize the visual artifacts associated with exit pupil coupling transitions, arrayed exit pupils should be separated by the optimum separation distance for eye pupil diameter. With the method of optimum exit pupil separation, boundary disruption artifacts are minimized with the maintenance of the optimum exit pupil separation distance for detected eye pupil diameter. Fortuitously, the optimum separation distance also minimizes the occurrence of exit pupil coupling transitions. Thus, the importance of maintaining the optimum separation distance is clearly evident.

With the switched singularly coupled exit pupil transition method, the necessity to maintain the optimum separation (or maximum separation, as applied to this method) is less critical. In fact, except for the image shift artifact, the separation of exit pupils has little impact with this coupling transition method. However, the image shift artifact is the most evident visual artifact associated with arrayed exit pupils, particularly with sparse or high spatial frequency display content. Minimizing the image shift artifact may be affected by minimizing the necessity to transition exit pupil couplings. This may be accomplished by presenting exit pupils that are separated by the maximum preferred distance for the detected eye pupil diameter. The model of preferred optimum exit pupil separation distance may also be applied in the estimation of the maximum separation distance for switched singularly coupled exit pupils.

It is feasible to implement alternative methods for the reduction or elimination of image shift artifacts with either coupling transition method. Theoretical engineering concepts for accomplishing this are discussed in section 8.6.

6. Head mounting apparatuses for arrayed exit pupil RSD's should be designed with the specific goal of minimizing z-axis pupil coupling error. As described in section 7.1.5.4, pupil coupling error that causes significant misalignment of the converged exit pupil with the plane of the eye pupil can severely impact the image quality of an arrayed exit pupil display. This reduction in image quality is caused by both image vignetting and by the effective enlargement of the region of coupling confusion in which severe boundary disruption artifacts are manifested.

With an ample effective exit pupil area provided by the arrayed exit pupil RSD more tolerance is provided for lateral pupil coupling errors. However, the coupling tolerance in the z-axis of alignment remains small and it is reduced as RSD field of view increases. Therefore, head mounted arrayed exit pupil RSD's must be afforded excellent stability in the z-axis to maintain good image quality. As a prudent measure, the z-axis positioning of the plane of arrayed exit pupils should be readily adjustable by the user, but the adjustment capacity must not compromise positional stability.

8.6 Recommended Research and Future RSD Concepts

This body of research was designed to provide fundamental, foundational knowledge for affecting efficient and effective human interface designs for retinal scanning displays. This goal has been well accomplished. However, as expected with a successful research effort, as many questions have been generated as have been answered. New questions arise with the newly acquired knowledge of RSD interfacing and visual system coupling concepts. New questions are now evident that demand additional investigations to uncover more answers in the quest to further develop RSD technology and utilize it to its maximum capacity. Also, new concepts for the engineering and interfacing of RSD's have evolved as new information was uncovered. These new display concepts also demand investigation. The following recommendations are submitted for additional RSD research and explorations related to the coupling of RSD's to the human visual system and to the advancement of RSD technology.

1. *Switched singularly coupled exit pupil RSD's*: The advantages of switched singularly coupled exit pupil RSD's are too attractive to ignore. The display power consumption reductions and optical advantages make this concept the clear next-step in RSD evolution. Engineering studies should be undertaken with the goal of developing the optical and electronic technology to make this RSD interfacing concept a reality.

Engineering explorations should investigate methods of producing multiple converged scan exit pupils for array presentation, methods of minimizing the quantity of scanning elements required to produce multiple exit pupils, and methods of optically or mechanically relocating exit pupils within the pupil array plane. Additional engineering efforts should approach the issue of integrating eye pupil tracking technology with RSD optics and mechanics for elegant methods of monitoring eye position in real time.

2. *Control logic for switched singularly coupled exit pupil RSD's*: The switched singularly coupled exit pupil method of affecting pupil coupling transitions presents a unique human interface challenge. The RSD system must detect the position and size of the eye pupil and determine which singular exit pupil position to activate at any given moment for the maintenance of pupil coupling. The control logic algorithms in an RSD system utilizing this technique will have a significant impact on display characteristics and on image quality. Specifically, the frequency with which pupil coupling transitions occur as well as the eye rotation and image position at which they occur will be a function of the control logic implementation. As image positional shifts may be experienced with pupil coupling transitions, it is prudent to implement control logic algorithms that help to minimize the perception of these perceptual artifacts.

From a visual perceptual and human interface perspective, two primary issues arise in consideration of control logic scenarios. First, exit pupil transitions affected during saccadic eye movements take advantage of saccadic suppression to reduce the perception of the image shift. Thus, control logic algorithms may be designed to maximize the occurrence of transitions during periods of eye motion. Second, maximum separation of exit pupils minimizes the necessity for coupling transitions. However, the maintenance of an exit pupil near the center of the eye pupil allows the greatest visual scanning area without affecting a coupling transition. Thus, a decision must be made about when to most efficiently affect a pupil transition for the minimization of

image shift artifacts. Logical trade offs must be made among the described considerations, and they must be made in milliseconds.

Detailed study of control logic perceptual characteristics is recommended. Studies may be initiated using prototype displays or with emulating apparatuses. The AEPE apparatus (section 2.1.3), modified with independently controllable light sources, with eye pupil tracking capacity, and with integrated computer control would satisfy the requirement for initial studies. Research in the area should be concerned with identifying viable pupil selection control algorithms that minimize visual artifacts associated with pupil coupling transitions.

Depending upon system speed, performance, and perceptual characteristics, it may be reasonable to combine the two methods of pupil coupling transition explored in Chapter 7. The simultaneous presentation of multiple exit pupils about the eye pupil may be a viable method for avoiding momentary interruptions of image presentation with rapid eye motion, particularly if system response is sluggish. These sub-arrays of exit pupils may be switched in position within the exit pupil array plane in accordance with prediction algorithms, historical data of eye motion, and display content position and type. Again, detailed study of control logic associated with these concepts is highly recommended.

3. Improved optimum separation models: While the preliminary models of optimum exit pupil separation provide a good estimate of the optimum or maximum exit pupil separation distance across a range of eye pupil sizes and for the recommended range of arrayed exit pupil diameters, additions and refinements to this model are recommended. Clearly, additional data collection would be prudent, utilizing a large cross section of the human population. Further, a variety of exit pupil characteristics should be examined, most notably the Gaussian profile exit pupil. As these models may affect the initial development of control logic for switched exit pupil RSD's, it is prudent to ensure their accuracy.

4. Idealized pupillary response models: As discussed in Chapter 6, the models of pupillary response are not idealized peak SC-1 sensitivity models with separate coupling error quantifications. Rather, uncontrolled coupling error from the peak SC-1 sensitivity position is inherent within the models and, thus, inseparable. Idealized models with error quantification, while somewhat difficult to obtain empirically, are a suggested goal for future research.

5. *Tests of pupillary response models robustness:* The pupillary response models derived in Chapter 6 should be tested for robustness. Human subject studies should be undertaken presenting a wide variety of display conditions to thoroughly test the models' robustness. Tests should be made using a variety of display imagery types, sizes, spatial frequencies, and dynamics. Significant deviations should be well documented to provide improved prediction performance for design engineers.

6. *Additional pupillary response studies:* While the pupillary response models derived herein are thorough, additional questions remain regarding human pupillary response to RSD stimuli. The observed oscillations in pupil response, particularly with monocular RSD stimulation, should be investigated and characterized. Correlations of these oscillations with experiences of binocular rivalry should be studied.

Models of pupillary response to dynamic RSD stimuli may be prudent, particularly if preliminary studies find marked differences from the response found with static stimuli. Dynamic stimuli should be well quantified and categorized to ensure the applicability of results to engineering endeavors.

7. *Longitudinal effects of small pupil accommodation:* As noted in section 2.2.1.7, the physiological response of small pupil accommodation is well explored except for longitudinal effects. As previous studies were interested in visual function and not in the advancement of displays using very small exit pupils, no study has been made of the long term impact of the accommodation system response changes that occur with small pupils. The literature review indicated that the magnitude of low frequency accommodation fluctuations increases markedly with the imposition of an unnaturally small pupil. This has been hypothesized to be a result of the visual system seeking mild image defocus on the retina in order to establish the accommodation of optimum focus by maintaining maximum image contrast.

With the advent of displays imposing unnaturally small exit pupils that may be presented repeatedly for hours at a time, a question arises regarding the long term impact of the increase oscillations of accommodation. It is quite likely that the visual system will adapt over a short exposure time with no adverse affects. However, it is possible that the increased actuation of the lens and ciliary bodies in the eye will cause fatigue, discomfort, or deleterious acuity effects. A well controlled ophthalmological longitudinal study is prudent to ensure safety with long term

frequent use of small exit pupil RSD's. In parallel, longitudinal human factors studies may examine human performance with RSD's as compared to more conventional display concepts. These studies may note human preference as well as performance and adaptation to the unique display concepts discussed in this body of research.

8. *z-axis coupling error modeling*: A useful and relatively easy model to develop would quantify the effects of z-axis coupling error with arrayed exit pupil RSD's. Based upon the singular z-axis model of deWit, this model could be hypothesized via geometrical analysis and validated with human subject studies [4, 5]. Specifically, this recommended research should seek to provide the engineering community with models for predicting the tolerance required of head-mounting apparatuses for arrayed exit pupil displays of various types. In particular, the two methods of pupil coupling transition should be modeled separately, as the effects on image perception with z-axis coupling error vary significantly between these two factors. RSD field of view should also be a primary variable for analysis.

9. *Alternative image shift suppression techniques*: It is feasible to employ alternative technique for the suppression of the arrayed exit pupil image shifts manifested with pupil coupling transitions. Methods for reducing the perception of this artifact should be explored.

One potential method for accomplishing this is to electronically shift the modulated RSD image in compensation. In the switched pupil RSD concept, the active exit pupil must be known to the system. Further, a quantification of the angular shift associated with each exit pupil may be determined in the design process. It seems reasonable that the scanning beam modulation could be adjusted with each coupling transition so that the normally exhibited image shift is directly compensated by an opposing electronically affected image shift. This shift would necessary "consume" a portion of the available RSD field of view, since additional display area must be made available at the periphery for electronic image shifting. However, the consumed display space would be small, probably near 1 degree visual angle for each exit pupil element across any array dimension. This method of reducing the perception of image shift due to exit pupil coupling transitions should be explored with engineering studies.

10. *Multiple presentation eye-activated RSD's*: Additional concepts for the evolution of RSD's should be examined with follow on research efforts. Specifically, the concept of

presenting multiple display images via independent RSD exit pupils, as described in section 7.3, should be explored further. This display concept seems remarkably promising as a means of presenting multiple augmented view displays while also providing a completely uncluttered natural view as the observer desires. The method of “turning on” a desired display is a completely natural human action, simply rotating the eye to a position that couples the exit pupil presenting the desired image. Both display engineering and human factors research should be undertaken to develop effective interface and information display concepts that take advantage of this unique RSD capability. Further, as this technique holds the potential for the presentation of very wide field of view displays by piecing together multiple displays in visual space, additional perceptual studies of this concept should be undertaken to determine fundamental perceptual characteristics and multiple image integration strategies.

Other research opportunities certainly exist beyond the few suggested here, but these ten recommendations stem directly from the current body of research and offer unique and exciting explorations. If pursued, these research efforts will undoubtedly reveal a plethora of new knowledge and information for the continued evolution of RSD technology and its coupling to the human visual system.

8.7 Closing Comments

The journey of this research effort has been both extraordinarily challenging and remarkably successful. All of the originally defined research objectives were met with a high degree of success, and an unexpectedly large body of ancillary knowledge was uncovered along with numerous new visual display concepts and experimental methods. Perhaps most significantly, new pathways have been revealed for additional journeys of discovery. Clearly, this research has helped to advance the evolution of RSD technology by providing foundational human interfacing and visual system coupling knowledge.

The human factors engineering community will benefit from this research effort, particularly from the knowledge of human visual perception of RSD's and from the models of human response and preference. The new visual interface concepts and experimental methods will also contribute to the human factors engineering body of knowledge. The display design and engineering community will benefit from the display concepts revealed by this work. Most

notably, the arrayed small exit pupil RSD and multiple display RSD provide concepts for exploration and development.

However, the author hopes that the greatest benefit of this research will come from through the utilization of new RSD displays partly derived from this research. Improved vision for low-vision patients to enrich lives, enhanced performance of aviation and military tasks to preserve our liberty, security, and safety, closer human connectivity with visual mobile communications, more efficient medical procedures for saving lives, all seem possible with the advancement of RSD technology.

The RSD offers a new and unique method of delivering visual information to the human mind. Many of the anticipated RSD developments described herein seem to offer an opportunity to greatly expand the bandwidth of visual information to the brain, perhaps offering an improved method of assimilating the ever increasing world of information in which we live and thrive. Only through continued advancement of human interface technology will we avoid an ever growing backlog of information assimilation that promotes stagnation, fatigue, and confusion, while placing limitations on our potential as individuals and as a species.

As this research has shown, the prospects for advancing RSD and visual display technology are excellent. This research represents one bright vector in this spreading technological advancement, and it opens numerous opportunities for further advances. It is this author's sincere hope that as the interface between human and machine continues to blur, the retinal scanning display and this research vector will prove to be distinct forward steps in this technological march. The march will continue. The human is a visual animal.

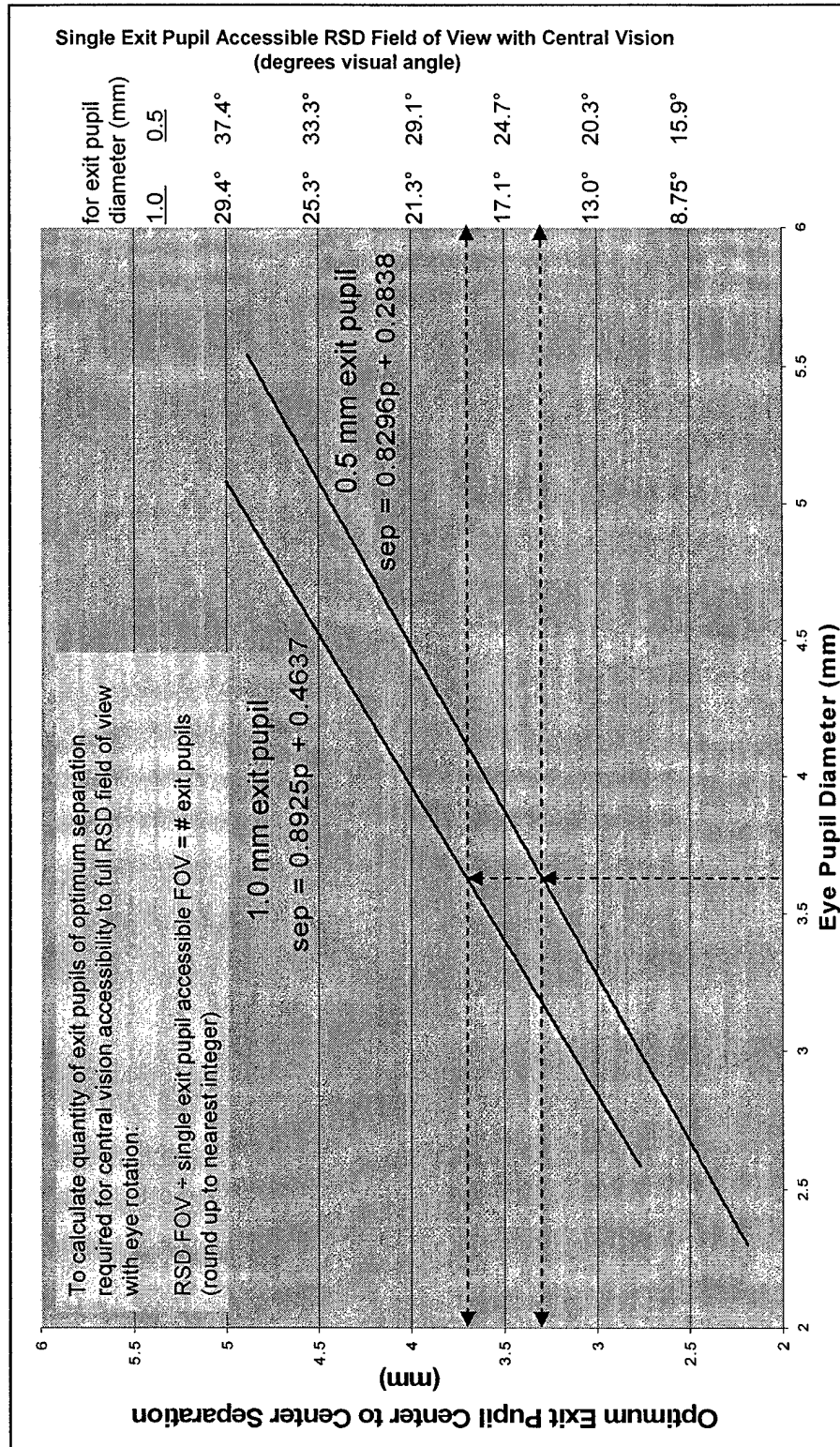


Figure 8.1: Relationships Among Eye Pupil Diameter, Exit Pupil Optimum Separation, and RSD Field of View Accessibility

Numerical References

1. Goldstein, E.B., *Sensation and Perception*. 5th Edition ed. 1999: Brooks/Cole Publishing Company.
2. Kollin, J.S. *A retinal Display for virtual-environment applications*. in *1993 international symposium, digest of technical papers*. 1993. Playa del Ray, CA: Society for Information Display.
3. Tidwell, M., *A Virtual Retinal Display for Augmenting Ambient Visual Environments*, in *Electrical Engineering*. 1995, University of Washington: Seattle. p. 1-108.
4. de Wit, G.C., R.A.E.W. Beek, and J.J.M. Braat. *Effects of a small exit pupil in an optical configuration for virtual reality*. in *Imaging Sciences and Display Technologies*. 1996. Berlin, Germany: Proceedings of the SPIE.
5. de Wit, G.C. and R.A.E.W. Beek, *Effects of a small exit pupil in a virtual reality display system*. *Optical Engineering*, 1997. **36**(8): p. 2158-62.
6. Johnston, R.S. and S.R. Willey. *Development of a commercial retinal scanning display*. in *Helmet- and Head-Mounted Displays and Symbology Design Requirements II*. 1995. Orlando, FL, USA: Proceedings of the SPIE.
7. Kleweno, C., Seibel, E., Kloeckner, K., Viire, E., and Furness, T.A. *Evaluation of a Scanned Laser Display as an Alternative Low Vision Computer Interface*. in *Proceedings of OSA Vision Science and Its Applications*. 1998.
8. Nagata, S., H.L. Pryor, and E.S. Viirre. *Visual image quality of a scanned light display in normal and low vision users*. in *ARVO Annual Meeting*. 1997. Ft Lauderdale, FL: Investigative Ophthalmology and Visual Science.
9. Capps, M.V., *Virtual Retinal Display (VRD) Technology*. 1999, http://www.cs.nps.navy.mil/people/faculty/capps/4473/projects/fiambolis/vrd/vrd_full.html.
10. Microvision Inc., *Microvision Home Page*. 2001, www.mvis.com.
11. Kollin, J.S. and M. Tidwell. *Optical engineering challenges of the virtual retinal display*. in *Novel Optical Systems Design and Optimization*. 1995. San Diego, CA, USA: Proceedings of the SPIE.
12. Silva, D., *Surgeons say hi-tech headgear makes the cut*, in *Puget Sound Business Journal*. 2000, American City Business Journals, Inc.

13. Owens, H., K. Bhat, and R.J. Jacobs, *Maxwellian and small pupils: effects on accommodation*. Invest. Ophthalmol. Visual Sci.[supplement], 1994. **35**: p. 1280.
14. Furness, T.A., *Virtual Retinal Display*, U.S. Patent #5467104, November 14, 1995, University of Washington: USA.
15. Melville, D., J.S. Kollin, and R. Johnston, *Miniature optical scanner for a two axis scanning system*, in *United States Patent Office*. 1996, University of Washington: United States of America.
16. Rodieck, R.W., *The First Steps in Seeing*. 1998, Sunderland, Massachusetts: Sinauer Associates, Inc.
17. Wandell, B.A., *Foundations of Vision*. 1995, Sunderland, Massachusetts: Sinauer Associates, Inc.
18. LeGrand, Y.L., *Light, Colour, and Vision*. 2nd ed. 1968, London: Chapman and Hall, Ltd. 564.
19. Boff, K.R. and Lincoln, J.E., *Section 1.1: Measurement of Light*, in *Human Engineering Data Compendium: Human Performance and Perception*, K.R. Boff and J.E. Lincoln, Editors. 1988, AAMRL: Wright-Patterson AFB, Ohio.
20. Stevens, S.S., *Brightness function: Effects of adaptation*. Journal of the Optical Society of America, 1963. **53**: p. 375-385.
21. Stevens, S.S., *Psychophysics*. 1975, New York, NY: John Wiley & Sons.
22. Bodmann, H.W., P. Haubner, and A.M. Marsden. *A unified relationship between brightness and luminance*. in *19th Session of the Commission Internationale de l'Eclairage*. 1979. Tokyo, Japan.
23. Teller, D.Y., *Vision and the Visual System*. 2000: University of Washington, Seattle, WA.
24. Boynton, R. and P. Kaiser, *Vision: The additivity law made to work for heterochromatic photometry with bipartite fields*. Science, 1968. **161**: p. 366-368.
25. Wagner, G. and R. Boynton, *Comparison of four methods of heterochromatic photometry*. Journal of the Optical Society of America, 1972. **62**: p. 1508-1515.
26. Wyszecki, G. and W.S. Stiles, *Color science : concepts and methods, quantitative data and formulae*. 2nd ed. ed. 1982, New York, NY: John Wiley & Sons.

27. Rushton, W.A.H., *Visual pigments in man*, in *Handbook of Sensory Physiology*, H.J.A. Dartnall, Editor. 1972, Springer-Verlag: New York, NY. p. 364-394.
28. Wald, G. and P.K. Brown, *Synthesis and bleaching of rhodopsin*. *Nature*, 1956. **177**: p. 174-176.
29. Baylor, D.A., B.J. Nunn, and J.L. Schnapf, *Spectral sensitivity of cones of the monkey Macaca Fascicularis*. *Journal of Physiology*, 1987(390): p. 145-160.
30. CIE, *Colorimetry (Official Recommendations of the International Commission on Illumination)*. 1971, CIE: Paris.
31. Boynton, R., *Human Color Vision*. 1979, New York: Holt, Rinehart, and Winston.
32. Hecht, E. and A. Zajac, *Optics*. 1974, Menlo Park, CA: Addison-Wesley Publishing Co.
33. Snyder, A.W., *The Stiles-Crawford effect - explanation and consequences*. *Vision Research*, 1973. **13**: p. 1115-1137.
34. Stacey, A. and C. Pask, *Spatial-frequency response of a photoreceptor and its wavelength dependence. I. Coherent sources*. *Journal of the Optical Society of America*, 1994. **11**(4): p. 1193-1198.
35. Pask, C. and A. Stacey, *Optical Properties of Retinal Photoreceptors and the Campbell Effect*. *Vision Research*, 1998. **38**(7): p. 953-961.
36. Horowitz, B.R., *Theoretical Considerations of the Retinal Receptor as a Waveguide*, in *Vertebrate Photoreceptor Optics*, J.M. Enoch and F.L. Tobey, Jr., Editors. 1981, Springer-Verlag: New York, NY. p. 219-300.
37. Enoch, J.M., *Retinal Receptor Orientation and Photoreceptor Optics*, in *Vertebrate Photoreceptor Optics*, J.M. Enoch and F.L. Tobey, Jr., Editors. 1981, Springer-Verlag: New York, NY.
38. Stiles, W.S. and B.H. Crawford. *The Luminous Efficiency of Rays Entering the Eye Pupil at Different Point*. in *Proceedings of the Royal Society of London*. 1933. London.
39. Jacobs, D.H., *The Stiles-Crawford Effect and the Design of Telescopes*. *Journal of the Optical Society of America*, 1944. **34**(11): p. 694.
40. Moon, P. and D.E. Spencer, *On the Stiles-Crawford Effect*. *Journal of the Optical Society of America*, 1944. **34**(6): p. 319-329.

41. Kelly, D.H., *Visual response to time-dependent stimuli. I. Amplitude sensitivity measurements*. Journal of the Optical Society of America, 1961. **51**: p. 422-429.
42. Robson, J.G., *Spatial and temporal contrast sensitivity functions of the visual system*. Journal of the Optical Society of America, 1966. **56**: p. 1141-1142.
43. Granit, R. and P. Harper, *Comparative studies on the peripheral and central retina: II. Synaptic reactions in the eye*. American Journal of Physiology, 1930. **95**: p. 211-228.
44. Boff, K.R. and Lincoln, J.E., *Section 1.5: Sensitivity to Temporal Variations*, in *Human Engineering Data Compendium: Human Performance and Perception*, K.R. Boff and J.E. Lincoln, Editors. 1988, AAMRL: Wright-Patterson AFB, Ohio.
45. de Lang, H., *Research into the dynamic nature of the human fovea - cortex systems with intermittent and modulated light: I. Attenuation characteristics with white and colored light*. Journal of the Optical Society of America, 1958. **48**: p. 777-784.
46. Brown, J.L., *Flicker and intermittent stimulation*, in *Vision and visual perception*, C.H. Graham, Editor. 1965, John Wiley & Sons: New York.
47. Dodt, J., *Electroretinogram response to intermittent stimuli*. Graefes Arch., 1952. **153**: p. 152.
48. Wu, S., S.A. Burns, and A.E. Elsner, *Effects of flicker adaptation and temporal gain control on the flicker ERG*. Vision Research, 1995. **35**: p. 2943-2953.
49. Burns, S.A. and A.E. Elsner, *Response of the retina at low temporal frequencies*. Journal of the Optical Society of America, 1996. **13**(3): p. 667-672.
50. Broca and Sulzer, *The brightness of brief pulses of light*. J. Physiol. Path. Gen., 1902. **4**: p. 632.
51. Baumgardt and Segal, *Temporal effects of brief stimuli*. C.R. Soc. Biol., 1946. **140**: p. 231.
52. Seguer, *De raritate Luminis*. 1740, Gottingen.
53. Talbot, F., in *Philosophy Magazine*. 1834. p. 327.
54. Nelson, T.M. and Bartley, Vision Research, 1964. **4**: p. 403.

55. Gilmer, *Examination of the Talbot-Plateau Law*. Journal of the Optical Society of America, 1937. **27**: p. 386.
56. Campbell, F.W. and J.G. Robson, *Applications of Fourier analysis to the visibility of gratings*. Journal of Physiology, 1968. **197**: p. 551-566.
57. Westheimer, G., *The Eye as an Optical Instrument*, in *Handbook of Perception and Human Performance*, K.R. Boff, L. Kaufman, and J.P. Thomas, Editors. 1986, John Wiley & Sons: New York.
58. Campbell, F.W. and R.W. Gubisch, *Optical quality of the human eye*. Journal of Physiology, 1966. **186**: p. 558-578.
59. Thompson, B.J., *Image Formation with Partially Coherent Light*, in *Progress in Optics*, E. Wolf, Editor. 1969, North-Holland Publishing Co.: New York, NY. p. 212-230.
60. Felipe, A., J.M. Artigas, and A.M. Pons, *Human contrast sensitivity in coherent Maxwellian view: effect of coherent noise and comparison with speckle*. Journal of the Optical Society of America, 1997. **14**(5): p. 972-983.
61. Farrell, R.J. and J.M. Booth, *Design Handbook for Imagery Interpretation Equipment*. 1984, Seattle, WA: Boeing Aerospace Company.
62. Stanley, P.A. and A.K. Davies, *The effect of field of view size on steady-state pupil diameter*. Ophthal. Physiol. Opt., 1995. **15**(6): p. 601-603.
63. Crawford, B.H., *The dependence of pupil size upon external light stimuli under static and variable conditions*. Proceedings of the Royal Society of London, 1936. **B121**: p. 376.
64. Reeves, P., *Rate of pupillary dilation and contraction*. Psychology Review, 1918. **25**: p. 330-340.
65. deLauney, L., *A note on the photopupil reflex*. Journal of the Optical Society of America, 1949. **39**: p. 364-367.
66. Campbell, F.W. and G. Westheimer, *Dynamics of accommodation response in the human eye*. Journal of Physiology, 1960. **151**: p. 285-295.
67. Leibowitz, H. and D.A. Owens, *New evidence for the intermediate position of relaxed accommodation*. Documenta Ophthalmologica, 1978. **46**: p. 133-137.

68. Campbell, F.W., J.G. Robson, and G. Westheimer, *Fluctuations of accommodation during steady viewing conditions*. Journal of Physiology, 1959. **145**: p. 579-594.
69. Gray, L.S., B. Winn, and B. Gilmartin, *Accommodation microfluctuations and pupil diameter*. Vision Research, 1993. **33**: p. 2083-2090.
70. Owens, H., B. Winn, B Gilmartin, and J. Pugh, *Effect of a topical beta-adrenergic receptor antagonist on the dynamics of steady-state accommodation*. Ophthal. Physiol. Opt., 1991. **11**: p. 99-104.
71. Stark, L.R. and D.A. Atchison, *Pupil size, mean accommodation response and the fluctuations of accommodation*. Ophthal. Physiol. Opt., 1997. **17**(4): p. 316-323.
72. Gray, L.S., B. Winn, and B. Gilmartin, *Effect of target luminance on microfluctuations of accommodation*. Ophthal. Physiol. Opt., 1993. **13**(3): p. 258-265.
73. Gray, L.S., B. Gilmartin, and B. Winn, *Accommodation microfluctuations and pupil size during sustained viewing of visual display terminals*. Ophthal. Physiol. Opt., 2000. **20**(1): p. 5-10.
74. Maxwell, J.C., *On the theory of compound colours, and the relations of the colours of the spectrum*. Phil. Trans. R. Soc., 1860. **150**: p. 57.
75. Westheimer, G., *The Maxwellian View*. Vision Research, 1966. **6**: p. 669-682.
76. Di Lollo, V., A. Siefert, G. Burchett, R. Rabeeh, and T. Ruman, *Phosphor persistence of oscilloscopic displays: A comparison of four phosphors*. Spatial Vision, 1997. **10**: p. 353-360.
77. Wolf, W. and H. Deubel, *P-31 phosphor persistence at photopic mean luminance level*. Spatial Vision, 1997. **10**: p. 353-360.
78. Viirre, E.S., R. Johnston, H. Pryor, S. Nagata, T. Furness, *Laser safety analysis of a retinal scanning display system*. Journal of Laser Applications, 1997. **9**: p. 253-260.
79. Kelly, J.P., H. Pryor, E. Viirre, and T. Furness, *Decreased Flicker Sensitivity with a Scanned Laser Display*. Investigative Ophthalmology and Visual Science [Supplement], 1998. **39**: p. S399.
80. Jenkins, F.A. and H.E. White, *Fundamentals of Optics*. 4th ed. 1976, New York, NY: McGraw-Hill, Inc.

81. Viirre, E., R. Johnston, H. Pryor, S. Nagata, and T. Furness, *The Virtual Retinal Display: A new technology for virtual reality and augmented vision in medicine*. in *Medicine Meets Virtual Reality*. 1998.
82. Kleweno, C., E. Seibel, E. Viirre, and T. Furness, *Evaluation of a scanned laser display as an alternative low vision computer interface*. in *Technical Digest of Vision Science and its Applications, Technical Meeting*. 1999. Santa Fe, New Mexico: Optical Society of America.
83. Arrington Research, *ViewPoint Eye Tracker*. 2002, www.arringtonresearch.com.
84. Gesture Central, *Gesture Central Eye Tracker*. 2002, www.gesturecentral.com/eyetracker/.
85. Tidwell, M., *Scanned retinal display with exit pupil selected based on viewer's eye position*, U.S. Patent #6352344, March 5, 2002, University of Washington: USA.
86. Microvision, *Microvision New Design Will Cut Micro Scanner Size*. 2002, www.mvis.com.
87. Ryer, A.D., *Light Measurement Handbook*. 1997, Newburyport, MA: International Light, Inc.
88. Boynton, P.A., et al. *Diagnostics for light measuring devices in flying-spot display measurements*. in *SPIE Conference 3954: Projection Displays 2000*. 1999.
89. Boynton, P.A. and E.F. Kelley. *Light measuring device diagnostics for the photometric and colorimetric measurement of flying-spot displays*. in *SPIE Conference 4295B*. 2001.
90. Pryor, H.L., S. Nagata, and E.S. Viirre. *Scanned Laser Display Power and Brightness Levels Compared to a CRT Image Standard*. in *ARVO Annual Meeting*. 1997. Ft Lauderdale, FL: Investigative Ophthalmology & Visual Science.
91. Hase, T., T. Kano, E. Nakazawa, and H. Yamamoto, *Phosphor materials for cathode-ray tubes*. *Advances in Electronics and Electron Physics*, 1990. **79**: p. 271-361.
92. Groner, R., M. Groner, P. Muller, W. Bischof, V. Di Lollo, *On the confounding effects of phosphor persistence in oscilloscopic displays*. *Vision Research*, 1993. **33**(913-917).
93. Di Lollo, V., W. Bischof, P. Walther-Mueller, M. Groner, *Phosphor persistence in oscilloscopic displays: Its luminance and visibility*. *Vision Research*, 1994. **34**: p. 1619-1620.

94. Bordens, K.S. and B.B. Abbott, *Research Design and Methods*. 3rd ed. 1996, Mountain View, CA: Mayfield Publishing Co.
95. Farrell, J.E., *An analytical method for predicting perceived flicker*. Behaviour and Information Technology, 1986. **5**: p. 349-358.
96. Pokorny, J. and V.C. Smith, *Colorimetry and Color Discrimination*, in *Handbook of Perception and Human Performance*, K.R. Boff, J.E. Lincoln, and J.P. Thomas, Editors. 1986, John Wiley and Sons: New York.
97. Applegate, R.A. and V. Lakshminarayanan, *Parametric representation of Stiles-Crawford functions: normal variation of peak location and directionality*. Journal of the Optical Society of America, 1993. **10**(7): p. 1611-1623.
98. de Wit, G.C., *Resolution matching in a retinal scanning display*. Applied Optics, 1997. **36**(22): p. 5587-93.

Bibliography

1. Applegate, R.A. and V. Lakshminarayanan, *Parametric representation of Stiles-Crawford functions: normal variation of peak location and directionality*. Journal of the Optical Society of America, 1993. **10**(7): p. 1611-1623.
2. Arrington Research, *ViewPoint Eye Tracker*. 2002, www.arringtonresearch.com.
3. Baumgardt and Segal, *Temporal effects of brief stimuli*. C.R. Soc. Biol., 1946. **140**: p. 231.
4. Baylor, D.A., B.J. Nunn, and J.L. Schnapf, *Spectral sensitivity of cones of the monkey Macaca Fascicularis*. Journal of Physiology, 1987(390): p. 145-160.
5. Bodmann, H.W., P. Haubner, and A.M. Marsden. *A unified relationship between brightness and luminance*. in *19th Session of the Commission Internationale de l'Eclairage*. 1979. Tokyo, Japan.
6. Boff, K.R., and Lincoln, J.E., *Section 1.1: Measurement of Light*, in *Human Engineering Data Compendium: Human Performance and Perception*, K.R. Boff and J.E. Lincoln, Editors. 1988, AAMRL: Wright-Patterson AFB, Ohio.
7. Boff, K.R., and Lincoln, J.E., *Section 1.5: Sensitivity to Temporal Variations*, in *Human Engineering Data Compendium: Human Performance and Perception*, K.R. Boff and J.E. Lincoln, Editors. 1988, AAMRL: Wright-Patterson AFB, Ohio.
8. Bordens, K.S. and B.B. Abbott, *Research Design and Methods*. 3rd ed. 1996, Mountain View, CA: Mayfield Publishing Co.
9. Boynton, P.A., et al. *Diagnostics for light measuring devices in flying-spot display measurements*. in *SPIE Conference 3954: Projection Displays 2000*. 1999.
10. Boynton, P.A. and E.F. Kelley. *Light measuring device diagnostics for the photometric and colorimetric measurement of flying-spot displays*. in *SPIE Conference 4295B*. 2001.
11. Boynton, R., *Human Color Vision*. 1979, New York: Holt, Rinehart, and Winston.
12. Boynton, R. and P. Kaiser, *Vision: The additivity law made to work for heterochromatic photometry with bipartite fields*. Science, 1968. **161**: p. 366-368.
13. Broca and Sulzer, *The brightness of brief pulses of light*. J. Physiol. Path. Gen., 1902. **4**: p. 632.

14. Brown, J.L., *Flicker and intermittent stimulation*, in *Vision and visual perception*, C.H. Graham, Editor. 1965, John Wiley & Sons: New York.
15. Burns, S.A. and A.E. Elsner, *Response of the retina at low temporal frequencies*. Journal of the Optical Society of America, 1996. **13**(3): p. 667-672.
16. Campbell, F.W. and R.W. Gubisch, *Optical quality of the human eye*. Journal of Physiology, 1966. **186**: p. 558-578.
17. Campbell, F.W. and J.G. Robson, *Applications of Fourier analysis to the visibility of gratings*. Journal of Physiology, 1968. **197**: p. 551-566.
18. Campbell, F.W., J.G. Robson, and G. Westheimer, *Fluctuations of accommodation during steady viewing conditions*. Journal of Physiology, 1959. **145**: p. 579-594.
19. Campbell, F.W. and G. Westheimer, *Dynamics of accommodation response in the human eye*. Journal of Physiology, 1960. **151**: p. 285-295.
20. Capps, M.V., *Virtual Retinal Display (VRD) Technology*. 1999, http://www.cs.nps.navy.mil/people/faculty/capps/4473/projects/fiambolis/vrd/vrd_full.html.
21. CIE, *Colorimetry (Official Recommendations of the International Commission on Illumination)*. 1971, CIE: Paris.
22. Crawford, B.H., *The dependence of pupil size upon external light stimuli under static and variable conditions*. Proceedings of the Royal Society of London, 1936. **B121**: p. 376.
23. de Lang, H., *Research into the dynamic nature of the human fovea - cortex systems with intermittent and modulated light: I. Attenuation characteristics with white and colored light*. Journal of the Optical Society of America, 1958. **48**: p. 777-784.
24. deLauney, L., *A note on the photopupil reflex*. Journal of the Optical Society of America, 1949. **39**: p. 364-367.
25. de Wit, G.C., *Resolution matching in a retinal scanning display*. Applied Optics, 1997. **36**(22): p. 5587-93.
26. de Wit, G.C. and R.A.E.W. Beek, *Effects of a small exit pupil in a virtual reality display system*. Optical Engineering, 1997. **36**(8): p. 2158-62.

27. de Wit, G.C., R.A.E.W. Beek, and J.J.M. Braat. *Effects of a small exit pupil in an optical configuration for virtual reality*. in *Imaging Sciences and Display Technologies*. 1996. Berlin, Germany: Proceedings of the SPIE.
28. Di Lollo, V., W. Bischof, P. Walther-Mueller, M. Groner, *Phosphor persistence in oscilloscopic displays: Its luminance and visibility*. Vision Research, 1994. **34**: p. 1619-1620.
29. Di Lollo, V., A. Siefert, G. Burchett, R. Rabeeh, and T. Ruman, *Phosphor persistence of oscilloscopic displays: A comparison of four phosphors*. Spatial Vision, 1997. **10**: p. 353-360.
30. Dodt, J., *Electroretinogram response to intermittent stimuli*. Graefes Arch., 1952. **153**: p. 152.
31. Enoch, J.M., *Retinal Receptor Orientation and Photoreceptor Optics*, in *Vertebrate Photoreceptor Optics*, J.M. Enoch and F.L. Tobey, Jr., Editors. 1981, Springer-Verlag: New York, NY.
32. Farrell, J.E., *An analytical method for predicting perceived flicker*. Behaviour and Information Technology, 1986. **5**: p. 349-358.
33. Farrell, R.J. and J.M. Booth, *Design Handbook for Imagery Interpretation Equipment*. 1984, Seattle, WA: Boeing Aerospace Company.
34. Felipe, A., J.M. Artigas, and A.M. Pons, *Human contrast sensitivity in coherent Maxwellian view: effect of coherent noise and comparison with speckle*. Journal of the Optical Society of America, 1997. **14**(5): p. 972-983.
35. Furness, T.A., *Virtual Retinal Display*, U.S. Patent #5467104, November 14, 1995, University of Washington: USA.
36. Gesture Central, *Gesture Central Eye Tracker*. 2002, www.gesturecentral.com/eyetracker/.
37. Gilmer, *Examination of the Talbot-Plateau Law*. Journal of the Optical Society of America, 1937. **27**: p. 386.
38. Goldstein, E.B., *Sensation and Perception*. 5th Edition ed. 1999: Brooks/Cole Publishing Company.
39. Granit, R. and P. Harper, *Comparative studies on the peripheral and central retina: II. Synaptic reactions in the eye*. American Journal of Physiology, 1930. **95**: p. 211-228.

40. Gray, L.S., B. Gilmartin, and B. Winn, *Accommodation microfluctuations and pupil size during sustained viewing of visual display terminals*. Ophthal. Physiol. Opt., 2000. **20**(1): p. 5-10.
41. Gray, L.S., B. Winn, and B. Gilmartin, *Accommodation microfluctuations and pupil diameter*. Vision Research, 1993. **33**: p. 2083-2090.
42. Gray, L.S., B. Winn, and B. Gilmartin, *Effect of target luminance on microfluctuations of accommodation*. Ophthal. Physiol. Opt., 1993. **13**(3): p. 258-265.
43. Groner, R., M. Groner, P. Muller, W. Bischof, and V. Di Lollo, *On the confounding effects of phosphor persistence in oscilloscopic displays*. Vision Research, 1993. **33**(913-917).
44. Hase, T., T. Kano, E. Nakazawa, and H. Yamamoto, *Phosphor materials for cathode-ray tubes*. Advances in Electronics and Electron Physics, 1990. **79**: p. 271-361.
45. Hecht, E. and A. Zajac, *Optics*. 1974, Menlo Park, CA: Addison-Wesley Publishing Co.
46. Horowitz, B.R., *Theoretical Considerations of the Retinal Receptor as a Waveguide*, in *Vertebrate Photoreceptor Optics*, J.M. Enoch and F.L. Tobey, Jr., Editors. 1981, Springer-Verlag: New York, NY. p. 219-300.
47. Jacobs, D.H., *The Stiles-Crawford Effect and the Design of Telescopes*. Journal of the Optical Society of America, 1944. **34**(11): p. 694.
48. Jenkins, F.A. and H.E. White, *Fundamentals of Optics*. 4th ed. 1976, New York, NY: McGraw-Hill, Inc.
49. Johnston, R.S. and S.R. Willey. *Development of a commercial retinal scanning display in Helmet- and Head-Mounted Displays and Symbology Design Requirements II*. 1995. Orlando, FL, USA: Proceedings of the SPIE.
50. Kelly, D.H., *Visual response to time-dependent stimuli. I. Amplitude sensitivity measurements*. Journal of the Optical Society of America, 1961. **51**: p. 422-429.
51. Kelly, J.P., H. Pryor, E. Viirre, and T. Furness, *Decreased Flicker Sensitivity with a Scanned Laser Display*. Investigative Ophthalmology and Visual Science [Supplement], 1998. **39**: p. S399.
52. Kleweno, C., Seibel, E., Kloeckner, K., Viire, E., and Furness, T.A. *Evaluation of a Scanned Laser Display as an Alternative Low Vision Computer Interface*. in *Proceedings of OSA Vision Science and Its Applications*. 1998.

53. Kleweno, C., E. Seibel, E. Viirre, and T. Furness, *Evaluation of a scanned laser display as an alternative low vision computer interface*. in *Technical Digest of Vision Science and its Applications, Technical Meeting*. 1999. Santa Fe, New Mexico: Optical Society of America.
54. Kollin, J.S. *A retinal Display for virtual-environment applications*. in *1993 international symposium, digest of technical papers*. 1993. Playa del Ray, CA: Society for Information Display.
55. Kollin, J.S. and M. Tidwell. *Optical engineering challenges of the virtual retinal display*. in *Novel Optical Systems Design and Optimization*. 1995. San Diego, CA, USA: Proceedings of the SPIE.
56. LeGrand, Y.L., *Light, Colour, and Vision*. 2nd ed. 1968, London: Chapman and Hall, Ltd. 564.
57. Leibowitz, H. and D.A. Owens, *New evidence for the intermediate position of relaxed accommodation*. *Documenta Ophthalmologica*, 1978. **46**: p. 133-137.
58. Maxwell, J.C., *On the theory of compound colours, and the relations of the colours of the spectrum*. *Phil. Trans. R. Soc.*, 1860. **150**: p. 57.
59. Melville, D., J.S. Kollin, and R. Johnston, *Miniature optical scanner for a two axis scanning system*, in *United States Patent Office*. 1996, University of Washington: United States of America.
60. Microvision Inc., *Microvision Home Page*. 2001, <http://www.mvis.com>.
61. Microvision Inc., *Microvision New Design Will Cut Micro Scanner Size*. 2002, www.mvis.com.
62. Moon, P. and D.E. Spencer, *On the Stiles-Crawford Effect*. *Journal of the Optical Society of America*, 1944. **34**(6): p. 319-329.
63. Nagata, S., H.L. Pryor, and E.S. Viirre. *Visual image quality of a scanned light display in normal and low vision users*. in *ARVO Annual Meeting*. 1997. Ft Lauderdale, FL: Investigative Ophthalmology and Visual Science.
64. Nelson, T.M. and Bartley, Vision Research, 1964. **4**: p. 403.
65. Owens, H., K. Bhat, and R.J. Jacobs, *Maxwellian and small pupils: effects on accommodation*. *Invest. Ophthalmol. Visual Sci.*[supplement], 1994. **35**: p. 1280.

66. Owens, H., B. Winn, B. Gilmartin, and J. Pugh, *Effect of a topical beta-adrenergic receptor antagonist on the dynamics of steady-state accommodation*. *Ophthalm. Physiol. Opt.*, 1991. **11**: p. 99-104.
67. Pask, C. and A. Stacey, *Optical Properties of Retinal Photoreceptors and the Campbell Effect*. *Vision Research*, 1998. **38**(7): p. 953-961.
68. Pokorny, J. and V.C. Smith, *Colorimetry and Color Discrimination*, in *Handbook of Perception and Human Performance*, K.R. Boff, J.E. Lincoln, and J.P. Thomas, Editors. 1986, John Wiley and Sons: New York.
69. Pryor, H.L., S. Nagata, and E.S. Viirre. *Scanned Laser Display Power and Brightness Levels Compared to a CRT Image Standard*. in *ARVO Annual Meeting*. 1997. Ft Lauderdale, FL: Investigative Ophthalmology & Visual Science.
70. Reeves, P., *Rate of pupillary dilation and contraction*. *Psychology Review*, 1918. **25**: p. 330-340.
71. Robson, J.G., *Spatial and temporal contrast sensitivity functions of the visual system*. *Journal of the Optical Society of America*, 1966. **56**: p. 1141-1142.
72. Rodieck, R.W., *The First Steps in Seeing*. 1998, Sunderland, Massachusetts: Sinauer Associates, Inc.
73. Rushton, W.A.H., *Visual pigments in man*, in *Handbook of Sensory Physiology*, H.J.A. Dartnall, Editor. 1972, Springer-Verlag: New York, NY. p. 364-394.
74. Ryer, A.D., *Light Measurement Handbook*. 1997, Newburyport, MA: International Light, Inc.
75. Seguer, *De raritate Luminis*. 1740, Gottingen.
76. Silva, D., *Surgeons say hi-tech headgear makes the cut*, in *Puget Sound Business Journal*. 2000, American City Business Journals, Inc.
77. Snyder, A.W., *The Stiles-Crawford effect - explanation and consequences*. *Vision Research*, 1973. **13**: p. 1115-1137.
78. Stacey, A. and C. Pask, *Spatial-frequency response of a photoreceptor and its wavelength dependence. I. Coherent sources*. *Journal of the Optical Society of America*, 1994. **11**(4): p. 1193-1198.

79. Stanley, P.A. and A.K. Davies, *The effect of field of view size on steady-state pupil diameter*. Ophthal. Physiol. Opt., 1995. **15**(6): p. 601-603.
80. Stark, L.R. and D.A. Atchison, *Pupil size, mean accommodation response and the fluctuations of accommodation*. Ophthal. Physiol. Opt., 1997. **17**(4): p. 316-323.
81. Stevens, S.S., *Brightness function: Effects of adaptation*. Journal of the Optical Society of America, 1963. **53**: p. 375-385.
82. Stevens, S.S., *Psychophysics*. 1975, New York, NY: John Wiley & Sons.
83. Stiles, W.S. and B.H. Crawford. *The Luminous Efficiency of Rays Entering the Eye Pupil at Different Points*. in *Proceedings of the Royal Society of London*. 1933. London.
84. Talbot, F., in *Philosophy Magazine*. 1834. p. 327.
85. Teller, D.Y., *Vision and the Visual System*. 2000: University of Washington, Seattle, WA.
86. Thompson, B.J., *Image Formation with Partially Coherent Light*, in *Progress in Optics*, E. Wolf, Editor. 1969, North-Holland Publishing Co.: New York, NY. p. 212-230.
87. Tidwell, M., *A Virtual Retinal Display for Augmenting Ambient Visual Environments*, in *Electrical Engineering*. 1995, University of Washington: Seattle. p. 1-108.
88. Tidwell, M., *Scanned retinal display with exit pupil selected based on viewer's eye position*, U.S. Patent #6352344, March 5, 2002, University of Washington: USA.
89. Viirre, E.S., Viirre, E.S., R. Johnston, H. Pryor, S. Nagata, T. Furness, *Laser safety analysis of a retinal scanning display system*. Journal of Laser Applications, 1997. **9**: p. 253-260.
90. Viirre, E., R. Johnston, H. Pryor, S. Nagata, and T. Furness, *The Virtual Retinal Display: A new technology for virtual reality and augmented vision in medicine*. in *Medicine Meets Virtual Reality*. 1998.
91. Wagner, G. and R. Boynton, *Comparison of four methods of heterochromatic photometry*. Journal of the Optical Society of America, 1972. **62**: p. 1508-1515.
92. Wald, G. and P.K. Brown, *Synthesis and bleaching of rhodopsin*. Nature, 1956. **177**: p. 174-176.

93. Wandell, B.A., *Foundations of Vision*. 1995, Sunderland, Massachusetts: Sinauer Associates, Inc.
94. Westheimer, G., *The Eye as an Optical Instrument*, in *Handbook of Perception and Human Performance*, K.R. Boff, L. Kaufman, and J.P. Thomas, Editors. 1986, John Wiley & Sons: New York.
95. Westheimer, G., *The Maxwellian View*. Vision Research, 1966. **6**: p. 669-682.
96. Wolf, W. and H. Deubel, *P-31 phosphor persistence at photopic mean luminance level*. Spatial Vision, 1997. **10**: p. 353-360.
97. Wu, S., S.A. Burns, and A.E. Elsner, *Effects of flicker adaptation and temporal gain control on the flicker ERG*. Vision Research, 1995. **35**: p. 2943-2953.
98. Wyszecki, G. and W.S. Stiles, *Color science : concepts and methods, quantitative data and formulae*. 2nd ed. ed. 1982, New York, NY: John Wiley & Sons.

Appendix A: List of Pupillary Response Experiment RSD Conditions

Each level of corneal flux density presented with the RSD in the pupillary response experiment of Chapter 6 may be characterized by the combination of display field of view and retinal illumination in troland. This alternative characterization may provide easier quantification of Maxwellian view displays in many cases. The following table summarizes all RSD presentation in the experiment.

Numbered Reference	RSD FOV (deg)	corneal flux density (cd/m ² * deg ²)	troland
1	5.0	100	182.7
2	5.0	500	743.8
3	5.0	1000	1320.1
4	5.0	5000	4654.7
5	5.0	10000	7813.2
1	12.0	100	31.7
2	12.0	500	129.1
3	12.0	1000	229.2
4	12.0	5000	808.1
5	12.0	10000	1356.5
6	12.0	50000	4425.0
7	12.0	100000	7412.5
1	20.0	100	11.4
2	20.0	500	46.5
3	20.0	1000	82.5
4	20.0	5000	290.9
5	20.0	10000	488.3
6	20.0	50000	1593.0
7	20.0	100000	2668.5
8	20.0	500000	9336.8
9	20.0	1000000	16507.8
1	28.0	100	5.8
2	28.0	500	23.7
3	28.0	1000	42.1
4	28.0	5000	148.4
5	28.0	10000	249.1
6	28.0	50000	812.8
7	28.0	100000	1361.5
8	28.0	500000	4763.7
9	28.0	1000000	8422.3

Appendix B: Equating Retinal Illumination of Corneal Flux Density Stimuli

A retinal illumination resulting from conditions defined by the natural view corneal flux density model of pupillary response of Stanley and Davies is desired to be matched with a Maxwellian view retinal illumination from the RSD (VRD Emulator) employing 632.8 nm HeNe laser light.

Begin with units of corneal flux density and with areas of desired stimuli disks.

Corneal flux density units: $\text{cd/m}^2 \text{ deg}^2$

Areas of RSD stimuli disks to be matched:

- 5 deg diameter $\rightarrow 19.63 \text{ deg}^2$
- 12 deg diameter $\rightarrow 113.10 \text{ deg}^2$
- 20 deg diameter $\rightarrow 314.16 \text{ deg}^2$
- 28 deg diameter $\rightarrow 615.75 \text{ deg}^2$

Dividing each desired corneal flux density value by RSD stimuli area in square degrees yields a luminance value in cd/m^2 for the source of the retinal illumination stimuli to be matched.

Example for 28 deg diameter RSD disk stimulus and $1,000,000 \text{ cd/m}^2 \text{ deg}^2$ corneal flux density:

$$1,000,000 \text{ cd/m}^2 \text{ deg}^2 \div 615.75 \text{ deg}^2 = 1624.04 \text{ cd/m}^2$$

Using the mean eye pupil diameter derived from Stanley and Davies model for $1,000,000 \text{ cd/m}^2 \text{ deg}^2$ corneal flux density level (2.6 mm), an estimate of retinal illumination may be calculated in either troland (td) or lumens per steradian (sr) by multiplying luminance by pupil area:

Example continued:

Pupil area: 5.31 mm^2

Retinal illumination: $5.31 \text{ mm}^2 \times 1624.04 \text{ cd/m}^2 = 8,623.7 \text{ td}$

$$8,623.7 \text{ td} \div 10^6 = 0.0086237 \text{ lumens/sr}$$

Multiplying the retinal illumination by an estimate of the solid angle of the RSD disk stimulus in steradians yields a value for the optical power in lumens of the stimulus.

Example continued:

$$0.0086237 \text{ lumens/sr} \times 0.1904 \text{ sr} = 0.001642 \text{ lumens}$$

Converting from lumens to watts for the 632.8 nm wavelength providing the VRDE scanned light yields a power level to ensure a match in retinal illumination to the mean retinal illumination affected by the natural view stimuli used by Stanley and Davies.

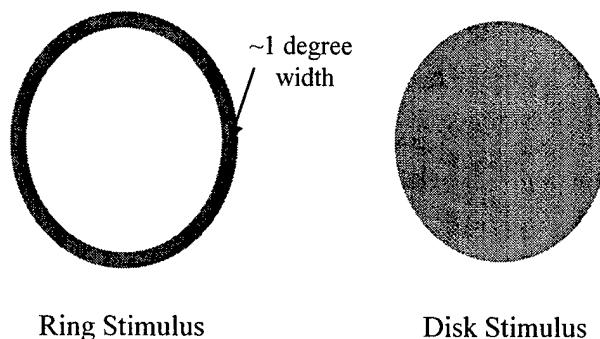
Example continued:

$$0.001642 \text{ lumens} \div 160.73 \text{ watts/lumen} = 10.215 \times 10^{-6} \text{ watts (10.215 } \mu\text{W)}$$

The required RSD power levels were produced by attenuating the VRDE laser energy with neutral density filters.

Appendix C: Example Stimuli Used in Pupillary Response Pilot Study and Exit Pupil Separation Study

Schematic of RSD ring and disk stimuli from pupillary response pilot study:



Ring and disk stimuli used in the pilot study were red in color with the HeNe laser 632.8 nm light. In each stimulus, the white collimated crosshair was centered within the ring or disk. Ring and disk stimuli ranged in diameter from 5 – 30 degrees visual angle, and the ring width was a consistent 1 degree visual angle.

Paragraph of text displayed in arrayed exit pupil explorations and pupil separation study:

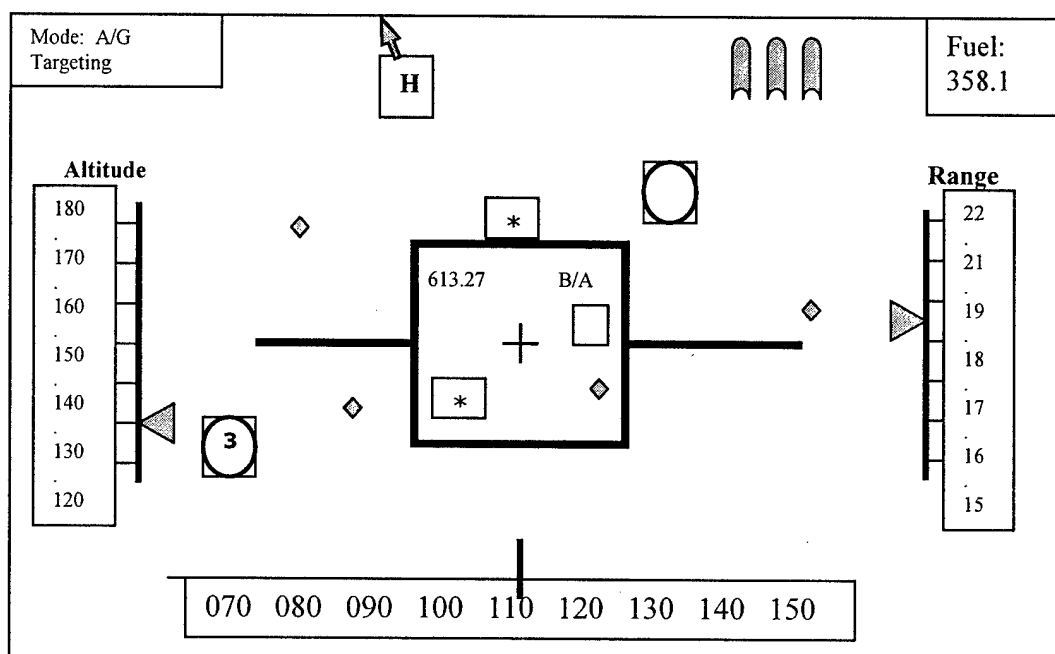
Figure 3.2 depicts relationships between the entrance pupil of the eye and two display exit pupils. This model assumes round exit pupils, that the diameters of the exit pupils are equivalent, and that the exit pupil diameters are significantly smaller than the entrance pupil diameter. Exit pupil separation distances are considered to be center-to-center. No special conditions are imposed on the arrangement or number of exit pupils.

If two exit pupil simultaneously enter the eye, overlapping images will result on the retina. In the absence of extreme image alignment precision, such overlapping would be distracting and detrimental to image interpretation. This circumstance is undesirable under most envisioned applications. Thus, exit pupil separation should be sufficient to avoid overlapping images.

Text was presented as white on black background so that in augmented display mode white text was imaged over the background scene.

Appendix C: Example Stimuli Used in Pupillary Response Pilot Study and Exit Pupil Separation Study continued...

Wire frame diagram used as sparse image content in arrayed exit pupil explorations:



Wire frame diagram was presented with black background, yellow text and numerals, and red lines. Image was presented in emulated RSD augmented view to contrast with the natural background scene.

Vita

Stuart L. Turner is a Lieutenant Colonel (select) in the United States Air Force. His career duties have included service as a B-52 bomber pilot, a research engineer, and an instructor at the U.S. Air Force Academy. He earned a Bachelor of Science degree in Physics from the University of Southern Mississippi in 1986. He earned a Master of Science degree in Systems Engineering from Wright State University in 1995. In 2002 he earned a Doctor of Philosophy at the University of Washington in Industrial Engineering while conducting research at the Human Interface Technology Laboratory.